PROCEEDINGS

The 10th HKBU-CSD Postgraduate Research Symposium

PG Day 2009

Department of Computer Science
Hong Kong Baptist University

August 31 & September 1, 2009

The 10th HKBU-CSD Postgraduate Research Symposium (PG Day) Program

August 31 Monday, 2009	
Time	**Sessions**
09:00-09:20	**On-site Registration** (LT1)
09:20-09:30	**Welcome**: Prof. Clement LEUNG (LT1)
09:30-10:30	**Keynote Talk**: Ms. Jenny Li IBM Master Inventor, Chief Technology Officer for the Energy and Utility Industry, IBM System and Technology Group in Poughkeepsie, NY (LT1) (Chair: Dr. Xiaowen CHU) **You Can Build a Smarter Planet**
10:30-10:45	Tea Break (LMC511)
10:45-12:45	Session I: (Chair: Benyun SHI) (LMC511)
	• **An Automatic Lip-reading Method Based On Polynomial Fitting** Meng LI • **Image Analysis based on the Local Features of 2D Intrinsic Mode Functions** Dan ZHANG • **Discriminability and Reliability Indexes: Two New Measures to Enhance Multi-image Face Recognition** Weiwen ZOU • **A Dynamic Trust Network for Autonomy-Oriented Partner Finding** Hongjun QIU
12:45-13:00	Noon Break (LMC511)
13:00-15:00	Session II: (Chair: Shang XIA) (LMC511)
	• **Control Behavior of 3D Humanoid Animation Object Using Reinforcement Learning** Yuesheng HE • **Optimize Write Performance for DBMS on Solid State Drive** Yu LI • **Cooperative Stochastic Differential Game in P2P Content Distribution Network** Xiaowei CHEN • **Social Knowledge Dynamics: A Case Study on Modeling Wikipedia** Benyun SHI
15:00-15:10	Tea Break (LMC511)
15:10-17:10	**Session III: (Chair: Dan ZHANG) (LMC511)**
	• **Edge Detection Combining Wavelet Transform and Canny Operator Based on Fusion Rules** Jian Jia PAN

	• **Modeling and Simulating Human Vaccinating Behaviors on a Disease Diffusion Network** Shang XIA • **Extracting Discriminating Binary Template for Face Template Protection** Yi Cheng FENG • **Incorporating Concept Ontology into Multi-level Image Indexing** Chun Fan WONG
17:10-17:20	Tea Break (LMC511)
17:20-19:20	**Session IV: (Chair: Xiaowei CHEN) (LMC511)**
	• **Hiding Emerging Pattern with Local Recoding Generalization** Wai Kit CHENG • **Estimation of the Number of Relevant Images in Infinite Databases** Xiaoling WANG • **Patient Journey Optimization Using A Multi-Agent Approach** Chung Ho CHOI • **Commentary-based Video Categorization and Concept Discovery** Kwan Wai LEUNG
September 1 Tuesday, 2009	
Time	**Sessions**
09:20-10:20	Session V: (Chair: Weiwen ZOU) (RRS905)
	• **Implementation of Multiple-precision Modular Multiplication on GPU** Kaiyong ZHAO • **L-BFGS and Delayed Dynamical Systems Approach for Unconstrained Optimization** Xiaohui XIE
10:30-11:30	**Distinguished Lecture**: David Lorge Parnas Pioneer in Software Engineering, Professor Emeritus, University of Limerick & McMaster University (LT1) (Chair: Prof. Jiming LIU, Head of Department of Computer, HKBU) **How Precise Documentation Allows Information Hiding to Reduce Software Complexity** **and Increase its Agility**
11:30-14:00	Noon Break
14:00-15:00	Dialogue with Prof. David Lorge Parnas (RRS905) (Chair: Weiwen ZOU)
16:30	**Awards Ceremony**: Best Paper & Best Presentation Awards (RRS905) (Chair: Prof. Jiming LIU) All students and faculty are invited

Table of Contents

An Automatic Lip-reading Method Based on Polynomial Fitting

Meng Li

Abstract

This paper addresses the problem of speaker-dependent isolate digits recognition using sole visual information. We employ intensity transformation and spatial filter to estimate the minimum enclosing rectangle of mouth in each frame. Thus, for each utterance, we can obtain two vectors composed of width and height of mouth, respectively. Then, we propose an approach to recognize the speech based on polynomial fitting. Firstly, both width and height vectors are normalized into the constant length via interpolation. Secondly, least square method is utilized to produce two 3-order polynomials that can represent the main trend of the two vectors, respectively, and reduce the noise caused by the estimate error. Lastly, positions of three crucial points (i.e. maximum, minimum and right boundary point) in each 3-order polynomial curve are recorded as a feature vector. For each utterance, we calculate the average of all vectors of training sample to make a template, and using Euclidean distance between the template and testing data to perform the classification. Experiments show the promising results of the proposed approach.

1 Introduction

Lip reading is to understand speech by visually interpret the lip movement of speakers [7]. This technique has potential attractive applications in speech recognition, human identification, and so forth [4, 9, 13].

So far, two kinds of features are widely used in lip reading system, namely image-based and model-based. In the image-based approach, the pixels of lip region are transformed by PCA, DWT or DCT, to become a feature vector [2, 5, 6]. Under the ideal environment, the accuracy of image-based approach is considerable high, but the performance will be degraded seriously in real environment. One main reason is that the approach is restricted by the illumination, mouth rotation and some other conditions. Thus, from the practical view point, the image-based approach is not the appropriate choice for automatic lip reading system. In the model based approach, shape and position of lip contours, tongue, teeth or some other features like width and height of mouth are modeled, and controlled by a set of parameters(e.g. Snake, ASM and AAM) [3, 8, 10, 12]. Model-based approach can invariant to the effects of scaling, rotation, translation and illumination. Hereby, with regard to the feature extraction, many researchers resort to the modal-based approach.

In this paper, we propose a lip reading approach under simple modal – the width and height of mouth. We employ intensity transformation and spatial filter to the image of ROI(Range Of Interesting) in gray scale space to localize the minimum enclosing rectangle of lip automatically. Then, give a video clip for an utterance, we can obtain two vectors composed of the width and hight of mouth from each frame, respectively. Based on the least square method, two 3-order polynomials are built to fit the width and height vector. The positions of three crucial points (i.e. maximum, minimum, and right boundary point) in each 3-order polynomial curve are recorded as a feature vector. For each utterance, we calculate the average of all vectors of training data to make a template, and use Euclidean distance between the template and testing data to perform the classification.

The remainder of this paper is organized as follows. Section 2 describes the visual feature, namely the minimum enclosing rectangle of mouth, extraction method. Section 3 presents our new approach for lip-reading recognition. In Section 4, we will conduct the experiment to compare our approaches with the existing methods. Finally, Section 5 draws a conclusion.

2 Lip localization and feature extraction

Before showing the details, a pre-processing is needed. The images captured by camera are comprised of RGB values. We heuristically project these RGB values into the gray-level space based on the following equation:

$$I = 0.299R + 0.587G + 0.114B. \quad (1)$$

In order to enhance the contrast between lip and surrounding skip region, we adjust the histogram of the image and make it equalized for the first step. Then we make an

accumulation of gray level value for each row of the image. The slopes of the curve contain the information about the boundaries between the lips and the surrounding skin region. The minimum value on the curve retained as the row position of mouth corner points or the nearby position, the row can be named as horizontal midline of mouth. The midline is shown in Figure 1.

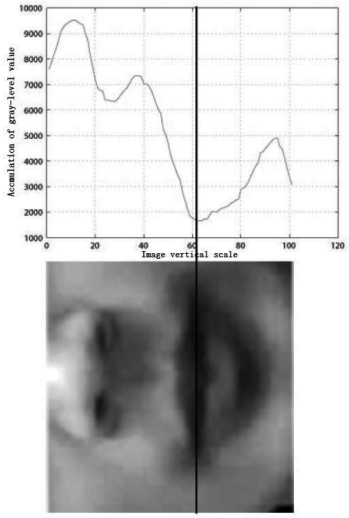

Figure 1. Accumulation curve of gray level value for each row. The vertical crossing line represents the relation between the horizontal midline of mouth and the minimum value of the accumulation curve.

The curve of gray level values along with the horizontal midline is saved in vector G. Building a sub-vector G_s by a segment of G which between the first maximum from left and the first maximum from right. Using the following equations to make the curve smooth and save it into a new vector which named C.

$$C_l^{(i)} = \begin{cases} G_s^{(i)} & (C_l^{(i-1)} > G_s^{(i)}) \\ C_l^{(i-1)} & (C_l^{(i-1)} \leq G_s^{(i)}) \end{cases} \quad i = 1, 2, \ldots, n \quad (2)$$

$$C_r^{(i)} = \begin{cases} G_s^{(i)} & (C_r^{(i+1)} > G_s^{(i)}) \\ C_r^{(i+1)} & (C_l^{(i+1)} \leq G_s^{(i)}) \end{cases} \quad i = n-1, n-2, \ldots, 1 \quad (3)$$

$$C = C_l + C_r \quad (4)$$

where C_l and C_r are assistant vectors, $C_l^{(i)}$ is the ith element in vector C_l, n is the dimension of the vector G. The initial values of the two vectors are shown in equation 5.

$$\begin{aligned} C_l^{(1)} &= G^{(1)} \\ C_r^{(n)} &= G^{(n)} \end{aligned} \quad (5)$$

Set the minimum of the most left and most right value in C as threshold. Elements in C less than the threshold build a new vector C' . Accordingly, the average can be calculated by the equation 6.

$$c_{avg} = \frac{\sum_{i=1}^{m} C'^{(i)}}{m} \quad (6)$$

The equation 7 is employed to adjust the contrast of image.

$$I_{out} = \begin{cases} 255 & (1.5c_{avg} < I_{in} < 1) \\ \frac{500}{c_{avg}} - 500 & (0 < I_{in} \leq 1.5c_{avg}) \end{cases} \quad (7)$$

where I_{in} is the input gray level value, and the I_{out} is the output.

For the adjusted image, a 11×1 searching block is performed along with the midline, the positions of the most left and right non-all white block are marked as the column of mouth corner candidates. The procedure is performed through an iterative process in the steps above, repeated until the position of mouth corner candidates no longer changed or the image turned into binary. Figure 2 illustrate the result of contrast adjustment and the the corresponding mouth corner estimate result.

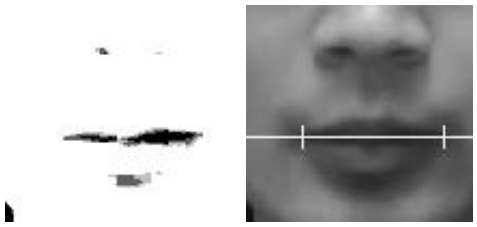

(a) (b)

Figure 2. Image of contrast adjust result (a) and mouth corner estimate result (b).

As shown in equation 8 and 9 , a 3×3 mask is employed to perform mean filter in the initial image.

$$M = \begin{bmatrix} \frac{1}{9} & \frac{1}{9} & \frac{1}{9} \\ \frac{1}{9} & \frac{1}{9} & \frac{1}{9} \\ \frac{1}{9} & \frac{1}{9} & \frac{1}{9} \end{bmatrix} \quad (8)$$

$$I^{(i+1)} = I^{(i)} * M \quad (9)$$

where the $I^{(i)}$ is the result of ith time filter. The times filter performed is determined by the equation 10.

$$\delta_i = dist(I^{(i+1)}, I^{(i)}) \tag{10}$$

where δ_i is the Euclidean distance between $I^{(i)}$ and $I^{(i+1)}$. The procedure should be ceased once δ_i less than a given threshold, and the $I^{(i+1)}$ can be marked as I_f.

Due to the position of left and right mouth corners have been estimated in section 2.1, we can utilize them to calculate the center of mouth easily. For each $I^{(i)}$, a gray value vector $G_{mu}^{(i)}$ is built by the segment from the center point to the top of image along with the normal direction respectively. Then the vector ΔG_{acc} is calculated by the equation 11.

$$\Delta G_{acc} = \sum_{i=1}^{n} (|G_{mu}^{(0)} - G_{mu}^{(i)}|) \tag{11}$$

The point correspond to extreme value of maximum (except boundary value) is retained as the row position of upper bound of mouth.

Then the subtracted image between $I^{(0)}$ and I_f can be calculated. For observing conveniently, an image inversing transformation is employed. The result is shown in Figure 3.

Figure 3. The subtracted image between source gray-scale $I^{(0)}$ and the filtered image I_f. For observing conveniently, an image inversing transformation is employed.

We get the gray level value along with the normal direction pass the middle point of mouth to the bottom of the image. The point perform extreme value of minimum (except boundary value) is retained as the row position of lower bound of mouth. The estimate of mouth upper and lower bound is shown in Figure 4.

3 Recognition method

For one utterance procedure, e.g. a isolate digit or a word, we can capture the video clip of speaker's lip motion, and split it into a frame sequence. Then, utilize the method

Figure 4. The estimate of mouth upper and lower bound.

described in Section 2 in each frame, we can get two vectors composed of width and height of mouth respectively. Since the time for each pronunciation is inconstant, a interpolation method is employed to make the length of two vectors same (in our paper, the length is 100), this two vectors are marked as F_w and F_h. A example is shown in Figure 5.

Since the range of lip motion for different people is inconstant, we use the radio between displacement and the original position of lip to represent the trend of motion. The normalization method is shown in equation 12 and 13.

$$F_w^{norm} = K\frac{(F_w - F_{w_1})}{F_{w_1}} \tag{12}$$

$$F_h^{norm} = K\frac{(F_h - F_{h_1})}{F_{h_1}} \tag{13}$$

where F_{w_1} is the first element in F_w, and K is a gain coefficient which make the motion trend more significant, in this paper, the value of K we get experimently is 30.

Then, we employ least square method so as to find two polynomials to fit F_w^{norm} and F_h^{norm}. The polynomial is like equation 14:

$$P = \sum_{k=0}^{n} a_k x^k \tag{14}$$

To find the coefficient a_k, we should make the following equation minimum.

$$I = \sum_{i=0}^{m} (\sum_{k=0}^{n} a_k x_i^k - y_i)^2 \tag{15}$$

The minimum of I is found by setting the gradient to zero. Since the equation 15 contains m parameters there are m gradient equations.

$$\frac{\partial I}{\partial a_i} = 2\sum_{i=0}^{m} (\sum_{k=0}^{n} a_k x_i^k - y_i) x_i^k = 0 \tag{16}$$

where y_i is the $F_{w_i}^{norm}$ or $F_{h_i}^{norm}$, m is the maximum index of vector which equal to 99, and x_i equal to $0.1i$ so as to

avoid the conditioned in coefficient matrix. Moreover, owing to the characteristic of human speech, n is chosen by 3. Thus, we can get the solution $A_w = [a_{w0}, a_{w1}, a_{w2}, a_{w3}]^T$ and $A_h = [a_{h0}, a_{h1}, a_{h2}, a_{h3}]^T$. A example of polynomial fitting result is shown in Figure 6.

The polynomial shapes for the same utterance are constrained to have similar expression. Thus, we can get the global maximum and minimum in the two polynomial marked as $(x_{w_{min}}, y_{w_{min}})$, $(x_{h_{min}}, y_{h_{min}})$, $(x_{w_{max}}, y_{w_{max}})$ and $(x_{h_{max}}, y_{w_{max}})$ to build the feature vectors which shown below:

$$F_w = [x_{w_{min}}, y_{w_{min}}, x_{w_{max}}, y_{w_{max}}, y_{w_{bound}}]^T \quad (17)$$

$$F_h = [x_{h_{min}}, y_{h_{min}}, x_{h_{max}}, y_{h_{max}}, y_{h_{bound}}]^T \quad (18)$$

where the y_{bound} is the most right value of polynomial when $x \in [0, 9.9]$ (e.g. $x = x_{99}$).

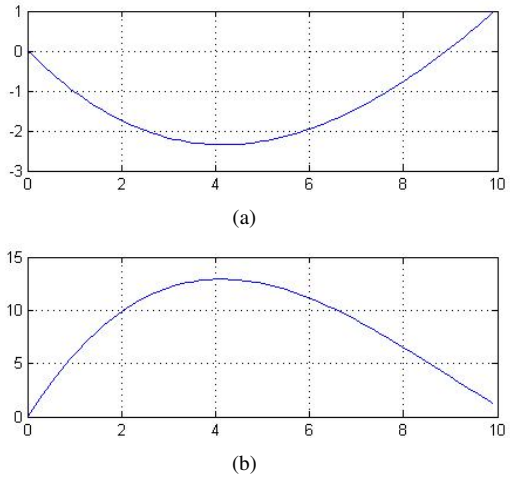

Figure 6. The curve of polynomial which fit to the width vector (a) and height vector (b) shown in Figure 5.

Moreover, for the feature vectors, if $x_{min} \notin [0, 9.9]$, both x_{min} and y_{min} are set to zero. In a similar way, we can determine the value of x_{max} and y_{max}. For example, as shown in Figure 6, the feature vectors are $F_w = [4.1558, -2.3476, 0, 0, 0.9460]^T$ and $F_h = [0, 0, 4.1266, 12.9164, 1.2969]^T$.

For each utterance, we calculate the average of all vectors of training data to make a template by following equations.

$$T_w^{i+1} = \frac{T_w^i + F_w}{2} \quad (19)$$

$$T_h^{i+1} = \frac{T_h^i + F_h}{2} \quad (20)$$

Digit	Phonetic Symbol	Digit	Phonetic Symbol
0	[liŋ]	5	[uː]
1	[jau]	6	[liou]
2	[ɤɻ]	7	[tɕʻ]
3	[san]	8	[baː]
4	[sɿ]	9	[tɕiou]

Table 1. The pronunciations of number 0 to 9 in Chinese mandarin.

where Ti is the template after i times trains employed, F is the new training data. For each classification, there is a template which involve two vectors.

When testing, we calculate the distance between each template and testing data via the following equation.

$$d = ||F_w - T_w|| \cdot ||F_h - T_h|| \quad (21)$$

that is, the input testing data is classified into the category which corresponding into the minimum d.

4 Experiment result

We conduct an experiment to demonstrate the performance of the proposed approach. The experiment environment is shown in Figure 7. The illumination source is a 18w fluorescent lamp which placed in front of speaker.The resolution of camera is 320×240, and the FPS(Frames Per Second) is 30.

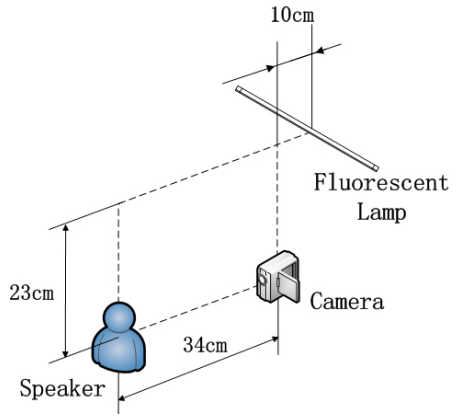

Figure 7. The illustration of experiment environment.

Our task is to recognize 10 isolate digits(0 to 9) in Chinese mandarin, which pronunciations are shown in Table 1.

There are 5 speakers(4 males and 1 female) take part into the experiment. For each digit, speakers were asked to re-

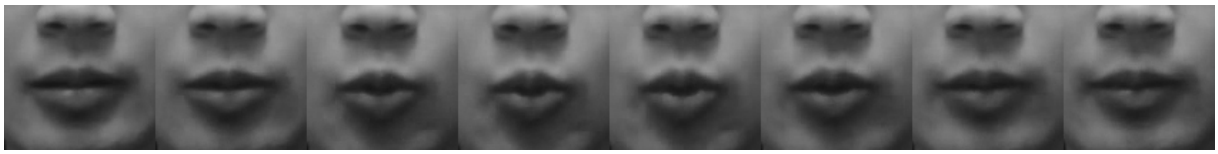

(a)

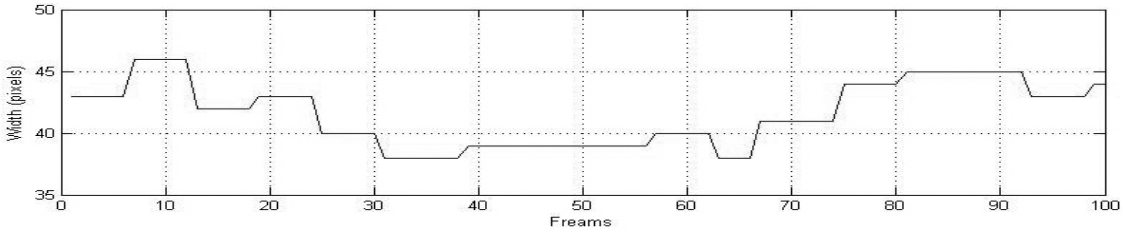

(b)

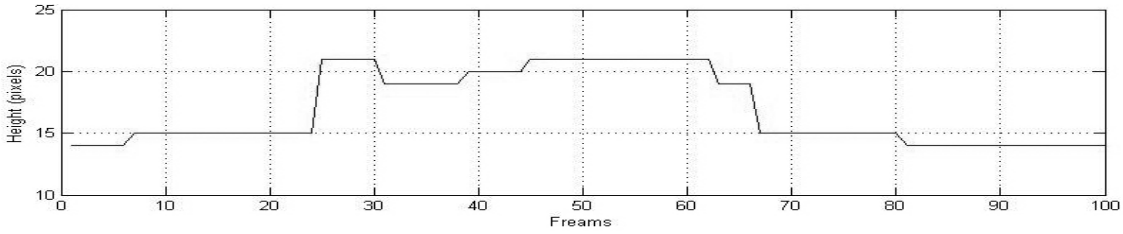

(c)

Figure 5. Some frames of the pronunciation of "5" in Chinese mandarin (a), and the corresponding width vector (b), height vector (c). In this illumination, although there are some noise caused by the estimate error, we can see that the main trend of width is original-narrow-original, and the height is original-high-original.

Digit	Accuracy	Digit	Accuracy
0	0.972	5	0.912
1	0.952	6	0.964
2	0.976	7	0.744
3	0.964	8	0.952
4	0.788	9	0.932

Table 2. The pronunciations of digits 0 to 9 in Chinese mandarin.

peat ten times to train the system, and fifty times to test. Figure 8 shows the performance of our approach with the different number of training samples. Moreover, Table 2 shows the recognition accuracy for each number with 10 training samples.

In order to compare with some existed approaches, we find two paper which also using width and height of mouth as the visual feature to perform the lip reading recognition. In [11], the recognition accuracy achieved under three

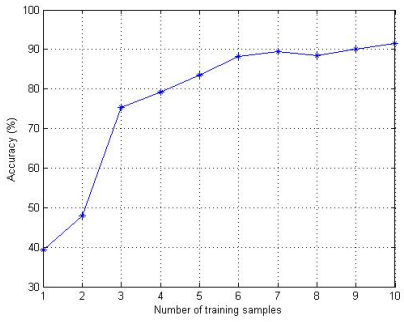

Figure 8. The testing result in different number of training samples.

Method	Accuracy
HMM	81.27%
RDA	77.41%
Spline	91.49%
ST Coding	77.20%
Our approach	91.56%

Table 3. The lip reading recognition accuracy obtain using different approaches.

	0	1	2	3	4	5	6	7	8	9
4	-	-	-	4	197	-	7	42	-	-
7	-	-	-	1	63	-	-	186	-	-

Table 4. The classification detail of "4" and "7" when number of training samples is 10.

method(HMM based, RDA based, and Spline based); the task is to recognize the isolate digits 0 to 9 in English. Moreover, in [1], the classification method is ST(spatio-temporal) coding based; the task is to recognize the isolate digits 0 to 9 in French. Table 3 shows the recognition performance obtained using different approaches.

Nevertheless, we have found that it is not enough to utilize the visual feature, i.e. the width and height of mouth, to distinguish some Chinese utterance, e.g. "4" and "7". Table 4 shows the classification detail of the two digits when number of training samples is 10. In future work, we will focus on how to find a more appropriate modal of mouth for the purpose of lip reading.

5 Conclusion

In this paper, we have proposed a new approach to automatic lip reading recognition based upon polynomial fitting. The feature vector of our approach have low dimensions and the approach need small testing data set. Experiments have shown the promising result of the proposed approach in comparison with the existing methods.

References

[1] A.R.Baig, R.Séguier, and G.Vaucher. Image sequence analysis using a spatio-temporal coding for automatic lip-reading. In *Proc. IEEE International Conference on Image Analysis and Processing*, pages 544–549, Venice, Italy, 1999.

[2] C.Bregler and Y.Conig. "eigenlips" for robust speech recognition. In *Proc. IEEE International Conference on Acoustics, Speech, Signal Processing*, pages 669–672, Adelaide, Australia, 1994.

[3] C.Neti, G.Iyengar, G.Potamianos, A.Senior, and B. Maison. Perceptual interfaces for information interaction: Joint processing of audio and visual information for human-computer interaction. In *Proc. International Conference on Spoken Language Processing*, Beijing, China.

[4] G.Potamianos, C.Neti, J.Luettin, and I.Matthews. Audio-visual automatic speech recognition: An overview. In G.Bailly, E.Vatikiotis-Bateson, and P.Perrier, editors, *Issues in Visual and Audio-Visual Speech Processing*. MIT Press, 2004.

[5] G.Potamianos and H.P.Graf. Discriminative training of hmm stream exponents for audio-visual speech recognition. In *Proc. IEEE International Conference on Acoustics, Speech and Signal Processing*, pages 3733–3736, Seattle,WA, 1998.

[6] G.Potamianos, J.Luettin, and C.Neti. Hierarchical discriminant features for audio-visual lvcsr. In *Proc. IEEE Internatioal Conference on Acoustics, Speech, Signal Processing*, pages 165–168, Salt Lake City, Utah, USA, 2001.

[7] J.Bulwer. *Philocopus, or the Deaf and Dumbe Mans Friend*. Humphrey and Moseley, 1648.

[8] J.Luettin and N.A.Thacker. Speechreading using probabilistic models. *Computer Vision and Image Understanding*, 65(2):163–178, 1997.

[9] J.Luettin1, N.A.Thacker, and S. Beet. Speaker identification by lipreading. In *Proc. IEEE International Conference on Spoken Language Processing*, pages 62–65, Philadelphia,USA, 1996.

[10] S.Dupont and J.Luettin. Audio-visual speech modeling for continuous speech recognition. *IEEE Transactions on Multimedia*, 2(3):141–151, 2000.

[11] S.L.Wang, W.H.Lau, A.W.C.Liew, and S.H.Leung. Automatic lipreading with limited training data. In *Proc. IEEE International Conference on Pattearn Recognition*, pages 881–884, 2006.

[12] S.Werda, W.Mahdi, and A.B.Hamadou. Colour and geometric based model for lip localisation: Application for lip-reading system. In *Proc. IEEE International Conference on Image Analysis and Processing*, pages 9–14, Modena, Italy, 2007.

[13] T.Chen and R.R.Rao. Audio-visual integration in multimodal communication. *Proceedings of the IEEE*, 86(5):837–851, 1998.

Image Analysis Based on the Local Features of 2D Intrinsic Mode Functions

Dan Zhang

Abstract

The Hilbert-Huang transform (HHT) is a novel signal processing method which can efficiently handle non-stationary and nonlinear signals. It firstly decomposes signals into a series of Intrinsic Mode Functions (IMFs) adaptively by the Empirical Mode Decomposition (EMD), then applies the Hilbert transform on the IMFs afterward. Based on the analytical signals obtained, the local analysis of the IMFs are conducted. This paper contains two main works. First, we proposed a new two-dimensional EMD (2DEMD) method, which is faster, better-performed than the current 2DEMD methods. Second, the Riesz transform are utilized on the 2DIMFs to get the 2D analytical signals. The local features (amplitude, phase orientation, phase angle, etc) are evaluated. The performances are demonstrated on both texture images and natural images.

1 Introduction

Texture [1] is ubiquitous and provides powerful characteristics for many image analysis applications such as segmentation, edge detection, and image retrieval. Among various texture analysis methods, signal processing methods are promising, which include Gabor filters [2], wavelet transforms [3], Wigner distributions and so forth. They characterize textures through filter responses directly.

Hilbert-Huang transform is a new signal processing method proposed by Huang et al [8, 10, 9]. It contains two kernel parts: Empirical Mode Decomposition (EMD) and Hilbert transform. First, it decomposes signals into a series of Intrinsic Mode Functions (IMFs) adaptively by the Empirical Mode Decomposition (EMD), then applies the Hilbert transform on the IMFs afterward. Based on the analytical signals obtained, the local analysis of the IMFs are conducted. Though Fourier spectral analysis and wavelet transform have provided some general methods for analyzing signals and data, they are still weak at non-stationary and nonlinear data processing. However, due to the fully data-driven process, the HHT is more efficient in this situation. It provides an efficient way for the local analysis.

As the kernel part of HHT, EMD works as a filter bank. It has a wide application in signal analysis including ocean waves, rogue water waves, sound analysis, earthquake time records as well as image analysis [19, 18, 16, 21, 20, 22, 23]. The EMD has been extended to 2DEMD. However, it countered a lot of difficulties such as inaccuracy of surface interpolation, high computational complexity and so forth [27, 29, 25, 26, 28, 31]. Finding a powerful 2DEMD is still a challenge. In this paper, we implemented a modified 2DEMD and study the local properties of the 2DIMFs by Riesz transform [4, 5]. The image after its Riesz transform, we can get the 2D analytical signal. The estimation of the local features is crucial in image processing. Generally, structures such as lines and edges can be distinguised by the local phase, the local amplitude can be used for edge detection.

This paper is organized as follows: Section 2 presents an introduction to HHT. In Section 3, the details of the modified 2DEMD are shown firstly, then we reviewed the Riesz transform. The simulation results are demonstrated in Section 4. Finally, the conclusions are given.

2 Hilbert-Huang transform

Hilbert-Huang transform was proposed by N.E.Huang in 1998. It contains two parts in terms of Empirical Mode Decomposition (EMD) and Hilbert transform. The signals are decomposed into a series of Intrinsic Mode Functions (IMFs), then Hilbert transform are applied on these IMFs to get analytic signals. Since this method is local, data-driven, it is capable of handling nonlinear and non-stationary signals.

EMD captures information about local trends in the signal by measuring oscillations, which can be quantized by a local high frequency or a local low frequency, corresponding to finest detail and coarsest content. Here we briefly review the sifting process of EMD. Four main steps are contained, S1, S2, S3 and S4 are abbreviation for Step 1 to Step 4. Given a signal x(t),

S1. Identify all the local minima and maxima of the input signals $x(t)$;

S2. Interpolate between all minima and maxima to yield two corresponding envelopes $E_{max}(t)$ and $E_{min}(t)$. Calculate the mean envelope $m(t) = (E_{max}(t) + E_{min}(t))/2$;

S3. Compute the residue $h(t) = x(t) - m(t)$. If it is less than the threshold predefined then it becomes the first IMF, go to Step 4. Otherwise, repeat Step 1 and Step 2 using the residue $h(t)$, until the latest residue meets the threshold and turns to be an IMF;

S4. Input the residue r(t) to the loop from Step 1 to Step 3 to get the next remained IMFs until it can not be decomposed further.

The analytical signal provides a way to compute the 1D signal's local amplitude and phase, which is obtained by the Hilbert transform on a real signal. The Hilbert transform $f_H(x)$ of a real 1D signal f is given by:

$$f_H(x) = f(x) * \frac{1}{\pi x},$$

where $*$ is convolution. $f_H(x)$ is the imaginary part of the signal. The analytical signal can be written as

$$f_A = f(x) + if_H(x) = a(t)e^{i\theta(t)},$$

in which, $a(t)$ is the amplitude, $\theta(t)$ is the phase.

Applying Hilbert transform on each IMF can evaluate the local properties such as amplitude and phase.

3 Local Analysis of 2DIMFs

3.1 The improved 2DEMD

Here we propose an alternative algorithm for EMD. Instead of using the envelopes generated by splines we use a low pass filter to generate a "moving average" to replace the mean of the envelopes. The essence of the sifting algorithm remains.

The moving average is the most common filter in digital signal processing. It operates by averaging a number of points from the input signal to produce each point in the output signal, it is written:

$$y[i] = \frac{1}{M} \sum_{j=0}^{M-1} x[i+j],$$

where $x[]$ is the input signal, $y[]$ is the output signal, and M is the number of points used in the moving average. It is actually a convolution using a simple filter $[a_i]_{i=1}^{M}, a_i = \frac{1}{M}$, and $[A_{i,j}]_{i=1,j=1}^{M,N}, A_{i,j} = \frac{1}{M \times N}$ for the 2-dimensional case.

Detection of local extrema means finding the local maxima and minima points from the given data. No matter for 1D signal or 2D array, neighboring window method is employed to find local maxima and local minima points. The data point/pixel is considered as a local maximum (minimum) if its value is strictly higher (lower) than all of its neighbors.

We illustrated 1-dimensional case and 2-dimensional case separately.

- 1-dimensional case:
  For each extrema map, the distance between the two neighborhood local maxima (minima, extrema, zero-crossing) has been calculated called as adjacent maxima (minima, extrema, zero-crossing) distance vector Adj_max ($Adj\_min, Adj\_ext, Adj\_zer$). Four types of window size:
  - Window-size I: $\max(Adj\_max)$;
  - Window-size II: $\max(Adj\_min)$;
  - Window-size III: $\max(Adj\_zer)$;
  - Window-size IV: $\max(Adj\_ext)$.
- 2-dimensional case:
  The window size for average filters is determined based on the maxima and minima maps obtained from a source image. For each local maximum (minimum) point, the Euclidean distance to the nearest local maximum (minimum) point is calculated, denoted as adjacent maxima (minimum) distance array Adj_max (Adj_min).
  - Window-size I: $\max(Adj\_max)$;
  - Window-size II: $\max(Adj\_min)$;

3.2 Monogenic signal

The analytic signal is the basis for all kinds of approaches which makes use of the local phase. The combination of a 1D signal and its Hilbert transform is called the analytic signal. Similarly, the combination of a image and its Riesz transform, which is the generalization of Hilbert transform, is called the monogenic signal [4, 5].

The monogenic signal is often identified as a local quantitative or qualitative measure of an image. Different approaches to an nD analytic or complex signal have been proposed in the past:

- Total Hilbert Transform, The Hilbert transform is performed with respect to both axes:

  $$H_T(\overrightarrow{v}) = jsign(v_1)sign(v_2)$$

  This transform is not a valid generalization of the Hilbert transform since it does not perform a phase shift of $\pi/2$.It can't meet orthogonality.

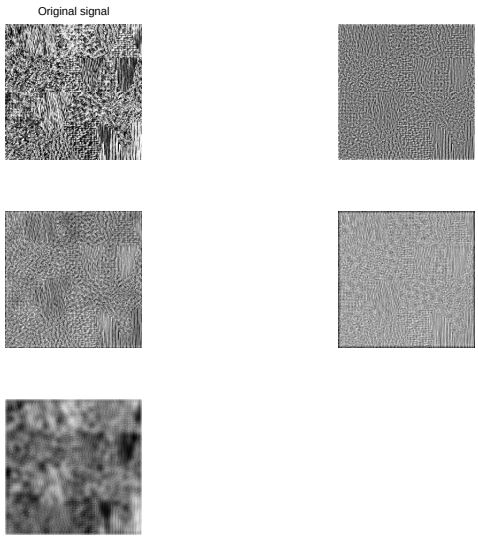

Figure 1. The 2DIMFs obtained by the improved 2DEMD.

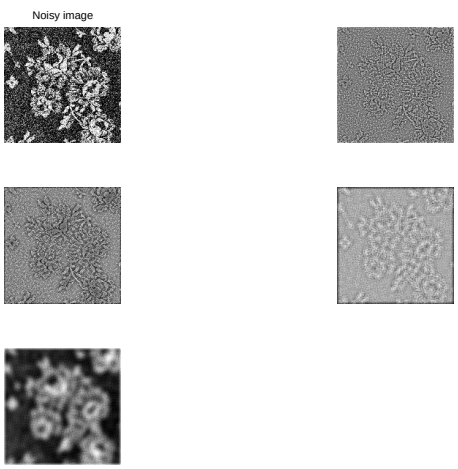

Figure 2. The 2DIMFs obtained by the improved 2DEMD on the noisy image.

- Partial Hilbert Transform, The Hilbert transform is performed with respect to a half-space that is chosen by introducing a preference direction:

$$H_T(\overrightarrow{v}) = jsign(\overrightarrow{v}, \overrightarrow{d}),$$

where $\overrightarrow{v} = (v_1, v_2)$ is one 2D vector, $\overrightarrow{d}$ is one preference direction. This transform missed the isotropy.

- Total Complex Signal,
- Hypercomplex Signal.

The Riesz transform [4, 5] is a multidimensional generalization of the Hilbert transform. The expression of Riesz transformed signal in the frequency domain:

$$F_R(\overrightarrow{v}) = \frac{i\overrightarrow{v}}{\overrightarrow{v}} F(\overrightarrow{v}) = H_2(\overrightarrow{v})F(\overrightarrow{v}),$$

where the transfer function H_2 of the Riesz transform is the generalization of the Hilbert transform, the corresponding space representation of Riesz transform is:

$$f_R(\overrightarrow{x}) = -\frac{\overrightarrow{x}}{2\pi|\overrightarrow{x}|^3} * f(\overrightarrow{x}) = h_2(\overrightarrow{x}) * f(\overrightarrow{x}).$$

The Riesz transformed signal and the original signal constitutes the 2D analytical signal, this is the monogenic signal.

$$f_M(\overrightarrow{x}) = f(\overrightarrow{x}) - (i, j)f_R(\overrightarrow{x}).$$

From this formulation, we see the 2D analytical signal is 3D vector and we can get the local features of the monogenic signal.

- Phase: Phase as we all know the polar representation of the complex $z = x + iy$ is $(r, \varphi) = (\sqrt{z\overline{z}}, \arg(z))$. Where $\overline{z}$ is the conjugate of z, $\arg(z)$ is the phase of the complex: $\arg(z) = a\tan 2(y, x) = sign(y)a\tan(|y|/x)$, $sign(y)$ represents the direction of rotation. The phase of the 2D analytical signal is:

$$a\tan 3(y, x) = \frac{\overrightarrow{x}_D}{|\overrightarrow{x}_D|} a\tan(\frac{|\overrightarrow{x}_D|}{< (0, 0, 1)^T, \overrightarrow{x} >}),$$

where $\overrightarrow{x}_D = (0, 0, 1)^T \times \overrightarrow{x}$ yields the direction of the rotation vector. The phase of the monogenic signal is:

$$\varphi(\overrightarrow{x}) = a\tan 3(f_M(\overrightarrow{x})) = \arg(f_M(\overrightarrow{x})).$$

- Amplitude: The local amplitude of $f_M(\overrightarrow{x})$ is:

$$|f_M(\overrightarrow{x})| = \sqrt{f_M(\overrightarrow{x})\overline{f_M(\overrightarrow{x})}} = \sqrt{f^2(\overrightarrow{x}) + |f_R(\overrightarrow{x})|^2},$$

given the local phase $\varphi(\overrightarrow{x})$ and the local amplitude $|f_M(\overrightarrow{x}|$ of a monogenic signal, it can be reconstructed by

$$f_M(\overrightarrow{x} = |f_M(\overrightarrow{x}|\exp((-j, i, 0)\varphi(x)).$$

2DEMD permits extracting multiscale components. The monogenic signal of each IMF permits to compute local amplitude, local phase and the local direction. We have shown this feature through experiment results for both natural textures and synthetic textures.

4 Experimental Results

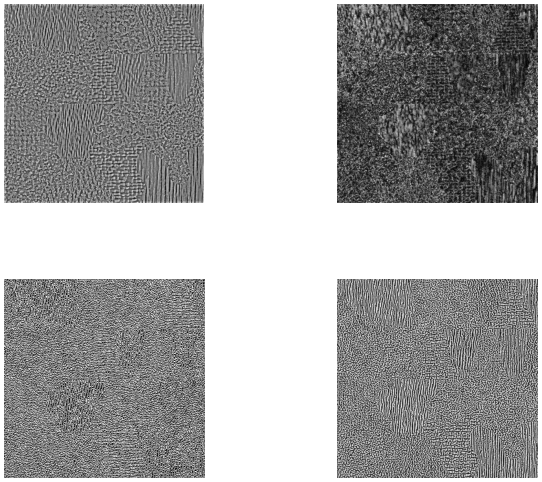

Figure 3. left-up: 1st IMF, right-up: amplitude, left-down: phase orientation, right-down: phase angle.

In all our numerical experiments we determine the window size in each decomposition with Window-size I. Unless otherwise specified we use $\alpha = 0.5$ for our stopping criterion.

We show the local features amplitude, phase orientation, phase angle extracted by SMV of the 1st IMF.

By having access to these representations of scenes or objects, we can concentrate on only one or several modes (one individual or several spatial frequency components) rather than the image entirety. The improved 2DEMD and Riesz local analysis offer a new and more promising way to analyze texture images.

5 Conclusions

This paper contains two main works. First, we proposed a new two-dimensional EMD (2DEMD) method, which is faster, better-performed than the current 2DEMD methods. Second, the Riesz transform are utilized on the 2DIMFs to

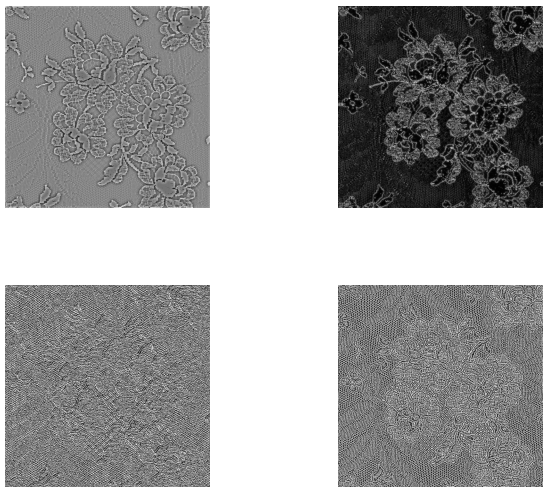

Figure 4. left-up: 1st IMF, right-up: amplitude, left-down: phase orientation, right-down: phase angle.

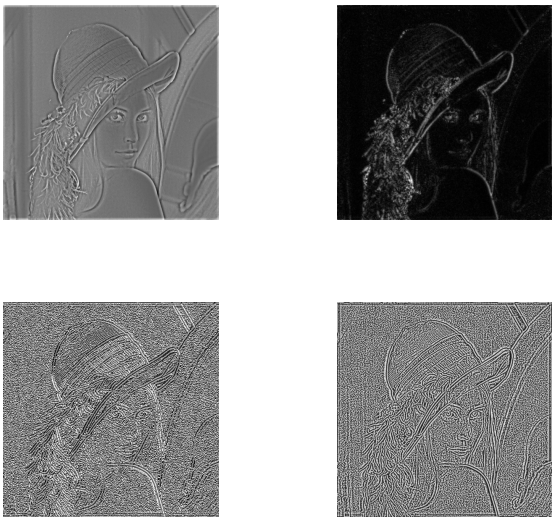

Figure 5. left-up: 1st IMF, right-up: amplitude, left-down: phase orientation, right-down: phase angle.

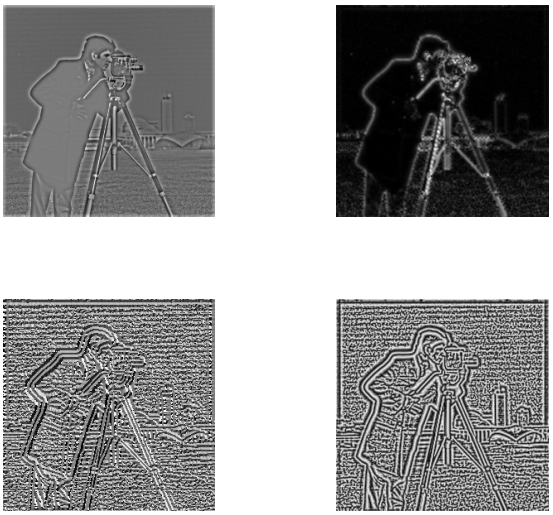

Figure 6. left-up: 1st IMF, right-up: amplitude, left-down: phase orientation, right-down: phase angle.

get the 2D analytical signals. The local features (amplitude, phase orientation, phase angle, etc) are evaluated. The performances are demonstrated on both texture images and natural images.

References

[1] Materka A and Strzelecki M, Texture analysis method: a review. *COST B11 report, Technical University of Lodz.*

[2] A. K. Jain and Farrokhnia F, Unsupervised texture segementation using Gabor filters. *Pattern Recognition, 24 (12), pp. 1167-1186, 1991.*

[3] Mallat S, Wavelets for a vision. *Proceedings of the IEEE, Vol. 84, Iss. 4, pp. 604-614, 1996.*

[4] Felsberg M and Sommer. G. The monogenic signal. *IEEE Trans Signal Process 49, 2001.*

[5] Felsberg M and Sommer. G. The Monogenic Scale-Space: A Unifying Approach to Phase-Based Image Processing in Scale-Space. *2004.*

[6] Felsberg M and Sommer. G. Structure multivector for local analysis of images. *Workshop on theoretical foundations of computer vision, SpringerVerlag, pp 93-104, 2001.*

[7] Felsberg M and Sommer. G. Low Level Image Processing with the Structure Multivector. *2002.*

[8] N. E. Huang, Z. Shen, S. R. Long, et al.. The empirical mode decomposition and the Hilbert spectrum for nonlinear and non-stationary time series analysis. *Proceedings of the Royal Society A, vol. 454, no. 1971, pp. 903C995, 1998.*

[9] HILBERT-HUANG TRANSFORM AND ITS APPLICATIONS. *Book in Interdisciplinary Mathematical Sciences, Vol. 5, edited by N. E. Huang, and Samuel S P Shen, 2005.*

[10] N. E. Huang, M. L. C. Wu, S. R. Long, et al.. A confidence limit for the empirical mode decomposition and Hilbert spectral analysis. *Proceedings of the Royal Society A, vol. 459, no. 2037, pp. 2317C2345, 2003.*

[11] S. R. Long. Applications of HHT in image analysis. in Hilbert-Huang Transform and Its Applications, N. E. Huang and S. S. P. Shen, Eds., World Scientific, River Edge, NJ, USA, 2005.

[12] Harishwaran Hariharan, Andrei Gribok, Besma Abidi, and Mongi Abidi. Multi-modal Face Image Fusion using Empirical Mode Decomposition. *The Biometrics Consortium Conference, Crystal City, VA, September 2005.*

[13] H. Hariharan, A. Koschan, B. Abidi, A. Gribok, and M.A. Abidi. Fusion of visible and infrared images using empirical mode decomposition to improve face recognition. *IEEE International Conference on Image Processing ICIP2006, Atlanta, GA, pp. 2049-2052, October 2006.*

[14] Bhagavatula, R., Marios Savvides, and M. Acoustics. Analyzing Facial Images using Empirical Mode Decomposition for Illumination Artifact Removal and Improved Face Recognition. *IEEE International Conference on Speech and Signal Processing, 2007 (ICASSP 2007). Vol. 1, Issue , 15-20 April 2007 pp. I 505-508.*

[15] J. C. Nunes, Y. Bouaoune, E. Delechelle, O. Niang, and Ph. Bunel. Image analysis by bidimensional empirical mode decomposition. *Image and Vision Computing Volume 21, Issue 12, Pages 1019-1026, November 2003.*

[16] Nunes J. C., Guyot S., and Deléchelle E. Texture analysis based on local analysis of the Bidimensional Empirical Mode Decomposition. In *Machine Vision and Applications 16, 3, pp. 0932-8092, 2005.*

[17] A. Linderhed. 2-D empirical mode decompositions in the spirit of image compression. *in Wavelet and Independent Component Analysis Applications IX, vol. 4738 of Proceedings of SPIE, pp. 1C8, Orlando, Fla, USA, April 2002.*

[18] A. Linderhed. Compression by image empirical mode decomposition. *IEEE International Conference on Image Processing, 2005 (ICIP 2005), Vol. 1, pp. I 553-6, 2005.*

[19] H. Hariharan, A. Gribok, M. Abidi, and A. Koschan. Image Fusion and Enhancement via Empirical Mode Decomposition. *Journal of Pattern Recognition Research, Vol. 1, No. 1, pp. 16-32, January 2006.*

[20] Sinclair, S. and Pegram, G. G. S. Empirical Mode Decomposition in 2-D space and time: a tool for space-time rainfall analysis and nowcasting. *Hydrol. Earth Syst. Sci. Discuss., 2, 289-318, 2005.*

[21] Jian Wan, Longtao Ren, and Chunhui Zhao. Image Feature Extraction Based on the Two-Dimensional Empirical Mode Decomposition. *2008 Congress on Image and Signal Processing, Vol. 1, pp. 627-631, 2008.*

[22] Jalil Taghia, Mohammad Ali Doostari and Jalal Taghia. An Image Watermarking Method Based on Bidimensional Empirical Mode Decomposition. *2008 Congress on Image and Signal Processing, Vol. 5, pp. 674-678, 2008.*

[23] Fauchereau, N., Sinclair, S., and Pegram, G. 2-D Empirical Mode Decomposition on the sphere, application to the spatial scales of surface temperature variations. *Hydrol. Earth Syst. Sci. Discuss., 5, 405-435, 2008.*

[24] C. Damerval, S. Meignen, and V. Perrier. A fast algorithm for bidimensional EMD. *IEEE Signal Processing Letters, vol. 12, no. 10, pp. 701C704, 2005.*

[25] Sharif M. A. Bhuiyan, Reza R. Adhami, and Jesmin F. Khan. Fast and Adaptive Bidimensional Empirical Mode Decomposition Using Order-Statistics Filter Based Envelope Estimation. *EURASIP Journal on Advances in Signal Processing, vol. 2008, Article ID 728356, 18 pages, 2008.*

[26] Sharif M. A. Bhuiyan, Reza R. Adhami, and Jesmin F. Khan. A novel approach of fast and adaptive bidimensional empirical mode decomposition. *IEEE International Conference on Acoustics, Speech and Signal Processing, 2008 (ICASSP 2008), pp. 1313-1316, 2008.*

[27] Sherman Riemenschneider, Bao Liu, Yuesheng Xu and Norden E. Huang. B-spline based empirical mode decomposition. *Hilbert-Huang Transform and Its Applications, Book chapter 2, 2005.*

[28] Louis Yu Lu. Fast intrinsic mode decomposition of time series data with sawtooth transform. *Technical report, Nov 2007.*

[29] Yong-Ping Huang, Xue-Yao Li and Ru-Bo Zhang. A research on local mean in empirical mode decomposition. *Proceedings of the 7th international conference on Computational Science, Part III: ICCS 2007, Lecture Notes In Computer Science, Vol. 4489, pp. 125-128.*

[30] Luan Lin, Yang Wang, and Haomin Zhou. A new approach to empirical mode decomposition. *Preprint.*

[31] Lixin Shen. Local mean and empirical mode decomposition. *Report on The Second International Conference on the Advances of Hilbert-Huang Transform and Its Applications, Guangzhou, Dec 2008. Preprint.*

Discriminability and Reliability Indexes: Two New Measures to Enhance Multi-image Face Recognition

Weiwen Zou

Abstract

In order to handle complex face image variations in face recognition, multi-image face recognition has been proposed, instead of using a single still-image-based approach. In many practical scenarios, multiple images can be easily obtained in enrollment and query stages, for example, using video. By accessing these images, a good "quality" image(s) will be used for recognition using conventional still-image-based recognition algorithms so that the recognition performance can be improved. However, existing methods do not fully utilize all images information. In this paper, two new measurements, namely discriminability index (DI) and reliability index (RI), are proposed to evaluate the enrolled and query images respectively. By considering the distribution of enrolled images from individuals, the discriminability index of each image is calculated and a weight is assigned. For testing images, a reliability index is calculated based on matching quality between the testing image and enrolled images. If the reliability index of a testing image is small, the testing image will be discarded as it may degrade the recognition performance. To evaluate and demonstrate the use of DI and RI, we adopt the recognition algorithm using combining classifiers with eigenface representations in input and kernel spaces. CMU-PIE , YaleB and FRGC databases are used for experiments. Experimental results show that the recognition performance, with three popular combination rules, can be increased by more than 10% on average with the use of DI and RI.

1 Introduction and Related Works

Research on face recognition has been performed for more than three decades and a number of encouraging results have been reported [18, 23]. However, some hard problems, such as outdoor illumination, still remain unsolved [12, 20, 23].

To overcome the remaining problems, a natural move is to change from single-frame image-based face recognition to multi-image-based recognition [3, 4, 5, 10, 21] as multiples frames in both enrollment and query phases provide additional information and can be easily obtained, for example, using video. In turn, multi-image face recognition has been proposed for solving the image variations problem. The common practice in multi-image recognition is to select a good visual quality frontal-view face image for recognition. While experimental results show that the recognition performance can be improved [16], non-frontal view good quality images, which can also be used to enhance the recognition performance, are discarded. That means, the available useful information are not fully utilized. To make use of multiple information, multi-image-based recognition methods were proposed.

Kruger *et al.* [15] proposed a new method to select frames from video. By applying an online-clustering algorithm on video, exemplar (representative frame) from each cluster is used to represent the cluster and used it as reference image in recognition system. Based on the cluster size, a weight (importance) is assigned to each representative frame. Hadid *et al.* [10] selected the representative images from video for recognition. They minimized distance between original images and the images to be selected as representative images, so that the most representative images are selected for recognition. However, representative images/exemplars do not guarantee they have high discriminability power.

Zhang *et al.* [22] assigned weights to testing images by evaluating similarity between the testing images and reference images based on the pose and facial expression. Thomas *et al.*[21] used a measurement called *Faceness* to assess the quality of the images. Based on Faceness, the images were selected in several selecting strategies, including N highest Faceness (NHF) and N evenly spaced from M highest faceness (NEHF). Experimental results showed that using the N highest faceness images did not get the best performance. Instead, using multi-images with ensuring face-

This paper has been submitted to *Pattern Recognition*, Jun 2009

ness diversity got the best result. Therefore, evaluating and selecting enrolled and testing images is an important task for multiple images face recognition system.

To overcome the existing problems in evaluating the enrolled and testing images, two new measurements are proposed in this paper. First, a discriminability index (DI) is proposed to measure the discriminative power of enrolled images in each individual. Second, a reliability index (RI) is proposed to measure the matching quality which reflects how good a face image can be used for face recognition. It is important to point out that both DI and RI are generic and can be integrated into most of the existing image-based algorithms.

The rest of this paper is organized as follows. Section 2 reports the proposed method in calculating the discriminability index for enrolled image and reliability index for testing image. Experimental evaluation on the two proposed indexes are given in Section 3. Finally, Section 4 gives the conclusions.

2 Proposed method

Consider the case that there are multiple images in probe ($\mathcal{P}$) and multiple images in gallery ($\mathcal{G}$). This paper proposes two new image measurements to evaluate how good the images are. A weight is then assigned to each image in probe and gallery set. The weight for both reference and testing images can be taken into account in the recognition process. It is important to note that there may have different ways to make use of DI and RI. In the experimental result section, we will demonstrate one of the ways of using DI and RI to improve the performance of multi-image face recognition system.

For multiple images in gallery set, discriminability index (DI) is developed to measure how discriminative an reference image is. A high discriminative (i.e. high DI) reference image means that such image is relatively far away from the classes boundary and has a relatively high tolerance to the intra-class variations. Then, a larger weight will be assigned to those reference images with high DI. Similarly, if a reference image is very close to the images in other classes, it will be easily affected by the intra-class variations. In turn, a smaller weight will be assigned.

For multiple images in probe set (testing set), reliability index (RI) is developed to measure how reliable the image is. A testing image with higher RI means that we have a higher confidence to treat the result is correct. Unlike existing schemes [15, 10, 21] selecting the representative images based on the face appearance, our proposed method calculates the RI by considering the matching quality of the image. This paper considers the distances between the testing image and the images in each class, as well as the distributions of the reference images in each class. The basic idea

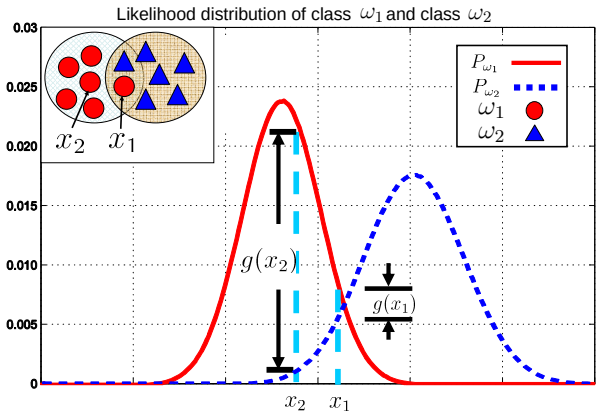

Figure 2. The distribution of ω_1 and ω_2. x_1 and x_2 are two reference image in ω_1.

of DI and RI is shown in Figure 1. Details in calculating DI and RI are given as follows.

Some useful notations are used in this paper: $\mathcal{P}$ represents the probe set while $\mathcal{G}$ represents the gallery set (reference images), $\mathcal{T}$ represents the training set; the small letters x, y, z represent still images; ω_i represents i-th class of the database.

2.1 Discriminability index (DI)

Discriminability index (DI) measures how much discriminative power of a reference image has. Since there is no generic definition of discriminative power of an image, this paper defines the discriminative power as the ability of an image distinguishing from images from other classes. Therefore, an image which is far away from the classes' boundary will have a high discriminative power. This discriminative power depends on two factors, namely the margin between a reference image and images from other classes, and the tolerance to intra-class variants which are caused by pose, illuminance, expression etc.

To clearly present and illustrate our idea on DI, we consider a two-class problem. As shown in Figure 2, x_1 and x_2 are two reference images which belong to the same class, ω_1. The distributions of ω_1 and ω_2 are overlapped. In practice, the classes distribution is always overlapped with each other due to intra-class variations, such as pose, illuminance, expression, occlusion. So the reference images will have different discriminative powers. Consider the probability likelihood $P(x_1|\omega_1)$, $P(x_1|\omega_2)$, $P(x_2|\omega_1)$ and $P(x_2|\omega_2)$, according to the discriminant function [7]

$$g(x) = P(x|\omega_1) - P(x|\omega_2) \quad (1)$$

we get $g(x_2) > g(x_1)$. This implies that x_2 is better than x_1

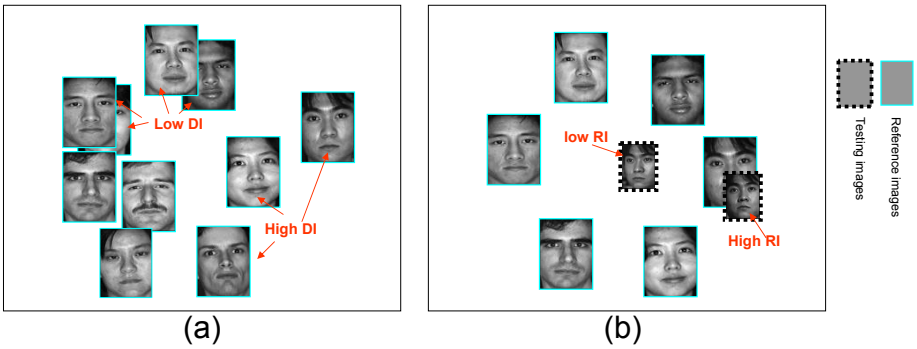

Figure 1. Demonstrating the idea of DI and RI. (a) Ten images from difference classes. Some of them overlap with others (low DI) while some are far away from others (high DI). (b) Two testing images matching with the reference images, one only has a short distance to the reference images (high RI) while another has similar distances to each class (low RI).

as a reference image. The reason is that if a testing image is close to x_2, it has a large gap (far away) from ω_2. That means we have high confidence to classify it to ω_1 but not ω_2. In turn, x_2 has a higher discriminative power. On the other hand, if a testing image is close to x_1, a noisy image of ω_2 may also be very close to x_1 due to relatively small $g(x_2)$. This leads the testing image be misclassified from ω_2 to ω_1. We have low confidence to classify x_1. x_1 has a relatively low discriminative power. Therefore, it is necessary to evaluate the discriminative power (discriminability index) of the enrolled is necessary.

A straightforward method to calculated the discriminability index (DI) is to calculate the involved likelihood probability. However, it is well-known that the likelihood distribution of the face images is not easy to model due to the high dimension of data and relatively small amount of training samples. Inspired by the success of calculating the probability from similarity [2], we estimate likelihood probability for DI calculation based on the similarity. According to Parzen window method, the probability can be estimated by:

$$P(x|\omega) = \frac{1}{n}\sum_{j=1}^{n}(\varphi_\omega(x, y_i)) \tag{2}$$

where y_i is the i-th neighbor of x in ω. Define the similarity between two images as

$$sim(x, y) = \frac{C_1 - \|x - y\|}{C_1} \tag{3}$$

where C_1 is a constant to normalize the similarity ranging from 0 to 1. Replace φ with Eq.(3), we have

$$P(x|\omega) = \frac{1}{nC_2}\sum_{j=1}^{n}(sim(x, y_i)). \tag{4}$$

where C_2 is a normalization constant. So DI can be defined as

$$\begin{aligned}
\mathrm{DI}_x &= g(x) \\
&= P(x|x \in \omega) - \max_k P(x|\omega_k) \\
&= \frac{1}{nC_2}\min_k\Big(\sum_{i=1}^{n}\Big(\frac{C_1 - \|x - y_i\|}{C_1}\Big)\Big) - \sum_{j=1}^{n}\Big(\frac{C_1 - \|x - y_j^k\|}{C_1}\Big)\Big)\Big) \\
&= C\min_k\sum_{i=1}^{n}(\|x - y_i^k\| - \|x - y_i\|)
\end{aligned} \tag{5}$$

where ω_k is the class which does not contain x_i, and $y_j^k \in \omega_k$ while $x, y_i \in \omega$, and $C = \frac{1}{nC_1C_2}$.

To alleviate influence of noise, Eq.(5) is performed several times with random selection of reference images of each class in the training set, and the average of DI will be considered as the final DI. Details of DI calculation is shown in Algorithm 1.

2.2 Reliability index (RI)

It is well-known that, in most of the cases, class distributions are overlapped. If testing images are in the overlapping area, they are not suitable for the using in recognition system. A straightforward solution for this problem is to check whether the testing image is suitable before using it for recognition. To evaluate how suitable the testing image is for recognition, matching quality is considered in this paper.

Matching quality reflects the relationship between the testing image and the reference images. High matching quality implies that such testing has a short distance to its

Algorithm 1 DI Calculation

Input: Reference images $\mathcal{G} = \{x_{ij}\}$, threshold for termination th, number of neighbors n, number of images to be selected N

Output: DI of each image in $\mathcal{G}$

Initial: $\mathrm{DI}_{ij} \leftarrow 0, \mathrm{DI}'_{ij} \leftarrow 0, \mathrm{DI}^*_{ij} \leftarrow \phi$;

repeat

$\mathrm{DI}'_{ij} \leftarrow \mathrm{DI}_{ij}$

for each x_{ij} **do**

randomly select N reference images from each class, denote as ω'_k

search the n-nearest neighbors in each ω'_k, denote as $\mathcal{N}^k_{x_{ij}}$

$\mathrm{DI}_{ij} \leftarrow \mathrm{DI}^*_{ij} \bigcup \{\frac{1}{n} \min_k \sum_{j=1}^{n} (\|x_{ij} - y^i_j\| - \|x_{ij} - y^k_j\|)\}$

end for

$\mathrm{DI}_{ij} \leftarrow avg(\mathrm{DI}^*_{ij})$

until $|\mathrm{DI}'_{ij} - \mathrm{DI}_{ij}| < th$

Output DI_{ij}

own class and has relatively long distances to other classes. Figure 3 (a) shows two testing images p_1 and p_2 which have different matching quality from the same class. The distance between p_1 and ω_1 is small, while the distances between p_2 and ω_1 , ω_2 and ω_3 are similar. For p_2, it locates in the overlapping area and its location causes ambiguity for classification, because a noisy image from other class (suppose ω_2) may locate at the same position of p_2. It should not be used for recognition. So p_1 has a higher matching quality than that of p_2, therefore it is more suitable for recognition. In this paper, reliability index (RI) is developed to evaluate the matching quality of testing images.

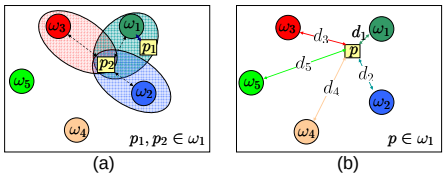

Figure 3. Matching quality and outlier. (a): Testing image p_1 has high matching quality while p_2 has low matching quality; (b)two kind of distances:$d_1 \in D_w$ and $d_2, d_3, d_4, d_5 \in D_b$. p has high matching quality if and only if d_1 is the only statistics outlier of D_b.

Based on the analysis above, the image with high matching quality has high discriminability which we develop in the Section 2.1. Since the class information of the testing images is not available, measuring matching quality by discriminability index is not suitable. Instead we use another cue which can access the image matching quality.

Considering the distances between the testing image (p) and the reference images ($\{x_{kj}\}_{k=1}^{C}$), define d_k, D_w, D_b as follows:

$$\begin{aligned} d_k &= \arg\min_j \|p - x_{kj}\| \\ D_w &= \{d | d = x' - x''\} \\ D_b &= \{d | d = y' - y''\} \end{aligned} \tag{6}$$

where x' and x'' are images from the same class, while y' and y'' are images from different classes respectively. Suppose testing image p is from ω_{k_0}. When matching a testing image p to the reference images $\{x_{kj}\}_{k=1}^{C}$, there are two kinds of distances, namely d_{k_0} and $d_k, k \neq k_0$. It is easy to shown that

$$d_{k_0} \in D_w \text{ and } d_k \in D_b (k \neq k_0) \tag{7}$$

If p have high matching quality, d_{k_0} is obviously less than other distances ($d_k, k \neq k_0$). Specifically, d_{k_0} should be the only one distance which is less than others significantly, if p has a high matching quality. As shown in Figure 3(b), $p \in \omega_1$ has high matching quality and d_1 is much smaller than that of d_2 to d_5. So the testing image with high matching quality leads d_{k_0} deviating from D_b. That means d_{k_0} is a statistics outlier [1] of D_b. Here, following the definition of Grubbs [9], a sample is called statistics outlier of a given set of samples, if and only if it appears to deviate markedly from other samples. Therefore, evaluating the matching quality of a testing image is equivalent to evaluating the probability that the corresponding d_{k_0} is the only statistics outlier of D_b.

However, as mentioned before, the class information of testing image p is not available. That means d_{k_0} cannot be determined when p is given. Instead, we propose to make use of d_{min} as a substitute for d_{k_0}, where $d_{min} = \min_k(d_k)$. If p has a high matching quality, d_{min} is equal to d_{k_0}, so d_{min} is the only outlier and replacing d_{k_0} with d_{min} is suitable. In contrary, if p has a low matching quality, there are two scenarios:

1) d_{min} is equal to d_{k_0},

2) d_{min} is less than d_{k_0}.

For 1), d_{min} is not the only statistics outlier of D_b, because p has similar distances to images from ω_{k_0} as well as other classes. For 2), d_{min} definitely is not an outlier of D_b, because d_{min} belongs to D_b. In both scenarios, d_{min} is not the only outlier of D_b. Therefore, p has a high matching quality (high reliability) if and only if d_{min} is the only significant outlier of D_b.

To evaluate whether d_{min} is the only statistics outlier, Q-test [6] is adopted. Though a number of algorithms have been proposed to detect outliers from a set of data [1, 11]

, Q-test is simpler and more suitable. That is because Q-test can handle scenario with only one outlier existing more effectively, while other existing methods, such as Grubb test [9] and t-test [13], consider the extrema as well as other samples as the candidate outliers. Moreover, Q-test is easy to implement and computationally efficient, as it dose not require calculation of the mean and standard deviation in advance.

In this paper, RI of p is defined as the Q-value [6] of the extreme (d_{min}) in Q-test, as follows:

$$\begin{aligned} \text{RI} &= \text{Q-value}(d_{min}) \\ &= \frac{\text{Gap}}{\text{Range}} \\ &= \frac{d_{min} - \min_k(\{d_k\} \setminus d_{min})}{\min\{d_k\} - \max\{d_k\}} \end{aligned} \tag{8}$$

Detailed calculation of RI is shown in Algorithm 2.

Algorithm 2 RI Calculation

Input: Reference images $\{x_{kj}\}_{k=1}^{C}$, testing image y_i
Output: RI_i

```
for each class k do
    d_k ← ||y_i − x_kj||
end for
Calculate the Q-value Q ← by Eq.[8]
output RI_i = Q-value
```

3 Experimental Results

This section demonstrates and evaluates the use of DI and/or RI with three public domain face databases. The results are presented into four parts. First, evaluation methodology of the comparative experiments are shown. Second, the use of DI and RI is reported. Third, three databases used in the experiments and the corresponding settings are discussed. Finally the experimental results are given. The results show that the proposed DI/RI can help the recognition system improving the performance.

3.1 Evaluation methodology

To evaluate the effectiveness of DI and RI, comparative experiments are performed based on the existing face recognition system integrating with and without DI and/or RI. As shown in Figure 4, the system consists of two independent modules, namely assessment module and recognition module.

In the assessment module, training images ($\{x_{kj}\}_{k=1}^{C}$) are assessed with proposed DI by Algorithm 1, while testing images ($\{p_i\}_{i=1}^{N_p}$) are assessed with RI by Algorithm 2. After these two assessments, DI of reference images and RI of testing images are obtain and then integrated with the existing face recognition in the way as mentioned in Section 3.2.

In the recognition module, two popular existing face recognition engines (namely Eigenface, and Kernel PCA) with combining classifiers are used to construct the recognition module. The face recognition engines match p_i to the reference images ($\{x_{kj}\}$), and output the similarity s_{ik} which is calculated by Eq.(9):

$$s_{ik} = \max_j (S(p_i, x_{kj})) \tag{9}$$

where $S(p_i, x_{kj})$ is the similarity calculated by the face recognition engine. Combining classifiers is used to draw the final result with multiple testing images. In this paper, three typical combining classifiers [14] are used, namely sum rule (SUM), product rule (PROD) and majority voting (MV). We do not make use of max/min rule, because max/min rule actually combine the results based on one maximal/minimal data rather than making use of all data.

3.2 Usage of DI and/or RI

This paper suggests one way to make use of DI and/or RI for face recognition. It is important to mention that there may have other better way to adopt DI/RI.

Based on determined DI/RI of each image, weights are assigned to reference images and testing images. For DI, a reference image x_{kj} is assigned with a weight which is defined as:

$$w_{kj} = (\frac{1 + \text{DI}_{kj}}{2}) \tag{10}$$

So w_{kj} is normalized to [0 1]. For RI, the testing images with low RI are discarded by assigning a weight of 0, while the ones with high RI are kept by assigning a weight of 1:

$$w_i' = \begin{cases} 1 & \text{if } \text{RI}_i > th, \\ 0 & \text{othervise.} \end{cases} \tag{11}$$

where th is a threshold determined by the Quotient Critical Value [6] of Q-test. In our experiments, we accept the testing images with 90% confidence level as an outlier.

3.3 Databases and experiment settings

Three public domain face databases, namely CMU-PIE [19], YaleB [8] and FRGC [17], are selected for experiments in this paper.

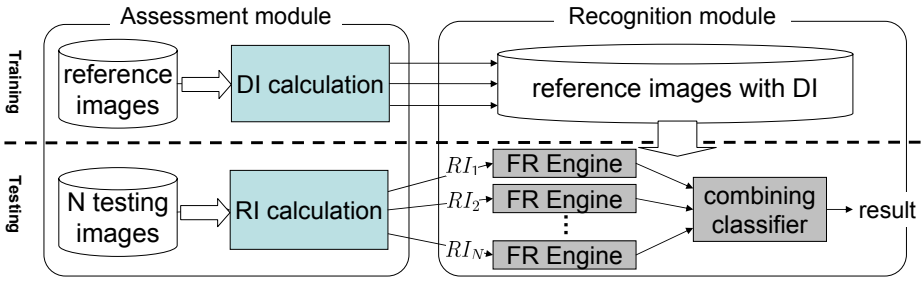

Figure 4. The block diagram of recognition system integrating with DI and RI .

CMU-PIE consists of 68 persons and each persons has 105 images(5 poses times 21 illumination); YaleB database consists of 38 persons with 64 different lighting conditions (totally 38 times 64 images); FRGC database consists of more than 300 persons with number of images ranging from 6 to 220. For FRGC database, we consider the person who has more than 50 images. For each person, 50 images with illumination, expression and wild pose variations are selected. After this selection, there are 311 classes by 50 images per class used in experiments.

By random selection, databases are divide into two separated sets (testing set and training set) in advance. The detailed setting of the experiments is shown in Table 1, where C is the number of individuals in the database, N_t is the number of training images per individual. Not all the images in training set will be used as reference images. N_r images in training set is randomly selected as reference images, and N_p images in testing set are randomly selected as probe.

All of the face images are extracted and aligned manually. Some images from three databases are shown in Figure 5.

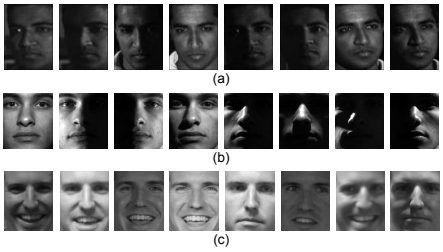

Figure 5. Sample images: (a) CMU-PIE ;(b) YaleB ; (c) FRGC .

3.4 Results and analysis

The results of three databases with different face recognition engines and difference combining classifiers are reported.

For CMU-PIE database, Eigenface representation is used in the recognition module and sum rule combining classifier is used to draw the final result. As shown in Figure 7(a), the results without using RI nor DI are used as benchmark. After using DI, the accuracy is improved from 68.4% to 76.9% (with $N_p = 15$) and from 74.1% to 84.5% (with $N_p = 55$); after using RI, the accuracy is improved to 73.3% (with $N_p = 15$) and 89.2% (with $N_p = 55$); after using both DI and RI, the system achieves the best result, and the accuracy improved to 73.5% (with $N_p = 15$) and 92.1% (with $N_p = 55$). The improvement ranges from 4.9% to 18.0%. Moreover, without DI nor RI, the improvement caused by increasing N_p is 5.7%, while it is 15.9% with both DI and RI. It can be seen from the results that integrating with DI and RI helps to improve the recognition system performance.

The robustness of the recognition system is evaluated by the standard deviation (StdDev) of the accuracy. The standard deviation of accuracy of CMU-PIE database on eigenface recognition engine with sum rule combining classifier is shown in Figure 6. The StdDev of methods using DI and/or RI is less than the one without DI nor RI. This implies that robustness of the recognition system is also improved by making use of DI and RI.

The additional computational time introduced by assessment module is estimated. For the case of CMU-PIE database with Eigenface engine and sum rule, it took 21.0 mins to calculate the DI of training images. That is, the time to calculate DI of one image is less than 3.8 seconds. It took 150 milliseconds to calculate RI of the testing images, specifically 40 microsecond per image, while the whole recognition procedure took 8.19 seconds on average. That means calculating RI in recognition phase only consumed 1.83% the total recognition time.

The experiments are repeated using majority voting and

Table 1. Experiment settings

database	C	N_t	N_r	N_p	variations
CMU-PIE	68	50	10	15∼55	pose, illumination
YaleB	38	32	4	15∼32	illumination
FRGC	311	20	4	15∼30	illumination, expression, mild pose

C is the number of individuals; N_t is the number of training images; N_r is the number of reference images; N_p is the number of testing images. (per individual)

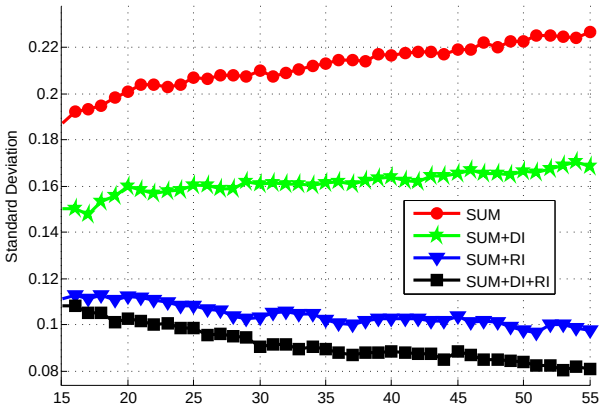

Figure 6. The standard deviation of results amount 100 times on CMU PIE with eigenface representation and sum rule.

product rule. Similar patterns are obtained, shown in Figure 7 (b) and (c), respectively. Moreover, replacing Eigenface representation with Kernel PCA representation, the experiments are repeated. The results are shown in Figure 8. It can be observed that the performances are improved after integrating DI and/or RI with the recognition system.

For YaleB database and FRGC database, the same experiments are conducted and the results are shown from Figure 9-12. It can be seen that same conclusions as that on CMU-PIE are drawn.

4 Conclusions

In this paper, two new measurements, discriminability index (DI) and reliability index (RI), are introduced. Differing from the existing image assessment methods, the proposed method is based on the discriminative power and the matching quality. These two new measurements help the multiple image based face recognition systems improving their performance. The experimental results show that after adopting the proposed DI and RI to the existing recognition algorithm, the recognition accuracy and the robustness of the performance are improved. The improvement of accuracy ranging from 4% to 30%.

Acknowledgement

This project was partially supported by Research Grant Council and Faculty Research Grant of Hong Kong Baptist University. The authors would like to thank CMU for providing the CMU-PIE database, Yale University for providing the YaleB database and University of Notre Dame for providing the FRGC database.

References

[1] V. Barnett and T. Lewis. *Outliers in Statistical Data*. John Wiley & Sons New York, 1994.

[2] S. Blok, D. Medin, D. Osherson Probability from similarity *AAAI Conference on Commonsense Reasoning* . AAAI Press: Stanford, CA, 2002

[3] K. Bowyer, K. Chang, P. Flynn, and C. X. Face Recognition Using 2-D, 3-D, and Infrared: Is Multimodal Better Than Multisample? . *Proceedings of the IEEE*, 94(11), 2006.

[4] S. Canavan, M. Kozak, Y. Zhang, J. Sullins, M. Shreve, and D. Goldgof. Face Recognition by Multi-Frame Fusion of Rotating Heads in Videos. In *IEEE International Conference on Biometrics: Theory, Applications, and Systems*, pages 1–6, 2007.

[5] K. Chang, K. Bowyer, and P. Flynn. An evaluation of multimodal 2D+ 3D face biometrics. *IEEE Transactions on Pattern Analysis and Machine Intelligence*, 27(4):619–624, 2005.

[6] W. Dixon. Analysis of extreme values. *The Annals of Mathematical Statistics*, pages 488–506, 1950.

[7] R.O. Duda, P.E. Hart and D.G. Stork *Pattern Classification*. Wiley New York, 2001

[8] A. Georghiades, P. Belhumeur, and D. Kriegman. From few to many: Illumination cone models for face recognition under variable lighting and pose. *IEEE Transactions on Pattern Analysis and Machine Intelligence*, 23(6): 643–660, 2001.

[9] F.E. Grubbs. Procedures for Detecting Outlying Observations in Samples *Technometrics*, 11(1): 1–21,1969.

[10] A. Hadid and M. Pietikainen. From still image to video-based face recognition: an experimental analysis. In *Proceedings of IEEE International Conference on Automatic Face and Gesture Recognition*, pages 813–818, 2004.

[11] V. Hodge and J. Austin. A survey of outlier detection methodologies. *Artificial Intelligence Review*, 22(2):85–126, 2004.

[12] A.K. Jain, S. Pankanti, S. Prabhakar, L. Hong, A. Ross, J.L. Wayman Biometrics: A Grand Challenge In *Proceedings of IEEE International Conference on Pattern Recognition (CVPR)*. IEEE Computer Society, 2004

[13] A. John. *Mathematical Statistics and Data Analysis*. Wadsworth & Brooks/Cole, 1988.

[14] J. Kittler, M. Hatef, R. P. W. Duin, and J. Matas. On combining classifiers. *IEEE Transactions on Pattern Analysis and Machine Intelligence*, 20:226–239, 1998.

[15] V. Kruger and S. Zhou. Exemplar-based face recognition from video In *Proceedings of IEEE International Conference on Automatic Face and Gesture Recognition*, pages 175 – 180, 2002.

[16] X. Liu, J. Rittscher and T. Chen. Optimal Pose for Face Recognition. *Proceedings of IEEE International Conference on Pattern Recognition (CVPR)*.IEEE Computer Society, vol(2), pp:1439-1446, 2006.

[17] P.J. Phillips, P.J. Flynn, T. Scruggs, K.W. Bowyer,*et al.*. Overview of the face recognition grand challenge In *Proceedings of IEEE International Conference on Pattern Recognition (CVPR)*.IEEE Computer Society, vol(1), pp:947-954, 2005.

[18] P.J. Phillips, W.T. Scruggs, A.J. O'Toole,*et al.*. FRVT 2006 and ICE 2006 Large-Scale Experimental Results *IEEE Transactions on Pattern Analysis and Machine Intelligence*, IEEE Computer Society, in press, 2009.

[19] T. Sim, S. Baker, and M. Bsat. The CMU pose, illumination, and expression database. *IEEE Transactions on Pattern Analysis and Machine Intelligence*, 25(12):1615–1618, 2003.

[20] X. Tan, S. Chen, Z. Zhou, and F. Zhang. Face recognition from a single image per person: A survey. *Pattern Recognition*, 39(9):1725–1745, 2006.

[21] D. Thomas, K. W. Bowyer, and P. J. Flynn. Multi-frame approaches to improve face recognition. In *Proceedings of IEEE Workshop on Motion and Video Computing*, pages 19–19, 2007.

[22] Y. Zhang and A. Martínez. A weighted probabilistic approach to face recognition from multiple images and video sequences. *Image and Vision Computing*, 24(6):626–638, 2006.

[23] W. Zhao, R. Chellappa, P. Phillips, and A. Rosenfeld. Face recognition: A literature survey. *ACM Computing Surveys*, 35(4):399–458, 2003.

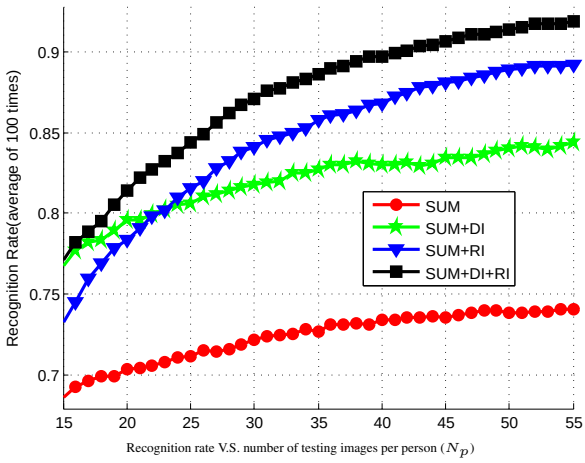

(a)

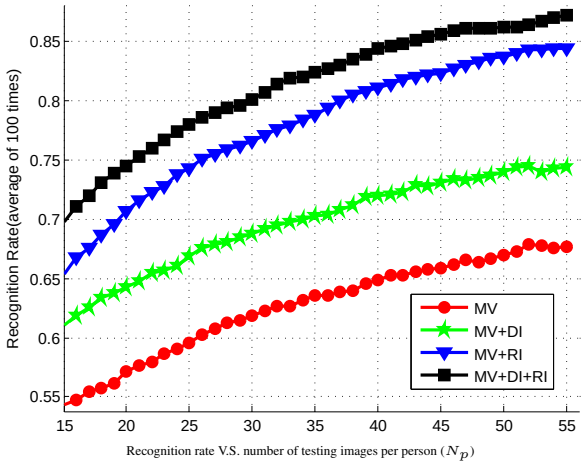

(b)

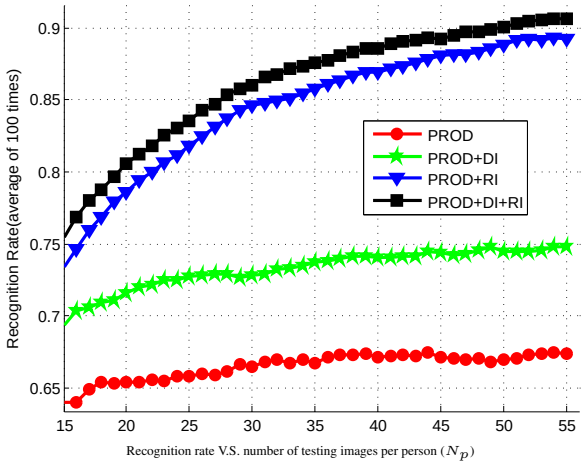

(c)

Figure 7. Results on CMU database with Eigenface representation :(a) Sum rule (SUM) (b) Majority voting rule (MV) (c) Product rule (PROD).

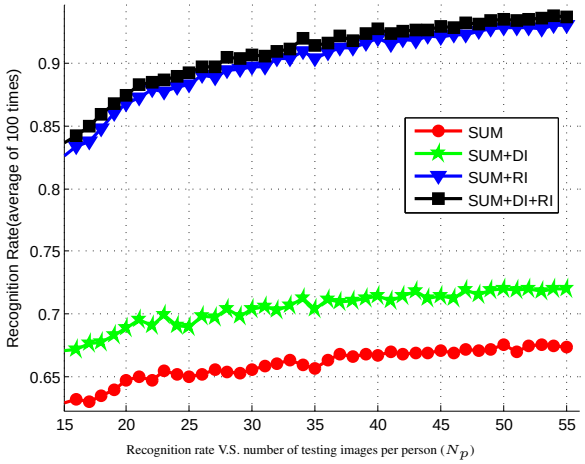

(a)

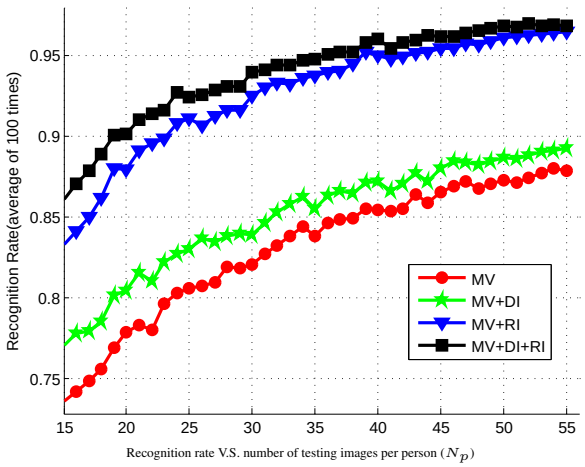

(b)

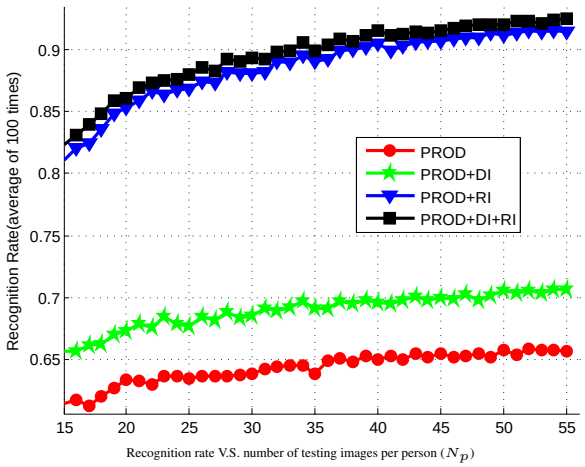

(c)

Figure 8. Results on CMU-PIE database with Kernel PCA representation :(a) Sum rule (SUM) (b) Majority voting rule (MV) (c) Product rule (PROD).

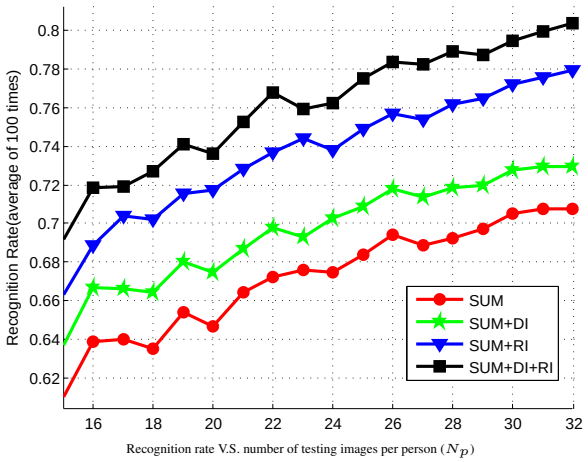

(a)

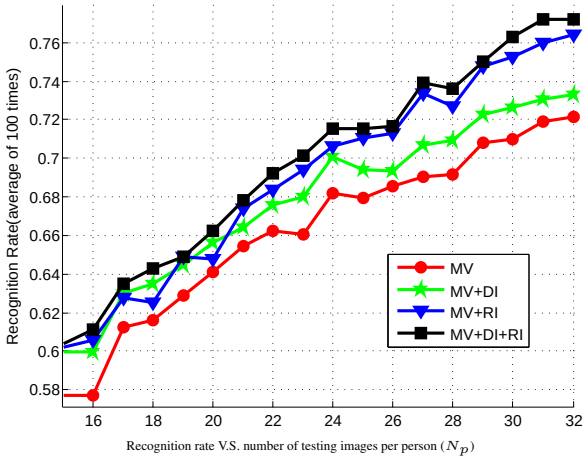

(b)

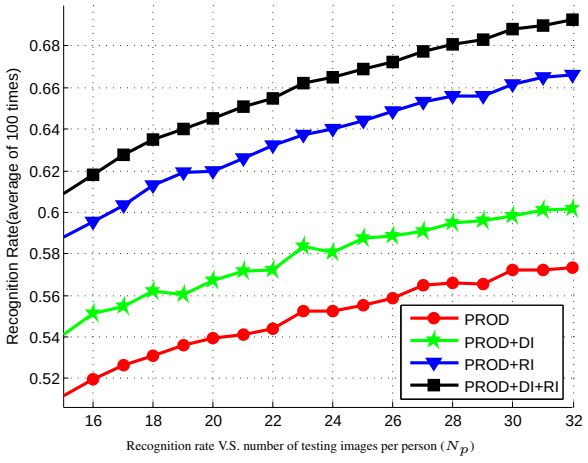

(c)

Figure 9. Results on YaleB database with Eigenface representation :(a) Sum rule (SUM) (b) Majority voting rule (MV) (c) Product rule (PROD).

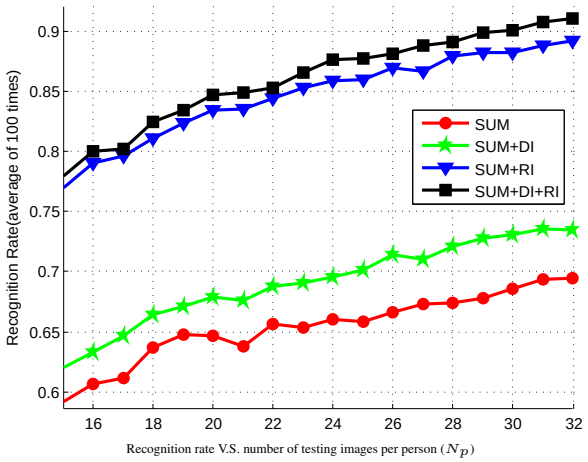

(a)

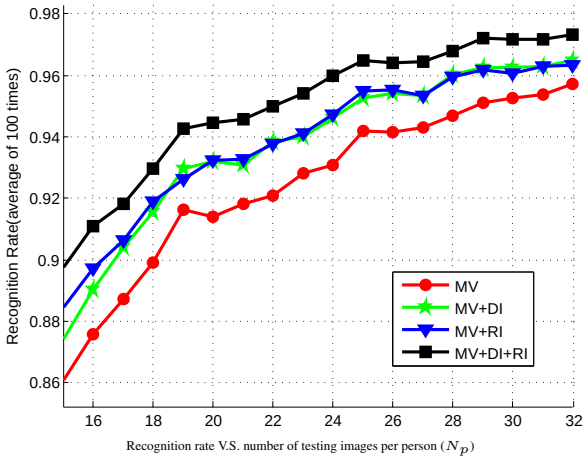

(b)

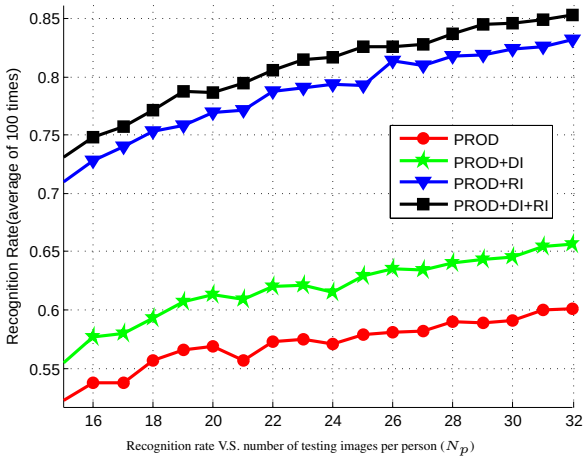

(c)

Figure 10. Results on YaleB database with Kernel PCA representation :(a) Sum rule (SUM) (b) Majority voting rule (MV) (c) Product rule (PROD).

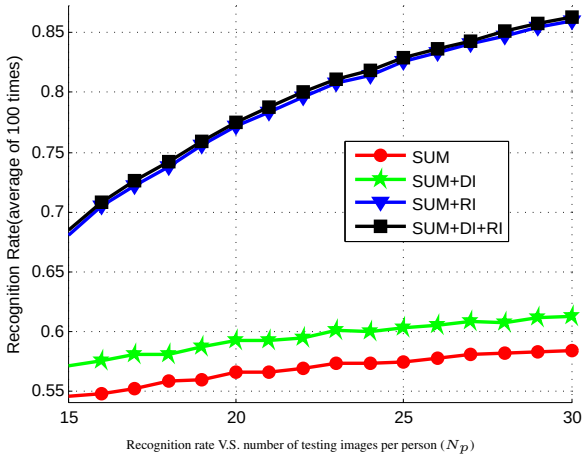

(a)

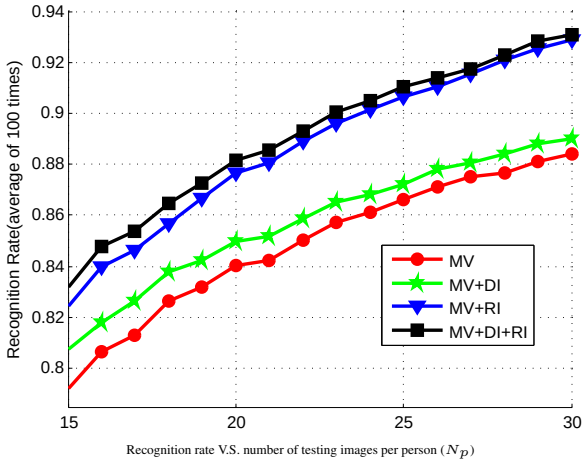

(b)

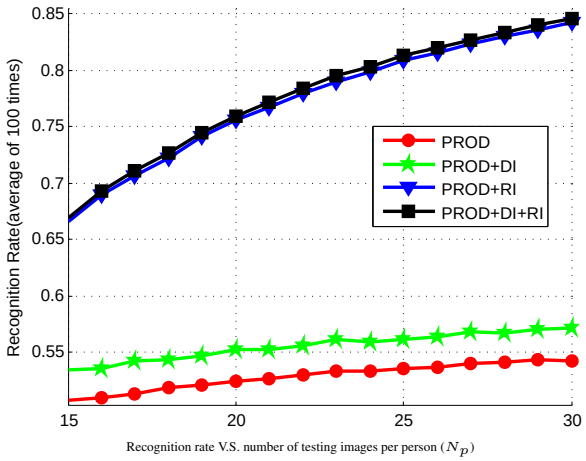

(c)

Figure 11. Results on FRGC database with Eigenface representation :(a) Sum rule (SUM) (b) Majority voting rule (MV) (c) Product rule (PROD).

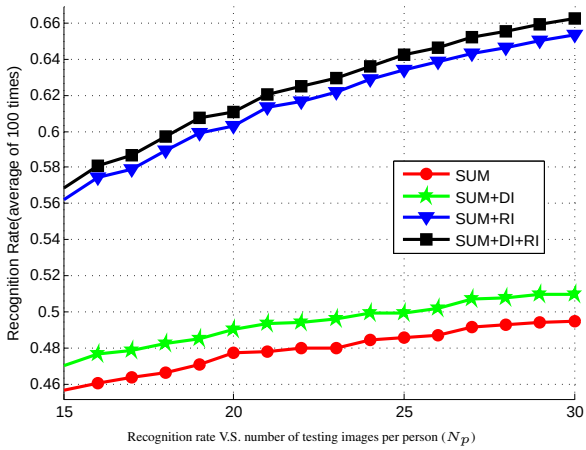

(a)

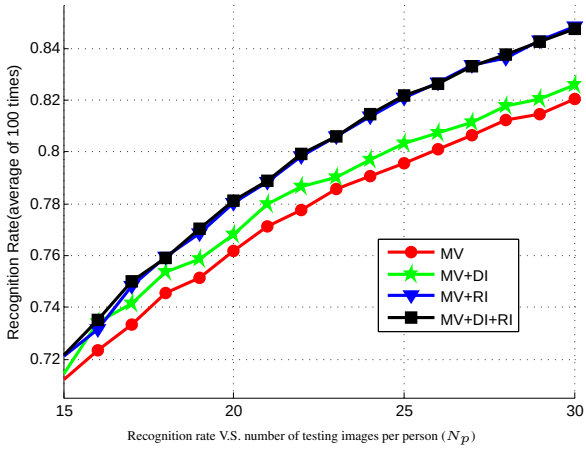

(b)

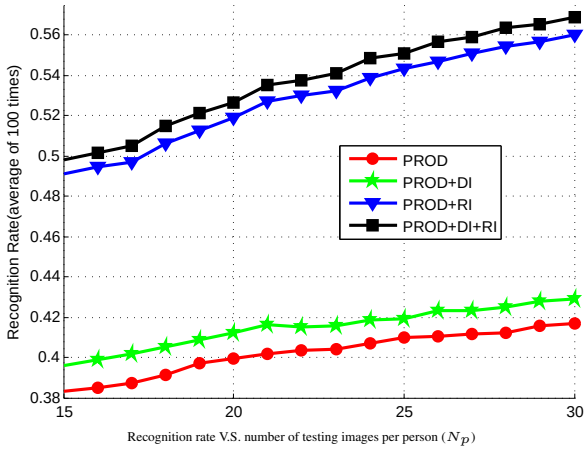

(c)

Figure 12. Results on FRGC database with Kernel PCA representation :(a) Sum rule (SUM) (b) Majority voting rule (MV) (c) Product rule (PROD).

A Dynamic Trust Network for Autonomy-Oriented Partner Finding

Hongjun Qiu*

Abstract

The problem of partner finding is to identify which entities (agents) can provide requested services from a group of entities. It can be found in open and distributed environments for such tasks as file sharing and resource allocation. Previous studies have shown that entities can refine and determine partners through measuring trust relationships, i.e., the beliefs of entities that others will accomplish a request for assigned services at hand. Entities dynamically change their beliefs through recalling their past experiences to quickly identify partners for new requests. This paper aims to observe whether those changes can enable entities efficiently find partners and hence provide services. We propose a dynamic network, which contains trust relationships as links among entities (nodes). Then, we investigate its structure and efficiency in the moments with different trust relationships. Autonomy-Oriented Computing (AOC) is applied to observe how the network dynamics emerge from local behaviors. A notion of autonomy is embodied in defining how entities activate their partner finding behaviors, whereas self-organization is realized to update the strength of trust relationships. Experimental results explicitly display a dynamic process of this network, changing from containing no link to having some stable links. Specially, in this process, the efficiency gradually gets enhanced.

1 Introduction

In a multi-entity network, entities (e.g., companies) usually look for some others (i.e., finding partners) to provide services beyond their own limited abilities. The problem of partner finding appears widely in real-world applications. Here, we take cloud computing as an example. In cloud computing, vendors (e.g., Google, Amazon and Microsoft) deploy numerous servers over the Internet, to store data or run programs in real time as requested by users [3]. The servers work together to deal with such requests from hundreds or thousands of users per second [4]. Hence, it is quite important for servers to immediately identify who can work together to accomplish requests.

Currently, researchers have introduced a notion of trust relationship as a measurement for identifying partners, to solve real-world problems in open, distributed and dynamic environments [2]. Trust relationships refer to entities' beliefs that others will provide services as needed [11]. In most cases, entities are inclined to choose partners from the ones in which their beliefs are relatively strong. Entities weaken their beliefs if the found partners cannot provide services. Otherwise, they strengthen their beliefs. They dynamically change the strength values of their beliefs with more and more such experiences. Thus, they can quickly identify partners at any time.

Many studies have been done in applying trust relationships to find partners. Golbeck [2] argues that trust relationships can be used to identify who can produce trustworthy online information. Sen et al. [1] compare three schemes of computing trust relationships in reducing the cost of finding partners from a small group of entities. Specially, they introduce a nearest neighbor algorithm as a scheme through recalling a fixed number of latest experiences of finding partners. To get rid of malicious entities from the group of potential partners, Kamvar et al. [6] build a matrix of weighted trust relationships through aggregating and normalizing based on a history of uploading files. They compute the left principal eigenvector of this matrix as their metric. More related work can be found in [5, 12, 13]. In such work, entities either measure the probabilities that others have successfully provided services before, or ask past partners for their beliefs about third-party ones.

However, it remains to clarify why and how trust relationships can make entities efficiently find partners in dynamic, distributed, real-world networks. This paper aims to solve this problem through proposing a dynamic trust network based on the bottom-up methodology of Autonomy-Oriented Computing (AOC). AOC can help us characterize how network dynamics emerge from local interactions through utilizing the ideas of autonomy and self-organization [7, 9, 8]. Here, network dynamics refers to the dynamics of network structure, network performances in providing services and so forth. Zhang et al. [14] have successfully characterized such dynamics of a distributed network, in which entities work together to provide various

*Prof. Jiming Liu is her corresponding supervisor

services. Their work shows the feasibility and rationality for the work in this paper.

In this study, the autonomy is embodied for entities (nodes) to find partners while a process of self-organization is realized to update trust relationships (links). Entities decide to activate which behaviors for partner search or selection through measuring their abilities and beliefs. They also immediately update their beliefs, once they receive the feedback from their latest partners. Specially, a positive feedback mechanism is emphasized, i.e., the strong beliefs become stronger while the weak become weaker. Experimental results show that our network quickly converges to be scale-free. With such a structure, entities quickly find partners for any request. These results explain why dynamic trust relationships are helpful for entities to find partners.

The reminder of this paper is organized as follows: Section 2 gives a detailed problem statement. Section 3 formulates a network on the basis of AOC. The network contains autonomous entities as nodes and self-organized trust relationships as links. In Section 4, we observe the structural emergence of this network and the dynamics of trust relationships. The efficiency in finding partners is also measured. Finally, the paper is concluded in Section 5.

2 Problem Statement

As mentioned above, the goal of this study is to examine the effects of dynamic trust relationships on finding partners in open, dynamic, and distributed networks, such as the Internet. It requires us to answer the following questions:

- How do entities update their trust relationships? What will they do if they never interact with their newly-found partners before? Will entities memorize the information about all of their past partners?
- What are the mechanisms for entities search and select partners? How do entities refine partners based on updated beliefs? How do entities identify their partners from their refinement results?
- Which parameters can we introduce to characterize the change of trust relationships, besides the variation of their strength? Is it enough to count the number of entities' trustees, associated by their beliefs?
- What is the efficiency in finding partners based on dynamically-changing trust relationships?

Previous studies have confirmed two preliminary phenomena. One is that entities prefer to interact with their trustees rather than strangers. The other is that entities strengthen their beliefs about another entity once it accomplishes a service request and vice versa. Based on the two phenomena, we attempt to answer the above questions in the following scenario.

Here, we assume that there exists a virtual network, which contains trust relationships as links and entities as nodes. In this network, entities are assigned with fixed abilities of providing certain services. Each of them can find a partner to satisfy a whole service request, which cannot be finished by itself. The request has a cost limit, i.e., the maximum number of times for finding partners. The partner will honestly inform whether it can finish this request. Then the finder can decide to strength or weaken its belief about this partner. If this partner cannot finish, it will transfer the request to the third entity, which is discovered as its partner. In other words, this request propagates among entities until it is accomplished or the number of finding times reaches the given cost limit.

Accordingly, the above questions can be translated into the following tasks:

1. Modeling a virtual network, in which distributed entities can find partners and update their beliefs.
2. Measuring structural characteristics at different moments to display the dynamics of the links among entities. The characteristics include network indegree (outdegree), the clustering coefficient and the harmonic mean of average path length (APL^{-1}).
3. Examining the efficiency in finding partners with two parameters, i.e.,
    - Accomplishment ratio: the ratio of the number of accomplished requests to the total number of requests;
    - Average propagation step: the average times that entities find partners for finishing requests.

3 Modeling a Dynamic Trust Network

3.1 Basic ideas

In this section, we will model a virtual network of distributed entities, i.e., a dynamic trust network. Then, we can characterize the structural dynamics of this network, as a reflection of dynamic trust relationships.

To meet the distributed, dynamic needs, we will define the network based on the methodology of AOC. AOC aims to characterize complex networks (e.g., large-scale, dynamic and distributed networks), through deploying a set of autonomy-oriented entities and defining their behavioral rules of self-organization [7, 10]. These entities activate different behaviors to finish a certain task or else, according to their different states, e.g., the number of entities they interacted before. Moreover, entities self-organize their coupling

relationships based on their received feedbacks, such as the state of other entities.

In this work, entities continually find partners in an autonomous manner, as well as self-organize trust relationships based on the feedback from partners.

For finding partners, entities activate one of well-defined search or selection behaviors in a probabilistic manner. The probability of activating each behavior is adaptive to new requests and entities' states (e.g., their beliefs).

A process of self-organization is realized to update trust relationships. At first, there is no trust relationship in the network. After a period of continually finding partners, entities maintain several trust relationships. The realization of this process lies in two aspects. On one side, entities' behaviors are defined to be exploratory or even stochastic. They may find strangers as their partners and create their beliefs about the newly-found partners. However, with positive feedback mechanisms, the newly-created beliefs may be weakened or even eliminated later. Therefore, only a part of generated relationships can remain. The remaining relationships can help entities effectively find partners to finish new requests. So, any request can be accomplished with a higher probability.

The network, entities and service requests are defined as follows:

Definition 1 *Let* $G^{'}(t)=< E, L^{'}(t) >$ *denote a dynamic network of trust-based entities on the basis of AOC. For brevity, we call it a dynamic trust network.* $E = \{e_1, \cdots, e_{N_e}\}$ *denotes the set of entities and* N_e *is the number of entities in the network.* $L^{'}(t) = \{l^{'}_{ij}(t)|e_i, e_j \in E\}$ *is the set of trust relationships at time* t.

Definition 2 *Let* $e_i =< ID, ability, rules >$ *denote an entity where* ID *is its identifier, i.e.,* $e_i.ID = i, i \in [1, N_e]$. *It can provide some services with different performances, i.e.,* $e_i.ability =< cw_1, \cdots, cw_{N_{service}} >$, *where* cw_j *denotes the performance on the* j*th type of service* t_j. $N_{service}$ *is the number of service types. The rules define when and how entities activate their behaviors.*

Definition 3 *A request can be formulated as* $r_m=< rw_1, \cdots, rw_{N_{service}}, T_{max} >$ *where* rw_j *denotes the performance requirement of the type of service* t_j. T_{max} *is the maximum number of times that entities are allowed to find partners.*

The two ideas from AOC are illustrated through describing the process of finding partners for finishing a request, which is specified in Section 3.5. Once a new request r_m is submitted to an entity e_i, this entity will perform the following:

1. **Evaluating**. Firstly, the entity will determine whether it can solely accomplish the new request by means of matching its ability with this request using a cosine-based similarity function $e_i.simRE(r_m)$. The request can be considered as accomplished once the value of $e_i.simRE(r_m)$ is larger than a threshold. The evaluation functions are specified in Section 3.4.

2. **Partner Search and Selection**. If the request cannot be accomplished and its T_{max} is not reached, the entity e_i will start finding partners. Firstly, it will search some candidates by means of activating one of search behaviors in a probabilistic manner. Then, it will select a candidate as its partner through activating one of selection behaviors also probabilistically. The probabilities are adaptive to the request and the states of the entity, e.g., its trust relationships. So, trust relationships will explicitly affect entities' partner finding. The detailed behaviors are given in Section 3.2.

3. **Updating**. The entity e_i will change its states once a partner is found. Firstly, it will deliver the whole request to its partner. Then, the partner e_j will honestly feedback its evaluating results $e_j.simRE(r_m)$. Finally, this entity will generate the trust relationship $l^{'}_{ij}$ if $l^{'}_{ij}(t)$ is not in the network. Otherwise, it will strengthen the relationship if the ability of this partner is relatively closer to this request, or weaken the trust relationship if not. The mechanisms of trust relationships are specified in Section 3.3.

3.2 The Local Autonomy of Entities

Three search behaviors and two selection behaviors are defined in this section. They will be probabilistically activated to realize the autonomy of entities. The probability of activating each behavior is determined with the degree of similarity between requests and entities' abilities, i.e., $e_i.simRE(r_m)$. When the degree is high, entities' neighbors will be discovered as partners with a high probability. Stochastic behaviors are given for entities to avoid being trapped in local-optima and for newcomers to join this network.

The detailed operations of search and selection behaviors are specified in below:

- **Neighbor-based search** $neighborSearch()$. An entity e_i will find some neighbors, which are not involved in the current request r_m, with the probability of $e_i.simRE(r_m)$. The probability will be adaptive to requests accordingly. Neighbors refer to its trustees. i.e., there are trust relationships from this entity to them.

- **Recommendation-based search** $recommendSear-ch()$. An entity e_i will discover candidates within a distance $maxD$ around itself with a probability of

$1 - e_i.simRE(r_m)$ when the receiving request is relatively near the entity's ability. That is, the entity will enlarge its search area from its neighbors to the area within a given distance. This behavior is inspired by two observations: 1) besides direct experiences, indirect experiences are also important for entities to make decisions; 2) communities have been discovered in many real-world networks, i.e., agents with similar interests cluster together. Here, the request far beyond the ability of an entity is likely out of its neighbors' abilities.

- **Random search** $randomSearch()$. An entity e_i will search in the whole network when it is a newcomer or its neighbors are all involved in the current request.
- **Trust-based select** $trustSelect()$. The entity e_i will select an entity e_j with the maximal degree of trust, $e_i.trust(e_j, t)$, from its candidates as its partner with a probability of $e_i.simRE(r_m)$. Entities are supposed to be more confident in selecting partners for requests which are relatively closer to its abilities.
- **Random select** $randomSelect()$. The entity e_i will stochastically select an entity from the candidate set $e_i.cand(r_m)$ as its partner with a probability of $1 - e_i.simRE(r_m)$.

3.3 The Mechanisms of Trust Relationships

We have introduced how trust relationships are applied in activating entities' behaviors for finding partners in the previous section. Now, we will introduce how they are changed based on the feedback from partners. Trust relationships are defined as follows:

Definition 4 *A link* l'_{ij}=$\{<$ e_i, e_j, $e_i.succ(e_j, t)$, $e_i.fail(e_j, t)$, $e_i.latestTime(e_j)$, $e_i.trust(e_j, t)$ $>|1 \leq i, j \leq N_e\}$ *reflects a trust relationship from* e_i *to* e_j *where*

- $e_i.succ(e_j, t)$ *and* $e_i.fail(e_j, t)$ *denote the numbers of successful and failed interactions, respectively;*
- $e_i.latestTime(e_j)$ *is the time of their latest interaction;*
- $e_i.trust(e_j, t)$ *is the degree of trust at time t, quantifying the belief that* e_j *will accomplish a new request from* e_i*. It is a numeric value in* $[\varepsilon, 1.0]$*, where the threshold* ε *will be described below.*

Once an entity e_i receives the feedback of its partner $e_j.simRE(r_m)$, a new relationship $l_{ij}(t)$ will be generated if it is not in the network. Otherwise, the existing relationship will be updated. The parameters of this relationship will be assigned as introduced below.

Firstly, the time of their latest interaction is set as the current time. Then, e_i will evaluate whether the partner is more suitable for the current request with Eq. 1 where λ is a threshold, $\lambda \in (0, 1)$.

$$e_i.QoI(e_j, r_m) = \begin{cases} true & \frac{e_j.simRE(r_m)}{e_i.simRE(r_m)} > (1 + \lambda); \\ false & otherwise \end{cases} \quad (1)$$

Other parameters will be assigned according to the result of $e_i.QoI(e_j)$. When the partner is more suitable for this request, i.e., $e_i.QoI(e_j, r_m) = true$, this interaction is regarded as successful and the number of their successful interactions increases. Otherwise, the number of failed interactions increases. Then, the degree of trust $e_i.trust(e_j, t)$ can be set with updated $e_i.succ(e_j, t)$ and $e_i.fail(e_j, t)$ as follows:

$$e_i.trust(e_j, t) = \frac{e_i.succ(e_j, t)}{e_i.succ(e_j, t) + e_i.fail(e_j, t)} \quad (2)$$

Trust relationships may be removed since the degree of trust is supposed to decay over time as follows:

$$\begin{aligned} e_i.trust(e_j, t) = e_i.trust(e_j, e_i.latestTime(e_j)) \\ - \eta * (t - e_i.latestTime(e_j)) \end{aligned} \quad (3)$$

where η is the decay factor, $\eta \in (0.0, 1.0)$. Once the degree of trust is less than a small negative numeric value ε, i.e., $e_i.trust(e_j, t) < \varepsilon$, the neighbor is interpreted as being no longer able to accomplish new requests from this entity, and the corresponding relationship will be eliminated. The threshold ε is empirically set, $\varepsilon \in (-0.05, 0)$.

In addition, entities will derive new trust relationships from the relationships already in the network. If the shortest distance from entity e_i to entity e_j is larger than a given threshold $maxD$, i.e., $e_i.shortestDis(e_j, t) > maxD$, e_i has no idea about the ability of e_j and the degree of trust $e_i.trust(e_j, t)$ is set as 0. Otherwise, the following functions can be used to compute the degree of trust for the derived relationships:

$$\begin{aligned} e_i.trust(e_j, t) &= \frac{\sum_{k=1}^{n_{ij}(t)} e_i^k.trustPath(e_j, t)}{n_{ij}(t)} \\ e_i^k.trustPath(e_j, t) &= \sum_{l'_{m_j}(t) \in L'(t)} (e_i^k.trustPath(e_m, t) \\ &\quad \times e_m.trust(e_j, t)) \end{aligned} \quad (4)$$

where $n_{ij}(t)$ is the number of the shortest paths from e_i to e_j and the function $e_i^k.trustPath(e_j, t)$ denotes the degree of trust derived from the kth shortest path. If e_j is a neighbor of e_i, $e_i^k.trustPath(e_j, t)$ will be computed with Eq. 3.

3.4 Evaluation Functions

We define two functions, $e_i.simRE(r_m)$ and $e_i.match(r_m)$, for entities to evaluate whether they can accomplish received requests in this section. A cosine-based function is given to compute the degree of similarity between request r_m and the ability of entity e_i, i.e.,

$$e_i.simRE(r_m) = \frac{\sum_{k=1}^{N_{service}} (r_m.rw_k * e_i.cw_k)}{\sqrt[2]{\sum_{k=1}^{N_{service}} r_m.rw_k^2 * \sum_{k=1}^{N_{service}} e_i.cw_k^2}} \quad (5)$$

When the value of $e_i.simRE(r_m)$ is larger than a threshold δ, $\delta \in (0, 1)$, the request r_m is assumed to be accomplished by the entity e_i, i.e.,

$$e_i.match(r_m) = \begin{cases} true & simRE(r_m) > \delta; \\ false & otherwise \end{cases} \quad (6)$$

3.5 The Algorithm

The trust network will evolve through continually finding partners based on the above-defined behaviors and trust relationships. Algorithm 1 describes how entities find partners once a new request is stochastically submitted. $search()$ and $select()$ represent entities activate a behavior of search and selection, respectively. $updateState()$ denotes that entities update their trust relationships. As defined before, $G'(t)$ represents the trust network at time t, i.e., t requests have been submitted to the network. If no request has ever been submitted, the network $G'(t)$ only contains N_e independent entities, i.e., $G'(0) =< \{e_1, \cdots, e_{N_e}\}, \emptyset >$.

Algorithm 1: The Autonomy-Oriented Partner Finding

Input: A new request r_m, the dynamic trust network $G^{'}(t)$
Output: The evolved network $G^{'}(t+1)$
begin
  // initialization phase
  stochastically select an entity e_i as the receiver of new request r_m;
  $current\_entity \leftarrow e_i$; $next\_entity \leftarrow null$;
  $flag \leftarrow true$;
  // self-organized computing phase
  while $r_m.T_{max} > 0$ **do**
    $matchResult \leftarrow current\_entity.match(r_m)$ based on Eq. 6;
    if $matchResult \neq$ *true* **then**
      $current\_entity.search()$;
      $next\_entity \leftarrow current\_entity.select()$;
      // update based on feedback
      $flag \leftarrow current\_entity.QoI(next\_entity, r_m)$ based on Eq. 1;
      $current\_entity.updateState(flag)$ based on Eq. 2;
      $current\_entity \leftarrow next\_entity$;
      $r_m.T_{max} = r_m.T_{max} - 1$;
    else
      $r_m.T_{max} = 0$;
    end
  end
end

4 Experiments

In the above, we have presented a dynamic trust network, which contains autonomous entities as nodes and self-organized trust relationships as links. This section gives some experiments toward the following objectives:

1. to characterize the dynamics of trust relationships by means of measuring network structural characteristics;
2. to measure the efficiency of the network in finding partners to accomplish requests.

4.1 Experimental Setting

Experimental parameters are listed in Table 1. The simulated network contains 1000 entities and can provide 5 types of services. Entities' abilities on providing each type of service are supposed to follow a power-law distribution and the power falls in the range of $[1, 2]$. That is, most entities provide certain type of service with a low performance, e.g., a low quality of service. A cycle denotes the time entities spent on finishing a request and updating corresponding trust relationships among them. The performance requirement and T_{max} of all requests are stochastically initialized. For each request, its requirement on each type of service is set to be in the field of $[0.0, 1.0]$ while its T_{max} is assigned with a random integer value in $(0, 999]$. The number of entities determines the upper limit of T_{max} since each entity is allowed to be found once for the same request. For fairness, we submit the same set of 100 requests after each cycle and test the efficiency of entities in finishing such requests.

4.2 The Dynamics of Trust Relationships

We examine the dynamics of trust relationships by measuring the structure characteristics, including the network

Table 1: The experimental parameters

$N_{service} = 5$	$N_{cycles} = 1500$	$N_{testRequest} = 100$
$N_e = 1000$	$\lambda = 0.2$	$maxD = 4$
$\delta = 0.95$	$\eta = 0.0003$	$\varepsilon = -0.02$

indegree (outdegree), the clustering coefficient, the harmonic mean of average path length APL^{-1} and the distributions of entities' indegree and outdegree. The results are shown in Fig. 1 and Fig. 2.

In Fig. 1, the values of three characteristics fluctuate relatively slightly after changing rapidly in the first 250 cycles. That means that entities dramatically generate and remove trust relationships at the beginning. Then, they find and maintain the relationships to their stable partners for any request later.

In Fig. 2, entities' indegree or outdegree approximately follow power-law distribution in the 100th, 500th, 1000th, 1500th cycles. Specially, we have observed that the phenomenon of a power-law distribution appears firstly at the 16th cycle. The power dynamically changes in the following cycles, as a result of more and more entities involve in finishing requests and then update their trust relationships. The result is quite interesting. It can be inferred that entities can more efficiently find their partners in such a structure, as to be discussed in the following section.

4.3 The Dynamics of Efficiency

In this section, we will examine the efficiency of our network in finding partners to finish the fixed 100 requests in different cycles. The measurements include:

- the accomplishment ratio $accompRatio$: the proportion of the number of accomplished requests to 100;
- the average steps $avgStep$: the average times entities find partners for finishing these requests;
- the standard deviation of propagation steps $stDevOfStep$.

As to be described later, the accomplishment ratio gradually increases, while the average steps and the standard deviation decrease. The efficiency gets enhanced with the change of trust relationships.

Table 2: The efficiency at different cycles

cycle	$accompRatio$	$avgStep$	$stDevOfStep$
0	0.937	52.242	61.603
1500	0.958	43.702	49.838

Fig.3 presents the dynamics of efficiency. Each point in curves is computed over 10 cycles. Entities may only

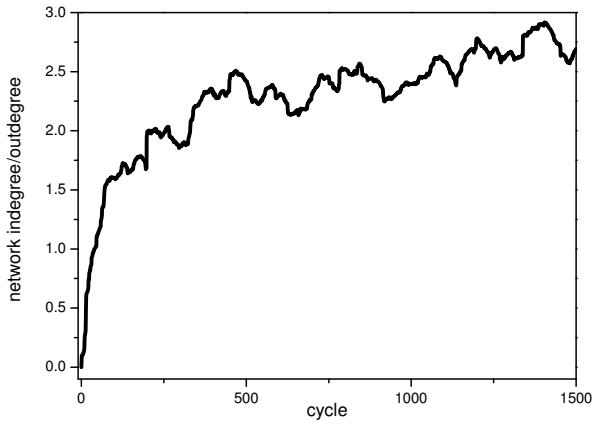

(a) the network indegree (outdegree)

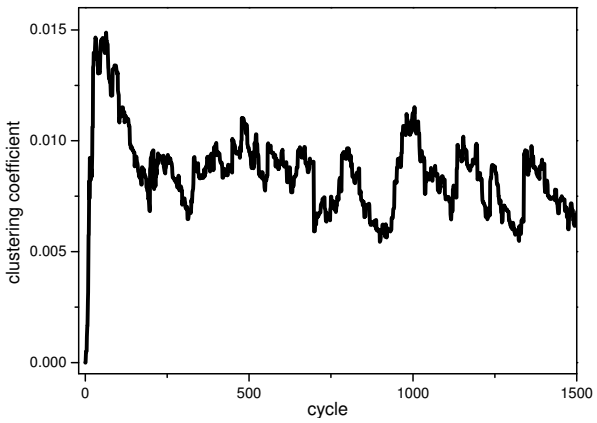

(b) the clustering coefficient

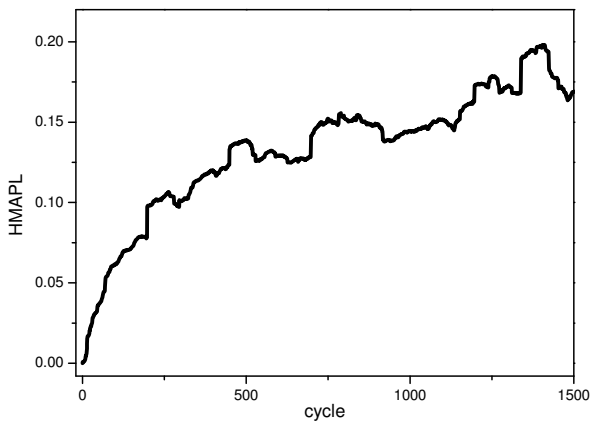

(c) the APL^{-1}

Figure 1: The dynamics of trust relationships with the measurement of (a) network indegree (outdegree), (b) clustering coefficient and (c) the harmonic mean of average path length.

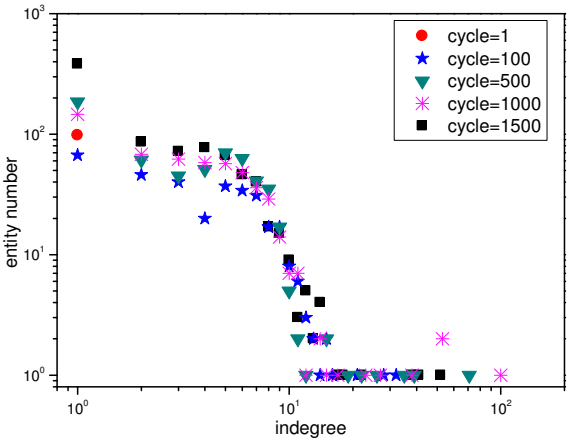

(a) the distribution of indegree

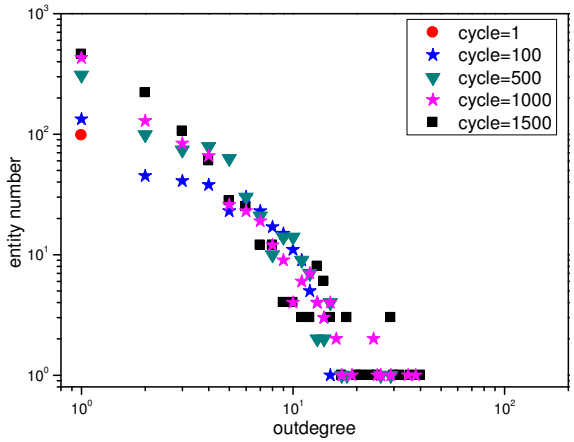

(b) the distribution of outdegree

Figure 2: The distributions of (a) entities' indegree and (b) outdegree at different cycles. Entities' indegree and outdegree approximately follow power-law distributions since the 16th cycle.

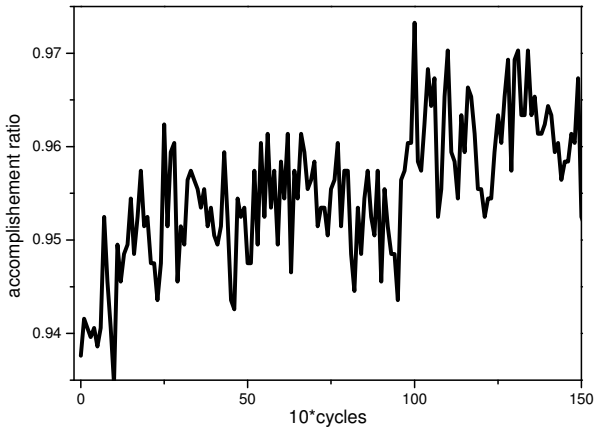

(a) the accomplishment ratio

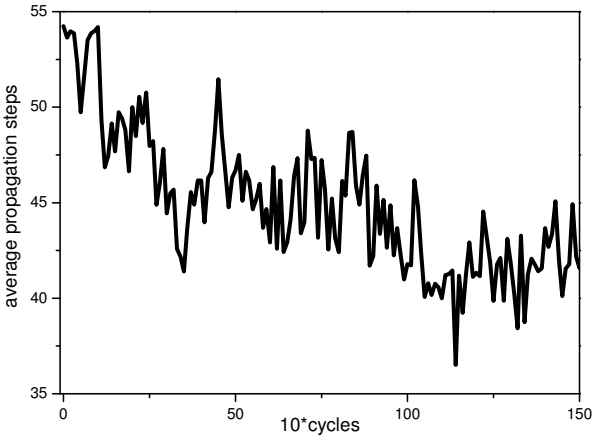

(b) the average steps

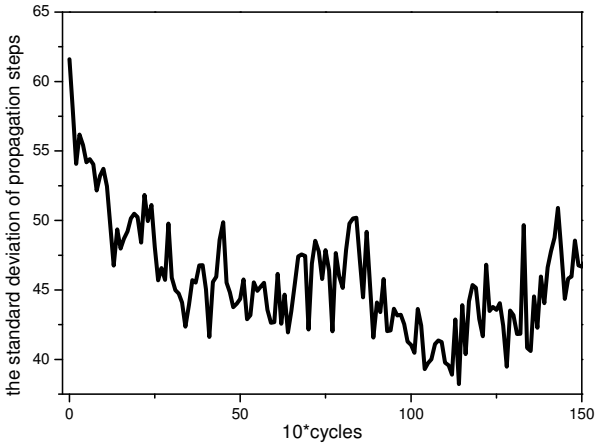

(c) the standard deviation of propagation steps

Figure 3: The dynamics of the efficiency with the three measurements: (a) the accomplishment ratio of 100 requests, (b) the average number of the times entities find partners for finishing the requests, (c) the standard deviation of the times spent on finding partners.

update 2 or 3 relationships in a cycle of updating, which hardly affects the efficiency. We can find that the upward or downward tendency in each sub-graph is quite clear. Table 2 gives the efficiency at the beginning cycle and ending cycle. The average steps decrease about 17.653%. It potently shows that the change of trust relationships leads to the high efficiency of finding partners.

5 Concluding Remarks

In this study, we are interested in characterizing dynamically-changing trust relationships in real-world applications. We attempt to understand why trust relationships can enable distributed entities quickly find partners to provide their requested services.

Specifically, we have proposed a dynamic trust network by means of utilizing the ideas of autonomy and self-organization from AOC. These ideas can help us understand how network-level phenomena emerge from entities' local behaviors. In this study, the notion of autonomy means that distributed entities (nodes) activate different behaviors based on their abilities and trust relationships. Self-organization refers to the process that entities change their relationships (links) with positive feedback mechanisms, according to the feedback from their partners.

Experimental results have shown that the network quickly converges to be scale-free. In other words, parts of dynamically-generated trust relationships remain relatively stable while others are eliminated. That is, the process of self-organization makes trust relationships emerge quickly. Meanwhile, the accomplishment ratio gradually rises while the average steps and the standard deviation of propagation steps gradually decrease. It can be inferred that, the convergence process of this network is accomplished with the enhancement of its efficiency in successfully finding partners.

References

[1] L. Erete, E. Ferguson, and S. Sen. Learning task-specific trust decisions. In *Proceedings of the 7th International Joint Conference on Autonomous Agents and Multi-Agent Systems*, 1477–1480, 2008.

[2] J. Golbeck. Weaving a web of trust. *Science*, 321(5896):1640–1641, 2008.

[3] M. Greeger. CTO roundtable: Cloud computing. *Communications of the ACM*, 52(8):50–56, 2009.

[4] B. Hayes. Cloud computing. *Communications of the ACM*, 51(7):9–11, 2008.

[5] A. Jøsang, R. Ismail, and C. Boyd. A survey of trust and reputation systems for online service provision. *Decision Support Systems*, 43:618–644, 2007.

[6] S. D. Kamvar, M. T. Schlosser, and H. Garcia-Molina. The eigentrust algorithm for reputation management in P2P networks. In *Proceedings of the 12th International World Wide Web Conference*, 640–651, 2003.

[7] J. Liu. Autonomy-oriented computing (AOC): The nature and implications of a paradigm for self-organized computing (keynote talk). In *Proceedings of the 4th International Conference on Natural Computation and the 5th International Conference on Fuzzy Systems and Knowledge Discovery*, 3–11, 2008.

[8] J. Liu, X. Jin, and K. C. Tsui. Autonomy-oriented computing (AOC): Formulating computational systems with autonomous components. *IEEE Transactions on Systems, Man, and Cybernetics-Part A: Systems and Humans*, 35(6):879–902, 2005.

[9] J. Liu, X. Jin, and K. C. Tsui. *Autonomy Oriented Computing: From Problem Solving to Complex Systems Modeling*. Springer, 2005.

[10] J. Liu and K. Tsui. Toward nature-inspired computing. *Communications of the ACM*, 49(10):59–64, 2006.

[11] S. P. Marsh. *Formalising Trust as a Computational Concept*. PhD thesis, University of Stirling, 1994.

[12] S. D. Ramchurn, T. D. Huynh, and N. R. Jennings. Trust in multi-agent systems. *The Knowledge Engineering Review*, 19(1):1–25, 2004.

[13] J. Sabater and C. Sierra. Review on computational trust and reputation models. *Artificial Intelligence Review*, 24:33–60, 2005.

[14] S. Zhang and J. Liu. Autonomy-oriented social networks modeling: Discovering the dynamics of emergent structure and performance. *International Journal of Pattern Recognition and Artificial Intelligence*, 21(4):611–638, 2007.

Control Behavior of 3D Humanoid Animation Object Using Reinforcement Learning

Yuesheng He

Abstract

The ability to learn is a potentially compelling and important quality for interactive 3D human avatars or virtual humans. To that end, we describe a practical approach to real-time learning for 3D virtual humans. Our implementation is grounded in the techniques of reinforcement learning and informed by insights from avatar's behavior training. It simulates the learning task for characters by enabling them to take advantage of predictable regularities in virtual graphical world and allowing them to make maximal use of any supervisory signals. We built an autonomous animated virtual human that can be trained with a technique used to train proper actions in the real world. Capabilities demonstrated include being trained to recognize and use shapes of 3D models' patterns as cues for actions, as well as to synthesize new actions from novel paths through its motion space. A key contribution of this paper is to demonstrate that by considering the three aspects on the problem of state, action, and reaction space discovery at the same time, by forming a value function on a manifold, the solution for each becomes easier. Finally, we articulate heuristics and design principles that make learning practical for synthetic animation human characters.

1 Introduction

We believe that interactive synthetic characters must learn from experience if they are to be compelling over extended periods of time. Furthermore, they must adapt in ways that are immediately understandable, important and ultimately meaningful to the virtual environment interacting with it. Computer system provides an excellent example of systems that do just this: 3D graphical human-like avatar[3][6].

Remarkably, virtual human do the actions with the effort of simulating our behavior, but little understanding of context and legend beyond their use as cues in the graphical environment. In addition, they are only able to learn causality if the events, actions and consequences are proximate in space and time, and as long as the consequences are motivationally significant[6].

Nonetheless, the learning avatars do allow them to behave human-like common sense and ultimately exploit the highly adaptive ability to different kinds of 3D environments.

Our belief is that by embedding the kind of learning of which avatars are capable into synthetic characters, we can provide them with an equally robust mechanism for adapting in meaningful ways to act like people in the 3D virtual environment which they are interacting.

In this paper, we describe a practical approach to real-time learning for 3D avatar characters that allows them to learn the kinds of things that people seem to learn so easily[7].

We ground our work in the machine learning theory of reinforcement learning, in which a creature learns to maximize reward in the absence of a teacher. Additionally, our approach is informed by insights from robot training, where a teacher is available. Robots and their trainers act as a coupled system to guide the robots exploration of its state, action, and state-action spaces . Therefore, we can simplify the learning task for autonomous animation characters by (a) enabling them to take advantage of predictable regularities in their world, (b) allowing them to make maximal use of any supervisory signals, either explicit or implicit, that the world offers, and (c) making them easy to train by interacting with virtual environment. Using this method, we implemented the autonomous animated avatar that can be trained with a technique used to train and behave like human. The synthetic avatar thus mimics some of a real human's ability to learn including:

- The best action to perform in a given context. What form of a given action is most reliable in producing reward;
- The relative reliability of its actions in producing a reward and altering its choice of action accordingly;
- To recognize new and valuable contexts such as shapes' patterns[1];

- To synthesize new and reasonable actions the training.

In order to accomplish these learning tasks, the system must address the three important problems of state, action and state-action space discovery. A key contribution of this paper is to show how these processes may be addressed in an integrated approach that guides and simulating the human-like processes. We emphasize that our behavioral architecture is one in which learning can occur, rather than an architecture that solely performs learning. As we will see, learning has important implications for many aspects of a general behavior architecture, from the design of the perceptual mechanism to the design of the 3D animation graphical system. Conversely, careful attention to the design of these components can dramatically facilitate the learning process. Hence, an important goal of this paper is to highlight some of these key design considerations and to provide useful insights apart from the approach that we have taken. We begin by surveying the framework of the approach. We then turn to a discussion of reinforcement learning. We introduce the core concepts and terminology, discuss the application of reinforcement learning to training avatar characters, and take on insights into the trial and error process. We then describe our approach, reviewing our key representations and processes for state, action and state-action space discovery. We present our experiment with different terrains, our virtual human, and discuss limitations of our approach. We conclude with a summary of what we see as the key lessons from our work.

2 Overview of The Framework

Motion action context is extensively used in computer animation, because it is able to describe all the subtleties of real human motion. By piecing together many some different type of short motion clips, we can further create novel but realistic motions. Consequently,the way of arranging the clips of motions to achieve specific goals is an important research topic[12].

A number of algorithms have been developed to represent plausible transitions between motion clips with graph structures. With these techniques, novel motions can be generated simply by building walks on the graph. For off-line applications, where the full motion specification is known in advance, a global sub-optimal or close-to-optimal solution that minimizes an objective function, such as a certain energy, can be found. In interactive applications, new input is continuously arriving and the decision for selecting the next clip needs to be made in a very short amount of time.

Therefore, only local search can be performed to generate motions in response to the dynamic 3D environments. The challenge for local search methods is to synthesize motions that require planning. Motion planning is important to achieve realistic results in many scenarios. For example, one may need to prepare well in advance to grasp an object at a particular location. Hence, first of all is to plan a total strategy of the action, then instead of trying to search a point-to-point path on the graph, we are going to face a dynamic changing 3D environment. Thus reinforcement learning techniques is used to train a motion controller off-line, which can make on-line decision quickly in any given situation. Some methods have been proposed in computer animation to utilize reinforcement learning to obtain policies for choosing actions that will increase long term expected rewards.

Thus, the whole motion can be separate into different clips. i.e. if the avatar want to go through a terrain full of obstacles, its motion can be constructed as Figure1shows. The state space and use dynamic programming to construct

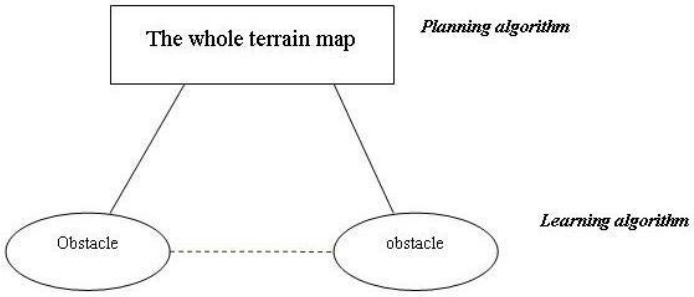

Figure 1. The framework of the the whole procedure of a virtual human's action in the 3D graphical environment.

a sample-based value function for actions.

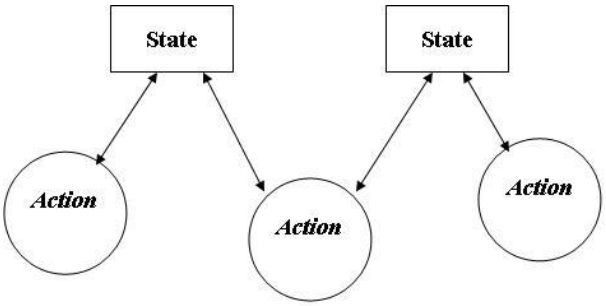

Figure 2. Every motion of a virtual human in the 3D graphical environment can be treated as a Semi-Markov Decision Process.

We will consider the action as a general class of random processes with trajectories in a metric space which are

	$DynamicProgramAlgorithm$
1	Q.Insert(Gx) and mark Gx as visited
2	while Q not empty do
3	x ← Q.GetFirst() //Get the priori queue
4	return SUCCESS
5	forall u-1 ∈ U-1(x)
6	x ← f-1(x', u-1)
7	if x not visited
8	Mark x as visited
9	Q.Insert(x)
10	else
11	Resolve duplicate x
12	return FAILURE

Table 1. The dynamic programming algorithm to update the value of action's policy.

continuous from the right and have limits from the left at any point of the half-line. These processes were continuous semi-Markov processes in according to the property of their first exit streams. The structure of the these processes of actions are showed on Figure 2 Thus, it is necessary to develop methods or to modernize traditional methods of investigation, which do not use the simple Markov property[12].

We can support value functions with to evaluate the actions' policy. Moreover, the above methods suffer from the limitation that the space of available motions is discrete. The parametric space is an abstract space defined by kinematic or physical attributes of motions. By parameterizing all motion samples in the space, and by blending among multiple motions, motion interpolation can create novel motions that have specific kinematic or physical attributes. We build a continuous parameterized motion space for similar motions that provide efficient control for interpolation.

To improve the action's policy π episode by episode, we adopt a value function Q and dynamic programm algorithm to achieve the goal Table 1[21].

To improve motion interpolation with the use of geometric statistics, treating interpolation as statistical prediction of missing data in the parametric space. We analyze interpolated human motions for physical correctness and show that the interpolated results are close to the physically correct motions. Cooper et al. proposed active learning to adaptively sample the parametric space so that the space can be well sampled with a reduced number of clips . Recently, researchers have also combined motion graphs with parametric synthesis to form richer, more complete motion spaces. In order to provide proper control, we present a way to learn parametric motion controllers, which can compute near-optimal parameters for motion synthesis for the 3D graphical environment in real-time.

3 Learning Algorithm on Manifold

In this section we describe a reinforcement learning framework to obtain motion controllers for interactive character animation. Using a database of atomic motion clips, our goal is to generate natural character motion as a sequence of clips. At each time step, the motion controller decides which motion clip best follows the user input and respects constraints imposed by the environment. This decision must be made quickly, since time lags are not allowed in interactive environments. The controller should also be able to achieve user objectives that require planning ahead of time. In addition, both user input and the environment should be represented using continuous parameters to allow for proper control.

We begin to introduce the Markov decision process (MDP) model for the control of the virtual human's action, and describe methods for approximately solving MDPs. This section is principally about choosing a basis for approximation of real-valued functions called value functions, which are central to solving Markov decision processes [13]. For in the most cases, previous work has modeled value functions as vectors in a Euclidean space to evaluate the action's policy π. One of the novel ideas is the approach to treat value functions as elements of a vector space on a graph or manifold [12]. This approach enables constructing basis functions that capture the large-scale (irregular) topology of the graph, and approximating (value) functions on these graphs by projecting them onto the space spanned by these bases.

A discrete Markov decision process (MDP) $M = (S, A, P^a_{s,s'}, R^a_{s,s'})$ is defined by a finite set of discrete states S, a finite set of actions A, a transition model $P^a_{s,s'}$ specifying the distribution over future states s' when an action a is performed in state s, and a corresponding reward model $R^a_{s,s'}$ specifying a scalar cost or reward [13].

Any optimal policy π defines the same unique optimal value function V which satisfies the nonlinear constraints:

$$V(s) = \max_a (R^a_{s,s'} + \gamma \sum_{s' \in S} P^a_{s,s'} V(s'))$$

where $Rsa = \sum_{s' \in S} P^a_{s,s'} R^a_{s,s'}$ is the expected immediate reward.

The Bellman operator T_π on the space of value function which is used to evaluate the policy π can be written as

$$T^\pi(V) = R_{s\pi(s)} + \gamma \sum_{s'} P^{\pi(s)}_{ss'} V(s')$$

Thus, the value function Vp associated with following a (deterministic) policy p can be defined as

$$V^\pi(s) = T(V^\pi(s)) = R_{s\pi(s)} + \gamma \sum_{s' \in S} P^{\pi(s)}_{ss'} V^\pi(s').$$

As it will be explained in the following part,in order to find the best policy π, we pose an optimization problem where the discrete values of temporal states are the variables. The goal of the optimization problem is to maximize the value function which requires determined by the states and actions, while enforcing the user's constraints.

Therefore, the question can be treated as a learning problem on a Riemannian manifold. There is a rich and well-developed theory of the Laplace operator on manifolds, which we can only briefly summarize here. The Laplace-Beltrami operator has been extensively studied in the general setting of Riemannian manifolds [16]. Riemannian manifolds have been actively studied recently in machine learning in several contexts, namely in the context of designing new types of kernels for supervised machine learning[17] and faster policy gradient methods using the natural Riemannian gradient on a space of parametric policies [18][19][20].

Although a full discussion of these perspectives is beyond this paper, they are worth noting in order to gain deeper insight into the many remarkable properties of the Laplacian.

The Laplacian is defined as

$$\Delta = divgrad = \frac{1}{\sqrt{\det g}} \sum_{i,j} \partial_i (\sqrt{\det g^{ij}} \partial_j)$$

where div and grad are the Riemannian divergence and gradient operators.

constraints in our optimization process. Detail vs. volume preservation. It is well known that the details of a shape at a point in space are preserved during a deformation if the local transformation that point undergoes is close to rigid.

To test our reinforcement learning algorithm's efficiency, we used a simulating environment in Matlab software.

This environment is based on Sutton and Barto's (1998)[21] Mountain Car Task as described in "Reinforcement Learning: An Introduction". This simulation program is running on the Matlab 7.02b as Figure 3 shows.

Consider a task where an agent must drive an underpowered car up a steep mountain road. Since gravity is stronger than the cars engine, even at full throttle the car cannot simply accelerate up the steep slope. The cars movement is described by two continuous output variables, position and velocity, and one discrete input representing the acceleration of the car.

In this application the state space S is naturally embedded in R_d as a sub-manifold, or some other type of geometrically structured subset. The shape of the manifold is showed in Figure 4.

The training used Q-learning algorithm in which the $\varepsilon - greedy$ policy should be used. We will randomly choose a 100 episode table to test the algorithm. The episodes will be truncated at 1000 time steps.

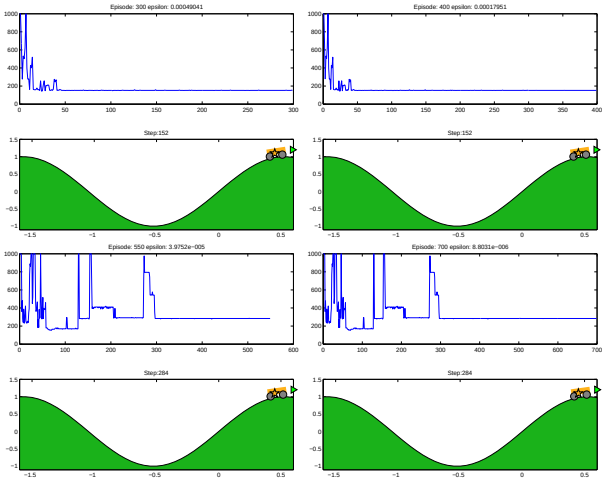

Figure 3. The clips of episodes of reinforcement learning training for the Mountain Car on the simulating software of Matlab. The up axes are representing the episode and steps and the down one is the animation clip of the simulation.

We used a Laplacian matrix as a window-based mask, i.e. it relies on a convolution mask to perform temporal filtering. We subtracted off all low frequency components from the original proto-value Qtable. Then we used high frequency edge descriptions to enhance the Qtable and compute a improved Qtable.

At the beginning, the Q table is all zero. After 100 episode training, we record a table. This table will be used in the two branches. One just keep on training without any change, the other will be transformed by laplace operator to improve the performances. The later's manifold shape shows in Figure 5.

Experimental results and comparisons with state-of-the-art methods are presented in Figure6 and Figure7. We will conclude all the result with a discussion and some future research directions in Section 5. In this section, we can make a conclusion that with the transformation for improving the Qtable, the improved one has a more stable and less steps training than original one. Moreover, the improved one's rewards are also better than original one.

4 Experimental Result

Our 3D graphical platform is the open source software : Delta3D.

Delta3D is an Open Source engine which can be used for games, simulations, or other graphical applications. Its modular design integrates other well-known Open Source

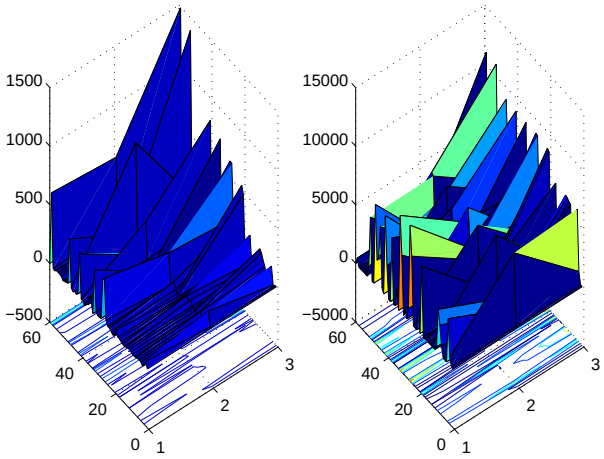

Figure 4. Qtable - The left one is the value function or Q function's manifold after 100 episode training, and the right one is it after 300 episode training.

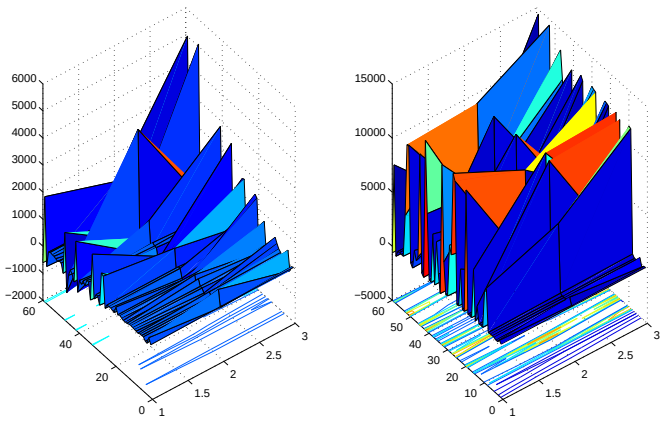

Figure 5. The Qtable Laplacian - The left one is the value function or Q function's manifold after 100 episodes training and laplacian improvement, and the right one is it after 300 episode training.

projects such as Open Scene Graph(OSG), Open Dynamics Engine(ODE), Character Animation Library (CAL3D), and OpenAL. Rather than bury the underlying modules, Delta3D just integrates them together in an easy-to-use API – always allowing access to the important underlying components. This provides a high-level API while still allowing the end user the optional, low-level functionality. Delta3D renders using OpenGL and imports a whole list of diverse file formats (.flt, .3ds, .obj, etc.).

Delta3D is released under the GNU Lesser General Public License (LGPL). The underlying modules may have their own licensing, but are at the minimum, considered Open Source and are freely distributable.

We used two virtual humans : "Cally" and "Paladin". Where they have a different ability and will behave differently to interact with the environments.

The task of the both avatars is to access the object (i.e. a beast), then interacts with it (i.e. shot a arrow to it).

The Cally and Paladin has different acting abilities and different absorb states which has been showed in Figure8, Figure9,Figure10 and Figure11.

The task of Cally and Paladin in a town is to access different kind of point to get reward. Cally can walk or jog to the object which show in the Figure12, and has two absorbing states which show in the Figure13. Paladin can walk, jog or sneak to the object which show in the Figure14, and has one absorbing state which shows in the Figure15.

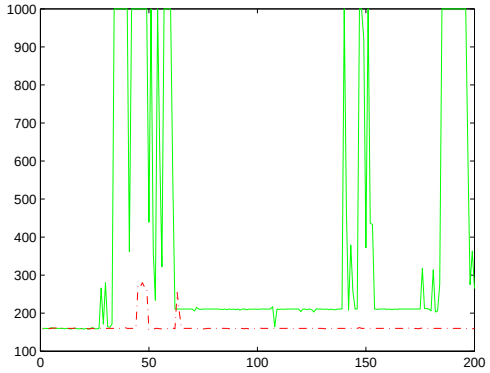

Figure 6. The steps (maximum is 1000) of training the Mountain Car. The green line is represented the Q function without any enhancement. And the red one is represented the Q table has been filtered by laplacian operator.

5 Conclusion and Discussion

This article presents a method for creating virtual human in the 3D graphical environment with learning ability on 3D animation. The example takes different 3D avatars which have different abilities to show different performance as the environment is dynamically changing. The result of blending actions animation presents that the virtual human has a more human-like behavior ,moreover intelligent ability to adapt the environment by learning ability.

We constructed a framework of controlling the motion of 3D human-like avatar by treating it as a Semi-Markov Decision Process.

By researching the reinforcement learning, we are able to choose the appropriate method to control the action of 3D human-like avatar. Besides, to treat the value function as a manifold which depends on the states and actions is proved to be a effective way to improve the Q function in the training process.

There are many opportunities to improve the techniques presented here. First, according to the shapes of manifold, there will be many powerful method to improve the performance of the learning algorithm. Second, if the virtual human can independently recognizes or classifies the objects and behaves in different way according to them, the system will be much better.

In this case, instead of making the animations frame by frame, the intelligent 3D avatar would be a powerful tools to achieve the work. Moreover, a more effective machine learning algorithm is one the key part of this area.

References

[1] Robert Osada, Thomas Funkhouser, Bernard Chazelle, and David Dobkin,Shape distributions, *ACM Transactions on Graphics*, Vol. 21, No. 4, October 2002, Page 807—832.

[2] Z.M. , D. Reidsma, A. Nijholt, Human Computing, Virtual Humans and Artificial Imperfection, *ICMI'06*, Page 179—184.

[3] Norman I.Badler, Cary B.Phillips, Bonnie Lynn Webber,*Simulating Humans: Computer Graphics Animation and Control*, 1993.

[4] T. Conde, D. Thalmann, An Integrated Perception for Autonomous Virtual Agents: Active and Predictive Perception, Computer Animation and Virtual Worlds, Volume 17, Issue 3-4, John Wiley, 2006

[5] Moccozet L, Thalmann N. M., Dirichlet Free-Form Deformation and their Application to Hand Simulation[J], *Proceedings Computer Animation97*, IEEE Computer Society, 1997, Page 93—102.

[6] Catherine Zanbaka1, Amy Ulinski, Paula Goolkasian, Larry F. Hodges, Social Responses to Virtual Humans: Implications for Future Interface Design, *CHI 2007 Proceedings*, Page 1561-1570.

[7] Edward M. Sims, Reusable, lifelike virtual humans for mentoring and role-playing, *Computers & Education*, 49 2007, Page 75-92.

[8] Lucio Ieronutti , Luca Chittaro, Employing virtual humans for education and training in X3D/VRML worlds, *Computers & Education*, Page 93-109.

[9] Weixiong Zhang, Randall W. Hill, Jr., A Template-Based and Pattern-Driven Approach to Situation Awareness and Assessment in Virtual Humans, *Agents*, 2000, Page 116—123.

[10] Z.M. , D. Reidsma, A. Nijholt, Human Computing, Virtual Humans and Artificial Imperfection, *ICMI'06*, Page 179—184.

[11] Sridhar Mahadevan: Fast Spectral Learning using Lanczos Eigenspace Projections. AAAI 2008, pp. 1472-1475.

[12] Sridhar Mahadevan and Mauro Maggioni, "Proto-Value Functions: A Laplacian Framework for Learning Representation and Control in Markov Decision Processes" , Journal of Machine Learning Research, pp. 2169—2231, vol. 8, 2007, MIT Press.

[13] M. L. Puterman. Markov decision processes. Wiley Interscience, New York, USA, 1994.

[14] A. Barto, and S. Mahadevan. Recent Advances in Hierarchical Reinforcement Learning. DiscreteEvent Systems: Theory and Applications, 13:41—77, 2003.

[15] F. Chung. Spectral Graph Theory. Number 92 in CBMS Regional Conference Series in Mathematics. American Mathematical Society, 1997.

[16] S Rosenberg. The Laplacian on a Riemannian Manifold. Cambridge University Press, 1997.

[17] J. Lafferty and G. Lebanon. Diffusion kernels on statistical manifolds. Journal of Machine Learning Research, 6:129—163, 2005.

[18] S. Kakade. A Natural Policy Gradient. In Proceedings of Neural Information Processing Systems. MIT Press, 2002.

[19] J. Bagnell and J. Schneider. Covariant policy search. In Proceedings of the International Joint Conference on Artificial Intelligence (IJCAI), pages 1019—1024, 2003.

[20] J. Peters, S. Vijaykumar, and S. Schaal. Reinforcement learning for humanoid robots. In Proceedings of the Third IEEE-RAS International Conference on Humanoid Robots, 2003.

[21] Sutton, R. S., and Barto, A. G. Reinforcement Learning C An Introduction. MIT Press, 1998.

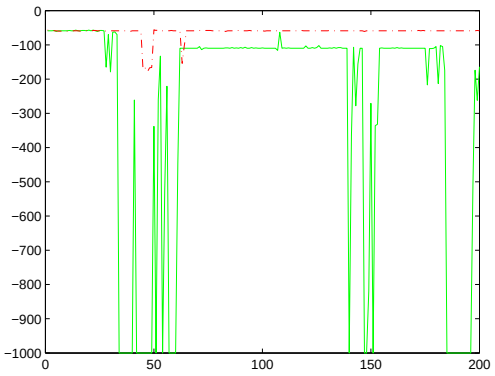

Figure 7. The rewards (every step without reaching the goal is -1, and with reaching the goal is 100) of training the Mountain Car. The green line is represented the value of Q function without any enhancement. And the red one is represented the Q table has been filtered by laplacian operator.

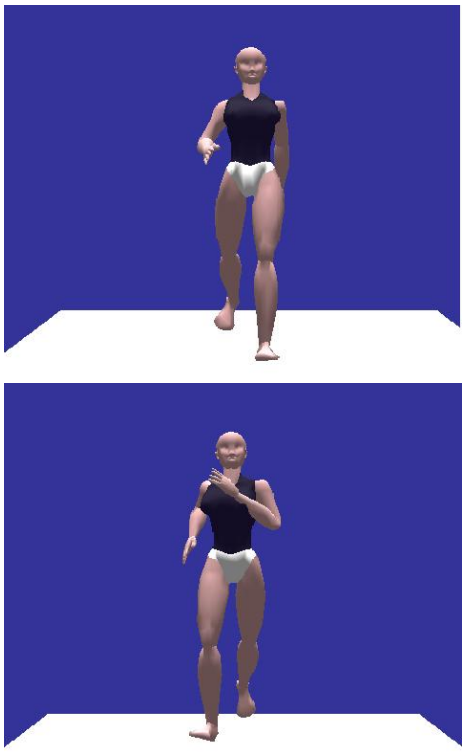

Figure 8. Cally has abilities of walk and jog to access the object. She has two different kinds of actions.

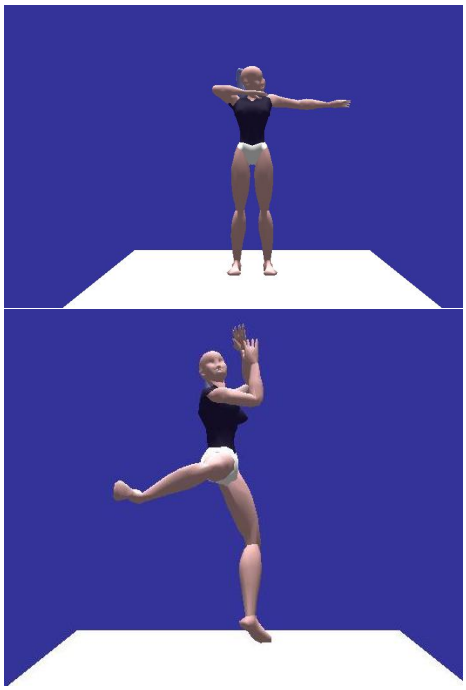

Figure 9. Cally has abilities of shotting an arrow and kicking the object. She has two different absorbing states.

Figure 10. Paladin has abilities of walk, jog and sneak to access the object. He has Three different actions.

Figure 11. Paladin has a ability of shotting the object. He has one absorbing state.

Figure 12. Cally 's typical action to access the object point in the town.

Figure 13. Cally chooses the action when reach the object point, if it is far, then she shot, otherwise, she will kick.

Figure 14. Paladin's typical action to access the object point in the town. Where the object is far, he walks, then he jogs, after that, he sneaks

Figure 15. Paladin reaches the proper position, then begin to shot.

Optimize write performance for DBMS on Solid State Drive

Yu Li

Abstract

Solid State Drive (SSD) is believed to be the replacement for magnetic disk in computer systems. SSD is a complex storage device composed of flash chips, controller hardware, and proprietary software that together provide a block device interface via a standard interconnect. Comparing to its fast sequential read/write and random read operations, the random write on SSD is generally believed to be poor. DBMS applications such as online transaction processing (OLTP) will suffer from it because of issuing random write stream to the storage. It is desirable to improve random write performance for these DBMS applications on SSD. Being different from previous solution in literature, we propose a solution which does not rely on modifying the firmware or hardware of SSD, but tries to decomposite the write streams of good write patterns from the archived write requests in a temporary focused area called StableBuffer. It is implemented as a software model called StableBuffer manager extending DBMS buffer manager. We discuss the motivation, design and implementation of StableBuffer manager, and report preliminary evaluation results.

1 Introduction

Solid State Drive (SSD) is believed to be the replacement for magnetic disk in computer systems. SSD is a complex storage device composed of flash chips (*i.e.*, NAND), controller hardware, and proprietary software (*i.e.*, firmware) that together provide a block device interface via a standard interconnect (*e.g.*, USB, IDE, SATA) [1]. Though it is made by assembling flash chips, the properties of SSD can not be easily derived from properties of flash chips. Because SSD read and write data in fixed sized blocks through a block interface, and integrates layers of software that manage block mapping(*i.e.*,, Flash Translation Layer, FTL), wear-leveling and error correction. In terms of IO performance, SSD does inherent characteristics of other flash storage media such as USB Flash memory and CompactFlash card. In general, sequential read/write and random read are believed to be fast on SSD, while random write on the other hand is believed to be slow.

The performance of random write of SSD is vital to DBMS applications such as online transaction processing (OLTP) . As often observed in OLTP applications, the access pattern to database is random and scattered with small granularity insert/delete/update requests, which cause the poor random write to be the bottleneck of whole system. Therefore, improve the overall write performance on SSD, especially when the write pattern trends to be random, is highly desired. In literature, Lee and Moon [10] studied this problem and proposed an in-page logging solution. The basic idea of in-page logging is that only write update logs inside the flash chip, and merge them with old data page when enough logs are collected. The in-page logging solution actually transfers random write stream to log appending stream which is naturally sequential. Even though lately merging logs into old data page costs extra resources, the transferred sequential logging appending stream actually save much more than random write stream. To implement the in-page logging mechanism, supporting from FTL, which is usually inside the firmware of SSD, is needed. However modifying the functions inside the firmware of SSD is not always possible to current commercial SSD products in market, which limits the in-page solution in practice.

Our focus in this paper is also to improve the write performance for DBMS applications. We try not to modify the firmware of SSD, and only to utilize the characteristics that SSD provides to developer. In the rest of this section, we describe the basic idea of our research by first introducing interesting characteristics of SSD as the motivation.

1.1 Good Write Patterns on SSD

Systematic performance studies [2, 6] show that the performance of IO on SSD is complex. It does not only sensitive to operation type (*i.e.*, read/write), but also sensitive to parameters such as access type (*i.e.*, sequential/random), granularity (*i.e.*, page size) and locality (*i.e.*, the distribution of addresses of accessed data). Recently a research work proposing a micro IO benchmark called uFlip for SSD by L. Bouganim et al [2] shows that, even different kinds of random write patterns perform different on SSD. They ac-

tually identified some good write patterns on SSD which could be considered as random. We will review them one by in following paragraphs.

1. *Random write limited to a focused area is fast.* A focused area is a small logical area of access addresses. For example, the space inside a pre-allocated small file smaller than 8MB can be viewed as a focused area. The size of a focus area is usually not bigger than the size of RAM in the controller of SSD. We name this kind of write pattern *focused random write*. According to result reported in uFlip paper, the response time of focused random write is only 1x$\sim$2x of the response time of sequential write, which is far better than the response time (17x$\sim$30x) of general random write to large area.

2. *Partitioned sequential write is fast.* As an example, write sequence "1[1],50,2,51,3,52,..." is an instance of partitioned sequential write pattern. It is similar to random write in global, but actually is mixture of two sequential write streams (*i.e.*, "1,2,3,..." and "50,51,52,..."). There are two sequential write streams, corresponding to two partitions. The response time of partitioned sequential write can be just 1x$\sim$2x of response time of sequential write, as long as there is not too many partitions (8$\sim$16).

3. *Ordered sequential write is fast.* As an example, the write sequence "1,3,5,7,9,11,..." is an instance of ordered sequential write pattern. The distance between addresses is $+2$. The distance could also be negative number, such as -2, such as the example "111,109,107,105,103,101...". The response time of ordered sequential write can be 1x$\sim$4x of response time of sequential write.

1.2 StableBuffer Idea

It is natural to thinkd about utilizing good write patterns (*i.e.*, sequential write, partitioned sequential write, ordered sequential write and clustered write patterns) to improve the write performance of SSD for DBMS applications. Suppose that we have several transactions concurrently committing pages to be written on SSD in an OLTP application. By only observing the combined write stream, it is generally random. So if we write pages one by one in their submission orders, the performance could be very poor. But actually some transactions may originally issue pages in good write pattern, or several write streams from different transactions may be combined to form instances of good write patterns. For instance, clustering pages by destination addresses may form focused random write stream. Then if we have the chance to delay each write request a little time, and collect enough write requests, we may either decomposite instances of good write patterns, or rearrange the write requests to follow good write patterns. Therefore we can only issue write requests to SSD by following good write patterns and the performance is improved.

However as the write requests are issued by online transactions, we usually have to flush them immediately to disk. Therefore we think about to write the pages temporarily first to a well managed place. In particular, we write them first to *StableBuffer*. StableBuffer is a temporary pre-allocated storage on SSD, and we limit it to be a focused area. In implementation, it can be implemented as small pre-allocated temporary file. Now with StableBuffer, the detailed process of writing a page will be

1. Page will be temporarily written to StableBuffer when it is issued. Since StableBuffer is a focused area, the temporarily write follows the focused random write pattern. And we keep some in memory data structures to record the temporarily write.

2. After we collect enough pages (usually when the StableBuffer is full), we decomposite some instance of good write pattern from StableBuffer. Pages of this instance will be read from StableBuffer and write again to their real destinations. The involved read request is a random read. The involved write request follows good write pattern.

We can roughly estimate the cost of write one page through StableBuffer. We denote the cost of sequentially writing one page as C. To flush one page to its destination through StableBuffer, there are two writes following good write patterns on SSD. According to the uFlip result, the cost is at most $4 \times C \times 2 = 8C$. There is another random read. But random read is even faster than sequential write on SSD. We at most add C cost to the total most, which is $C + 8C + C = 9C$. Now consider that we directly flush the page to SSD. Since it could follow a random write pattern, the cost could be as big as $13C \sim 30C$ according to the result of uFlip paper. We can easily notice that, although it writes same page twice, the StableBuffer idea is still able to improve the overall performance.

It is remarkable that the StableBuffer idea does not require modification on firmware and hardware of SSD. We can implement it as a software model inside the buffer manager of DBMS, which is the focus of our current research. In the rest of this paper, we discuss the design of StableBuffer manager in section 2 and 3. After that, we present some preliminary evaluation result in section 4 and list the related work in section 5. Finally, we conclude the paper in section 6.

[1]We use simple number to denote the logical address of a page.

2 System Overview

Fig. 1 gives an overview of the StableBuffer manager. It is an extension of traditional DBMS buffer manager. New components such as *StableBuffer*, *StableBuffer Translation Table* and *Write Stream Decompositors* are added.

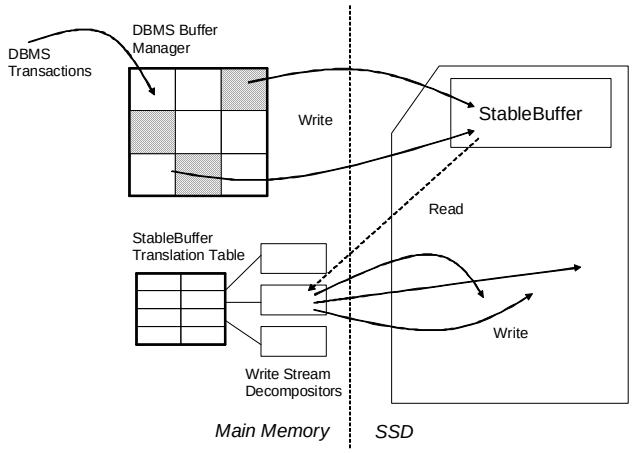

Figure 1: The System Overview of StableBuffer Manager

1. *StableBuffer* is an pre-allocated focused area on SSD. It is usually implemented as small pre-allocated temporary file. The size of the StableBuffer should not exceeds the size of the RAM in the controller of SSD. For example, in a 16GB MTron MSD-SATA-3525 SSD, the size should be less than 8MB. The StableBuffer will be accessed in the granularity of pages, which has the same size as pages in buffer manager of DBMS.

2. *StableBuffer Translation Table* is a data structure maintaining the mapping between the offset of page inside the StableBuffer and the destination address. For example, if a page is issued to write to address `12345678AB` but now temporarily written to the `32`th slot of StableBuffer, a mapping entry "`<12345678AB, 32>`" is inserted into StableBuffer Translation Table. In order to facility fast lookup, insert and delete, StableBuffer Translation Table can be implemented as a hash table.

3. *Write Stream Decompositors* are programs finding instances of good write patterns. They run in concurrent threads, scan the entries of StableBuffer Translation Table and try to decomposite instances of good write patterns. When StableBuffer runs out of slots, some instance of good write patterns will be selected to be read its pages from StableBuffer and then written to their destinations. Thus some of the slots of StableBuffer will be freed for new coming pages.

Now we elaborate how a page is written through StableBuffer manager. Consider that a dirty page is issued by a transaction (as you can see in up left corner of Fig. 1). First it goes through a traditional DBMS buffer manager and may result as a random write to SSD. When we get the write request, we try to write the page to StableBuffer (shown in up center of Fig. 1). If we find a free slot in StableBuffer, the page is written and a new mapping entry will be inserted into StableBuffer Translation Table. Otherwise, we have to free some slots of StableBuffer first. The Write Stream Decompositors will be examined one by one to select an instance of good write patterns (the details will be discussed in section 3). With an instance, we read its pages from StableBuffer, write them to their destinations according to the mapping entries in StableBuffer Translation Table. After that we delete these entries from StableBuffer Translation Table. Now we have free slots of StableBuffer and can write the issued page to it. In either case, we only write pages to StableBuffer, which is a focused area, or write pages in good write patterns. Though we pay extra IO and computation cost in managing StableBuffer, it is still could be better than directly write pages in the order they are issued.

Notice that when write a page into StableBuffer, besides inserting mapping entry to StableBuffer Translation Table, its destination address and a timestamp should also be embedded into the metadata of the page. This is to serve the recovery of StableBuffer Translation Table after the system crush. For a page at offset O whose destination address is D, by comparing its timestamp T to the latest update time T_0 of page at destination D, we know whether the page is swapped out from StableBuffer. In detail, if $T > T_0$, the page is not swapped out yet. Therefore we can insert a mapping entry "$<D, O>$" to StableBuffer Translation Table. Otherwise (*i.e.*, $T \leq T_0$), since the page is already swapped out, we can mark the Oth slot of StableBuffer as free.

Because pages could be temporary stored in StableBuffer, we have to query StableBuffer when answer the request of retrieving page by transaction through DBMS buffer manager. In detail, when get a request of retrieving some page at D, first we need to check whether there is an entry "$<D, O>$" in StableBuffer Translation Table. If there is, we read page at Oth slot in StableBuffer and return it. Otherwise we issue a read request to SSD for the page at D. By implementing StableBuffer Translation Table as a hash table on D, this query to StableBuffer is efficient and will not harm overall performance.

3 Write Stream Decompositors

Fig. 2 illustrates how write stream decompositors work in StableBuffer manager. Write Stream Decompositors are programs which scan the entries of StableBuffer Transla-

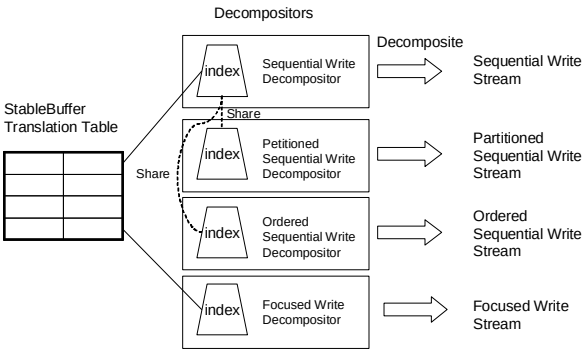

Figure 2: The Framework of Decompositors

tion Table for instances of good write patterns. They are designed to work concurrently, and may identify different instances of different good write patterns sharing same set of entries. They may require local data structures to track on relevant information of entries in StableBuffer Translation Table. For example, a sequential write decompositor may build a search tree index on destination addresses of mapping entries to facility the searching process. These data structures can be viewed as an index on entries of StableBuffer Translation Table. Some decompositor can share other's index to save the system recourses. E.g., partitioned sequential write can reuse the index of sequential write decompositor to search sequential write instances. As every index should be updated whenever insert/delete entry to/from StableBuffer Translation Table, sharing index between decompositors can save both computation resource and memory.

With multiple instances of good write patterns, selecting which instance to swap out from StableBuffer becomes a non-trivial problem. Intuitively, we trend to select the instance of write pattern which performs the best on SSD. For example, if there are instances of sequential write and focused random write pattern, we should select the instance of sequential write, because the performance of sequential write is usually better than focused random write. On the other hand, how many slots the instance can free from StableBuffer is also important. The reasons are: First the write sequence of local short instances of good write patterns could be random in global. For example, consider the write sequence "1,2,56,57,6,7,42,43,3,4,...". It is random in global, but actually could be generated by every time selecting instance of sequential write with two pages, *i.e.*, "1,2", "56,57", "6,7", "42,43", "3,4" and so on. Second selecting short instances may cause frequent demands on freeing slots for new write requests because each time few slots can be freed. Since updating StableBuffer Translation Table and indices does consume system resources, these frequent demands could cause a degeneration on overall performance. Therefore, in our solution, we select the instances $\{I_i\}$ of different write patterns $\{P_i\}$ based on formula 1,

$$min\{\frac{T_i}{L_i}\} \quad (1)$$

where T_i is average time needed to write single page of the write pattern P_i and L_i is the size of I_i. In particular, we will select the instance with fastest write speed and biggest size.

In our system, we propose four write stream decompositors, corresponding to four good write patterns described in section 1. Following we will discuss the function, design and implementation of them one by one.

Sequential Write Decompositor

This decompositor maintains a search tree index on the destination addresses of mapping entries. The decompositor scans the index in the ascending order of destination addresses to find continuous subsequences on destination address. Each continuous subsequence is corresponding to an instance of sequential write. Finally the largest continuous subsequence will be return as the decomposition result.

Partitioned Write Decompositor

Partitioned write stream is a group of instances of sequential write with same length, so it can share the search tree index of Sequential Write Decompositor. When to decomposite, the Partitioned Write Decompositor first finds continuous subsequences similar to Sequential Write Decompositor. After that, it groups continuous subsequences according to their lengths. Any group with two or more continuous subsequences is then an instance of partitioned write. The largest group will be return as the decomposition result.

Ordered Write Decompositor

Ordered write differs from sequential write in that there is fix distance between destination addresses. But it can also reuse the search tree index of Sequential Write Decompositor. When scan the entries, we try to find not the continuous subsequence, but subsequence with even distance between destination addresses. Finally the largest subsequence will be returned as the decomposition result.

Focused Write Decompositor

Focused Write Decompositor searches for clusters of entries whose destination addresses are focused in small area. It maintains a hash index of entries of StableBuffer Translation Table. In detial, given an entry "$< D, O >$", it will be hashed into bucket $\lfloor D/M \rfloor$, where M is the upper bound of size of focused area of the SSD. It is clear that either a page cluster is inside a bucket, or at most expands to two sibling buckets. When to decomposite, we can efficiently find the

biggest cluster by scanning the buckets in ascending order. The biggest cluster will be returned as the decomposition result.

4 Preliminary Performance Evaluation

We have implemented a prototype StableBuffer manager on top of a Windows desktop PC equipped a 16GB MTron MSD-SATA-3525 SSD. In the prototype, StableBuffer is implemented as a pre-allocated temporary file with the size not exceeding 8MB, and it is accessed with a page oriented interface. The prototype can read write stream from write trace file. All four kinds of decompositors described in section 3 are implemented.

In our preliminary performance evaluation, we use the write trace from Oracle 11g DBMS running TPC-C benchmark. The benchmark simulates an enterprise OLTP retailing application, which processes transactions keeping insert/delete/update records from a 8GB database. Therefore the write addresses in write trace expand from 0 to 8GB. In total there are 488623 write requests in our write trace for testing. The page size is set to be 4KB, and the StableBuffer is configured to be 8MB, corresponding to 2048 pages.

We compare the performance of StableBuffer with the Direct method, which processes write requests one by one in their appearing order in the trace file. Fig. 3 shows the evaluation result. We can see that there is a 1.5x performance gain with StableBuffer against Direct.

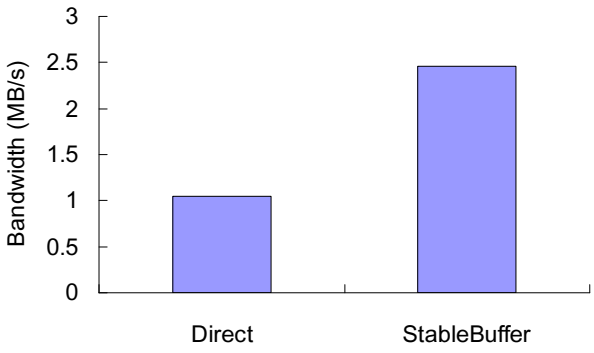

Figure 3: Evaluation result on Oracle 11g TPC-C Trace

5 Related Work

Database management on flash-based storage media has attracted increasing research attention in recent years. Early work focused on assembling flash chips to simulate traditional hard disk [8, 4, 9] and guaranteeing long life span of data [3, 5, 9]. Recent research work starts to tune DBMSs to meet the characteristics of flash disks for a better performance. In view of the asymmetric read/write speed and the erase-before-write limitation, Wu et al. [14] proposed log-based indexing scheme for flash memory. Observing that the log-based indexing scheme is not suitable for read-intensive workload on some flash devices, Nath and Kansal [12] developed an adaptive indexing method that adapts to the workload and storage device. Lee and Moon [10] presented a novel storage design called in-page logging (IPL) for DBMS in order to overcome the possible write issues. S. Chen [7] investigated exploiting flash devices to improve the synchronous logging performance of DBMS.

More recently there are more and more research works focus on improving DBMS performance on Solid State Drive. Agrawal et al. [1] first published a paper on revealing the internal architecture showing that the SSD is indeed very different devices comparing to simple flash-based disks, such as USB flash memory, Compact Flash card and Secure Disk card. uFLIP by Bouganim et al. [2] proposes a microbench mark to help researchers systematically understanding flash IO pattern on SSD. It also provides several interesting hints on the best practices when write pages on SSD in the conclusion part. In parallel, Feng et al. [6] did a similar work to Bouganim. In their work they also point out that fragmentation can cause unignorable performance degeneration. [11] investigated how the performance of standard DBMS algorithm is affected when the conventional magnetic disk is replaced by SSD. [13] presented fast scanning and joining method for relational DBMS on SSD.

6 Conclusion

We focus our study on overcoming poor random write performance of SSD for DBMS applications. Different from previous research work, we propose the StableBuffer solution which does not rely on modifying the firmware or hardware of SSD. It is motivated by systematic study of IO performance of various write patterns on SSD. The basic idea is to decomposite the write streams of good write patterns after archiving the write requests into a temporary focused area called StableBuffer. It is implemented as a software model inside DBMS buffer manager. Preliminary evaluation result shows that there is 1.5x performance gain with StableBuffer manager on TPC-C benchmark trace.

References

[1] N. Agrawal, V. Prabhakaran, T. Wobber, J. D. Davis, M. Manasse, and R. Panigrahy. Design tradeoffs for ssd performance. In *ATC'08*, pages 57–70. USENIX Association, 2008.

[2] L. Bouganim, B. T. Jónsson, and P. Bonnet. uflip: Understanding flash io patterns. In *CIDR*, 2009.

[3] L. Chang. On efficient wear leveling for large-scale flash-memory storage systems. In *SAC'07*, pages 1126–1130, 2007.

[4] L. Chang, T. Kuo, and S. Lo. Real-time garbage collection for flash-memory storage systems of real-time embedded systems. *Trans. on Embedded Computing Sys.*, 3(4):837–863, 2004.

[5] Y. Chang, J. Hsieh, and T. Kuo. Endurance enhancement of flash-memory storage systems: an efficient static wear leveling design. In *DAC'07*, pages 212–217, 2007.

[6] F. Chen, D. A. Koufaty, and X. Zhang. Understanding intrinsic characteristics and system implications of flash memory based solid state drives. In *SIGMETRICS '09*, pages 181–192. ACM, 2009.

[7] S. Chen. Flashlogging: exploiting flash devices for synchronous logging performance. In *SIGMOD '09*, pages 73–86. ACM, 2009.

[8] A. Kawaguchi, S. Nishioka, and H. Motoda. A flash-memory based file system. In *USENIX Winter*, pages 155–164, 1995.

[9] H. Kim and S. Lee. A new flash memory management for flash storage system. In *COMPSAC'99*, page 284, 1999.

[10] S. Lee and B. Moon. Design of flash-based dbms: an in-page logging approach. In *SIGMOD '07*, pages 55–66, 2007.

[11] S.-W. Lee, B. Moon, C. Park, J.-M. Kim, and S.-W. Kim. A case for flash memory ssd in enterprise database applications. In *SIGMOD*, pages 1075–1086, 2008.

[12] S. Nath and A. Kansal. Flashdb: Dynamic self-tuning database for nand flash. Technical Report MSR-TR-2006-168, Microsoft Research, 2006.

[13] D. Tsirogiannis, S. Harizopoulos, M. A. Shah, J. L. Wiener, and G. Graefe. Query processing techniques for solid state drives. In *SIGMOD '09*, pages 59–72. ACM, 2009.

[14] C. Wu, T. Kuo, and L. P. Chang. An efficient b-tree layer implementation for flash-memory storage systems. *Trans. on Embedded Computing Sys.*, 6(3):19, 2007.

Cooperative Stochastic Differential Game in P2P Content Distribution Networks

Xiaowei Chen

Abstract

Pareto-optimal resource allocation is one of the major goals in game-theoretic solutions for peer-to-peer content distribution network. These solutions have been designed that force the participants to behave more cooperatively to reach the overall efficiency as well as individual efficiency of a distributed system. But there exist many issues when these solutions are applied in stochastic differential environment which is more realistic. In this paper, we propose an incentive framework based on cooperative stochastic differential game. In this framework, peers can cooperate with each other and get Pareto-optimal bandwidth allocation without any binding agreements. We prove the payoff distribution procedure can achieve dynamic Shapley value by using equilibrating transitory compensation during peers' cooperation and make peers follow the original optimality principle and cooperative state trajectory path. Our incentive framework is more flexible and realistic than previous game-theoretic solutions. It can build cooperation relationship in stochastic dynamic peer-to-peer network without the limitation of time consistency.

1. Introduction

The Peer-to-Peer (P2P) paradigm offers obvious advantages for the fast distribution of large content in the Internet. As reported in an ipoque report [1] in 2009, P2P generates most traffic in all regions. Just as in previous years, and BitTorrent is the dominating P2P protocol followed by HTTP in all regions but South America (There is another P2P protocol which leads the pack before BitTorrent and eDonkey in South America).

Though the swarming principle supports P2P content distribution protocol in a non-cooperative environment and exploits the two-way interest of peers in different blocks which the other one provides, the cooperation of peers is not a matter of course. Most of the peers behave selfishly and are interested in maximizing their own download rates, the mutual interest results in peers, which bargain for bandwidth with each other. P2P faces the problem of free-riding [2] where peers consume resources solely without contributing anything to the network. Therefore, reputation systems and/or incentive mechanisms are implemented in P2P applications frequently.

A very popular example is the BitTorrent protocol [3] where a peer uploads to others from which it receives the highest download rates. This strategy is inspired by the tit-for-tat principle that is well known from game theory. Here, a player adopts the strategy, which his opponent used in the previous round. By cooperating in the first step the tit-for-tat strategy proved very effective in the repeated prisoner's dilemma [4].

Unfortunately, simulation-based studies for BitTorrent reveal a high variability in the download rates [5] and unfairness in terms of the ratio of uploaded to downloaded data [6]. Tit-for-tat strategy may look beneficial from a local perspective, but from a more global perspective, they are not effective. Piatek [7] shows that increased upload contribution only marginally improves download rates, and peers have no reason to contribute once they have satisfied their immediate demands.

These results lead to two questions. Firstly, from the user perspective: Does another strategy exist which outperforms BitTorrent's tit-for-tat strategy? This means with such kind of strategy a user can fairly increase its download performance according to it upload performance. Secondly, from the angle of a protocol designer: Does a strategy exist which ensures fairness between peers although peers behave selfishly?

Users in a P2P social network are strategic and rational, and they are likely to manipulate any incentive systems to maximize their own payoff. They will even cheat if they believe it could help maximize their payoff. Hence, game theory is a proper tool to model the interaction among peers, and to analyze the optimal and cheat-proof cooperation strategies. But there exist many issues when the proposed solutions are applied in stochastic differential environment which is more realistic.

Our work tries to answer the above two questions based on game theory. We design an incentive framework based on cooperative stochastic differential game to achieve Pareto-optimal bandwidth allocation fairly without any binding agreements. Our contributions are:

- We analyze the root issue of BitTorrent tit-for-tat strategy from game theory prospective and reveal the reason that why this strategy cannot achieve its original goal.
- We clearly define the basic elements of game theory from P2P content distribution network's prospective, which lay a solid foundation to help us explore the essence of incentive framework based on game theory in P2P content distribution network.
- We present a general incentive framework based on cooperative stochastic differential game. It adopts an analytically tractable "payoff distribution procedure" which would lead to subgame-consistent solutions. We prove the payoff distribution procedure can achieve dynamic Shapley value by using equilibrating transitory compensation during peers' cooperation and make peers follow the original optimality principle and cooperative state trajectory path.

1.1 Related work

We now briefly present some related work. Micro-payment [8] is probably the earliest work on designing incentive protocol for P2P networks. It relies on a centralized server and uses virtual currency to provide incentive for resource sharing. Since then, much efforts are focused on incentive mechanisms for P2P systems [9] and wireless networks [10]. Vishnumurthy [11] shows that shared history based incentives can overcome the scalability problem of private history based mechanisms and one can use DHT to implement the shared history incentive mechanism. One shared history based incentive is the reciprocative strategy [12]. It makes decisions according to the reputation of requesters and is studied via simulation only.

There are some existing works on designing a particular incentive mechanism. Feldman [13] assumes that each peer has a fixed strategy with a certain distribution while we assume peers can adapt their strategies. In [14], authors show that a proportional strategy can lead to market equilibria but the result does not generalize to multiple strategies.

Pareto-optimal resource allocation is one of the major goals in game-theoretic solutions for peer-to-peer content distribution network. The above solutions have been designed that force the participants to behave more cooperatively to reach the overall efficiency as well as individual efficiency of a distributed system. But there exist many issues when these solutions are applied in stochastic differential environment which is more realistic. Our paper focuses on the incentive mechanism design in cooperative stochastic differential environment in P2P content distribution systems.

1.2 Paper organization

The balance of the paper is organized as follows. In section 2, we analyze the root issue of tit-for-tat strategy and reveal the reason that why this strategy cannot achieve its original goal. In section 3, we clearly define the basic elements and their properties of game theory from P2P content distribution network's view. In section 4, we present a general incentive framework based on cooperative stochastic differential game and prove its effectiveness. Finally, section 5 concludes this paper.

2. Analysis of Tit-for-Tat Strategy

From section 1, we know that the swarming principle supports P2P content distribution protocol in a non-cooperative environment. But under non-cooperative environment, the profit of each peer and whole system will be far away from Pareto-optimality, even hurting each other. The result must be "solitary, poor, nasty, brutish and shot" [15]. The difficulty of cooperation is rooted from free-riding problem in many situations. As a matter of fact, the reason is the temporary profit of each peer exits conflicts.

Based on this analysis, many researchers induct game theory as tool to solve this problem. Because static non-cooperative game often leads to lose-lose situation, so the static cooperative game which can build Pareto-optimality is applied in P2P systems. But there is an assumption in static cooperative game that peers can meet a binding agreement. Actually, whether there is a binding agreement is the watershed between non-cooperative game and cooperative game. The Shapley value in cooperative game is a very important solution which can create a unique fairly profit distribution which can achieve Pareto-optimality. Unfortunately, binding agreement has not one hundred percent sanction in real P2P systems. There always exist conflicts between individual rationality and group rationality.

Under this circumstance, strategic conflict resolution becomes a way of building cooperation in non-cooperative P2P environment. We realize that repeated game still can bring on Tragedy of Common, but there can exist cooperation in infinite repeated game. The most used strategy is tit-for-tat which is implemented in BitTorrent protocol. Here we should be noted that infinite repeated game is a very special game model which often does not exist in real P2P systems. That is why the tit-for-tat strategy often cannot achieve fairness bandwidth allocation.

On one hand, since peers interact in time and decisions generally lead to effects over time, it is only a slight exaggeration to claim that "P2P content distribution is a dynamic game". Dynamic or differential game investigates interactive decision making over time. On the other hand, the dynamic cooperation among pees often changes stochastically. For example, there are unstable network bandwidth and unexpected lost connection among peers, etc. Yeung [16] introduced the paradigm of randomly-furcating stochastic differential games to make it possible to study stochastic elements via branching payoffs under the format of differential games.

Cooperative games hold out the promise of socially optimal and group efficient solutions to problems involving strategic actions. Formulation of optimal peer behavior is a fundamental element. In dynamic cooperative games, a stringent condition on cooperation and agreement is required: In the solution, the optimality principle must remain optimal throughout the game, at any instant of time along the optimal state trajectory determined at the outset. This condition is known as dynamic stability or time consistency. In other words, dynamic stability of solutions to any cooperative differential game involved the property that, as the game proceeds along an optimal trajectory, players are guided by the same optimality principle at each instant of time, and hence do not possess incentives to deviate from the previously adopted optimal behavior throughout the game.

In the presence of stochastic elements, a more stringent condition, subgame consistency, is required for a credible cooperative solution. In particular, a cooperative solution is subgame-consistent if an extension of the solution policy to a situation with a later starting time and any feasible state brought about by prior optimal behavior would remain optimal. Along with Yeung and Petrosyan's significant breakthrough in

the study of cooperative stochastic differential games [17], we propose an incentive framework based on their contributions and apply it in P2P content distribution networks.

Before we introduce our incentive framework, we need to define the basic elements of game theory from P2P content distribution network's prospective to lay a solid foundation and help us explore the essence of incentive framework based on game theory.

3. Basic Elements of Game Theory

In P2P content distribution environment, we need provide clear definition of the following basic elements in game theory: player, action, information, strategy, payoff, rationality, objective, order of play, outcome and equilibrium.

Definition 1. *Player* is peer which can make decisions in P2P content distribution.

Player must have more than one action to be selected. Normally, there are at least two peers in P2P content distribution. Except player, there can exist pseudo-player, namely, nature. *Nature* is a player or mechanism without objective. It will randomly choose action as pre-defined probability.

In general, player is assumed as rational.

Definition 2: *Action* is decision variable of player in a specific time point. We use $a_i \in A_i$ denotes a specific action of *i*-th player. A_i denotes the action sets that the player can select.

The action of player can be discrete or continuous. In P2P content distribution networks, we can view it as the bandwidth that a peer wants to upload.

Definition 3: *Information* is knowledge of peer in P2P content distribution game. We use information set to describe information. In game theory, an *information set* is a set that, for a particular player, establishes all the possible moves that could have taken place in the game so far, given what that player has observed so far.

If the game has *perfect information*, every information set contains only one member, namely the point actually reached at that stage of the game. Otherwise, it is *imperfect information* that some players cannot be sure exactly what has taken place so far in the game and what their position is.

An item of information in a game is *common knowledge* if all of the players know it (it is mutual knowledge) and all of the players know that all other players know it and all other players know that all other players know that all other players know it, and so on.

Complete information requires that every player know the strategies and payoffs of the other players but not necessarily the actions. If and only if the type, strategy space and payoff function of each peer are all common knowledge, we call the game has complete information, otherwise, it has incomplete information. We assume the information in a game is complete. If not, we can use Harsanyi Transformation which adds *nature* as a player in the game to make an incomplete information game transform as a complete but imperfect information game, or Bayesian game.

Definition 4: A player's *strategy* in a game is a complete plan of action for whatever situation might arise; this fully determines the player's behavior. A player's strategy will determine the action the player will take at any stage of the game, for every possible history of play up to that stage.

There are two kinds of strategies: pure strategy and mixed strategy. A pure strategy provides a complete definition of how a player will play a game. A mixed strategy is an assignment of a probability to each pure strategy. This allows for a player to randomly select a pure strategy.

We use $s_i \in S_i$ denotes a specific strategy of *i*-th player. S_i denotes the strategy set or strategy space.

Definition 5: *Payoffs* are numbers which represent the motivations of players. Payoffs may represent profit, quantity, "utility," or other continuous measures, or may simply rank the desirability of outcomes. In P2P content distribution networks, payoff of a peer is the download bandwidth of a peer. We use u_i denotes payoff of *i*-th player.

Definition 6: *Rationality* implies that every player is motivated by maximizing his own payoff. In a stricter sense, it implies that every player always maximizes his utility, thus being able to perfectly calculate the probabilistic result of every action. Rationality can be classified as individual rationality and group rationality.

Definition 7: If each player's preference can be represented as expected payoff function, then player has a clear and definite *objective* that optimizes its payoff function by strategy or choosing actions.

Definition 8: In game theory, each player has time point to select action. These time points are called decision nodes. Decision nodes can have sequence which is called as *order of play*. In differential game, players can take actions simultaneously or with sequential order.

Definition 9: *Outcome* is a set of moves or strategies taken by the players, or their payoffs resulting from the actions or strategies taken by all players.

Definition 10: *Equilibrium* is the combination of optimal strategies among all players. In an equilibrium, each player of the game has adopted a strategy that they are unlikely to change. We use s_i^* denotes optimal strategy of *i*-th player.

4. Cooperative Stochastic Differential Game

4.1 Incentive Framework

The balance of the According to Yeung [16] and [17], we know that the dynamic stability of a solution of a cooperative differential game is the property that, when the game proceeds along an optimal trajectory, at each instant of time the players are guided by the same optimality principles, and hence do not have any ground for deviation from the previously adopted "optimal" behavior throughout the game.

In the presence of stochastic elements, a more stringent condition, subgame consistency, is required for a credible cooperative solution. A cooperative solution is subgame consistent if an extension of the solution policy to a situation

with a later starting time and any feasible state brought about by prior optimal behaviors would remain optimal.

Consider the cooperative game $\Gamma_c(x_0, T-t_0)$ in which the players agree to act to maximize their joint payoff and adopt a certain mechanism governing the sharing of the players' payoffs. t_0 and x_0 are start time and start state. To achieve group rationality, the players adopt the cooperative controls $[\psi_1^{(t_0)*}(t,x), \psi_2^{(t_0)*}(t,x)]$. A set of controls $[\psi_1^{(t_0)*}(t,x), \psi_2^{(t_0)*}(t,x)]$ provides an optimal solution to the stochastic control problem $\Psi(x_0, T-t_0)$. The optimal cooperative state trajectory follows the stochastic path $\{x^*(s)\}_{s=t_0}^{T}$.

At time t_0, with the state being x_0, the term $\xi^{(t_0)i}(t_0, x_0)$ denotes the expected share/imputation of total cooperative payoff (received over the time interval [t_0, T]) to player i guided by the agreed-upon optimality principle.

Now, consider the cooperative game $\Gamma_c(x_\tau^*, T-\tau)$ in which the game starts at time $\tau \in [t_0, T]$ with initial state $x_\tau^* \in X_\tau^*$, and the same agreed-upon optimality principle as above is adopted. Let $\xi^{(\tau)i}(\tau, x_\tau^*)$ denote the expected share/imputation of total cooperative payoff given to player i over the time interval [τ, T].

Following Yeung and Petrosyan [17], we formulate a payoff distribution over time so that the agreed imputations can be realized. Let the vectors $B^\tau(s) = [B_1^\tau(s), B_2^\tau(s)]$ denote the instantaneous payoff of the cooperative game at time $s \in [\tau, T]$ for the cooperative game $\Gamma_c(x_\tau^*, T-\tau)$. In other words, player i, for $i \in \{1, 2\}$, obtains a payoff equaling $B_i^\tau(s)$ at time instant s. A terminal value of $q^i(x^*(T))$ is received by player i at time T.

In particular, $B_i^\tau(s)$ and $q^i(x^*(T))$ constitute a Payoff Distribution Procedure (PDP) for the game $\Gamma_c(x_\tau^*, T-\tau)$. $B_i^\tau(s)$ is equilibrating transitory compensation, $q^i(x^*(T))$ is optimal terminal value. Subgame consistency guarantees that the solution imputations throughout the game interval in the sense that the extension of the solution policy to a situation with a later starting time and any feasible state brought about by prior optimal behaviors would remain optimal. Equilibrating transitory compensation is developed for the implementation of subgame consistency cooperation scheme.

In stochastic environment, the compensation $B_i(\tau)$ player i receives at time τ given the state $x_\tau^* \in X_\tau^*$ is the sum of

(*i*) Player *i*'s agreed upon marginal share of total expected cooperative profit,

(*ii*) Player *i*'s agreed upon marginal share of his own expected non-cooperative profit plus the instantaneous effect on his non-cooperative expected payoff when the change in the state variable x_τ^* follows the cooperative trajectory instead of the non-cooperative path, and

(*iii*) Player *i*'s agreed upon marginal share of Player *j*'s non-cooperative profit plus the instantaneous effect on Player *j*'s non-cooperative payoff when the change in the state variable *x* follows the optimal trajectory instead of the non-cooperative path.

In P2P content distribution networks, consider the scenario in which *n* peers, and peer *i*'s objective is:

$$E_{t_0}\{\int_{t_0}^{T} g^i[s, x_i(s), u_i(s)]\exp[-\int_{t_0}^{s} r(y)dy]ds + \exp[-\int_{t_0}^{s} r(y)dy]q^i(x_i(T))\} \quad \text{for} \quad \text{for } i \in [1, 2, \ldots, n] \equiv N,\ g^i(\bullet) \geq 0, q^i(\bullet) \geq 0 \tag{1}$$

where $x_i(s) \in X_i$ denotes the current bandwidth of peer *i*, $u_i \in U^i$ is the control vector of peer *i*, denotes the upload bandwidth of peer *i* can provide, $\exp[-\int_{t_0}^{s} r(y)dy]$ is discount factor which can be viewed as a peer's opportunity cost, and $q^i(x_i(T))$ is the terminal payoff which can be viewed as the future potential current value (bandwidth) in terminal time. $g^i[s, x_i(s), u_i(s)]$ denotes the instantaneous bandwidth that peer *i* can get. In particular, $g^i[s, x_i(s), u_i(s)]$ and $q^i(x_i)$ are positively related to x_i.

The state dynamics of the game is characterized by the set of vector-valued stochastic differential equations:

$$dx_i(s) = f^i[s, x_i(s), u_i(s)]ds + \sigma[s, x_i(s)]dz_i(s), \quad x_i(t_0) = x_i^0 \tag{2}$$

where $\sigma[s, x_i(s)]$ is a $m_i \times \Theta_i$ matrix, and $z_i(s)$ is a Θ_i - dimensional Wiener process and the initial state x_i^0 is given. Let $\Omega_i[s, x_i(s)] = \sigma[s, x_i(s)]\sigma[s, x_i(s)]^T$ denote the covariance matrix with its element in row *h* and column ζ denoted by $\Omega_i^{h\zeta}[s, x_i(s)]$. For $i \neq j$, $x_i \cap x_j = \varnothing$, and $z_i(s)$ and $z_j(s)$ are independent Wiener processes. Trough the above processes, we import stochastic environment factors in dynamic cooperation joined by multiple peers. We also used $x_N(s)$ to denote the vector $[x_1(s), x_2(s), \ldots, x_n(s)]$ and x_N^0 denotes the vector $[x_1^0, x_2^0, \ldots, x_n^0]$.

Consider a coalition of a subset of peers $K \subseteq N$. There are *k* peers in the subset *K*. The participating peers can gain more bandwidth that would be difficult for them to obtain on their own, and hence the state dynamics of peer *i* in the coalition *K* becomes

$$dx_i(s) = f^i[s, x_K(s), u_i(s)]ds + \sigma[s, x_i(s)]dz_i(s), \quad x_i(t_0) = x_i^0 \quad \text{for } i \in K \tag{3}$$

where $x_K(s)$ is the concatenation of the vectors $x_j(s)$ for $j \in K$. In particular, $\partial f_i^K[s, x_K, u_i] / \partial x_j \geq 0$, for $j \neq i$. Thus positive effects on the state of peer *i* could be derived from the other peers within the coalition. Without much loss of generalization, the effect of x_j on $f_i^K[s, x_K, u_i]$ remains the same for all possible coalitions *K* containing peers *i* and *j*.

4.2 The Dynamic Shapley Value Imputation

Consider the above cooperation involving n peers. The member peers would maximize their joint profit and share their cooperative profits according to the Shapley value. The Shapley value is one of the most commonly used sharing mechanism in static cooperation games with transferable payoffs. Besides being individually rational and group rational, the Shapley value is also unique. The uniqueness property makes a more desirable cooperative solution relative to other solutions like the Core or the Stable Set. Specifically, the Shapley value gives an imputation rule for sharing the cooperative profit among the members in a coalition as:

$$\varphi^i(v) = \sum_{K \subseteq N} \frac{(k-1)!(n-k)!}{n!}(v(K) - v(K \setminus i)) \quad \text{for } i \in N \tag{4}$$

where $K\backslash i$ is the relative complement of i in K, $v(K)$ is the profit of coalition K, and $[v(K) - i(K\backslash i)]$ is the marginal contribution of peer i to the coalition K.

Given the assumption that $v(K)$ is super-additive, the Shapley value yields the desirable properties of individual rationality and group optimality. Though the Shapley value is used as the profit allocation mechanism, there exist two features that do not conform with the standard Shapley value analysis. The first is that the present analysis is dynamic so that instead of a one-time allocation of the Shapley value, we have to consider the maintenance of the Shapley value imputation over the cooperation horizon. The second is that the profit $v(K)$ is the maximized profit to coalition K, and is not a characteristic function (from the game in which coalition K is playing a zero-sum game against coalition $N\backslash K$).

To maximize the cooperation's profits the peers would adopt the control vector $\{\psi_N^{(t_0)N*}(t, x_N^{t*})\}_{t=t_0}^T$ over the time $[t_0, T]$ interval, and the corresponding optimal state trajectory $\{x_N^{t*}(t)\}_{t=t_0}^T$ would result. At time t_0 with state $x_N^{t_0}$, the peers agree that peer i's share of profits be:

$$v^{(t_0)i(t_0, x_N^0)} = \sum_{K \subseteq N} \frac{(k-1)!(n-k)!}{n!}[W^{(t_0)K}(t_0, x_K^0) - W^{(t_0)K\setminus i}(t_0, x_{K\setminus i}^0)] \quad \text{for } i \in N \tag{5}$$

However, the Shapley value has to be maintained throughout the cooperation horizon $[t_0, T]$. In particular, at time $\tau \in [t_0, T]$ with the state being $x_N^{\tau*}$, the following imputation principle has to be maintained:

Condition 1. At time τ, peer i's share of profits be:

$$v^{(\tau)i(\tau, x_N^{\tau*})} = \sum_{K \subseteq N} \frac{(k-1)!(n-k)!}{n!}[W^{(\tau)K}(\tau, x_K^{\tau*}) - W^{(\tau)K\setminus i}(\tau, x_{K\setminus i}^{\tau*})] \quad \text{for } i \in N \text{ and } \tau \in [t_0, T] \tag{6}$$

Condition 1 satisfies the property of Pareto optimality throughout the game interval and guarantees individual rationality throughout the game interval. Pareto optimality and individual rationality are essential properties of imputation vectors. Moreover, if Condition 1 can be maintained, the solution optimality principle – sharing profits according to the Shapley value – is in effect at any instant of time throughout the game along the optimal state trajectory chosen at the outset. Hence time consistency is satisfied and no peers would have any incentive to depart the cooperation. Therefore a dynamic imputation principle leading to formula (6) is dynamically stable or time consistent.

Crucial to the analysis is the formulation of a profit distribution mechanism that would lead to the realization of Condition 1. This will be done in the next section.

4.3 The Dynamic Shapley Value Imputation

In this section, a profit distribution mechanism will be developed to compensate transitory changes so that the Shapley value principle could be maintained throughout the venture horizon. From Yeung [16] and [17], we can get the following theorem.

Theorem 1. A payment to peer $i \in N$ at time $\tau \in [t_0, T]$ equaling

$$\begin{aligned} B_i(\tau) = & \\ & -\sum_{K \subseteq N} \frac{(k-1)!(n-k)!}{n!}\{[W_t^{(\tau)K}(\tau, x_K^{\tau*})\big|_{t=\tau}] - [W_t^{(\tau)K\setminus i}(\tau, x_{K\setminus i}^{\tau*})\big|_{t=\tau}] \\ & +([W_{x_N^{\tau*}}^{(\tau)K}(t, x_K^{\tau*})\big|_{t=\tau}] - [W_{x_N^{\tau*}}^{(\tau)K\setminus i}(\tau, x_{K\setminus i}^{\tau*})\big|_{t=\tau}]) \\ & \times f^N[\tau, x_N^{\tau*}, \psi_N^{(\tau)N}(\tau, x_N^{\tau*})]\} \end{aligned} \tag{7}$$

will lead to the realization of the Condition 1.

Since the partial derivative of $W^{(\tau)K}(\tau, x_K^{\tau*})$ with respect to x_j, where $j \notin K$, will vanish, a more concise form of Theorem 1 can be obtained as:

Theorem 2. A payment to peer $i \in N$ at time $\tau \in [t_0, T]$ leading to the realization of the Condition 1 can be expressed as:

$$\begin{aligned} B_i(\tau) = & \\ & -\sum_{K \subseteq N} \frac{(k-1)!(n-k)!}{n!}\{[W_t^{(\tau)K}(\tau, x_K^{\tau*})\big|_{t=\tau}] - [W_t^{(\tau)K\setminus i}(\tau, x_{K\setminus i}^{\tau*})\big|_{t=\tau}] \\ & +\sum_{j \in K}[W_{x_j^{\tau*}}^{(\tau)K}(t, x_K^{\tau*})\big|_{t=\tau}] f_j^N[\tau, x_N^{\tau*}, \psi_N^{(\tau)N}(\tau, x_N^{\tau*})] \\ & -\sum_{h \in K\setminus i}[W_{x_h^{\tau*}}^{(\tau)K\setminus i}(\tau, x_{K\setminus i}^{\tau*})\big|_{t=\tau}] f_h^N[\tau, x_N^{\tau*}, \psi_h^{(\tau)N}(\tau, x_N^{\tau*})]\} = \\ & \sum_{K \subseteq N} \frac{(k-1)!(n-k)!}{n!}\{[W_t^{(\tau)K}(\tau, x_K^{\tau*})\big|_{t=\tau}] - [W_t^{(\tau)K\setminus i}(\tau, x_{K\setminus i}^{\tau*})\big|_{t=\tau}] \\ & +[W_{x_N^{\tau*}}^{(\tau)K}(t, x_K^{\tau*})\big|_{t=\tau}] f_K^N[\tau, x_N^{\tau*}, \psi_K^{(\tau)N}(\tau, x_N^{\tau*})] \\ & -[W_{x_{K\setminus i}^{\tau*}}^{(\tau)K\setminus i}(t, x_{K\setminus i}^{\tau*})\big|_{t=\tau}] f_{K\setminus i}^N[\tau, x_N^{\tau*}, \psi_{K\setminus i}^{(\tau)N}(\tau, x_N^{\tau*})] \end{aligned} ,$$

where $f_K^N[\tau, x_N^{\tau*}, \psi_K^{(\tau)N}(\tau, x_N^{\tau*})]$ is a column vector containing $f_i^N[\tau, x_N^{\tau*}, \psi_i^{(\tau)N}(\tau, x_N^{\tau*})]$ for $i \in K$.

The vector $B(\tau)$ serves as a form equilibrating transitory compensation that guarantees the realization of the Shapley value imputation throughout the game horizon. Note that the instantaneous profit $B_i(\tau)$ offered to peer i at time τ is conditional upon the current state $x_N^{\tau*}$ and current time τ. One can elect to express $B_i(\tau)$ as $B_i(\tau, x_N^{\tau*})$. Hence an instantaneous

payment $B_i(\tau, x_N^{\tau^*})$ to player $i \in N$ yields a dynamically stable solution to the cooperation.

5. Conclusion

In this paper, we analyze the root of issues derived from BitTorrent tit-for-tat strategy, reveal that the cooperative stochastic differential environment is more realistic than the current proposed mechanism. Based on the clear definition of basic game theory elements from P2P content distribution prospective, we propose an incentive framework which peers can cooperate with each other and get Pareto-optimal bandwidth allocation without any binding agreements. We prove the payoff distribution procedure can achieve dynamic Shapley value by using equilibrating transitory compensation during peers' cooperation and make peers follow the original optimality principle and cooperative state trajectory path. Our incentive framework is more flexible and realistic than previous game-theoretic solutions. It can build cooperation relationship in stochastic dynamic peer-to-peer network without the limitation of time consistency.

References

[1] IPOQUE Report. Internet Study 2008-2009, http://portal.ipoque.com/downloads/index/get/?id=265, 2009.

[2] E. Adar and B. A. Huberman. Free riding on Gnutella. *First Monday*, 5(10), Oct. 2000.

[3] B. Cohen. Incentives build robustness in BitTorrent. In *Proc. 1st Workshop on Economics of Peer-to-Peer Systems*, Berkeley, June 2003.

[4] M. J. Osborne. *An Introduction to Game Theory*. Oxford University Press, 2004.

[5] M. Izal, G. Urvoy-Keller, E. W. Biersack, P. Felber, A. A. Hamra, and L. Garc´es-Erice. Dissecting BitTorrent: Five months in a torrent's lifetime. *In Passive and ActiveMesurements*, pages 1–11, April 2004.

[6] A. R. Bharambe, C. Herley, and V. N. Padmanabhan. Analyzing and improving BitTorrent performance. Technical Report MSR-TR-2005-03, Microsoft Research, 2005.

[7] M. Piatek, T. Isdal, A. Krishnamurthy, T. Anderson, One hop reputations for peer to peer file sharing workloads, *in NSDI08*, pp. 1-14.

[8] P. Golle, K. Leyton-Brown, and I. Mironov. Incentives for sharing in P2P networks. *In 3rd ACM Conf. on Electronic Commerce*, 2001.

[9] T. B. Ma, C. M. Lee, J. C. S. Lui, and K. Y. Yau. Incentive and Service Differentiation in P2P Networks: A Game Theoretic Approach. *IEEE/ACM Trans. on Networking*, 14(5), 2006.

[10] S. Zhong, J. Chen, and Y. Yang. Sprite: a simple, cheat-proof, creditbased system for mobile ad-hoc networks. *In INFOCOM*, IEEE, 2003.

[11] V. Vishnumurthy, S. Chandrakumar, and E. Sirer. Karma: A secure economic framework for peer-to-peer resource sharing. *In Workshop on Economics of Peer-to-Peer Networks*, 2003.

[12] M. Feldman, K. Lai, I. Stoica, and J. Chuang. Robust incentive techniques for peer-to-peer networks. *In ACM EC'04*, 2004.

[13] M. Feldman, C. Papadimitriou, J. Chuang, and I. Stoica. Free-riding and whitewashing in peer-to-peer systems. *In Workshop on Practice & theory of incentives in networked systems*, 2004.

[14] F. Wu and L. Zhang. Proportional response dynamics leads to market equilibrium. *In ACM STOC*, 2007.

[15] Thomas Hobbes. Leviathan. 1651. http://publicliterature.org/books/leviathan/xaa.php

[16] Yeung, D.W.K.: Infinite horizon stochastic differential games with branching payoffs. *Journal of Optimization Theory and Applications*, 111, No. 2, 445–460, 2001.

[17] Yeung, D.W.K., Petrosyan, L.: Subgame consistent cooperative solutions in stochastic differential games. *Journal of Optimization Theory and Applications*, 120, No.3, 651–666, 2004.

Social Knowledge Dynamics: A Case Study on Modeling Wikipedia

Benyun Shi

Abstract

We show the current research progresses and focuses on Wikipedia to try to understand principles behind social knowledge dynamics. Wikipedia is a popular web-based encyclopedia, which can be edited freely and collaboratively by its users. This kind of truly collaborative and social platform provides a good opportunity for sociologist, physicists, computer scientists, and other researchers on traditional social knowledge dynamics to better understand the evolution of social cognition - that is, the ability of a group of people to remember, think, and reason. We survey recent research work on how to characterize global features of Wikipedia and how to model the growth of Wikipedia. While previous work mainly focus on statistical analysis of a mass of date from Wikipedia, it is extremely hard to understand the nature behind the Wikipedia phenomena. In this work, we try to study how to build bottom-up models based on autonomy-oriented computing (AOC) to better understand the nature and fundamental principles of social knowledge dynamics through a case study of Wikipedia.

1 Introduction

Wikipedia is a freely available online encyclopedia, that anyone can create, edit, as well as delete articles. The unique character of the free editing policy and the large number of participants make the success of Wikipedia. Each article of Wikipedia can be treated as a collective knowledge of a group of users who have made updates on it. Sociologists define knowledge as follows. "*Knowledge is embodied in people gathered in communities and networks. The road to knowledge is via people, conversations, connections and relationships. Knowledge surfaces through dialog, all knowledge is socially mediated and access to knowledge is by connecting to people that know or know who to contact.*" In terms of this definition, the evolution of Wikipedia can be treated as a type of social knowledge dynamics for the following reasons: i) the formation of each article of Wikipedia is contributed by a collective of users that gathered together on the page of the article, ii) users on the article page can exchange their knowledge through "talk" page (i.e., user interaction), iii) users with similar opinions or users who act frequently on a specific article may form community on the article, and iv) the underlying structure of some articles may inversely influence uses' knowledge on some other articles. In this case, finding principles behind about the evolution of Wikipedia may help to have a better understanding about social knowledge dynamics.

Social knowledge dynamic is a research branch of social dynamics. Social dynamics mainly focuses on the study of a society of individuals to react to inner and/or outer changes and tries to find ways to explain some social phenomena. Researches [7] on social dynamics have shown that interesting global patterns, such as phase transition and criticality in culture dynamics [8], can emerge from even a group of simple individuals (in term of their behavior rules and/or relationships). Understanding the driven force behind such emergence is the first step for us to realize the complex real world. Previous studies show that individual's social behaviors play important roles in this process. For example, Surowiecki's "The Wisdom of Crowds" [20] discusses the question about why the many are smarter than the few and how collective wisdom shapes business, economies, societies and nations.

The physics community [7] has long aimed at the discovery of fundamental principles behind emergent properties, such as phase transition, of the social systems by local dynamic models, for example, the simple sand pile model [6]. However, for any investigation of local dynamic models of social dynamics, there are two levels of difficulty: i) the definition of sensible and realistic microscopic models, and ii) the usual problem of inferring the macroscopic phenomenology out of the microscopic dynamics of such models. However, without intact data of social activities, it is extremely hard i) to build a realistic microscopic model, and ii) to observe explicit macroscopic phenomena. With a millions of articles, hundreds of thousands of contributors, and tens of millions of fully recorded article revisions, Wikipedia's freely available database [2] made it possible to study how human knowledge is recorded and organized through an open collaborative process.

In this work, we survey recent research work on how to characterize microscopic features of Wikipedia and how

to model the growth of Wikipedia. These previous work mainly focus on statistically analyzing a mass of data from Wikipedia, and building statistical models to explain some macro-level patterns. We argue that the macro-level analysis and modeling is not enough to understand the nature of the evolution of Wikipedia, as well as social knowledge dynamics, for the reason that the real Wikipedia is driven by the social dynamics, including user-to-user interactions, use-to-group interactions, and group-to-group interactions, rather than simple stochastic processes.

We then discuss how to build bottom-up models based on autonomy-oriented computing (AOC) [12] to better understand the nature and fundamental principles of social knowledge dynamics. AOC defines and deploys a system of local autonomy-oriented entities, which spontaneously interact with their environment and operate based on their behavior rules. Since the features of AOC match the formation of Wikipedia very well, we believe the AOC-based models can help us to understand the whole Wikipedia system, the topic evolution, and the dynamic of user communities on Wikipedia.

The rest of this work is organized as follows. In section 2, we briefly introduce the roles of Wikipedia in the development of Web 2.0. In section 3, we summarize the microscopic phenomena analysis of Wikipedia data dump. In section 4, we survey the recent studies of modeling of Wikipedia growth. In section 5, we discuss the possibility of designing AOC-based model to study the nature and fundamental principle of social knowledge. Finally, we conclude our work in section 6.

2 Roles of Wikipedia

Wikipedia relies on server-side technology that allow both registered and anonymous users to make instant update (i.e., create, edit, delete) to a page or link via a web interface. It has archiving systems that record all previous edits of a page and make it simple to revert to an earlier version. This archiving system ensures that no permanent harm can be caused by cankered editing. The key technology behind Wikipedia is its online heavyweight Web-based collaboration. Ed H. Chi's work [9] on Web 2.0 technologies provides the following social web collaboration spectrum (Figure 1).

At the lightweight end of the social collaboration spectrum, researchers are focusing on information-foraging and behavioral models. In the middle the spectrum, mathematicians and social scientists are developing new theories and algorithms to model, mine, and understand social structure. While at the heavy end of the spectrum, researchers should focus on studying what hinders and fosters coordination on large group projects, which is especially important for understanding collaborative co-creation system such as

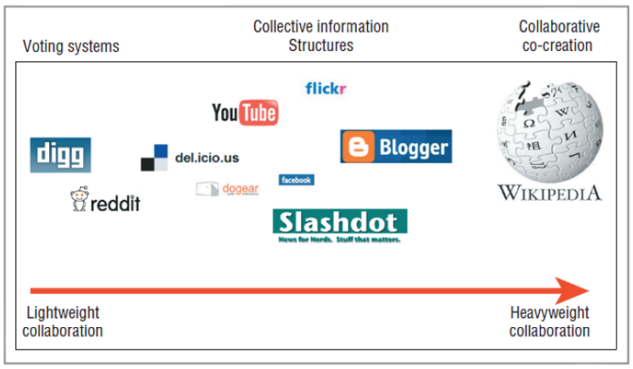

Figure 1. Social Web collaboration spectrum. (adopted from Fig. 2 in [9].)

Wikipedia.

For the richness of data from Wikipedia, it is important to understand features behind these data so that further studies can be carried out. In the next section, we summarize the recent data analysis about Wikipedia.

3 Related Work on Wikipedia

Since Wikipedia provides rich data sources to download, including i) articles, ii) categories, iii) images and multimedia, iv) user, help, and talk pages, and v) redirects, templates and broken links, there are many work on analyzing these data with different purposes. For example, D. Spinellis and P. Louridas [19] analyzed the evolution of the ratio between incomplete and complete articles, and the relation of references and definitions of articles. They found that "the addition of new articles in not a purely random process following the whims of its contributors but that references to nonexistent articles trigger the eventual creation of a corresponding article". R. Almeida et al. [3] studied the updates of articles in Wikipedia, and found that the evolution of updates is governed by a self-similarity process. A. Kittur et al. [11] proposed a mapping approach to study the distribution of topics in Wikipedia. Also, there are also other researches [21] focusing on visualization of history flow of Wikipedia.

In this work, we mainly focus on the analysis where Wikipedia is treated as complex networks, where the articles of Wikipedia represent the nodes of the network while the hyperlinks pointing from one article to another are treated as links. Many characteristics [17] of complex networks can be used to analyze the structure of Wikipedia, for instance, degree distribution, clustering, path length, network topology, reciprocity, motifs, and so on. Here, we briefly introduce analysis results for three characteristics that may relate to bottom-up model designing.

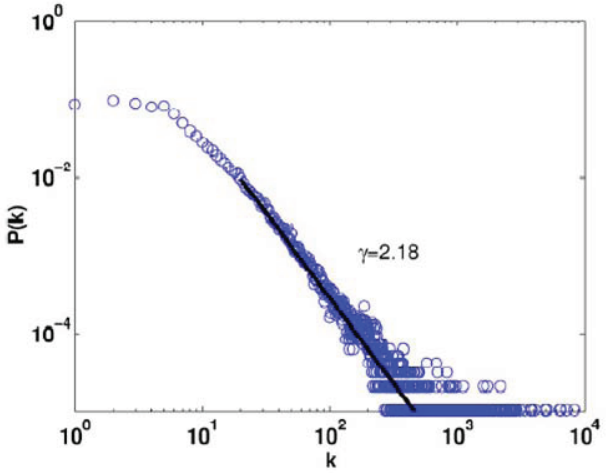

Figure 2. In-degree distribution of Japan Wikipedia. (adopted from Fig. 3 in [23].)

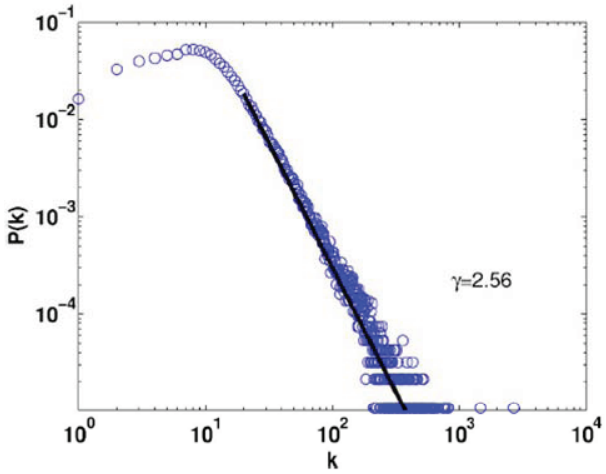

Figure 3. Out-degree distribution of Japan Wikipedia. (adopted from Fig. 4 in [23].)

3.1 Degree distribution

The in-degree (respectively, out-degree) of a node in Wikipedia network measures the number of articles that link into the article (respectively, the number of articles that the article links to as references). In most cases, two articles sharing a link reflect some kinds of relations in term of their contents. Hence, analyzing degree distributions (both in- and out-degree distributions) of Wikipedia may help to understand the article structure of Wikipedia, and may future help to understand the intrinsic relation of different kinds of knowledge.

V. Zlatic et al. [23] presented an analysis of Wikipedia in several languages as complex networks. They found that both the in-degree and out-degree of distributions of most Wikipedia follow power-law distributions. Figures 2-3 are examples of in-degree and out-degree distributions of the Japan Wikipedia.

The similar degree distributions for different kinds of languages supports the assumption that the Wikipedia in different languages represent realizations of the same process of network growth, which in turn shows that there must be some fundamental principles behind the social knowledge dynamics. Hence, various statistical models can be proposed to study the Wikipedia growth. We will introduce these models in section 4.

However, most of recent work analyze Wikipedia network as a whole. We argue that to have a better understanding of knowledge dynamic, it is necessary to do analysis about Wikipedia on different granularity (e.g., analysis on topic level to measure the topic distribution; analysis within different topics to measure the distribution of articles in a specific topic). By doing so, we can observe whether or not the observed scale-free phenomena exist in the Wikipedia structure. In other words, does self-similarity exist?

3.2 Reciprocity and feedback loops

Another interesting features observed in Wikipedia network is their reciprocity [23]. Reciprocity quantifies mutual "exchange" between two nodes. Reciprocal links are just the links pointing from the node i to the node j for which exists a link pointing from node j to the node i. The reciprocity is then defined as

$$\rho = \frac{L_{bd}/L - \bar{a}}{1 - \bar{a}}$$

where L_{bd} represents the number of bidirectional links, i.e., links for which a reciprocal link exists. L is the total number of directed links and $\bar{a} = \frac{L}{N(N-1)}$ is the density of links.

Another feature that similar with reciprocity is feedback loops in the networks. A feedback loop in Wikipedia network can be defined as a loop with directed links that start from and end with the same node. The ecological study in [11] observed that the number of feedback loops in the species network is correlated with system lifetime. Though there have not many papers dealing with the origin of reciprocity or network evolution models that capture this quantity, we believe that reciprocity and feedback loops play important roles in the evolution of Wikipedia. In this case, analysis about reciprocity and feedback loops on Wikipedia is necessary and important work before designing models on Wikipedia to understand social knowledge dynamics.

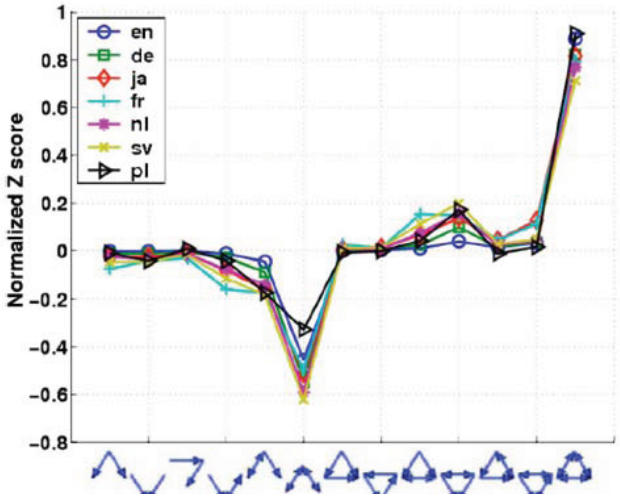

Figure 4. The triadic motif profiles of Wikipedias. (adopted from Fig. 10 in [23].)

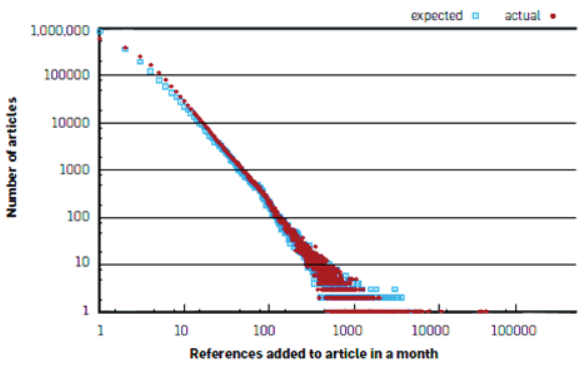

Figure 5. Frequency distribution of the expected and actual number of references added each month to each article (adopted from Fig. 3b in [19]).

3.3 Motifs

Motifs introduced in [16] are small subgraphs (in [16], triadic subgraphs are concerned) of networks, which are used to systematically study similarity in the local structure of networks. By comparing significance profiles of the original network with that of randomly generated networks, networks with similar local structure can be grouped together. Interesting results shows that networks with similar functions may have similar motif profiles (see Fig. 1 in [16] for more details).

By analyzing the motifs in Wikipedia network, V. Zlatic et al. [23] show that the triadic motif significance profiles of Wikipedia networks with different languages are very similar, though Wikipedia networks with different have different size. In Figure 4, the x axis depicts all possible triadic motifs of a directed network, while the y axis represents the normalized Z score [16] for a given motif.

The similar motif significance profiles for different languages indicate that there maybe exist common fundamental principles that drive the growth of Wikipedia. Then, what are the principles behind this? Do these principles related to principles that drive the social knowledge dynamics? We should keep these questions in mind when we design models to discover the essential principles.

4 Modeling Wikipedia's Growth

In this section, we will mainly focus on the scale-free phenomena in Wikipedia. The models for scale-free can be divided into two groups: i) scale-free as the result of an optimization or phase transition process [2], and ii) scale-free as the results of a growth model, such as preferential attachment. Recent study [18] also shows that scale-free can also be formed by deliberate removal.

It is impossible to examine the emergence of scale-free in other big real-world networks, as there is no full record of their evolution. Wikipedia provides a platform to allow us to witness, and validate preferential attachment. Two models based on preferential attachment will be introduced in this section to explain two different power law phenomena. We believe that lots of research should be down in the future to find more fundamental principles.

4.1 Model about reference

The following model is from the study of D. Spinellis and P. Louridas in [19]. Consider a model where at each time step t a month, a variable number of articles and r_t references are added. The references are distributed among all entries following a probability $p(k_{i,t}) = \frac{k_{i,t}}{\sum_{j,t} k_{j,t}}$, with the sums and the connectivity calculated at the start of t. The expected number of references added to entry i at month t is then $E(k_{i,t}) = r_t p(k_{i,t})$. The authors find a close match between the expected and the actual numbers in Wikipedia data. Figure 5 shows a log-log plot of frequency distribution of the expected and actual number of articles gaining a number of references in a month.

4.2 Model about degree distribution

The following model is from the work of V. Zlatić et al. [22]. The model consists of two steps. In the first one a new node, introduced in the network at time t and therefore labeled as t, attaches to the network with m outgoing links.

The probability that the given link, from these m links, will attach itself to some node $s < t$ is proportional to the in-degree $k_i(s)$ of the node s. In the second step for every new link with the probability r a new reciprocal link is formed between nodes s and t. The results also show a perfect fit between the in-degree distribution of Wikipedia and the expected distribution of this model. See figures 2-3 in [22] for more details.

Though these two models could be used to reflect some principles behind network growth, such as preferential attachment, we should realize that the real Wikipedia is driven by the social dynamics, including user-user interactions, use-group interactions, and group-group interactions, rather than the simple stochastic processes. Autonomy-oriented computing provides a bottom-up way to study the global emergence of Wikipedia. In the next section, we will discuss the possibility of adopting AOC-based model [12] to design the social knowledge dynamics mechanisms.

5 AOC-Based Models

AOC defines and deploys a system of local autonomy-oriented entities, which spontaneously interact with their environment and operate based on their behavior rules. Self-organization as a soul of AOC allows entities to self-organize both their relationships and their local dynamics, with respect to some predefined settings, so that problems with various complicated properties can be adaptively solved. Feedbacks (both positive and negative) play important roles in self-organization process. The fundamental difference of positive feedback and negative feedback is that i) positive feedbacks aim at accelerate aggregations with non-linear amplification (e.g., reproduction), while ii) negative feedback (e.g., collective regulation) aim at self-correction/self-tuning.

The features of AOC match the formation of Wikipedia very well in terms of i) Wikipedia is formed by editing of spontaneous users, ii) users may interact/discuss with each other in "talk" page of each article, iii) contents of other pages may give feedbacks to regulate or aggregate users decisions, and iv) communities can be formed during the evolution of Wikipedia, which inversely play important roles for Wikipedia's evolution.

In this case, what are the fundamental behavior rules of entities to form global patterns of Wikipedia? How do entities self-organize themselves during the evolution of Wikipedia? Do these rules and self-organization reflect the formation rule of social knowledge and social organization? To answer these questions, we should carefully define entities behavior rules and relation structures during model designing.

In the rest of this section, we propose three possible research directions on Wikipedia for our future research.

5.1 Wikipedia as a system

Any natural systems have processes of birth, boom, and death. As a collaborative system based solely on users' spontaneous actions, what's the driven of its birth, boom, and death?

Robert M. May [13] [14] has studied the impact of interaction strength, connectance, on stability of large complex ecosystems. His results and subsequent work indicate that large randomly assembled ecosystems tend to be less stable as they increase in complexity, where the complexity is measured by the connectance and the average interaction strength between species. R. Mehrotra et al. [15] have studied an evolutionary model that exhibits spontaneous growth, stasis, and then a collapse of its structure. They find that the typical lifetime of the system increase with the diversity of its components. They also find that the number of feedback loops play important roles in the process of collapse of the system. There are also other researchers trying to understand nature behind some phenomena of complex system, such as catastrophe [10], punctuated equilibrium [5], and so on.

We argue that as a system, Wikipedia may also have similar phenomena as the ecosystems do. However, up to now, most existing models are based on statistical analysis or stochastic simulations, which are not enough to reflect real-world phenomena as we argued in section 1. Hence, in the future, we would like to build AOC-based models to simulate and analyze the Wikipedia system.

5.2 Topic evolution on Wikipedia

Previous work on topic mining focus on mining specific topics from a large volume of data, where for most cases, i) the data are static (some researches on dynamic topic mining adopt time windows to reflect the topic evolution), and ii)the mining processes are based on sematic/content analysis.

However, in Wikipedia, topics are dynamically evolving as a result of users dynamics. Different with traditional topic evolution problem, we can treat the topic evolution on Wikipedia as a results of user-to-user interactions, or even the interaction among groups of users. In this case, we can further observe the evolution of social knowledge.

While traditional data mining strategies cannot explain the driven force behind the evolving the topics, we argue that AOC-based model on Wikipedia topics may reveal some principles by focusing on entities/topics local interactions and collective regulations. The studies on culture evolution [8] [4] may provide some ideas on this research aspect.

5.3 User community dynamics on Wikipedia

Traditional community discovery algorithms [1] are mostly based on the quantitative measure of modularity Q. The modularity is defined as $Q = \sum_i (e_{ii} - a_i^2)$, where e_{ii} measures the fraction of edges that have both ends pointing at nodes in group i, and a_i measures the fraction of edges whose end points belong to at least one of vertices in group i. Some researchers [1] argue that the linkage-based measurement cannot reflect multiple relationships.

In Wikipedia, each user may associate into multiple articles. While for each article, there will be multiple users acting on it. This kind of bi-party network may provide novel definitions of community so that new approaches about community evolution can be proposed. Also, by AOC-based models, communities may emerge from entities local interactions, and may further dynamically evolve as entities activities change over time.

For above mentioned research aspects, many work need to be done in the future to get more deep understanding about Wikipedia and its dynamics.

6 Conclusion

In this work, we survey both the macro- and microscopic studies about Wikipedia. For the macroscopic study, we focus on the data analysis of Wikipedia, especially on the Wikipedia network analysis, and find many interesting phenomena. For the microscopic study, we introduce two statistical models based on preferential attachment to fit the scale-free phenomena in Wikipedia. Since the real Wikipedia is driven by the user dynamics rather than simple stochastic processes, it is necessary to design AOC-based models to study the essential rules behind the Wikipedia dynamics. Several research aspects are proposed for future study at the end of this paper.

References

[1] Community Discovery. http://www.cscs.umich.edu/ crshalizi/notebooks/community-discovery.html.

[2] Download Wikipedia. http://download.wikimedia.org.

[3] R. Almeida, B. Mozafari, and J. Cho. On the evolution of wikipedia. *In Proceeding of International Conference on Weblogs and Social Media*, 2007.

[4] R. Axelrod. The dissemination of culture: A model with local convergence and global polarization. *Journal of Conflict Resolution*, 41(2):203–226, 1997.

[5] P. Bak and K. Sneppen. Punctuated equilibrium and criticality in a simple model of evolution. *Physical Review Letters*, 71(24):4083–4086, 1993.

[6] P. Bak, C. Tang, and K. Wiesenfeld. Self-organized criticality. *Physical Review A*, 38(1):364–374, 1988.

[7] C. Castellano, S. Fortunato, and V. Loreto. Statistical physics of social dynamics. *Reviews of Modern Physics*, 81:591–646, 2009.

[8] D. Centola, J. C. Gonzalez-Avella, V. M. Eguiluz, and M. S. Miguel. Homophily, cultural drift, and the co-evolution of cultural groups. *Journal of Conflict Resolution*, 51(6):905–929, 2007.

[9] E. H. Chi. The social web: Research and opportunities. *Computer in Computer*, 41(9):88–91, 2008.

[10] S. A. Kauffman. *The Origins of Order: Self-Organization and Selection in Evolution*. Oxford University Press, 1993.

[11] A. Kittur, E. H. Chi, and B. Suh. What's in wikipedia? mapping topics and conflict using socially annotated category structure. *In Proceeding of the* 27^{th} *Annual CHI Conference on Human Factors in Computing Systems*, pages 4–9, 2009.

[12] J. Liu. Autonomy-oriented computing: The nature and implications of a paradigm for self-organized computing. *Keynote Talk at The* 4^{th} *International Conference on Natural Computation, and the* 5^{th} *International Conference on Fuzzy Systems and Knowledge Discovery*, pages 3–11, 2008.

[13] R. M. May. Will a large complex system be stable? *Nature*, 238:413–414, 1972.

[14] R. M. May. Qualitative stability in model ecosystems. *Ecology*, 54(3):638–641, 1973.

[15] R. Mehrotra, V. Soni, and S. Jain. Diversity sustains an evolving network. *Journal of the Royal Society Interface*, 6(38):793–799, 2009.

[16] R. Milo, S. Itzkovitz, N. Kashtan, R. Levitt, S. Shen-Orr, I. Ayzenshtat, M. Sheffer, and U. Alon. Superfamilies of evolved and designed networks. *Science*, 303(5663):1538–1542, 2004.

[17] M. E. J. Newman. The structure and function of complex networks. *SIAM Review*, 45(2):167–256, 2003.

[18] M. Salathé, R. M. May, and S. Bonhoeffer. The evolution of network topology by selective removal. *Journal of Royal Society, Interface*, 2(5):533–536, 2005.

[19] D. Spinellis and P. Louridas. The collaborative organization of knowledge. *Communications of the ACM*, 51(8):68–73, 2008.

[20] J. Surowiecki. *The Wisdom of Crowds: Why the Many are Smarter than the Few and How Collective Wisdom Shapes Business, Economies, Societies, and Nations*. Doubleday, 2004.

[21] F. B. Viégas, M. Wattenberg, and K. Dave. Studying cooperation and conflict between authors with history flow visualizations. *In Proceedings of the Conference on Human Factors in Computing Systems*, pages 575–582, 2004.

[22] Vinko and H. Štefančić. Model of wikipedia growth based on information exchange via reciprocal arcs. *Physics and Society*, 2009.

[23] V. Zlatic, M. Bozicevic, H. Stefancic, and M. Domazet. Wikipedias: Collaborative web-based encyclopedias as complex networks. *Physical Review E*, 74(1), 2006.

Edge Detection Combining Wavelet Transform and Canny Operator Based on Fusion Rules

Jianjia Pan

Abstract

Aiming for the problem of discarding some important details of high-frequency sub-image when detecting the edge based on wavelet transform, and the edge detection result is poor because of the noise influence. This paper proposed a new edge detection algorithm based on wavelet transform and canny operator. In the wavelet domain, the low-frequency edges are detected by canny operator, while the high-frequency edges are detected by solving the maximum points of local wavelet coefficient model to restore edges after reducing the noise by wavelet. Then, both sub-images edges are fused according to fusion rules. Experiment results show the proposed method can detect image edges not only remove the noise effectively but also enhance the edges and locate edges accurately.

Keywords:

Edge detection; Wavelet transform; Canny operator; Image denoise; Fusion rules;

1. Introduction

Edge detection plays an important role in computer vision and image analysis, and is an important processing in the image analysis and pattern recognition. Edges are the abrupt change points in the image which are the basic features of the image. These abrupt change points give the locations of the image contour that shows the important feature [1]. The edge representation of an image reduces the amount of data to be processed, and it retains important information about the shapes of objects in the scene. The description of an image is easy to integrate into a large number of recognition algorithms used in computer vision and other image processing applications [10].

Wavelet analysis developed rapidly as a useful research method, this method based on multi-scale wavelet is one of the new edge detection methods [10]. The traditional edge detection method based on wavelet transform is to perform the wavelet multi-resolution for image firstly, and then extract the low-frequency sub-image to further process, which will discard some important details and the effect of edges extracting will be affected by lots of noise in the high-frequency sub-images [2]. In this paper, we proposed a new fusion algorithm based on wavelet transform and canny operator to detect image edges, which can reduce the noise and obtain the continuous and distinct edges.

2. Image decomposition based on Wavelet transform

Based on image decomposition model of wavelet transform, the original image can be divided into low-frequency information and high-frequency information. After two-dimensional frequency decomposition of wavelet transform, low-frequency information can be decomposed low-frequency area LL and high-frequency area LH, high-frequency information can be decomposed low-frequency area HL and high-frequency area HH. LL shows the smoothing image of the original image which contains the most information of the original image. LH preserves the vertical edge details. HL preserves the horizontal edge details. HH preserves the diagonal details which are influenced by noise greatly. The result can be decomposed as needed. The process is shown in Figure.1

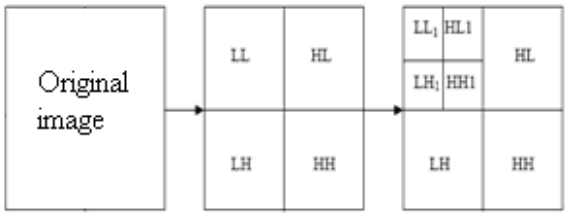

Figure.1 Image decomposition based on wavelet transform

3. Fusion algorithm of edge detection combining wavelet transform and canny operator

Though the edge extracted by wavelet transform can reduce the most noise of the image, the real edges of the image are also mixed with much noise, especially HH areas are affected by the noise greatly. Thus many methods of edge detection will discard these HH areas [5]. The four areas obtained from two-dimensional decomposition of wavelet transform contain the useful information of the original image, so these areas should be used completely when detecting the image edges. This paper presents a new fusion algorithm based on wavelet transform and canny

operator to detect image edges, which can reduce the noise and obtain the continuous and distinct edges.

3.1. Low-frequency sub-image edge detecting based on canny operator

The LL area shows the smoothing image of the original image which contains the most information of the original image. Canny operator is a edge detecting operator based on an optimal algorithm, which has the most stringent criterions of edge detecting. The good effect will be obtained adopted canny operator when processing the image contaminated by additive white Gaussian noise. So canny operator [3,9] are adopted to detect the edges of the low-frequency sub-image. The realization process is as follows.

(1) Smoothing image. Gaussian function is used to smooth the image; the method use 5×5 Gaussian template and the original image to weight neighborhood [4]. Denote any point (x, y) of the image as the center when processing and extracting 5×5 neighborhood, the weighting neighborhood can be indicated as follows:

$$I^*(x,y)=\frac{1}{5\times 5}\sum_{i=-2}^{2}\sum_{j=-2}^{2}I(x+i,y+j)\times M(2+i,2+j)$$

x=1,2,…,m; y=1,2,…,n (1)

Where the pixel value of the low-frequency sub-image is $I(x, y)$, M is Gaussian template, the pixel value of the smoothed image is $I^*(x, y)$.

(2) Computing gradient direction and amplitude. Computing gradient direction and amplitude of smoothed image $I^*(x,y)$ adopting first order partial finite difference of 2×2 neighborhood.

$$M(x,y)=\sqrt{g_x^2(x,y)+g_y^2(x,y)} \quad (2)$$

$$Q(x,y)=\arctan[g_x(x,y),g_y(x,y)] \quad (3)$$

$$f_x=\begin{bmatrix}-1/2 & 1/2\\ -1/2 & 1/2\end{bmatrix} \qquad f_y=\begin{bmatrix}1/2 & 1/2\end{bmatrix} \quad (4)$$

Where g_x and g_y are the results of the original image filtered along rows and lines.

(3) Gradient image with non-maximum suppression. If the gradient amplitude of the pixel is no less than the gradient amplitude between two adjacent pixels in the gradient direction, the point can be judged as the edge point possibly.

(4) Dual threshold method of detecting and connecting the edges. Select two thresholds, Hth and Lth. Hth denotes the high threshold and Lth denotes the low threshold to process the gradient image. Where Hth=Lth*h, h=1.5 ~ 2. There will be two detecting results, one resulted from high threshold detecting, and the other resulted from low threshold detecting. Connecting the edge contour from the former and finding weak edge points from the latter to recoup the former edge gaps when connecting to the endpoint.

Through adopting canny operator to detect the low-frequency sub-image can obtain clear edge image which will miss some real edges and exist some sham edges. Thus the edges of the high-frequency sub-images should be fused.

3.2. High-frequency sub-image edges detecting based on wavelet transform

After two-dimensional frequency decomposition of wavelet transform, there will be three high-frequency sub-images LH、HL and HH where contain the noise and the details of the image. When extracting the edges from the high-frequency sub-images, the result will be affected because of much noise. Thus, this paper presents that the noise should be reduced before extracting the edges from the high-frequency sub-images. The algorithm can not only keep the important details of the high-frequency sub-images but also restrain the noise.

3.3. Denoising algorithm of the high-frequency sub-images based on wavelet transform

Among the wavelet coefficients of the high-frequency sub-image, the wavelet coefficients which have smaller amplitude present the most noise part, and the wavelet coefficients which have larger amplitude present the details of the image [2]. Based on the characteristic of the high-frequency sub-images, we proposed a method based on wavelet transform to reduce the noise in the high-frequency sub-images. The wavelet coefficients are multiplied by a denoising factor which is relative to their own coefficients' value. This denoising factor is less than 1 and will decrease if the absolute value of the wavelet coefficients increases. This algorithm considers energy distribution property of the wavelet decomposition of the image globally, and obtains a better denoising result, which support the foundation for extracting the edge of the high-frequency sub-images. The process function is as follows.

$$F(x,y)=\begin{cases}w(x,y) & |w(x,y)\ge 3\sigma|\\ 0 & |w(x,y)\le |aver|\\ w(x,y)\times k & else\end{cases} \quad (5)$$

Where $w(x,y)$ denotes the high-frequency coefficient, $F(x,y)$ denotes the high-frequency coefficient gained after denoising; σ、$aver$ indicate the variance and the mean value of the high-frequency coefficient in different wavelet decomposition levels. On the basis of the statistic property of the wavelet coefficients, k is a function which is relative to the coefficient:

$$k = e^{-aw(x,y)+b} - 1 \quad (6)$$

When $w(x,y)$ is greater than 3σ, $w(x,y)$ can be considered as consisting of the signal completely. So k=1, it will be:

$$e^{(-3\sigma a+b)} - 1 = 1 \quad (7)$$

When $w(x,y)$ is smaller than $aver$, $w(x,y)$ will approaches 0, it will be:

$$e^{-a\times aver+b} - 1 = 0 \quad (8)$$

It can be obtained from the two upper equations:

$$a = \frac{-\ln 2}{3\sigma - aver} \qquad b = a \times aver \quad (9)$$

Denoising factor k will be obtained when a and b substituted into the equation (6).

$$k = e^{-\frac{\ln 2}{3\sigma-aver}\times w(x,y)+\frac{-\ln 2}{3\sigma-aver}\times aver} - 1 \quad (10)$$

Denoising algorithm will be computed when k substituted into equation (5). This algorithm is aiming for the wavelet coefficients multiplied by different denoising factors from different wavelet decomposition levels and different high-frequency sub-image, which can reduce the image noise and keep useful details.

3.4. Edge detecting of denoising high-frequency sub-image based on wavelet transform

After eliminating noise of the high-frequency sub-image, the edges of the high-frequency sub-image can be detected using wavelet modulus maxima algorithm [7]. The wavelet modulus maxima algorithm is obtained from an irregular sampling based on multiscale wavelet transform which can describe mechanism singularity of the signal. The wavelet modulus maxima algorithm can describe multiscale edges of the target in the image which has translation, scale and rotation-invariant performance. Thus the wavelet modulus maxima algorithm is an effective algorithm to detect the edges. The realization process is as follows:

$\theta(x,y)$ denotes Gaussian smoothing function, supposing:

$$\theta_s(x,y) = \frac{1}{s^2}\theta\left[\frac{x}{s},\frac{y}{s}\right] \quad (11)$$

Calculating the partial derivative of the smoothing function $\theta(x,y)$, the wavelet function will be:

$$\phi_s^1(x,y) = \frac{\partial\theta(x,y)}{\partial x} = \frac{1}{s^2}\phi^1\left[\frac{x}{s},\frac{y}{s}\right] \quad (12)$$

$$\phi_s^2(x,y) = \frac{\partial\theta(x,y)}{\partial y} = \frac{1}{s^2}\phi^2\left[\frac{x}{s},\frac{y}{s}\right] \quad (13)$$

Convolution of $f(x,y)$ will obtain two components of two dimensional wavelet transform in scale s:

$$W_s^1 f(x,y) = f * \phi_s^1(x,y) \quad (14)$$

$$W_s^2 f(x,y) = f * \phi_s^2(x,y) \quad (15)$$

The gradient module in scale s is:

$$M_s f(x,y) = \sqrt{\left|W_s^1 f(x,y)\right|^2 + \left|W_s^2 f(x,y)\right|^2} \quad (16)$$

The angel in scale s is:

$$A_s f(x,y) = \arctan\left[\frac{W_s^2 f(x,y)}{W_s^1 f(x,y)}\right] \quad (17)$$

Detecting the edges of the high-frequency sub-images LH、HL and HH using wavelet modulus maxima algorithm. Computing the local modulus maxima of three sub-images after wavelet transform using equation (16) and (17), then their edge images G_{LH}, G_{HL} and G_{HH} will be obtained. Those high-frequency sub-images contain the details of the original image, so we proposed that the wavelet coefficients of three edge images should be computed with weighting fusion rules. Computing formula [13] is described as follows:

$$D_H(i,j) = r_{LH} * D_{LH}(i,j) + r_{HL} * D_{HL}(i,j) + r_{HH} * D_{HH}(i,j) \quad (18)$$

Where $D_{LH}(i,j)$、$D_{HL}(i,j)$、$D_{HH}(i,j)$ indicate the wavelet coefficients corresponding to the edge images G_{LH}、G_{HL} and G_{HH}. $D_H(i,j)$ denotes the wavelet coefficient after fusion. r_{LH}、r_{HL} and r_{HH} indicate the corresponding weights, the sum of the three weights is 1.

After these processes, we can get the edges of the low-frequency sub-image and the weighting edges of the high-frequency sub-images. The final edge images are obtained through wavelet composition from the fusion edge sub-images [13].

4. Experimental results

In order to verify the efficiency and accuracy of the proposed algorithm, some images with 256 gray-level are used as experimental subjects. Figure 2 shows the edge detect result of image 'Lena'. Figure.3 shows the edge detect result of the tire image. Figure.4 shows the edge detect result of the noisy image Lena (SNR=15.8dB). The experimental results show that our proposed algorithm, which combined wavelet transform and canny operator to detect the edges, can reduce the noise and obtain the continuous and distinct edges.

(a) The original image

(b) Detecting result by wavelet Algorithm

(c)Detecting result by proposed algorithm

Figure.2 Edge detecting result of the 'Lena' image

(a) The original image

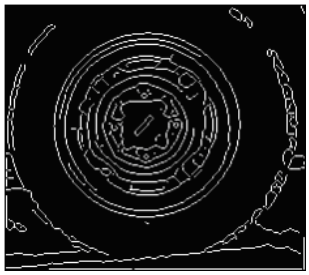

(b) Detecting result by wavelet Algorithm

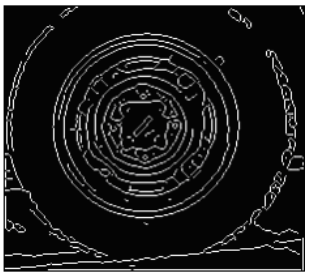

(c)Detecting result by proposed algorithm

Figure.3 Edge detecting result of the tire image

(a) The original noisy image (SNR=15.8dB)

(b) Detecting result by wavelet Algorithm

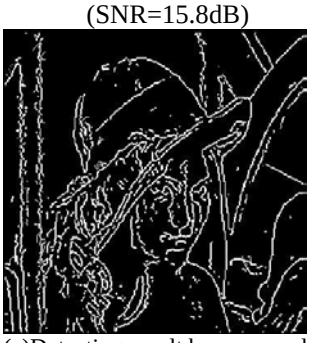

(c)Detecting result by proposed algorithm

Figure.4 Edge detecting result of the noisy image Lena

5. Conclusion

Aiming for the problem of discarding some important details of high-frequency sub-images when detecting the edge based on wavelet transform, and the effect of edge extracting is poor because of the noise. This paper proposed a new edge fusion detection algorithm based on wavelet transform and canny operator, its advantages are to reduce the noise simply and keep the fine image edges. Experiment results show that using this method to detect the image edges can not only get rid of the noise effectively but also enhance the image edge's details and locate the edge accurately.

References:

[1] MALLAT S, HW ANG W L. “Singularity Detection and Processing with Wavelets”. IEEE Trans 2002, IT-38(2):617-643.

[2] MALLAT S. “Multi-frequency Channel Decomposition of Images and Wavelet Models”. IEEE Trans 1998, AS-SP-37(12) :2091-2110.

[3] Yanlong-Chen, Chenghu-Zhu. “Improved Edge Detection Algorithm Based on Canny Operator”. Computer Applications and Software. 2008, vol.25(8):51-53.

[4] Wenyao-Liu. “Photoelectric Image Processing”. Publishing house of electronics industry, 2002, vol.11:106-107

[5] Musheng-Chen. “A New Method of Image Denoising Based on Wavelet Transform”. Optical Technique, 2006, vol.32(5):796-798.

[6] Zhang L, Bao P. “Edge Detection by Scale Multiplication in Wavelet Domain”. Pattern Recognition Letters, 2002, vol. 23(14):1771-1784

[7] Zhu-lihua, Ji-xiaoping. “The application of wavelet modulus maxima algorithm in the image retrieval”. SCI-tech information development and economy. 2007, vol.17(3): 169-170

[8] Wen-Ge, Liqun-Gao. “Fusion Based Algorithm of Edge Detection Combining Wavelet Transform with Morphology”. Journal of Northeastern University. 2008, vol.29(4):477-479

[9] J.F. Canny, “A computational approach to edge detection,” IEEE Transactions on Pattern Analysis and Machine Intelligence, 1986 ,vol.8, pp.679-698

[10] Mitra Basu, “Gaussian-Based Edge-Detection Methods—A Survey”, IEEE Transactions on Systems, Man, and Cybernetics, Part C, 2002, Vol.32(3), pp. 252-260

[11] A. L. Yuille and T. A. Poggio, “Scaling theorems for zero-crossings,” IEEE Transactions on Pattern Analysis and Machine Intelligence, vol.8, pp.15–25, 1986.

[12] P. Bao and L. Zhang, “Noise Reduction for Magnetic Resonance Image via Adaptive Multiscale Products Thresholding,” IEEE Transactions on Medical Imaging, vol.22, pp. 1089-1099, 2003.

[13] Pajares G . "A wavelet-based image fusion tutorial". Pattern Recognition，2004，vol.37(9)：1855—1872.

Modeling and Simulating Human Vaccinating Behaviors On a Disease Diffusion Network

Shang Xia

Abstract

As human is the host of disease infection, its social interactions and vaccinating behaviors influence the dynamics of disease spreading. Previous disease diffusion models are mainly based on the homogeneous mixing assumption, which assumes that individuals in population are identical to each other in terms of disease infection. This assumption ignores inherent heterogeneities in both human contact patterns and individuals' possible behavioral choices. By comparison, we design a disease diffusion model, in which a SIV disease model transmits on a social contact network with scale free topology. We assume that each individual in population will make their self-interest decisions, vaccinating or not, according to the perceived payoff of different choice. Under the AOC modeling framework we incorporate human decision making features, e.g. self-interest choice, following neighbors, panic irrationality, etc, into individual's behavioral sets, and observe how the individual-level decision making behaviors can directly determinate the global-level disease diffusion dynamics and inversely how the disease spreading influence individuals' vaccinating choices.

1. Introduction

In recent years, several serious epidemic outbreaks show that disease diffusion is no longer confined within a local region but involved every corner of the world. These epidemic outbreaks share some common complex characteristics, such as quick spreading through continents, intense outbreak in a certain population communities, unexpected lower new infection case or even sudden disappearance [1][2]. How to characterize or even predict these complex disease diffusion patterns is critical important and urgent, for we do not know when and where a new epidemic attack will happen.

However, even armed with the most progressive biochemistry theories and brilliant innovations of modern biotechnology, it is still hard to trace the expansion of disease spreading. Based on the analysis of epidemic spreading datas, these complexities should be blamed to the combination of disease infections and human social contact behaviors. Human long range travels facilitate the disease spreading cross nations or even continents; individuals' vaccination attitude or self-interest behaviors will greatly influence the potential disease diffusion. Interactions between individuals are both the infection mediums and the information exchange channel. Hence, the problems of epidemic spreading are involved both the macro disease diffusion dynamics and micro human behavioral patterns.

How to understand the relationship between heterogeneities of human social interactions and disease diffusion dynamics is one of the most prominent challenges in epidemic spreading research. The previous analysis of disease diffusion is mainly based on statistical model and differential equations, e.g. homogenous mixing assumption, assuming that individuals in a population have the same probability to contact with each other and thus have the equal chance to be infected by infectious ones [3][4]. These assumptions failed to reveal the complexity in both diffusion dynamics and individual behavioral heterogeneities and thus obscure the veiled correlation between local human individual behaviors and global epidemic spreading dynamics, which we can call it local-global relationship for short.

To analyze the local-global relationship, a methodology called Autonomy-Oriented Computing (AOC) provides a fundamental framework to investigate the emergent complex patterns in epidemic spreading system. AOC emphasize the modeling of autonomy in the entity of a complex system and designing the self-organization mechanism of them to achieve a global level emergent dynamics. In this study, we will build a multi-agent system model following the modeling framework of AOC. In our model, we present the disease infection system as an autonomy agent system which is located on a social contact network with a scale free topology. For the artificial behavior construction, we specify the individuals' vaccinating decision making mechanisms and individual interaction rules. Thus, based on the performance measurement, we can investigate the

relationship between the agents' local behaviors and the global dynamics of disease diffusion process.

The reminder of this paper is organized as follows: section 2 gives a basic formulation structure of our simulation model. Section 3 formulates a social contact network with a scale free topology. In Section 4, we introduce the SIV disease diffusion model to represent close contact disease transmission. Section 5 designs a behavior mechanism for individual decision making. Finally, the paper is concluded in Section 6.

2. Basic Formulation Structure

As mentioned above, the goal of this study is to design a simulation model which can examine the relationship between individuals' local behaviors and global disease diffusion dynamics.

The basic formulation structure includes the following parts, as shown in Figure 1:

1. Social contact network. This network, in which nodes stand for autonomy agents and edges characterize contact, represents the heterogeneity in individuals' neighborhood interactions.
2. Local decision making mechanism. In each time unit, individual will make a vaccination decision based on three concerns: (1) respective payoff of vaccinating or not, (2) history records of vaccination decisions, (3) environmental evaluations.
3. Disease infection model. Infectious disease can stochastically spread along edges of connected individual pairs in terms of interaction quality and vaccination decisions.
4. Global characteristics of disease diffusion process. These Global features include (1) Population immunization patterns, which characterizes individuals' decisions of vaccination in population level, (2) Epidemics spreading dynamics, which reflect the individuals' infection state on the population communities.

Thus, we can investigate the coupling relationship between local individuals' behaviors and global epidemics spreading dynamics.

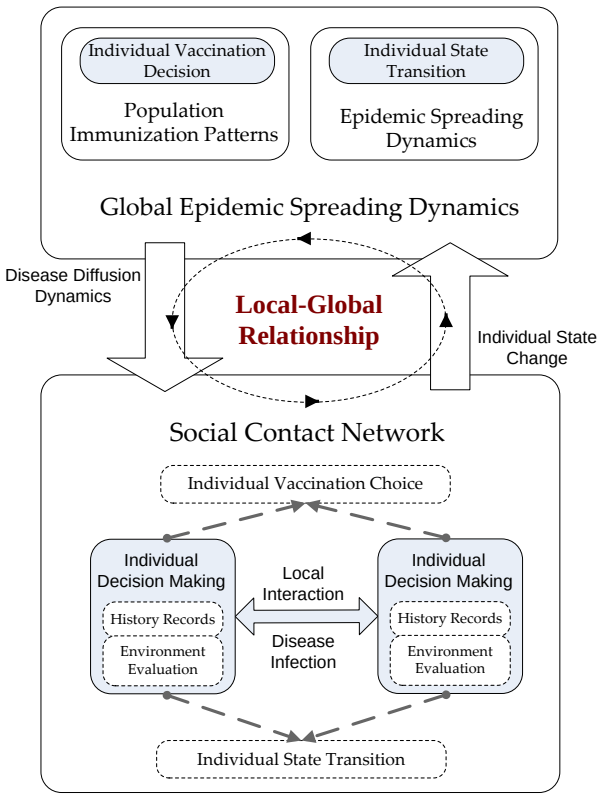

Figure 1, Basic formulation structure of epidemic spreading model

3. Social Contact Network

Many epidemics spreading through human populations are mainly based on individuals' physical interactions. These individual level interactions can be thought to form a network with nodes, standing for hosts, and links, representing interactions. During an epidemic outbreak, the spreading of individuals' infection can be viewed as disease diffusion along network links. So the features of human contact pattern can be interpreted as the structural complexity of social contact network.

To build a contact network model, the statistical data are needed to exploit the properties of real human interaction patterns. Many progresses have been achieved, such as tracing all infected individuals and their contacts during or following an outbreak [10], surveying individuals in populations [11] and using census [12], and social characteristic [13] and so on. Among all these properties of real human contact patterns in epidemic spreading process, scale free network draws more and more concerns. Scale-free network is characterized by degree distributions which follow a power law distribution meaning that a small fraction of nodes have highly connected edges [14]

(Figure2.b). Scale-free properties have been found in many fields, such as information technology (e.g. the Internet, the World Wide Web) [15][16] and biological systems (e.g. metabolic, protein interactions, transcription regulation and protein domain)[17~21].

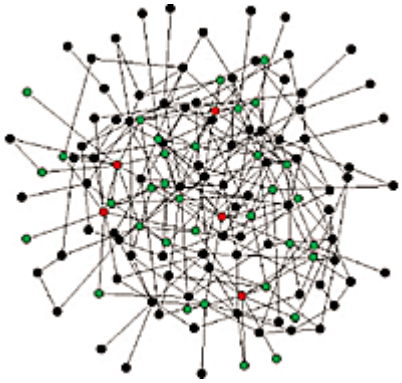

(a) Random Network

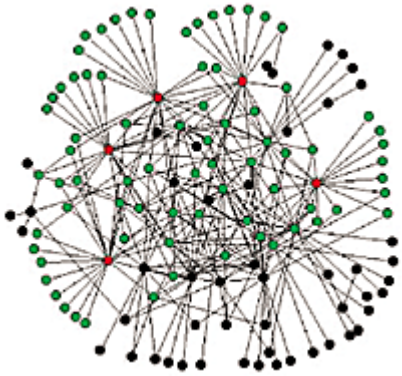

(b) Scale Free Network

Figure 2, In the random network, the five nodes with the most links (red) are connected to only 27% of all nodes (green). In the scale-free network, the five most connected nodes (red) are connected to 60% of all nodes (green). (Source Link: Scale-Free Networks)

In this study, a social contact network explicitly represents individual host interactions which are the medium for epidemic spreading. In this network, a node represents an individual host which might be infected by neighbors or infect its neighbors; an edge between two nodes represents an interaction relationship that is a disease transmission path; the weight value of an edge can be interpreted as the quality of individual interaction. A node's degree is the number of edges attached to it and the degree distribution of a network is the frequency distribution of degrees throughout the entire population, which is a reflection of the heterogeneity of individuals contact patterns.

This social contact network is medium for disease diffusion and with a scale free topology to characterize the individuals' contact pattern. It will focus exclusively on the epidemiological impact of the heterogeneity of contact pattern, although other structural characteristics of network, such as node clustering, community structure, or degree correlation, are also important factors to influence the disease diffusion process. For another aspect, the network model is also assumed to be a static network, which means the contact pattern is supposed to be fixed in the epidemic spreading process.

4. SIV Disease Infection Model

In the research of epidemic spreading process, many sophisticated models are proposed to simulate the disease diffusion mechanism, such as SIS/SIR model [22], spatial metapopulation models [23][24]. However these traditional models are mainly based on mixing assumption and differential equations, which characterize the statistical features of disease infection.

In this section, we will describe a SIV disease infection model on the social contact network. A scale free social contact network with N nodes and average neighbor size v can be generated under the preferential attachment rule [14]. We assume that individual nodes have three possible states in disease infection process, susceptible state (S), infected state (I) and vaccinated state (V) (Figure 3). The disease infections are only transmitted through neighborhood links that the susceptible individual can be infected by its direct infectious neighbors and infected nodes can transmit infection to its direct neighbors. If the individual is vaccinated, so it is safe from disease infection until expiration of vaccination efficacy.

4.1. Disease Percolation

In this study, we suppose the disease transmission is a percolation process through the contact network. In each time unit, the infected node will randomly select a direct neighbor to spread disease infection. The probability of a neighbor node being selected P_{Trans} is proportional to its edge weight value in terms of that of the whole neighbors.

$$P_{Trans(i,j)} = \frac{w_{ij}}{\sum_{k \in neighbor} w_{ik}} \quad (1)$$

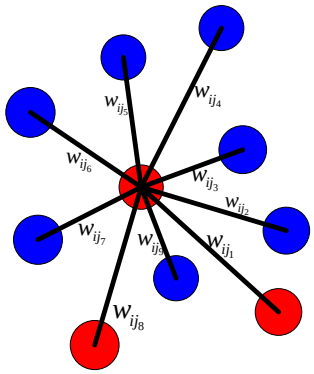

Figure 3, SIV Disease Model

In each time units, if the selected neighbor is in susceptible state, disease infection is successful and the state of the selected one will be changed into infected state; if the selected neighbor is in infected state or vaccinated state, disease infection is failed.

4.2. Individual Infection

If a susceptible node is not vaccinated, it will face the risk of being infected by its infectious neighbors. As we have mentioned the probability of infectious individual e_i to infect its susceptible neighbor e_j is $P_{Trans(i,j)}$. Thus, a susceptible node e_j with $n_{\inf}$ infectious neighbors will have a total probability $\lambda_{\inf}$ that node e_j becomes infected in the current time unit.

$$\lambda_{\inf} = 1 - \prod_{i=n_{\inf}} (1 - P_{Trans(i,j)}) \quad (2)$$

If a node is infected, the duration of infection can be drawn from a gamma probability distribution function with a mean of $1/\gamma$ and a variance of V_γ time units, which simulate the difference among population on the demography characteristics. After this infection duration, the infected node can be either died with a probability $d_{\inf}$ as a cost of disease infection, or recovered with a probability $1-d_{\inf}$ to susceptible state without any residual immunity.

Here must points out that the dead infected individual does not means to erase the node from the network. It just represents a possible severe punishment for individual's infection, which is an important factor for individuals' decision making.

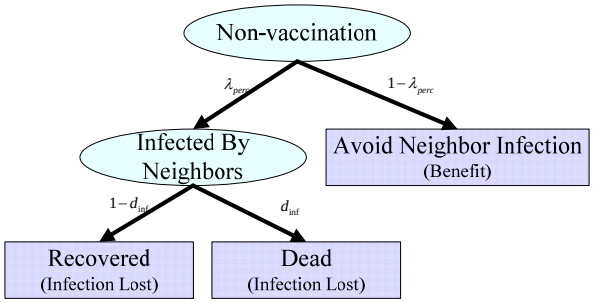

Figure 4, Individual state transition without vaccination

4.3. Individual Vaccination

If the node adopts vaccination choice, it will face death risk caused by the side effect of vaccination. We assume that the death possibility caused by vaccination is d_{vac}, and the efficacy of the vaccine to provide successful protection from disease infection is ε. If the vaccination do not have any side-effects but still fail to immunize the node, the current node will keep in the susceptible state faced with the risk of disease infection.

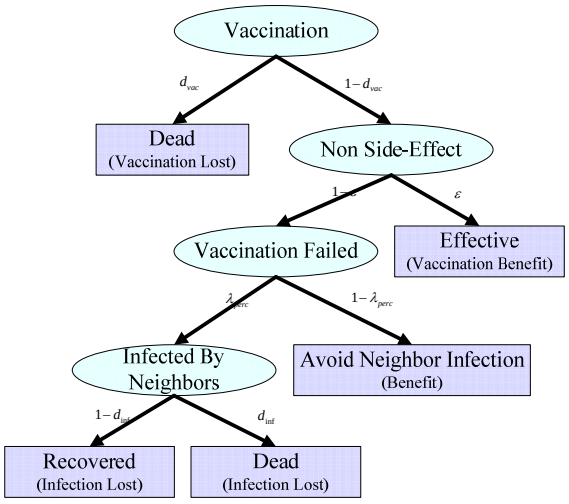

Figure 5, Individual state transition with vaccination

5. Individual Vaccinating Decision Making

In the disease infection and vaccination model, each individual face with two kinds of risk, risk of disease infection, and risk of vaccination's side-effect or failure. As the vaccination coverage increase, the infection risk is decreased relatively due to the herd immunity. Hence, the incentive for individual to vaccination is also reduced, which in turn will accelerate the disease transmission. This effect of individuals' behavior on disease diffusion

dynamics can be treated in game theoretical analyses of infection dynamics and vaccination choice.

In this section, we will incorporate individuals' vaccinating behaviors into disease infection model. And the following four aspects will influence individuals' decision making:

1. Perceived payoff value of vaccination and non-vaccination on current status.
2. Individuals' history decision making experience.
3. Environment Evaluation for global disease diffusion dynamics and local neighbors' statuses.
4. Individuals' biased preferential choice based on the above three criteria.

By incorporating individual behaviors into disease infection model, we can observe the correlation between local individual actions to the global epidemic dynamics.

5.1. Perceived Payoff Functions

In a given time unit, a susceptible individual can choose either vaccination or non-vaccination based on payoff value P_v (vaccination) and P_N (non-vaccination) relatively. Individuals will weigh the benefits of vaccinating, such as immunization protection from neighborhood infection but with small vaccine death risks and some probability vaccine failure, against the benefits of non-vaccinating, such as eliminating risk of vaccine but with possibly infection risk.

Payoff value P_N for non-vaccinating

If the individual does not vaccinate, it can be either infected with perceived infection probability $\lambda_{\inf}$ or not with probability $1-\lambda_{\inf}$. If the susceptible individual escapes the neighbor infections the payoff value will be L_{sus}. If the current susceptible individual is infected, and after its infection duration it is died with probability $d_{\inf}$, leaving the payoff value in this step zero. If the individual survives from infection with probability $1-d_{\inf}$, the payoff value for this circumstance is $L_{\inf}$. Hence, the overall payoff value of non-vaccinating individual choice is

$$P_N = (1-\lambda_{\inf})\bullet L_{sus} + \lambda_{\inf}\bullet[(1-d_{\inf})\bullet L_{\inf}] \qquad (3)$$

Payoff value P_v for vaccinating

If a person chooses to vaccinate, then either the vaccine has vital side-effect with probability d_{vac}, or not with the relative probability $1-d_{vac}$. We also suppose that the vaccine without side-effect will be truly efficacious to provide immunization with probability ε, or fail to protect individuals just leaving it still in the susceptible state. If the individual successful vaccinate itself, the payoff value in this step is L_{vac}. If the individual choose vaccination but the vaccine has neither side-effect to death nor efficacy to immunization, the relative payoff in this circumstance is the same the non-vaccinating individuals. Thus, the overall payoff value for vaccinating individuals is

$$P_V = (1-d_{vac})\{\varepsilon L_{vac} + (1-\varepsilon) \bullet\{(1-\lambda_{\inf})\bullet L_{sus} + \lambda_{\inf}\bullet[(1-d_{\inf})\bullet L_{\inf}]\}\} \qquad (4)$$

In summary, there are four payoffs for individuals' decision.

1. If individual is died either for the disease infection or for side-effect of vaccination, the payoff is zero.
2. If the susceptible individual escapes from disease infection, the payoff is L_{sus},
3. If the infected individual recovers from disease infection, the payoff is $L_{\inf}$,
4. If the susceptible individual is successful vaccinated, the payoff is L_{vac}.

Based on the common sense, it is reasonable to expect that $L_{\inf} < L_{sus} < L_{vac}$, for individual benefit of successful vaccination is the biggest, and that of recovered individual is the least, the benefit of susceptible individual is in the middle.

5.2. History Experience

Each individual in the social contact network has a record of its past experience of vaccination decision making. Individual will evaluate the necessary of vaccination based on the real efficacy of past vaccination memory.

There are four kinds of records for each individual's to vaccination adoption.

1. Individual is vaccinated, and successfully defend infection attacks at least once.
2. Individual is vaccinated, but no infection attack happens in the duration of vaccine.
3. Individual is non-vaccinating, and successfully escapes from infection attacks.
4. Individual is non-vaccinating, but infected by its infectious neighbors.

We assume each of the records above have a payoff value h_{vac}^{+}, h_{vac}^{-}, h_{non}^{+}, h_{non}^{-} respectively. We also suppose that $h_{vac}^{+} = -h_{vac}^{-}$, $h_{non}^{+} = -h_{non}^{-}$, which are the decision judgment based on the disease diffusion result. Hence, in

time unit k the historical evaluation of vaccinating behaviors $H_{vac}(k)$ (vaccination history) and $H_{non}(k)$ (non vaccination history) can be updated as following:

$$H_{vac}(k) = \lambda_{decay} \bullet H_{vac}(k-1) + h_{vac}(k) \quad (5)$$

$$H_{non}(k) = \lambda_{decay} \bullet H_{non}(k-1) + h_{non}(k) \quad (6)$$

λ_{decay} is decay ratio, meaning that the most recent records have a bigger influence on individuals' decision making.

5.3. Environment Evaluation

We assume that each individual has a full ability to communicate with its direct neighbors, but a confined global information achievement. For local interaction, the individual can detect its neighbor's state and vaccination choice of last time. For global information, we suppose that individuals can get the global infection rate as a severity estimation criterion. Thus these environment evaluation parameters will influence individuals' vaccination decision making process.

r_{vac} is the proportion of the vaccinated neighbors to all neighbors.

$$r_{vac} = \frac{n_{vac}}{n_{neigb}} \quad (7)$$

$r_{\inf}$ is the proportion of the infected neighbors to all neighbors.

$$r_{\inf} = \frac{i_{vac}}{n_{neigb}} \quad (8)$$

$R_{\inf}$ is the infection rate in the global network.

$$R_{\inf} = \frac{I}{N} \quad (9)$$

5.4. Individual Biased Preference Rules

In each time unit, individuals' vaccination decision making is based on three parts (Figure 5):
(1) Payoff function P_V and P_N;
(2) History records H_{vac} and H_{non};
(3) Environment estimation r_{vac}, $r_{\inf}$ and $R_{\inf}$.

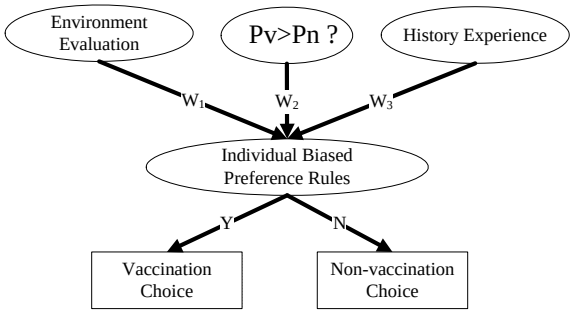

Figure 6, Individual Biased Preference Rules

We assume some biased preference rules to simulate human's irrational decision making behaviors.

- Individuals are more incline to rely on their history experience.
- Individuals are likely to simulate its neighbor's behaviors.
- Pandemic scare is based on individuals' irrational estimation.

Thus, based on the above biased preference assumptions, we can design the decision making functions as following:

$$E_{vac}(k) = P_V(k) + \xi_i^1 \bullet H_{vac}(k) + \xi_i^2 \bullet [tg(\frac{\pi}{2} \bullet r_{vac}) + tg(\frac{\pi}{2} \bullet R_{\inf})] \quad (10)$$

$$E_{non}(k) = P_N(k) + \zeta_i^1 \bullet H_{non}(k) + \zeta_i^2 \bullet [tg(\frac{\pi}{2} \bullet (1 - r_{vac})) + tg(\frac{\pi}{2} \bullet (1 - R_{\inf}))] \quad (11)$$

If $E_{vac}(k) > E_{non}(k)$, the current individual will adopt the vaccination choice, or vice versa. ξ_i^1 ζ_i^1 are parameters to modify the influence of history experience for vaccination and non-vaccination. ξ_i^2 ζ_i^2 are variables to control the impact of environment estimations.

Function $tg(\frac{\pi}{2} \bullet r_{vac})$ is designed to simulate individual's neighbor following feature. If the proportion of vaccinated neighbors is increased the current will more inclined to adopt vaccination. Function $tg(\frac{\pi}{2} \bullet R_{\inf})$ tries to describe the potential epidemic scare. If the global infection rate is near 100%, each individual will irrationally adopt vaccination instead of balancing payoff gains.

6. Conclusions

It is now well recognized notion that human's behaviors will influence the epidemic spreading. What kinds of relationship coupling the local individual behavioral patterns to the global disease diffusion dynamics is still obscure. Aimed to investigate this core problem in epidemic control, we design a SIV infection model incorporated with complex human behaviors under AOC modeling framework. In this model, we try to investigate what kinds of impact the human behavior will impose on the disease diffusion process, such as self-interest choice, following neighbors, panic irrationality, etc, and inversely what kind of influence will the epidemic dynamics have on individuals' decision making, e.g. mass infection case or scare infection rate. Based on this model, we expect a clear picture to portray the skeleton about the local global relationship in epidemic spreading process.

Reference

[1] L. Meyers, M. Newman, B. Pourbohloul. Predicting epidemics on directed contact networks. Journal of Theoretical Biology, 240(3): 400-418, 2006.

[2] S. M. Poutanen. Identification of severe acute respiratory syndrome in Canada. *New England Journal of Medicine*, 348:1995-2006, 2003.

[3] H. W. Hethcote. Mathematics of Infectious Diseases. *Society for Industrial and Applied Mathematics Review*, 42(4): 599-653, 2000.

[4] Timothy C. Reluga. An SIS Epidemiology Game with Two Subpopulations. *Journal of Biological Dynamics*, 27(1):1-19, 2008.

[5] A. Prisic, C. Bauch. Social contact networks and Disease Eradicability under voluntary vaccination policy. *PLoS Computational Biology*, 5(2), 2009.

[6] A. Perisic, C. Bauch. A simulation analysis to characterize the dynamics of vaccinating behavior on contact networks. *BMC Infectious Diseases*, 77(9), 2009.

[7] M. Keeling. The implications of network structure for epidemic dynamics. *Theoretical Population Biology*, 67(1):1-8, 2005.

[8] S. Bansal, B.T. Grenfell, L.A. Meyers. When individual behavior matters: Homogeneous and network models in epidemiology. *Journal of the Royal Society Interface*, 4(16): 879-891, 2007.

[9] J. Liu. Autonomy-Oriented Computing (AOC): The nature and implications of a paradigm for self-organized computing (keynote talk). *In Proceedings of the 4th International Conference on Natural Computation and the 5th International Conference on Fuzzy Systems and Knowledge Discovery*, 3-11, 2008.

[10] A. S. Klovdahl, Z. Dhofier, G. Oddy, J.O. Hara, S. Stoutjesdijk, A. Whish. Social networks in an urban area: First Canberra Study. *Journal of Sociology*, 13(2): 169-172, 1977.

[11] S. Eubank, H. Guclu, V.S. Kumar, M.V. Marathe, A. Srinivasan, Z. Toroczkai, N. Wang. Modeling disease outbreaks in realistic urban social networks, *Nature*, 429: 180-184, 2004.

[12] L.A. Meyers, B. Pourbohloul, M.E. Newman, D.M. Skowronski, R.C. Brunham. Network theory and SARS: Predicting outbreak diversity. *Journal of Theoretical Biology*, 232(1), 71-81, 2005.

[13] M.E. Halloran, I. M. Longini, A. Nizam, Y. Yang. Containing bioterrorist smallpox, *Science*, 298: 1428-1432, 2002.

[14] A.L Baraba´si, R. Albert. Emergence of scaling in random networks, *Science*, 286: 509-512, 1999.

[15] R. Albert, H. Jeong, A.L. Barabasi. The diameter of the World Wide Web. *Nature*, 401: 130-131, 1999.

[16] M. Faloutsos, P. Faloutsos, C. Faloutsos. On power-law relationships of the Internet topology. *Computer Communication Review*, 29(4):251-262, 1999.

[17] S. Wuchty. Scale-free behavior in protein domain networks. *Molecular Biology and Evolution*, 18(9): 1694-1702, 2001.

[18] L. Giot, J. S. Bader, C. Brouwer, A. Chaudhuri, B. Kuang, Y. Li, Y.L. Hao, C.E. Ooi, B. Godwin, E.A. Vitols. Protein interaction map of Drosophila melanogaster, *Science*, 302(5651): 1727-1735, 2003.

[19] P. Bork, L. J. Jensen, C. V. Mering, A.K. Ramani, I. Lee, E.M. Marcotte. Protein interaction networks from yeast to human. *Current Opinion in Structural Biology*, 14(3): 292-299, 2004.

[20] V. Hatzimanikatis, C. Li, J. A. Ionita, L. J. Broadbelt. Metabolic networks: Enzyme function and metabolite structure. *Current Opinion in Structural Biology*, 14(3): 300-306, 2004.

[21] N.M. Luscombe, M.N. Babu, H. Yu, M. Snyder, S. A. Teichmann, M. Gerstein. Genomic analysis of regulatory network dynamics reveals large topological changes, *Nature*, 431: 308-312, 2004.

[22] M.J. Keeling, K.T.D. Eames. Networks and epidemic models. *Journal of The Royal Society Interface*, 2(4):295–307, 2005.

[23] B. M. Bolker, B. T. Grenfell. Mass vaccination to control chickenpox: the influence of zoster. *Proceedings of the National Academy of Sciences of the United States of America Proc. Natl*, 93(14):7231-7235,1996.

[24] M.J. Keeling, B.T. Grenfell. Disease extinction and community size: Modeling the persistence of measles. *Science*, 275:65-67, 1997.

Extracting Discriminative Binary Template for Face Template Protection

Yicheng Feng

Abstract

This paper addresses the security issues of the face biometric templates stored in a database. In order to improve the security level of the stored face templates, cryptographic techniques are commonly employed. Since most of such techniques require a binary input, thresholding is usually employed to binarize the real valued face features. While binary templates are obtained, the discriminability of the original templates may be affected and so is the recognition performance. In order to overcome this limitation, this paper proposes a new approach to discriminative extract binary templates from original face templates. A projection is applied before thresholding such that the thresholding can fit the projected data distribution better, which makes the extracted binary templates more discriminative. A discriminability index is constructed to measure the discriminability of the extracted binary templates and the projection matrix is optimized. The proposed method is evaluated on three public domain databases, namely FERET, CMU-PIE and FRGC. Experimental results show that, in comparison to the existing thresholding-based methods, the proposed method improves the GAR by around $11\% - 13\%$ *at a FAR of* 1%.

1 Introduction

Biometrics is a reliable, robust and convenient way for person authentication [9, 10, 6]. With the success of the biometrics research in the last two decades, several large scale recognition systems have been successfully deployed. With the growing use of biometrics, there is a rising concern about the security and privacy of the stored biometric templates (which refer to a set of features extracted from raw biometric data) stored in a database or a smartcard. Recent studies [11] show that simple attacks on a biometric system, such as hill climbing, are able to recover the raw biometric data from a stolen biometric template. Moreover, the attacker may be able to make use of the stolen template to access the system or cross-match across databases. A comprehensive analysis of eight types of attacks [6] on a biometric system has been reported. Therefore, biometric template security [9, 10, 6, 18] has been an important issue in deploying a biometric system.

In order to overcome the security and privacy problems [6, 7, 9], a number of biometric template protection algorithms have been reported in the last few years. These methods can be broadly categorized into two approaches, namely biometric cryptosystem approach and transformation-based approach. The basic idea of both the approaches is that instead of storing the original biometric template, the transformed/encrypted template is stored. In case the transformed/encrypted biometric template is stolen or lost, it is computationally hard to reconstruct the biometric template and the original raw biometric data from the transformed/encrypted template. Generally speaking, the transform-based approach suffer from a trade-off between dicriminability and security of the transformed templates while biometric cryptosystems may provide both enhanced security and acceptable discriminability. Cryptographic technique is employed in the last step in the cryptosystems approach to enhance the security of the templates. Error-correcting schemes are applied to deal with the intra-class variance thus the discriminability of the encrypted templates will not degrade too much. However, most of the protection algorithms in biometric cryptosystem approach require a binary template or integer data (most for the fuzzy vault scheme [5]) for encryption. That means, the input template has to be converted into a binary or integer template before encryption. The fuzzy vault scheme is mostly applied to fingerprint. The minutiae of fingerprint are unordered set of points, which the fuzzy vault scheme is just able to encrypt. For face recognition algorithms like PCA or LDA schemes, the situation is much different because the extracted templates are ordered real value vectors with large range, which causes a problem to apply the fuzzy vault scheme. On the other hand, there are schemes to transform the original face templates into binary strings for protection. In order to satisfy the input requirements, thresholding is a typically employed in existing algorithms [12, 13, 14, 15, 16, 17]. While the binary template can be obtained, some useful and discriminative information in the original (real valued) template may be lost after thresholding leading to degraded matching accuracy (discriminability) [12, 13]. And existing approaches lack of discriminabil-

ity evaluation of the thresholding process.

In view of the limitations on existing thresholding-based algorithms, this paper provide a discriminability optimized thresholding scheme. Directly optimize the thresholds may have some problems. For security issues, the information content of the quantized binary templates should be maximized such that a brute-force attack will be most expensive to break the system. To maximize the information content of the bits, the thresholds should be set to make half of the corresponding bits in the binary templates to be "0" and half to be "1". Which implies the thresholds should be set as the mean value of the corresponding elements of the original templates (called max-entropy rule). It means that the thresholds are already determined. And binary templates with maximum information content imply that they already get certain discriminability, which are shown clearly in experiments. So thresholds optimization makes little sense. Here we choose another approach. Before thresholding, an orthonormal projection process is applied to rotate the data position such that the thresholding fits the data distribution better. And the projection matrix is optimized such that the output binary templates after thresholding will have maximum discriminability. And we turn the whole thresholding process including the projection into an approximation process. The output binary templates is approximated by a linear function of original templates such that we can avoid the non-linear thresholding function while constructing the objective function.

The rest of this paper is organized as follows. Section 2 gives a brief review of the existing binarization schemes. Our proposed algorithm is then reported in Section 3. Experimental results and analysis are given in Sections 4. Finally, Section 5 gives the conclusion.

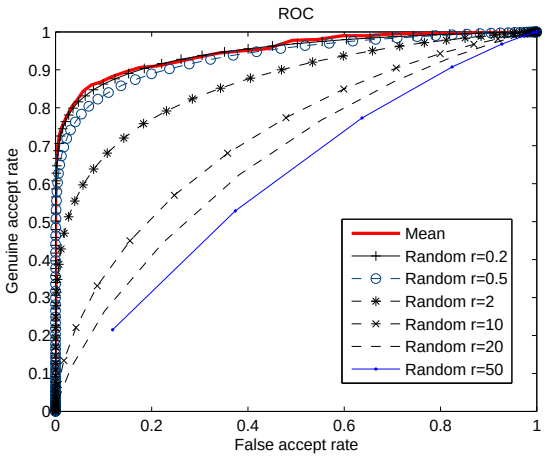

Figure 1. The effect of adjusting thresholds: The curves show performances in FERET database of binary templates extracted by a straightforward thresholding process. symbol "Mean" means the thresholds are set as the mean values of the original templates. "Random" means thresholds are randomly chosen with a Gaussian distribution, in which the mean of the distribution is mean of the original templates and variance of the distribution is r times of the variance of the original templates. The random thresholds are generated 100 times for experiment and the curves represent the average performance. It shows clearly that when r is closer to 0 the performance is higher, implying that thresholds with mean value of original templates are already close to optimal.

2 Review on Existing Binarization Schemes

A comprehensive survey on biometric template protection has been reported in [9, 8]. This section mainly reviews the existing binarization schemes in biometric template protection.

Monrose $et\ al.$ [12, 13] first proposed a binarization scheme, who described a cryptographic key generation scheme from biometrics. The biometric data is transformed into a binary string called "feature descriptor" which has relatively small intra-class variance and large between-class variance. This binary string is generated by a thresholding technique based on mean and standard deviation of the biometric data.

Goh and Ngo [15] proposed a biohashing scheme. In their scheme, the original templates are first transformed using random mapping. Each element of the transformed template is thresholded to either 0 or 1, thus converting the template into binary form. Different versions of Biohashing algorithms [14, 17] have been proposed in the last few years but their binarization schemes are quite similar.

Chang and Roy [22] proposed a fingerprint binarization scheme. It draws lines to the original fingerprint. The difference of numbers of minutiae lying in each side of the lines are used to construct an integer number vector. PCA is applied decorrelate the vector and the deccorelated vector is then quantized to bits with threshold 0.

Nagar $et\ al.$ [24, 23] proposed a scheme to generate binary helper data from fingerprint. It first extract a minutiae descriptor from the minutiae of fingerprint with the orientation and ridge frequency information, then quantizes each element of the minutiae descriptor into 2^5 or 2^4 integer values. These values are converted to bits with Gray codes (because the converted Gray codes from neighbor value differ only 1 bit).

Kevenaar $et\ al.$ [25] proposed a face template binariza-

tion scheme. It statistically estimates the means and variances of the enrolled original templates. The means are used as thresholds for quantization which converts the original templates into bits. The scheme also constructs an index with the means and variances to measure the reliability of the converted bits. Only bits with high reliability are selected for recognition.

Linnartz and Tuyls [26] proposed a quantization scheme with quantization step size q. It did not directly extract the bit string from biometric data but link a binary secret to the biometric data. A binary string secret S is selected. For the original reference template X, a helper data W is constructed such that elements of $S+W$ are multiples of q and the quantized values of $X+W$ have the same parities of corresponding bits in S. For a testing template Y, $W+Y$ is quantized to an integer number vector and then the parity of the vector is checked to extract a bit string S'. S and S' is compared for decision.

Feng $et\ al.$ [19, 20, 21] proposed a class-distribution-preserving transform (CDP transform) for binarization. Distinguishing points are determined. The distance between each distinguishing point and the face template is calculated and thresholded. With optimal positioning of the distinguishing points, the transform optimizes the discriminability of the binary strings. Thus the discriminability-preserving ability of this scheme is justified. But note that it is still a thresholding-based approach.

3 Proposed Algorithm: Optimized Thresholding with Projection

3.1 Basic Idea

To binarize a biometric feature vector (template), the most straightforward and common way is to apply a quantization/thresholding algorithm, which is applied in most of the existing schemes. However, lack of discriminability analysis is still a problem for the binarization approach. Do the transformed binary templates have enough discriminability or not? In this paper we do a primary research to propose a new thresholding approach which provides a discriminability index, and optimize such index to extract binary templates having optimal discriminability. As we mentioned before, directly optimizing the thresholds is not effective. Here we choose a different approach (illustrated in Figure 2) to solve the optimization problem. Before thresholding, an orthonormal projection is applied to transform the input original templates into a new domain. The projection matrix is optimized such that the output binary templates after thresholding have optimal discriminability. The thresholds in the thresholding is fixed with the max-entropy rule.

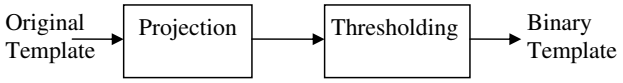

Figure 2. The proposed thresholding scheme with projection.

An orthonormal projection will not change the relative positions of the original templates in the feature space, thus after the projection the discriminability of the original templates will be completely preserved. This is quite important because if the projection cause discriminability lost, it will contradict our purpose to maximize the discriminability. And an orthonormal projection can rotate the original templates in feature space to new positions, such that the thresholding can fit the data distribution better. The two-dimensional case is illustrated in Figure 3. The thresholding in each dimension (abscissa and ordinate) can be treated as a line that divides the feature space into two halves. Given two classes of points as Figure 3 illustrated, directly adjust the abscissa and ordinate thresholds would not completely separate the two classes (illustrated in sub-figure (a)). However, after projection, thresholding in abscissa can completely separate the two classes (illustrated in sub-figure (b)). So, when the thresholds are fixed, we can optimize the projection matrix such that the thresholding well separates different classes of rotated templates, therefore provide high discriminability to the quantized binary templates. Since thresholding will cause rather complicated formulation to construct the discriminability index, the whole thresholding (including projection) process is converted to an approximation process in latter steps.

3.2 Optimize Thresholding through Approximation

To measure the discriminability of the binary templates, we adopt the concept of within-class variance and between-class variance. The within-class variance and the between-class variance are defined for each class respectively, therefore different optimized projection matrices can be chosen for different classes such that they can fit the distribution of each class better than a matrix for all classes. The within-class variance and between-class variance are defined as Equation (1) and (2):

$$D_W(\Omega) = \frac{\sum_{p\in\Omega} ||w(p) - w_\Omega||^2}{\sum_{p\in\Omega} 1} \quad (1)$$

$$D_B(\Omega) = \frac{\sum_{p\notin\Omega} ||w(p) - w_\Omega||^2}{\sum_{p\notin\Omega} 1} \quad (2)$$

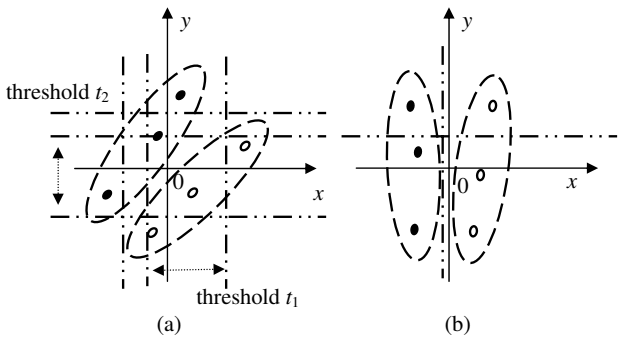

Figure 3. The effort of projection to thresholding (a) scenario of the original thresholding, thresholds are directly optimized; (b) thresholding with projection. The solid an hollow points represent templates in two different classes (illustrated with ellipses). It shows clearly that the thresholding in (b) separates two classes.

where $D_W(\Omega)$ and $D_B(\Omega)$ represents the within-class variance and between-class variance of class Ω. w_Ω denotes the reference binary template that represents Ω and $w(p)$ represents the binary template transformed from original template p. With the defined within-class variance and between-class variance, the discriminability is defined as $D_B(\Omega) - D_W(\Omega)$. Here w_Ω needs to be determined and we do not directly generate w_Ω from the training data, but find it through optimization together with the projection matrix such that the discriminability is maximized. Assume the projection matrix is M. $D_B(\Omega)$ and $D_W(\Omega)$ are subject to M and w_Ω. Then the objective function is constructed as Equation (3):

$$(M_{opt}, w_{opt}) = \underset{M, w_\Omega}{\operatorname{argmin}}(D_B(\Omega) - D_W(\Omega)) \qquad (3)$$

As we mentioned before, directly optimize such an objective function is unconvenient because of the thresholding function. So before optimization, we first turn the thresholding function to an approximation process.

In our proposed thresholding process, the original template p is first projected with an orthonormal matrix M to $u = M^T p$, and then thresholded with Equation (4):

$$b_j = \begin{cases} 1 & : \quad h_j \geq t_j \\ -1 & : \quad h_j < t_j \end{cases} \qquad (j = 1, 2 \ldots k) \qquad (4)$$

where h_j are components in u. Because of the max-entropy rule, t_j should be the mean value of h_j. A normalization process with Equation (5) can turn the equation to be simpler with all thresholds 0:

$$q = \frac{p - \overline{p}}{||p - \overline{p}||} \qquad (5)$$

where $\overline{p}$ denotes the mean vector of all the original templates. With such a normalization, Equation (4) turns to Equation (6):

$$b_j = \begin{cases} 1 & : \quad a_j \geq 0 \\ -1 & : \quad a_j < 0 \end{cases} \qquad (j = 1, 2 \ldots k) \qquad (6)$$

where a_j are the elements in $v = M^T q$.

Equation (6) can be further turned into an approximation process (Equation (7)):

Given an unit vector $v = (a_1, a_2 \ldots a_k)$, it is transformed to a binary string $w'(v) = (b_1, b_2 \ldots b_k) \in \{1, -1\}^k$ with the following equation:

$$w'(v) = \underset{\omega}{\operatorname{argmin}} ||v - \frac{\omega}{\sqrt{k}}|| \qquad (7)$$

where $w'(v)$ represents the binary template transformed from v.

It can be shown that

$$||v - \frac{\omega}{\sqrt{k}}||^2 = \sum_{j=1}^{k} (a_j - \frac{b_j}{\sqrt{k}})^2$$

is minimum if and only if b_j satisfies Equation (6). So Equation (7) is equivalent to Equation (6), thus $w'(v) = w(p)$.

Substitute $v = M^T q$ into Equation (7), we have

$$w''(q) = w'(v) = \underset{\omega}{\operatorname{argmin}} ||M^T q - \frac{\omega}{\sqrt{k}}|| \qquad (8)$$

So our binarization scheme $w(p)$ can be turned into an approximation process $w''(q)$ as Equation (8) describes. Denote $e = \frac{M w_\Omega}{\sqrt{k}}$. Therefore,

$$\begin{aligned} & ||w_\Omega - w''(q)|| \\ = \; & \sqrt{k} || \frac{w_\Omega}{\sqrt{k}} - M^T q + M^T q - \frac{w''(q)}{\sqrt{k}} || \\ \leq \; & \sqrt{k} (|| \frac{w_\Omega}{\sqrt{k}} - M^T q|| + ||M^T q - \frac{w''(q)}{\sqrt{k}}||) \\ \leq \; & 2\sqrt{k} || \frac{w_\Omega}{\sqrt{k}} - M^T q|| \\ = \; & 2\sqrt{k} || \frac{M w_\Omega}{\sqrt{k}} - M M^T q|| \\ = \; & 2\sqrt{k} ||e - q|| \end{aligned} \qquad (9)$$

Notice here $|| \frac{w_\Omega}{\sqrt{k}} - M^T q||$ is no less than $|| \frac{w''(q)}{\sqrt{k}} - M^T q||$ because $\frac{w''(q)}{\sqrt{k}}$ is closet to $M^T q$ (Equation (8)).

On the other side,

$$\begin{aligned} & ||w_\Omega - w''(q)|| \\ = \; & \sqrt{k}||\frac{w_\Omega}{\sqrt{k}} - M^T q + M^T q - \frac{w''(q)}{\sqrt{k}}|| \\ \leq \; & \sqrt{k}||\frac{w_\Omega}{\sqrt{k}} - M^T q|| + \sqrt{k}||M^T q - \frac{w''(q)}{\sqrt{k}}|| \\ = \; & \sqrt{k}||q - e|| + \sqrt{k}||M^T q - \frac{w''(q)}{\sqrt{k}}|| \end{aligned}$$

implies

$$\begin{aligned} & |(||w_\Omega - w''(q)|| - \sqrt{k}||q - e||)| \\ \leq \; & \sqrt{k}||M^T q - \frac{w''(q)}{\sqrt{k}}|| \end{aligned} \quad (10)$$

Here $||M^T q - \frac{w''(q)}{\sqrt{k}}||$ is minimized with optimal $w''(q)$. To let the approximation error as small as possible, Equation (5) makes $M^T q$ an unit vector and scalar $\sqrt{k}$ is used such that $\frac{w''(q)}{\sqrt{k}}$ is a normalized vector too. Without $\sqrt{k}$,

$$||M^T q - w''(q)|| \geq ||w''(q)|| - ||M^T q|| = \sqrt{k} - 1$$

causing large approximation error. With $\sqrt{k}$, $\frac{w''(q)}{\sqrt{k}}$ is a unit vector thus the norms of $M^T q$ and $\frac{w''(q)}{\sqrt{k}}$ provide no contribution to the approximation error, resulting in small approximation error. Then Equation (10) implies that

$$||w_\Omega - w''(q)|| \approx \sqrt{k}||\frac{w_\Omega}{\sqrt{k}} - M^T q|| \quad (11)$$

Denote $m = \sum_{p \notin \Omega} 1$ and $n = \sum_{p \in \Omega} 1$. Substitute Equation (9) into Equation (1) and (11) into (2). Since $w''(q) = w'(v) = w(p)$, we have

$$D_W(\Omega) = \frac{\sum\limits_{p \in \Omega} ||w(p) - w_\Omega||^2}{n} \leq 4k \frac{\sum\limits_{q \in \Omega} ||q - e||^2}{n} \quad (12)$$

and

$$D_B(\Omega) = \frac{\sum\limits_{p \notin \Omega} ||w(p) - w_\Omega||^2}{m} \approx k \frac{\sum\limits_{q \notin \Omega} ||q - e||^2}{m} \quad (13)$$

Equation (13) implies that a large $D'_B(\Omega)$ leads to large $D_B(\Omega)$. Equation (12) indicates that a small $D'_W(\Omega)$ leads to a small $D_W(\Omega)$. So the objective function is changed to

$$(M_{opt}, w_{opt}) = \underset{M, w_\Omega}{\operatorname{argmin}}(D'_B(\Omega) - D'_W(\Omega)) \quad (14)$$

where

$$D'_B(\Omega) = \frac{\sum\limits_{q \notin \Omega} ||q - e||^2}{m}$$

and

$$D'_W(\Omega) = \frac{\sum\limits_{q \in \Omega} ||q - e||^2}{n}$$

.

From Equation (14) we can see that with the approximation process, the terms including binary templates in the objective functions are replaced by terms with original templates. Therefore, there is no need to consider the correlation between bits and the thresholding process, thus solves the problems mentioned before. In Equation (14) M and w_Ω are only related to e. So we can first optimize e and then choose M and w_Ω to fit the optimized e:

$$e_{opt} = \underset{e}{\operatorname{argmax}}(\frac{\sum\limits_{q \notin \Omega} ||q - e||^2}{m} - \frac{\sum\limits_{q \in \Omega} ||q - e||^2}{n}) \quad (15)$$

with constraint

$$||e|| = 1 \quad (16)$$

.

The constraint is because $e = M\frac{w_\Omega}{\sqrt{k}}$ is an unit vector. After e_{opt} is found, w_{opt} is randomly generated and M_{opt} is constructed such that $\frac{M_{opt} w_{opt}}{\sqrt{k}} = e_{opt}$.

However, we should notice that the objective function can only ensure $D'_B(\Omega)$ is large, but can not ensure that $D'_W(\Omega)$ is small. So the following constraint

$$e \cdot q_\Omega \geq \theta \quad (17)$$

is required. Here q_Ω is the normalized mean vector of Ω and θ is a threshold smaller than 1. This constraint ensure that $D'_W(\Omega)$ is relatively small.

3.3 Solve the Objective Function

The objective function is first expanded as follows:

$$\begin{aligned} & \sum_{q \notin \Omega}(||q - e||^2)/m - \sum_{q \in \Omega}(||q - e||^2)/n \\ = \; & (\sum_{q \notin \Omega} ||q||^2 - 2\sum_{q \notin \Omega} q \cdot e)/m + ||e||^2 \\ & -(\sum_{q \in \Omega} ||q||^2 - 2\sum_{q \in \Omega} q \cdot e)/n - ||e||^2 \\ = \; & (\sum_{q \notin \Omega} ||q||^2/m - \sum_{q \in \Omega} ||q||^2/n) \\ & +2(\sum_{q \in \Omega} q/n - \sum_{q \notin \Omega} q/m) \cdot e \end{aligned}$$

where $\cdot$ denotes inner product. Assume r is the normalized vector of $\sum_{q \in \Omega} q/n - \sum_{q \notin \Omega} q/m$. According to the above equation, to maximize the objective function is equivalent to maximize $r \cdot e$.

Apply the Gram-Schmidt algorithm to randomly generate an orthonormal basis $\{s_1, s_2 \dots s_k\}$ where $s_1 = q_\Omega$. Denote Q to be the orthonormal matrix using $s_1, s_2 \dots s_k$ as columns. Then From Equation (17), we have

$$e^T Q Q^T q_\Omega \geq \theta \tag{18}$$

Denote $z = Q^T e = (x_1, x_2 \dots x_k)$. According to Equation (16), z is an unit vector. Because of the construction of Q, $Q^T q_\Omega = (1, 0, \dots 0)$. Substitute these two terms into Equation (18), we have

$$x_1 \geq \theta \tag{19}$$

Denote $l = Q^T r = (y_1, y_2 \dots y_k)$. Since r is an unit vector, l is an unit vector. Therefore,

$$r \cdot e = r^T Q Q^T e = l^T z = \sum_{j=1}^{k} x_j y_j$$

And

$$\begin{aligned} \sum_{j=1}^{k} x_j y_j &= x_1 y_1 + \sum_{j=2}^{k} x_j y_j \\ &\leq x_1 y_1 + (\sum_{j=2}^{k} x_j^2 \cdot \sum_{j=2}^{k} y_j^2)^{\frac{1}{2}} \\ &= x_1 y_1 + \sqrt{1 - x_1^2}\sqrt{1 - y_1^2} \end{aligned}$$

$\sum_{j=1}^{k} x_j y_j$ will achieve its maximum if and only if

$$x_j = \frac{\sqrt{1 - x_1^2}}{\sqrt{1 - y_1^2}} y_j \qquad j = 2 \dots k$$

Denote $\phi = \arccos x_1$, $\varphi = \arccos y_1$. Then,

$$\begin{aligned} \sum_{j=1}^{k} x_j y_j &= x_1 y_1 + \sqrt{1 - x_1^2}\sqrt{1 - y_1^2} \\ &= \cos\phi \cos\varphi + \sin\phi \sin\varphi \\ &= \cos(\varphi - \phi) \end{aligned}$$

From Equation (19), we have the restriction for ϕ:

$$0 \leq \phi \leq \arccos\theta$$

If $\varphi \leq \arccos\theta$ (that is, $y_1 \geq \theta$), set $\phi = \varphi$, $r \cdot e$ can achieve the maximum value 1. If $\varphi > \arccos\theta$, Then $0 < \varphi - \phi < \pi$. $\cos(\varphi - \phi)$ will be maximum when $\varphi - \phi$ is minimum. So ϕ should be $\arccos\theta$. That is, $r \cdot e$ will achieve its maximum when

$$x_1 = \begin{cases} y_1 & : \quad y_1 \geq \theta \\ \theta & : \quad y_1 < \theta \end{cases}$$

and

$$x_j = \frac{\sqrt{1 - x_1^2}}{\sqrt{1 - y_1^2}} y_j \qquad j = 2 \dots k.$$

Then, $e_{opt} = Qz = Q[x_1, x_2 \dots x_k]^T$.

After e_{opt} is found, w_Ω is randomly generated and M_{opt} is constructed such that $M_{opt} w_\Omega / \sqrt{k} = e_{opt}$.

3.4 Algorithm Implementation

In enrollment,

- Normalize the original feature vectors with Equation (5).
- Construct M and w_Ω for class Ω.
- w_Ω is used as the reference template and encrypted with the fuzzy commitment scheme for protection.
- The encrypted w_Ω and M are stored in database.

In authentication,

- when input a query p, the corresponding M is released.
- Normalize p to q with Equation (5). And then q is projected to $v = M^T q$.
- Threshold q to $w''(q) = (b_1, b_2 \dots b_k)$ with Equation (6).
- Compare $w(p)$ with w_Ω to make a decision.

4 Experimental Results

In the experiments, three public databases namely CMU PIE, FERET and FRGC are applied to evaluate the performance of our proposed thresholding with orthonormnal projection (TOP) algorithm. The Fisherface [1] scheme is used for feature extraction. The detailed parameters settings are shown in Table 1, where n_c is the number of individuals in the database, n_p denotes the total number of images from each individual, n_t is the number of images used for training from each individual. In our TOP algorithm, the paramter θ is chosen 0.8.

Table 1. The experiment settings

Database	n_c	n_p	n_t
CMU PIE	68	105	10
FERET	250	4	2
FRGC	350	40	5

Our proposed TOP algorithm is also compared with the recent developed Random Multi-space Quantization

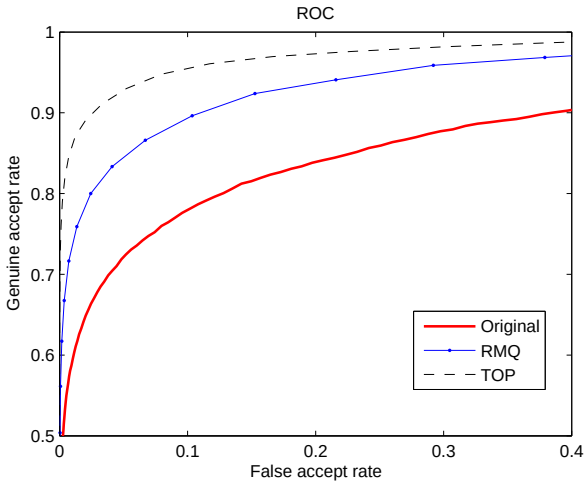

Figure 4. Experimental results on the CMU PIE database.

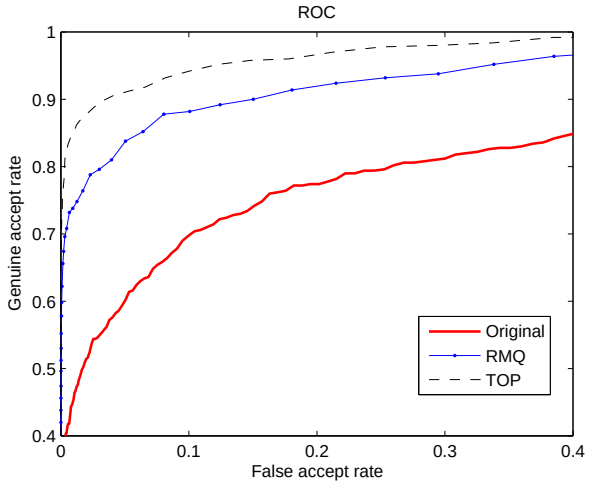

Figure 5. Experimental results on the FERET database.

Table 2. The GARs(%) of the experiments with fixed FAR=0.01

Database	Original	RMQ	TOP
CMU PIE	59.26	73.53	85.99
FERET	45.47	74.01	85.09
FRGC	26.28	67.40	78.35

Table 3. The EERs(%) of the experiments

Database	Original	RMQ	TOP
CMU PIE	17.32	10.37	6.30
FERET	21.66	11.29	7.44
FRGC	31.75	13.38	10.05

(RMQ) algorithm. The RMQ algorithm, as a binarization scheme, is also used for face recognition and has similar procedure with our scheme. It also does a projection before thresholding, though the purpose of the projection is much different from ours. For fair comparison, we use a randomly generated orthonormal matrix in the projection step of the RMQ algorithm, therefore the projection step does not reduce the dimension of the face template and will not cause information lost. So it will get higher performance than a normal RMQ algorithm.

The experimental results are shown in Figure 4-6. Symbol "Original" represents the original Fisherface algorithm without protection. The figures show clearly that our algorithm outperforms the RMQ algorithm. Following the popular setting, we fix the FAR at 0.01 and compare the GAR. The results are shown in Table 2. We also measure the equal error rate (EER) and the results are shown in Table 3. In all three databases, our proposed method gives the highest GAR and lowest EER.

The security of the proposed scheme depends on the security of the extracted binary templates, which are protected by cryptosystems scheme like the fuzzy commitment scheme. Since this part is not our main concern, we assume the protecting scheme provides enough security thus it is very computationally expensive for attackers to extract the binary templates from the protected data. Then attackers would have to guess the binary template with what they got. It should be mentioned that the projection matrix M_{opt} is unprotected and may be exposed to attackers. However, this would not help the attackers because the only relationship between M_{opt} and w_Ω is equation $M_{opt}w_\Omega/\sqrt{k} = e_{opt}$, where e_{opt} is kept secret to attackers. And as we know, w_Ω is randomly generated. So the entropy of w_Ω is the length of it, that is, k bits. And this is also the security level of our proposed algorithm.

5 Conclusions

This paper has proposed a new method to generate a binary face template from a real valued face template. The original face templates are first projected with an orthonormal matrix, and then thresholded to binary templates. The orthonormal matrix is optimized such that the extracted binary templates can get highest discriminability. Three public domain available face databases have been used to evaluate the proposed method. The experimental results show that the proposed method has good performance and outperforms the RMQ algorithm for comparison. The security of

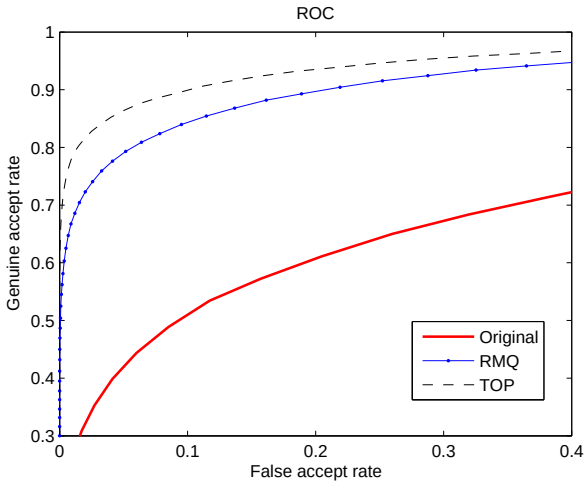

Figure 6. Experimental results on the FRGC database.

the proposed algorithm is just the length k of the extracted binary template, which is quite sufficient when k is large (say 40).

References

[1] P N Belhumeur, J P Hespanha and D J Kriegman, "Eigenfaces vs. fisherfaces: Recognition using class specific linear projection", *IEEE Trans. on PAMI*, 19(7), pp. 711-720, 1997.

[2] S Z Li, "Face Recognition Based on Nearest Linear Combinations," *Computer Vision and Pattern Recognition*, pp. 839-844,1998.

[3] R L Rivest, "The MD5 Message-Digest Algorithm," *RFC1321, Network Working Group, MIT Laboratory for Computer Science and RSA Data Security, Inc.*, 1992.

[4] J Daugman, "The Importance of Being Random: Statistical Principles of Iris Recognition," *Pattern Recognition*, Vol. 36, No. 2, pp. 279-291, 2003.

[5] A Juels and M Sudan. "A Fuzzy Vault Scheme", *IEEE International Symposium on Information Theory*, 2002.

[6] N Ratha, J Connell and R Bolle, "Enhancing security and privacy in biometric-based authentication systems," *IBM Systems Journal*, Vol. 40. No. 3, pp. 614 - 634, 2001.

[7] S Prabhakar, S Pankanti and A K Jain, "Biometric Recognition: Security and Privacy Concerns," *IEEE Security and Privacy Magazine*, Vol. 1, No. 2, pp. 33-42, March-April 2003.

[8] A K Jain, K Nandakumar and A Nagar, "Biometric template security," *EURASIP Journal on Advances in Signal Processing*, Vol. 8, 2008.

[9] U Uludag, S Pankanti, S Prabhakar and A K Jain, "Biometric cryptosystems: issues and challenges," *Proceedings of the IEEE*, vol. 92, no. 6, pp. 948-960, 2004.

[10] A K Jain, A Ross and S Pankanti, "Biometrics: A Tool for Information Security", *IEEE Transactions on Information Forensics and Security*, Vol. 1, No. 2, pp. 125-143, 2006.

[11] A Alder, "Images can be regenerated from quantized biometric match score data", *Proceedings of Canadian conference of Electrical and Computer Engineering*, pp. 469-472, 2004.

[12] F Monrose, M K Reiter and S Wetzel, "Password Hardening Based on Key Stroke Dynamics," *Proc. ACM Conf. Computer and Comm. Security*, pp. 73-82, 1999.

[13] F Monrose, M Reiter, Q Li and S Wetzel, "Cryptographic Key Generation from Voice," *Proc. IEEE Symp. Security and Privacy*, pp.202-213, May 2001.

[14] A Teoh, D Ngo and A Goh, "Biohashing: Two Factor Authentication Featuring Fingerprint Data and Tokenised Random Number," *Pattern Recognition*, vol. 37, no. 11, pp. 2245-2255, Nov. 2004.

[15] A Goh and D C L Ngo, "Computation of cryptographic keys from face biometrics", *in Proc. 7th IFIP TC6/TC11 Conf. Commun. Multimedia Security*, vol. 22, pp. 1-13, 2003.

[16] D Ngo, A Teoh and A Goh, "Biometric Hash: High-Confidence Face Recognition", *IEEE transactions on circuits and systems for video technology*, vol. 16, no. 6, 2006.

[17] A Teoh, A Goh and D. Ngo, "Random Multispace Quantization as an Analytic Mechanism for BioHashing of Biometric and Random Identity Inputs," *IEEE Transactions on Pattern Analysis and Machine Intelligence*, vol. 28, no. 12, pp. 1892-1901, Dec. 2006.

[18] N Ratha, S Chikkerur, J Connell and R Bolle, "Generating Cancelable Fingerprint Templates", *IEEE Transactions on Pattern Analysis and Machine Intelligence*, vol.29, no.4, pp. 561-572, 2007.

[19] Y C Feng, P C Yuen and A K Jain, "A Hybrid Approach for Face Template Protection," *Proceedings of SPIE Defense and Security Symposium*, 2008.

[20] Y C Feng and P C Yuen, "Class-Distribution Preserving Transform for Face Biometric Data Security," *Proceedings of IEEE International Conference on Acoustics, Speech, and Signal Processing (ICASSP)*, pp. 141-144, 2007.

[21] Y C Feng and P C Yuen, "Selection of Distinguish Points for Class Distribution Preserving Transform for Biometric Template Protection," *Proceedings of IEEE International Conference on Biometrics (ICB)*, pp. 636-645, 2007.

[22] E C Chang and S Roy, "Robust extraction of secret bits from minutiae," *in Proceedings of 2nd International Conference on Biometrics*, pp. 750C759, 2007.

[23] A Nagar, K Nandakumar and A K Jain, "A Hybrid Biometric Cryptosystem for Securing Fingerprint Minutiae Templates," *Pattern Recognition Letters*, 2009.

[24] A Nagar, K Nandakumar and A K Jain, "Securing fingerprint template: Fuzzy vault with minutiae descriptors," *International Conference on Pattern Recognition*, pp. 1-4, 2008.

[25] T A M Kevenaar, G J Schrijen, M Veen, A H M Akkermans, "Face recognition with renewable and privacy preserving binary templates," *IEEE Workshop on Automatic Identification Advanced Technologies*, pp. 21-26, 2005.

[26] J P Linnartz, P Tuyls, "New Shielding Functions to Enhance Privacy and Prevent Misuse of Biometric Templates," *Audio and Video-Based Biometric Person Authentication*, 2003.

Incorporating Concept Ontology into Multi-level Image Indexing

R.C.F. Wong and C.H.C. Leung

Abstract

The huge availability of multimedia data in the World Wide Web, and its exponential growth from the past few years, has made the search, indexing and maintenance of the information a hard and time consuming task when they are carried out manually. Image indexing has been become one of the most popular activities on the Internet as the effectiveness of image indexing depends on meaningful indexing. In this paper, we propose an extension of image annotation models which are incorporating concept ontology for multi-level image indexing. Our system is evaluated quantitatively using more than 100,000 web images and around 1,000,000 tags. Experimental results indicate that this approach is able to deliver highly competent performance.

1 Introduction

The huge availability of multimedia data in the World Wide Web (WWW), and its exponential growth from the past few years, has made the search, retrieval and maintenance of the information a hard and time consuming task, specially when these tasks have to be carried out manually, image retrieval has been become one of the most popular activities on the Internet. As the number of images available in online repositories is growing dramatically, exploring the frontier between image and language is an interesting and challenging task. Research in image retrieval has reflected the dichotomy inherent in the semantic gap, and is divided between two main categories: concept-based image retrieval and content-based image retrieval. The former focuses on retrieval by objects and high-level concepts, while the latter focuses on the low-level visual features of the image.

Low-level visual features are indicated by visual content descriptors in order to support users in accessing the knowledge embedded in images. These methods aim at capturing image similarity by relying on some specific characteristic of images; typically, these models are based on color, texture and shape[23, 35, 12, 32, 4, 6]. As discussed in [34], in order to compute these descriptors, the image often has to be segmented into parts, which aims to determine image objects. Current methods of image segmentation include[16, 9, 31, 13, 24]: partitions, sign detection, region segmentation. They compute general similarity between images based on statistical image properties[18, 3, 29, 2, 27, 1, 22]. Some studies[20, 13] include users in a search loop with a relevance feedback mechanism to adapt the search parameters based on user feedback. Semantic annotation of the image database combined with a region based image decomposition is used, which aims to extract semantic properties of images based on spatial distribution of color and texture properties[23, 10, 35, 12, 32, 15]. However, an advantage of using low-level features is that, unlike high-level concepts, they do not incur any indexing cost as they can be extracted by automatic algorithms. In contrast, direct extraction of high-level semantic content automatically is beyond the capability of current technology. Some research[5] focuses on implicit image annotation which involve an implicit and, in consequence, augments the original indexes with additional concepts that are related to the query.

The pioneering work[8] to extract semantic concept from the metadata of images conducts statistical analysis on the data fields of metadata to discriminate and classify scenes of images. In [26, 17], researchers make use of image metadata to address the problems of classifying images into mutually exclusive classes and use ”scenes mode” of the acquisition device to provide scene classifications. Although their contribution focuses on binary classifications of images (for example, indoor-outdoor scenes and sunset or not), these papers offer both strategic directions for future works and provide important steps towards progress in this area

With the advent of Semantic Web technology, ontology is playing a key role as the core element of knowledge representation architecture in Semantic Web. Some effort [14, 25, 30, 7, 19] has been made for image retrieval using Semantic Web techniques.

Our work is related to generative modelling approaches. In [34], a semantic annotation technique named Automatic Semantic Annotation (ASA) approach is developed which is based on the use of image parametric dimensions and metadata . Using decision trees and rule induction, a rule-based approach to formulate explicit annotations for images fully automatically is developed, so that, semantic query

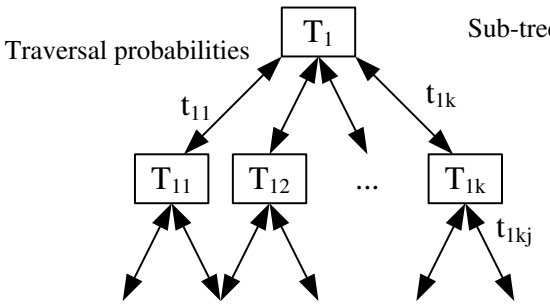

Figure 1. Ontology expansion

such as "sunset by the sea in autumn in New York" can be answered and indexed purely by machine. In this paper, we propose an extension of such image annotation models by using ontology-based expansion and contextual feature-based index expansion. Our system is evaluated quantitatively using more than 100,000 web images and over 990,000 tags. Experimental results indicate that this approach is able to deliver highly competent performance.

2 Ontology and Contextual Index Expansion

2.1 Ontology-based expansion

An ontology is a representation of a set of concepts within a domain and the relationships between those concepts. It is used to reason about the properties of that domain, and may be used to define the domain.

In certain applications, the presence of particular objects in an image often implies the presence of other objects. If term $U \Rightarrow V$, and if only U is indexed, then searching for V will not return the image in the result, even though V is present in the image. The application of such inferences will allow the index elements T_i of an image to be automatically expanded according to some probability which will be related to the underlying ontology of the application.

There are two types of expansion:

(a) Aggregation hierarchical expansion

This relates to the aggregation hierarchy of sub-objects that constitute an object. The objects can be classified as:

(i) concrete, where the relevant objects are well-defined (e.g. an "orchestra" expanded to violins, trumpets, clarinets etc.)

(ii) abstract, where the objects are not concretely defined (e.g. although "conflict" is not a definite visual object, it contains certain common characteristics).

Associated with each branch is a tree traversal probability t_{ij} (Fig. 1) which signifies the probability of occurrence of the branch index given the existence of the parent index. In general, the traversal probabilities of different object classes exhibit different characteristics, with $t_{ij} > t'_{mn}$ for t_{ij} belonging to the concrete object class, and t'_{mn} belonging to the abstract object class.

(b) Co-occurrence expansion

This relates to the expectation that certain semantic objects tend to occur together. The relevant weighting may be expressed as a conditional probability given the presence of other objects. An expansion to associate an image object O_j given the presence of object O_i is taken to be indexable when $Prob[O_j|O_i] \geq h$, where h is a preset threshold value that depends on the tradeoff between precision and recall performance of the system. More generally, complex probabilistic rules taking the form $Prob[O_j|O_1, ..., O_n] \geq h$ will be applied. The ontology expansion tree may be traversed bi-directionally in the course of the expansion. Top-down traversal will lead to an expansion factor > 1, while bottom-up traversal will have an expansion factor < 1 at each level of expansion. There are, in general, many sub-trees whose roots are the nodes of the ontology expansion. Each sub-tree may be fully expanded, and it has an expansion reliability factor $0 < r < 1$, which signifies the dependability and completeness of the associated expansion. For high precision retrieval ($\pi \approx 1$), only sub-trees having a significant reliability factor need to be traversed, and nodes with a small value for r will be pruned. Decision rules linking expansibility with π and r can be determined.

2.1.1 Semantic Knowledge from WordNet

As for redefining image indexing, the most popular way is to simplify the semantic knowledge into the semantic similarity between concepts, WordNet, is one of these applica-

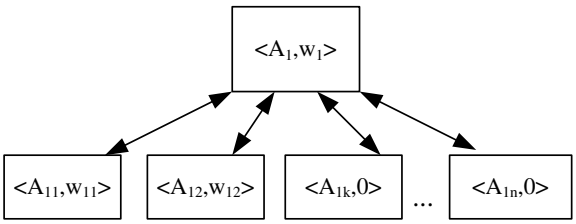

A particular annotation class A1 may exhibit a certain degree of ambiguity covering the n subclasses $A_{11,...}A_{1n}$. Our disambiguation algorithm will partially pinpoint the precise annotations by making use of a set of modal images, where each annotation concept C_i will have associated with it a representative set of modal images that are external to the images to be annotated.

Figure 2. Annotation Disambiguation

tions of semantic lexicon for the English language and general knowledge base and commonsense reasoning engine.

However, this thesaurus based approach has its limitations: lots of detailed semantic knowledge present has been lost and also it does not provide a quantitative measure of the semantic similarity between concepts. Various measures**??** have been proposed to derive the semantic similarity from WordNet, but they are subject to refundment and sometimes need for contradict with human ratings. Also, WordNet has limited coverage and has a lack of effective word-sense disambiguation ability and most of the text representation enrichment strategies, which append or replace document terms with their hypernym and synonym, are overly simple. The purpose of the work is both to produce a combination of dictionary and thesaurus that is more intuitively usable, and to support automatic text analysis and artificial intelligence applications.

2.1.2 Normalized Google Distance

Realizing the limitations of computing the semantic similarity from WordNet, some research are relying on the largest text database, i.e., the WWW, to mine the semantic relation between concepts automatically. Normalized Google distance(NGD)[11] is proposed to calculate the relationship between two concepts by their correlation in the search result from Google search engine when querying both concepts. The definition of NGD is as follows,

$$NGD(x,y) = \frac{max\{logf(x), \log(y)\} - logf(x,y)}{logN - min\{lgof(x), logf(y)\}}, \quad (1)$$

$f(x)$ and $f(y)$ are the numbers of the web pages returned by Google search engine when typing x and y as the search term respectively. $f(x,y)$ denotes the number of pages containing both x and y, as reported by Google.

2.1.3 Wikipedia Distance

Wikipedia is the worlds largest collaboratively edited source of encyclopedic knowledge. In spite of its utility, its contents are barely machine-interpretable. Each article in Wikipedia describes a single topic; its title is a succinct, well-formed phrase that resembles a term in a conventional thesaurus. Meanwhile, each article must belong to at least one category of Wikipedia. Hyperlinks between articles keep many of the same semantic relations as defined. WikiRelate[28] was the first to compute measures of semantic relatedness using Wikipedia. The Wikipedia Link Vector Model (WLVM)[21] uses Wikipedia to provide structured world knowledge about the terms of interest. Their approaches are using the hyperlink structure of Wikipedia rather than its category hierarchy or textual content[33].

Probability of WLVM is defined by the total number of links to the target article over the total number of articles. Thus if t is the total number of articles within Wikipedia, then the weighted value w for the link $a \rightarrow b$ is:

$$w(a \rightarrow b) = |a \rightarrow b| \times log(\sum_{x=1}^{t} \frac{t}{|x \rightarrow b|}), \quad (2)$$

where a and b denotes the search terms.

2.2 Contextual feature-based index expansion

Here, we shall establish associations between low-level features with high-level concepts, and such associations will take the following forms.

(a) Associating basic features with semantic concepts

The presence of certain low-level features F may suggest a finite number of m object possibilities. The expansion will be carried out by examining all $Prob[O_j|F] > 0, j = 1, 2, ..., m$. The object O_k that maximizes the probability expression will be indexed. Sometimes, a combination of basic features may be used to infer the presence of high-level concepts for inclusion in the semantic index. Thus, in more complex situations, maximization will need to be carried out on the probabilities $Prob[O_j|F_1, ..., F_n]$ which correlates an object with multiple feature occurrences.

(b) Exploiting contextual constraints

Basic features alone may not be sufficient to infer the presence of specific objects, but such features if augmented by additional information may lead to meaningful inferences. When a particularly context is known, a concept may be indexed more precisely. Such contextual information will typically be provided through ontological expansion, which may lead to the creation of a new index term, or a revision of the score of an existing index term. In general, we will need to consider the probabilities $Prob[O, |\overrightarrow{F}, \overrightarrow{O}]$, where $\overrightarrow{F}, \overrightarrow{O}$, are respectively the available feature set (an element of which may be a vector) and the object set. This will give rise to an iterative feedback loop where the determination of new objects will lead to new meaningful feature-object combinations, where further objects may be determined.

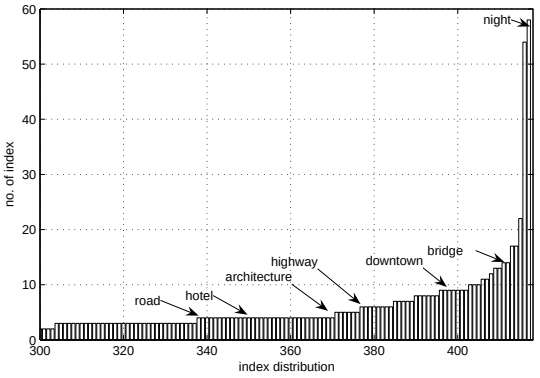

Figure 3. Index distribution associate with night scene images

3 Experiment Setup

We are introducing ontology technique into the image indexing problem and using the sub-objects as surrogate terms for general queries is to improve the precision in the image sets. Here we exploit WordNet, NGD and WLVM Distance to assist our experiments. In order to produce a list of tags that are more intuitively usable, we perform a semantic lexicon checking by all three algorithms, where numeric, symbol characters misjudge phase have been removed, and in consequence 289,399 tags with 7,982 keywords are formed. The quality assessment of the machine-inferred boundaries between parts of the depicted scenes is based on the precision. In our evaluation, we decide that a relevant image must include a representation of the category in such a manner that a human should be able to immediately associate it with the assessed concept.

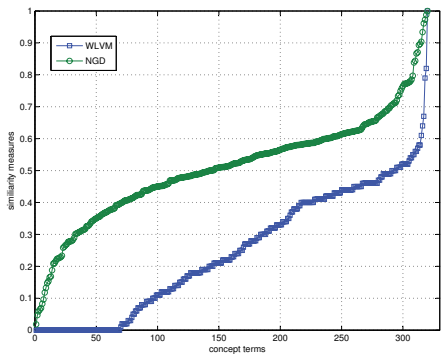

Figure 4. Similarity measurement of LVMD and GND

3.1 Experimental Results

In relation to image acquisition, many images may be broken down to few basic scenes, such as nature and wildlife, portrait, landscape and sports. In the case of aggregation hierarchical expansion of ontology-based expansion, we decided to test our system using the aggregation hierarchy of basic categories ”night scenes” and extend the image hierarchy to find a sub-scene ”night scene of downtown”. In [34] by using decision trees and rule induction, a rule-based approach to formulate explicit annotations for images fully automatically has been developed. To extend the approach, firstly, we annotate night scenes based on the prior rule-based approach to extract 422 out of 103,527 images. We also gather 1108 tags associated with those images and totally 417 unique terms are formed. We list the top 117 out of 417 unique terms list in Fig. 3.

By using Wordnet, ”downtown” can be expanded to ”business district”, ”commercial district”, ”city center” and ”city district”, while ”city district” can be expanded to ”road”, ”building”, ”architecture”, ”highway” and ”hotel”. For both NGD and WikiRelate, we compare the distances between ”downtown” and all associated tags, and Table 1 compares NGD and WLVM by their performance of semantic relatedness measures. Only the top 20 and last 5 measures obtained by the different approaches are shown. Across all three expansion algorithms, WordNet, WLVM and GND, we see that NGD deliver better accuracy compared to WLVM. WordNet can only expand few concepts and cannot directly compare to its competitors.

Table 1. Performance of semantic relatedness measures

top	WLVM	NGD
1	downtown (100%)	downtown (100%)
2	airport (79%)	driving (99%)
3	street (55%)	harbor (97%)
4	landmark (54%)	station (96%)
5	park (52%)	train (93%)
6	freeway (50%)	street (90%)
7	urban (48%)	lights (90%)
8	city (46%)	trails (89%)
9	transportation (44%)	transportation (87%)
10	highway (44%)	highway (87%)
11	tower (43%)	city (84%)
12	construction (40%)	airport (84%)
13	hotel (40%)	camp (80%)
14	road (40%)	bridge (78%)
15	car (38%)	museum (78%)
16	railway (35%)	outside (78%)
17	bridge (34%)	freeway (77%)
18	architecture (33%)	airplane (77%)
19	airplane (28%)	urban (77%)
20	station (27%)	railway (77%)
...	...	...
413	corinth (0%)	auckland (0%)
414	destiny (0%)	han (0%)
415	dual (0%)	berlin (0%)
416	great (0%)	barcelona (0%)
417	greek (0%)	new (0%)

4 Conclusion

In this paper, we propose an extension of image indexing models which uses ontology-based expansion with WordNet, WLVM and NGD. Our system is evaluated quantitatively, and experimental results indicate that this approach is able to deliver highly competent performance. Our approach, not only demonstrates the applicability of ontology to the image annotation problem, but also using the subobjects as surrogate terms for general queries is to improve the precision in the image sets.

[1] G. Amato and C. Meghini. Combining features for image retrieval by concept lattice querying and navigation. *International Conference on Image Analysis and Processing Workshops*, 0:107–112, 2007.

[2] J. Amores, N. Sebe, and P. Radeva. Context-based object-class recognition and retrieval by generalised correlograms. *IEEE Transactions on Pattern Analysis and Machine Intelligence*, 29(10):1818–1833, October 2007.

[3] V. Athitsos, J. Alon, S. Sclaroff, and G. Kollios. Boostmap: A method for efficient approximate similarity rankings. *IEEE Computer Society Conference on Computer Vision and Pattern Recognition*, 02:268–275, 2004.

[4] I. Azzam, A. G. Charlapally, C. H. C. Leung, and J. F. Horwood. Content-based image indexing and retrieval with xml representations. *Proceedings of the International Symposium on Intelligent Multimedia, Video and Speech Processing, Hong Kong*, pages 181–185, 2004.

[5] I. A. Azzam, C. H. C. Leung, and J. F. Horwood. Implicit concept-based image indexing and retrieval. In *Proceedings of the IEEE International Conference on Multi-media Modeling*, pages 354–359, Brisbane, Australia, January 2004.

[6] I. A. Azzam, C. H. C. Leung, and J. F. Horwood. A fuzzy expert system for concept-based image indexing and retrieval. *International Conference on Multimedia Modeling Conference*, 0:452–457, 2005.

[7] K. Barnard, P. Duygulu, N. de Freitas, D. Forsyth, D. Blei, and M. Jordan. Matching words and pictures. *Journal of Machine Learning Research*, 3:1107–1135, 2003.

[8] M. Boutell and J. Luo. Photo classification by integrating image content and camera metadata. In *ICPR '04: Proceedings of the Pattern Recognition, 17th International Conference on (ICPR'04) Volume 4*, pages 901–904, Washington, DC, USA, 2004. IEEE Computer Society.

[9] Y. Chen, J. Z. Wang, and R. Krovetz. Content-based image retrieval by clustering. In *MIR'03: Proceedings of the 5th ACM SIGMM international workshop on Multimedia information retrieval*, pages 193–200, New York, NY, USA, 2003. ACM.

[10] J. S. Cho and J. Choi. Contour-based partial object recognition using symmetry in image databases. In *SAC'05: Proceedings of the 2005 ACM symposium on Applied computing*, pages 1190–1194, New York, NY, USA, 2005. ACM Press.

[11] R. L. Cilibrasi and P. M. Vitanyi. The google similarity distance. *IEEE Transactions on Knowledge and Data Engineering*, 19(3):370–383, 2007.

[12] D. Cremers, M. Rousson, and R. Deriche. A review of statistical approaches to level set segmentation: Integrating color, texture, motion and shape. *International Journal of Computer Vision*, 72(2):195–215, 2007.

[13] R. Datta, J. Li, and J. Z. Wang. Content-based image retrieval: approaches and trends of the new age. In *MIR'05: Proceedings of the 7th ACM SIGMM international workshop on Multimedia information retrieval*, pages 253–262, New York, NY, USA, 2005. ACM.

[14] L. Fan and B. Li. A hybrid model of image retrieval based on ontology technology and probabilistic ranking. *Web Intelligence*, 0:477–480, 2006.

[15] K. Hornsby. Retrieving event-based semantics from images. *International Symposium on Multimedia Software Engineering*, 00:529–536, 2004.

[16] R. Krishnapuram, S. Medasani, S. H. Jung, Y. S. Choi, and R. Balasubramaniam. Content-based image retrieval based on a fuzzy approach. *IEEE Transactions on Knowledge and Data Engineering*, 16(10):1185–1199, 2004.

[17] W. Ku, M. S. Kankanhalli, and J. H. Lim. Using camera settings templates (”scene modes”) for image scene classification of photographs taken on manual/expert settings. In *The Pacific-Rim Conference on Multimedia*, pages 10–17, 2007.

[18] J. Li and J. Z. Wang. Automatic linguistic indexing of pictures by a statistical modeling approach. *IEEE*

Transactions on Pattern Analysis and Machine Intelligence, 25(9):1075–1088, 2003.

[19] H. Lieberman and H. Liu. Adaptive linking between text and photos using common sense reasoning. *Adaptive Hypermedia and Adaptive Web-Based Systems, Second International Conference, AH 2002, Malaga, Spain*, pages 2–11, May 2002.

[20] D. Liu and T. Chen. Content-free image retrieval using bayesian product rule. *IEEE International Conference on Multimedia and Expo*, 0:89–92, 2006.

[21] D. Milne and I. H. Witten. An effective, low-cost measure of semantic relatedness obtained from wikipedia links. In *WIKIAI'08: first AAAI Workshop on Wikipedia and Artificial Intelligence*.

[22] A. P. Natsev, A. Haubold, J. Tešić, L. Xie, and R. Yan. Semantic concept-based query expansion and re-ranking for multimedia retrieval. In *International conference on Multimedia*, pages 991–1000, New York, NY, USA, 2007. ACM.

[23] R. Pawlicki, I. Kókai, J. Finger, R. Smith, and T. Vetter. Navigating in a shape space of registered models. *IEEE Transactions on Visualization and Computer Graphics*, 13(6):1552–1559, 2007.

[24] A. Perina, M. Cristani, and V. Murino. Natural scenes categorization by hierarchical extraction of typicality patterns. *International Conference on Image Analysis and Processing*, pages 801–806, 2007.

[25] A. Popescu, G. Grefenstette, and P. A. Moellic. Using semantic commonsense resources in image retrieval. In *International Workshop on Semantic Media Adaptation and Personalization*, pages 31–36, Washington, DC, USA, 2006. IEEE Computer Society.

[26] P. Sinha and R. Jain. Classification and annotation of digital photos using optical context data. In *The International Conference on Image and Video Retrieval*, pages 309–318, 2008.

[27] K. Stevenson and C. H. C. Leung. Comparative evaluation of web image search engines for multimedia applications. *IEEE International Conference on Multimedia and Expo*, 0:4 pp., 2005.

[28] M. Strube and S. P. Ponzetto. Wikirelate! computing semantic relatedness using wikipedia. July 2006.

[29] Y. Sun, S. Shimada, and M. Morimoto. Visual pattern discovery using web images. *MIR'06: Proceedings of the 8th ACM international workshop on Multimedia information retrieval*, pages 127–136, 2006.

[30] A. M. Tam and C. H. C. Leung. Semantic content retrieval and structured annotation: Beyond keywords. *ISO/IEC JTC1/SC29/WG11 MPEG00/M5738, Noordwijkerhout, Netherlands*, March 2000.

[31] N. Vasconcelos. From pixels to semantic spaces: Advances in content-based image retrieval. *IEEE Computer*, 40(7):20–26, 2007.

[32] J. Vogel, A. Schwaninger, C. Wallraven, and H. H. Bülthoff. Categorization of natural scenes: Local versus global information and the role of color. *ACM Transactions on Applied Perception*, 4(3):19, 2007.

[33] M. Völkel, M. Krötzsch, D. Vrandecic, H. Haller, and R. Studer. Semantic wikipedia. In *WWW '06: Proceedings of the 15th international conference on World Wide Web*, pages 585–594, New York, NY, USA, 2006. ACM.

[34] R. C. F. Wong and C. H. C. Leung. Automatic semantic annotation of real-world web images. *IEEE Transactions on Pattern Analysis and Machine Intelligence*, 30(11):1933–1944, November 2008.

[35] T. Zöller and J. M. Buhmann. Robust image segmentation using resampling and shape constraints. *IEEE Transactions on Pattern Analysis and Machine Intelligence*, 29(7):1147–1164, July 2007.

Hiding Emerging Pattern with Local Recoding Generalization

Michael Wai-Kit Cheng

Abstract

*When data is published to public, it is vastly preferable to publish meaningful data and yet protect embedded sensitive patterns. This process is often referred to as privacy preserving data publishing (*PPDP*). In this paper, we investigate* PPDP *in the context of frequent itemsets mining – one of the fundamental data-mining concepts – and emerging patterns (*EP*s) – patterns that have a high classification power. More specifically, we want to hide all* EP*s embedded in data while publishing the data with a minimal distortion on its frequent itemsets. We propose a novel heuristic solution that captures the unique properties of hidding* EP*s and incorporates with local recoding generalization. To guide a bottom-up recoding generalization, a metric is derived based on (i) frequent-itemset distortion that quantifies the quality of published data and (ii) the degree of reduction in emerging patterns in each recoding generalization. We have implemented our proposed solution and experimentally verified its effectiveness using two benchmark datasets.*

1 Introduction

Organizations often publish or share their data to support subsequent data analysis for various reasons, for instance, advancing medical research [27] or raising customer satisfaction level [32]. In many cases, data may involve personal information or company's secrets which are not supposed to be disclosed in normal circumstances. Protecting the published data against privacy breaching is often of top priority. Nonetheless, people may still choose to relinquish certain privacy for a greater good, but only when they can be assured that the published data will be properly sanitized.

Studies on data sanitization can be dated back to the earlier work on statistical disclosure control [1]. For instance, it is a common requirement to remove personal identifiers from published data using mechanisms like masking (e.g., ID="123456(7)" → ID="123***(*)") and substitution (e.g., name="Donald" → name="YxfG1L") to ensure anonymization. However, the privacy-breaching challenge goes beyond that. It has been clear that combinations of quasi-identifiers, e.g., the demographic attributes, can allow sensitive information such as personal identity, facts, or forbidden patterns to be inferred, and thus disclosed [34]. Given that data publishing is still a must in many situations, there has been a stream of work called *privacy-preserving data publishing* (PPDP), emerged in recent years to flight against the privacy-breaching challenge [13]. The particular type of PPDP considered in this paper tries to sanitize the data to be published so that some specified sensitive patterns could not be discovered and meanwhile, certain statistical properties of the published data are preserved as far as possible to support subsequent analysis.

In this paper, we argue that emerging patterns embedded in data can carry important intelligence (e.g., newly emerging sales opportunities revealed in sales records) that data owners may want to hide before they publish them for further analysis. In particular, emerging patterns has known to have a high classification power where EP-based classifiers can often be more accurate than classifiers with C5.0, naive Bayes and CAEP. At the meantime, frequent itemset mining is a classical data mining technique and has already been well-supported by commercial data mining software. Published data may be evidently subjected to such an analysis. Therefore, we study a novel form of PPDP where the sensitive information to be protected is emerging patterns in datasets and the data analysis is frequent itemset mining.

More specifically, given two transactional datasets D_1 and D_2, a threshold of growth rate ρ and a threshold of support σ, we want to determine a sanitization operation G on both D_1 and D_2 such that the emerging patterns with a growth rate higher than ρ are eliminated and the distortion of σ-frequent itemsets is minimized. (The details of the problem formulation shall be given in Section 3.)

Example 1.1: Let us consider an example from a demographic dataset [36], which contains some census information of the United States. We divide the dataset into two: (i) people who earned more than $50/year and (ii) people who do not. When we set ρ to be 35, we find that there are 8 emerging patterns. One emerging pattern in (ii) is (never-married, own-child). In other words, in [36], there are at least 35 times more people who have never married and have their own child in (ii) than (i). We remark that (never-married, own-child) is not a frequent itemset of the entire dataset when $\sigma = 0.4$.

The example shows that emerging patterns may reveal certain sensitive information from data. For applications like publishing census reports, sanitizing data might not be legitimate. But for applications related to business intelligence, protecting customer data and cooperations' interests become a necessity. We speculate that in many other scenarios, one may prefer to sanitize such sensitive information embedded in data before publishing. ∎

Different data sanitization approaches have been proposed in the literature for PPDP [12] (as well as other privacy preservation related fields), which could be roughly categorized into recoding generalization [20, 5, 15, 19, 34, 28, 40, 35, 31] and perturbation [2, 8, 10, 18]. In this paper, recoding generalization is adopted. Recoding generalization has been extensively used in the context of k-anonymization which was originally proposed in [34]. Recoding generalization is (intuitively) a value-grouping process according to a given attribute generalization hierarchy. Since the attribute hierarchy is always published with the data, data recipients can correctly interpret every generalized values that appear in the sanitized data. Therefore, the sanitized data can be "blurred" but is not lost. This work focuses on exploring the possibilities of adopting recoding generalization in the context of hiding emerging patterns.

A sanitization is obviously unacceptable if a data mining technique would either (i) reveal sensitive information or (ii) produce a highly distorted result from the sanitized data. These two competing objectives make the problem technically intriguing.

We remark that hiding emerging patterns is more technically challenging than some related works on hiding frequent itemsets [30, 2]. The reason is that the *apriori anti-monotone* property of frequent itemsets does not hold for emerging patterns. Thus, the search space of emerging patterns cannot be pruned as effectively as that of frequent itemsets. Furthermore, recoding generalization may hide an emerging pattern as well as generating new emerging patterns. To the best of our knowledge, there has not been work on adopting recoding generalization techniques to hide emerging patterns.

The paper is organized as follows. In Section 2, we give a brief summary on the research on PPDP. In Section 3, we present the background and notations used and give the formal problem statement of this paper. In Section 4, we discuss the recoding generalization technique adopted to solve this problem. Section 5 gives an overview of our algorithm. Section 6 derives the heuristics that quantifies the quality of a recoding generalization. Section 7 discusses a number of optimizations related to solving this PPDP problem. In Section 8, we present an experimental evaluation that verifies the effectiveness of our proposed algorithm. Section 9 concludes this work and discusses future works.

2 Related Work

There have been recent research efforts on various aspects of PPDP. In this section, we highlight some relevant, admittedly non-exhaustive PPDP techniques.

Anonymity measure and recoding generalization. In an analysis of a demographic dataset with external information [35], it has been shown that personal identity can be recovered from a published dataset, even the identifiers have been removed. The notion of k-anonymity [35] was thus introduced. A published data is said to be k-anonymized if at least k individuals are linked with a particular record in the published data even if the data may be cross-referenced with external information. Each group of items with indistinguishable attribute values is called an equivalence class. To further improve k-anonymity, ℓ-diversity [25] was proposed to require also each sensitive value in each equivalence class to appear at most $1/\ell$ times.

Given a particular measure, recoding generalization [34, 40, 23] is commonly adopted to achieve anonymization. Recoding generalization has two advantages over the perturbation approach for data sanitization,. First, the dataset sanitized by recoding generalization is still semantically consistent with the original one. The information conveyed by a generalized dataset always contains the truth, even though it is "blurred". In contrast, perturbation techniques may generate fake information. These may not be acceptable in many real applications, e.g., a database with patient information. Second, since the attribute hierarchy is often published with the dataset, the generalized values in the published dataset can be always interpreted. We adopt recoding generalization, to protect emerging patterns.

The notion of information preservation. There has been a stream of work on k-anonymity which also makes an attempt to preserve as much information of the original dataset as possible [5, 16, 14]. For example, [5, 16] considers the preservation of classification accuracy during the sanitization process. [14] investigates the preservation of cluster structures of the data. In addition, there has been some recent work studying the trade-off effect between privacy and utility [24] in the context of PPDP. However, they are not designed to tackle some particular patterns.

Frequent itemset hiding. There has been previous work [30, 33, 29] on hiding frequent itemsets for PPDP. In particular, users specify a subset of frequent itemsets, namely sensitive frequent itemsets, that are not supposed to be disclosed to public. The main objective of this related work is to sanitize the data such that the sensitive frequent itemsets are removed from the sanitized data while non-sensitive frequent itemsets are retained as many as possible. In our study, we focus on hiding emerging patterns, which makes a different contribution to PPDP.

We remark that the previous work on frequent-itemset hiding used techniques like removing sensitive data, introducing random and unknown data. Recoding generalization has not been adopted in this stream of work.

Emerging patterns. Intuitively, EPs are some distinctive features from one class to the others. Much previous effort [17, 38, 11, 7] has been spent on using EPs for building classifiers. The results of these efforts have shown that the accuracy of EP-based classifiers can often be higher than those of traditional classifiers, such as, C5.0 and naive Bayes. Due to the high classification power, EP-based classifiers have been used for predicting the likelihood of diseases such as acute lymphoblastic leukemia [21] and discovering knowledge in gene expression data [22].

Although EPs have been found useful in classification, there have not been studies on EPs with PPDP. Previous work on EPs focuses on the mining efficiency. Mining EPs has been technically intriguing. First, the total number of EPs in large datasets can be huge. In the worst case, the total number of EPs is exponential to the total number of attributes in transactions. Second, there has not been a corresponding notion of the apriori anti-monotone property of frequent itemsets in EPs. As such, the search space pruning strategies of frequent-itemset mining cannot be adopted to EP mining. There have been a border-based approach [4], constraint-based approach [41] and jumping emerging patterns [3] to improve the efficiency of EP mining.

3 Background and Problem Statement

In the following, we present the definitions, notations used and the problem statement of the paper.

Let D be a transactional dataset and $I := \{i_1, i_2, ..., i_n\}$ be a finite set of distinct items in D. A transaction t may have a set of nominal attributes A and each attribute takes values from a set $V_i \subseteq I$, where the domain $\mathcal{D}$ is $V_1 \times V_2 \times ... \times V_{|A|}$. We make two simple remarks about these notations. (i) While we assume transactional data with nominal attributes, data of a continuous domain can be casted into nominal data, e.g., by defining ranges. (ii) One may consider a relation as a set of transactions of a fixed arity.

$Supp_D(X)$ denotes the support of an itemset $X \subseteq I$ in a dataset D, which can be computed as $\frac{|\{t \mid X \in t \wedge t \in D\}|}{|D|}$. Given a support threshold σ, X is said to be a *σ-frequent itemset* if $Supp_D(X) \geq \sigma$. The growth rate of an itemset is the ratio of its support in one dataset to that in the other.

Definition 3.1: [6] Given two datasets, namely D_1 and D_2, the *growth rate* of an itemset X, denoted as $GR(X, D_1, D_2)$, from D_1 to D_2 is defined as $GR(X, D_1, D_2) =$

$$\begin{cases} 0 & \text{, if } Supp_{D_1} = 0 \text{ and } Supp_{D_2} = 0 \\ \infty & \text{, if } Supp_{D_1} = 0 \text{ and } Supp_{D_2} > 0 \\ \frac{Supp_{D_2}(X)}{Supp_{D_1}(X)} & \text{, otherwise.} \end{cases}$$ ∎

Intuitively, given two datasets, emerging patterns (EPs) [6] are the itemsets whose support increases significantly from one dataset to another. The formal definition of EPs can be given as follows.

Definition 3.2: [6] Given a growth rate threshold ρ and two datasets $D_1$and D_2, an itemset X is said to be a *ρ-emerging pattern* (ρ-EP) from D_1 to D_2 if $GR(X, D_1, D_2) \geq \rho$. ∎

An emerging pattern with a growth rate ∞ (i.e. itemset that appears in one dataset but not the other) is called a *jumping emerging pattern*.

For ease of presentation, we may skip σ, ρ, D_1 and D_2 of EPs when they are not essential to our discussions.

Example 3.1: Table 1 shows a hypothetical dataset D of Adult dataset [36]. More description of the dataset can be found in Section 8. We opt to present some nominal attributes of Adult for discussions. Each record (or transaction) represents a person. Let us consider two subsets of D: D_1 contains the people who are married and D_2 contains the people who never marry before. From Table 1, we find the following patterns, among many others.

- The pattern (MSE, manager) has a support 75% in D_1 and 20% in D_2. Therefore, the growth rate of (MSE, manager) from D_1 to D_2 is 3.75. When we set ρ to 3, (MSE, manager) is a ρ-emerging pattern in D_2. Obviously, when we set ρ to 4, (MSE, manager) is not a ρ-emerging pattern.
- High-school graduate (HS) has a support 0% in D_1 but 20% in D_2. Hence, its grwoth rate from D_2 to D_1 is infinite. (HS) is a jumping emerging pattern in D_1.
- Suppose that the threshold support for frequent itemset σ is set to 50%. Neither (MSE, manager) nor (HS) is a σ-frequent itemset of D. In comparison, (manager) is a σ-frequent itemset, whose support is 77.8%. ∎

Using the above notations, we state the formal problem statement of this paper below (visualized in Figure 3).

Problem statement. Given two datasets (D_1, D_2), σ and ρ, we want to sanitize (D_1, D_2) to (D'_1, D'_2) such that no ρ-EPs can be mined from (D'_1, D'_2) while the distortion between σ-frequent itemsets of (D_1, D_2) and those of (D'_1, D'_2) is minimized. ∎

4 Global vs Local Recoding Generalization

Our proposed algorithm for hiding emerging pattern is derived from local recoding generalization. In this section,

Table 1. A hypothetical subset of `Adult`

ID	Edu.	Martial	Occup.	Rel.	Race	Sex
1	BA	married	executive	wife	black	F
2	MSE	married	manager	husband	black	M
3	MSE	married	manager	wife	white	F
4	MSE	married	manager	husband	black	M
5	BA	never	manager	NA	white	M
6	MSE	never	manager	NA	white	F
7	HS	never	repair	NA	black	M
8	BA	never	manager	NA	white	M
9	BA	never	manager	NA	black	F

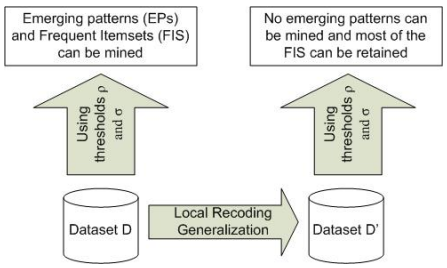

Figure 1. The problem statement illustration

we give a brief overview on global and local recoding generalization, or *recoding* for simplicity, and its variations.

Recoding. In privacy-preserving data mining, recoding has been a popular technique for sanitizing datasets in order to achieve anonymization. The key idea of recoding is to modify a value into a more general value such that more tuples will share the same values and cannot be distinguished individually. Thus, anonymization can be achieved. In this work, we recode emerging patterns with some non-emerging values. As a result, the corresponding patterns become less emerging after recoding. Such a recoding process is repeated until the desired anonymization is reached.

Variations of recoding. In the following, we describe the there types of recoding. In this work, we adopt the last recoding technique.

1. Single-dimensional global recoding. Single-dimensional global recoding has been studied in [5, 15, 19, 34]. It performs recoding on the domain of an attribute in a dataset. It recodes a value of the domain to another (generalized) value. That is, if a particular value is recoded, the attribute of all the tuples containing that particular value will be recoded. It is evident that datasets are very often over-generalized by this recoding.

2. Multidimensional global recoding. Multidimensional global recoding was first proposed in [20]. It generalizes data at "cell" level. This recoding relies on the notion of *equivalence classes*. An equivalence class of attributes A is a set of tuples T where $\pi_A(T)$ is a singleton. That is, the tuples in T has the same value in attributes A. In multidimensional global recoding, the tuples in an equivalence class (of a set of attributes) are generalized together. By doing so, both original and generalized values may exist in the recoded dataset. When compared to the previous global recoding, multidimensional global recoding generalizes data in a finer granularity. Hence, this recoding over-generalizes data less often.

Example 4.1: Let us revisit the dataset in Table 1 and the emerging pattern (`MSE`, `manager`). The pattern is related to the attributes of education background (`Edu.`) and occupation (`Occup.`). Regarding (`Edu.`, `Occup.`), the equivalence classes in D_2 are $\{\{5, 8, 9\}, \{6\}, \{7\}\}$, where the numbers are the IDs. In multidimensional global recoding, we may recode the `Edu.` attribute of $\{2, 3, 4\}$ and $\{5, 8, 9\}$. For instance, we may recode `BA` and `MSE` into degree holder `Deg`. After such a recoding, all `BA`, `MSE` and `Deg.` appear in the recoded dataset. We remark that (`Deg.`, `manager`) is not an emerging pattern since its growth rate is 75%/60% = 1.25. ∎

3. Multidimensional local recoding. Local recoding has been studied in [9, 28, 40, 23] in the context of k-anonymity. It performs generalization at cell level as well. It also relies on equivalence classes. Its difference between the multidimensional global recoding is that it does not require the entire equivalence class to be recoded, as long as anonymity has been achieved. For instance, we may recode $\{8, 9\}$, as opposed to $\{5, 8, 9\}$, with $\{2, 3, 4\}$ in Example 4.1. The growth rate of (`Deg.`, `manager`) in the recoded dataset is 75%/40% = 1.875. Hence, (`Deg.`, `manager`) is not ρ-emerging when $\rho = 3$.

In this paper, we focus on this recoding. In the subsequent discussions, we use the term *local recoding* to refer to multidimensional local recoding.

5 Overview on hiding emerging patterns

In this section, we present an overall algorithm `hide-eps` (shown in Figure 2) to hide emerging patterns with a minimal distortion in frequent itemsets. Its details shall be discussed shortly. Then, we provide some details of the heuristics in `hide-epse` in Section 6.

Overall algorithm. We give the main ideas of Figure 2. First, we find the frequent itemsets to be preserved (Line 03) and the emerging patterns to be hidden (Line 04). In Line 05, we select an emerging pattern to hide. Next, we carry out a local recoding `local-recoding` (Line 06). This process is repeated until there is no more emerging pattern to hide (Lines 07-08).

The main tasks of the local recoding `local-recoding` are to compute (i) the equivalence classes of an emerging pattern e to generalize (Line 03) and (ii) the corresponding utility gain (details in Section 6) to guide us to choose an equivalence class for local recoding (Line 06). To avoid be-

Procedure `hide-eps`
Input: two datasets, D_i and D_j, the threshold of
the growth rate and frequent itemsets ρ and σ,
the heuristic parameters p and q,
a temperature t_0 and the cooling parameter α
Output: transformed datasets (D_i, D_j)

01 initialize a hashtable H to optimize
computing equiv. classes; $t = t_0$
02 **do**
03 F := `mine-fis`$(D_i \cup D_j, \sigma)$
04 E := `mine-eps`(D_i, D_j, ρ)
05 e := `next-overlapping-ep`(E)
06 **if** e is not null
(D_i, D_j) := `local-recoding`$(D_i, D_j, e, F, t, \alpha)$
07 **if** $t > 0.01$ **then** $t = \alpha \times t$
08 **while** $E \neq \emptyset$
09 **return** (D_i, D_j)

Procedure `local-recoding`
Input: two datasets, D_i and D_j, an emerging pattern e
a frequent itemset F, a temperature t_0
Output: transformed datasets (D_i, D_j)

01 **let** D_i be the dataset where e has a higher support
02 $t := t_0$; $u = 0$ //initialization
03 compute equiv. classes C of D_j of the attr. of e
04 //compute the heuristic function of local recoding
05 denote c_e be the equiv. class of e in D_i
06 **for each** c_k in C
$H[c_e][c_k]$:= `util_gain`$(G_{(c_e,c_k)}, E)$ //heap
$r[c_k] = exp^{\frac{H[c_e][c_k]}{t}}$
$sum = sum + r[c_k]$
07 **find** k s.t. $r[c_k]/sum <$ `rand`$(1) < r[c_{k+1}]/sum$
D_i := `recode`(D_i, c_e, c_k)
D_j := `recode`(D_j, c_e, c_k)
08 **return** (D_i, D_j)

Figure 2. Overall algorithm

ing trapped at some local sub-optima, we present our algorithm in a simulated-annealing style search (Lines 06-08).

Next, we provide the details of the overall algorithm.

The effect of local recoding on frequent itemsets. We first remark that global recoding may only merge some frequent itemsets, shown in Figure 3 (a). Hence, the change in frequent itemsets due to global recoding can be determined easily. However, local recoding may lead to a non-trivial change in frequent itemsets, shown in Figure 3 (b). The reason is that by the definition of local recoding, two tuples, even in the same equivalence class, are not always recoded together. This leads to a few possible effects on the frequent itemsets. First, since some of the values of the attributes A have been recoded to a generalized value, a frequent itemset may not be frequent after a local recoding. Second, multiple frequent itemsets may be recoded into one generalized frequent itemset. Third, a frequent itemset may not be affected by a local recoding. The first case is only possible

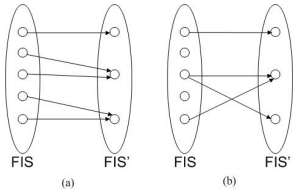

Figure 3. The relationship between F and F' in (a) global recoding (b) local recoding

with local recoding whereas the second and third cases may appear correspondingly in global recoding as well.

The above complication leads to Line 04 of `hide-eps`, which mines the current frequent itemsets in each iteration of local recoding.

The selection of emerging patterns for hiding. In the worst case, there are $O(|E| \times (|D_1| + |D_2|) \times \mathcal{D} \times \mathcal{H})$ possible local recodings on a set of emerging patterns E, where $\mathcal{D}$ is the total size of the domains of the attributes of E and $\mathcal{H}$ is the total height of the hierarchy of the attributes of E. In the worst case, local recoding allows tuple-wise recoding, which leads to the term $|D_1| + |D_2|$. While there may be search algorithms to explore an optimal local recoding on E, we employ a simple and efficient solution to avoid exploring a large search space – we hide an emerging pattern, one-at-a-time (Line 05 of `hide-eps`, `next-overlapping-ep`), based on equivalence classes.

The pseudocode of `next-overlapping-ep` has been omitted, since it is straightforward but tedious. Here, we present its intuitions. Given a set of emerging patterns E, `next-overlapping-ep` determines the emerging pattern e in E such that it overlaps with the remaining emerging patterns the most. The intuition is that reducing the growth rate of e may indirectly reduce the growth rate of the overlapping emerging patterns as well. We verify this with some preliminary experiments that this approach consistently outperforms generalizing the most independent, the longest or the shortest emerging patterns first.

The search algorithm. The algorithm is presented in a simulated anneanling style in Figure 2. We have implemented a deterministic search to analyze our heuristics (Section 6).

6 Heuristics for Guiding Local Recoding

In this section, we present the formulation of the utility gain (`util_gain`) adopted to guide the local recoding process `local-recoding`, discussed in Figure 2. The main idea is that we consider a local recoding perferrable if it results in a small distortion in the frequent itemsets and at the same time it reduces the growth rate of an emerging pattern significantly. In the following two subsections 6.1 and 6.2, we present the details of the metrics for measuring (i) the distortion of frequent itemsets and (ii) the reduction in the growth rate of emerging patterns, respectively.

6.1 Metric for the distortion on frequent itemsets

Recoding is a process of grouping existing values to some new generalized values. After a recoding, some σ-frequent itemsets may not be frequent anymore and some may contain generalized values.

Example 6.1: Let us reconsider the recoding in Example 4.1. We set σ to be 4. Recoding `BA` and `MSE` into `Deg.` leads to a new frequent itemset (`Deg.`, `manager`), which contains both non-generalized and generalized values. (`MSE`, `manager`) is not frequent after the recoding. ∎

Therefore, we need a metric for measuring the distortion in the *σ-frequent itemsets* of D and D'. For presentation clarity, we will present our proposed metric for global recoding followed by its adaption for local recoding.

Distortion metric for single-dimensional global recoding. In global recoding, no frequent itemsets "disappear" after in a recoding (recall Figure 3 (a)). However, *some* frequent itemsets may appear in a generalized form. That is, a particular frequent itemset f in D will always have a corresponding itemset in the generalized frequent itemsets in D', in either the original or generalized form.

Inspired by the distortion metric proposed in [23], we propose a metric for measuring the *recoding distance* ($RDist$) between the original and generalized form of a tuple. Then, we define a metric called *value distance* (VD) which measures the distance between the original and generalized form of a single attribute value. We will use VD as a building block for the definition of distortion (RD). Since a recoding always assumes an attribute hierarchy, we may skip the hierarchy H when it is clear from the context.

Definition 6.1: *Recoding Distance (RDist):* Consider a recoding G which generalizes a set of attribute values V to a single generalized value v_g. The recoding distance of G is:

$$RDist(G) = |V|,$$

where $|V|$ is the number of leave nodes (non-generalized values) under v_g in the attribute hierarchy. ∎

Definition 6.2: *Value Distance (VD):* Let h be the height of the hierarchy of an attribute H, where level h is the most generalized level and level 0 is the most specific level. Consider a value v at level p is generalized to a value v' at level q. Let G_i denote the recoding which generalizes an attribute from level $i-1$ to i, where $0 < i \leq h$. The *value distance* between v and v' is:

$$VD(v, v') = \sum_{i=p}^{q} \frac{i \cdot RDist(G_i)}{h}.$$

∎

Value distance is mainly unfavorable to recoding (i) many values together into one single generalized value and (ii) a value into a generalized value that is close to the top

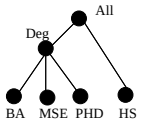

Figure 4. An attribute hierarchy of `Edu`.

of the hierarchy. This gives us a measure on the distortion of a value affected by a recoding.

Next, we extend VD to measure the distortion of a tuple due to recoding.

Definition 6.3: *Tuple Distance (TD):* Suppose a tuple $f = (v_1, v_2, \ldots, v_n)$ is generalized to $f' = (v'_1, v'_2, \ldots, v'_n)$. The tuple distance between f and f' is defined as:

$$TD(f, f') = \sum_{i=1}^{n} VD(v_i, v'_i).$$

∎

Finally, the distortion of between frequent itemsets due to a recoding is defined.

Definition 6.4: *Recoding Distortion (RD):* Let $F = \{f_1, f_2 \ldots f_n\}$ be a set of *σ-frequent itemsets* in D and $F' = \{f'_1, f'_2 \ldots f'_m\}$ be the set of *σ-frequent itemsets* in D', where $m \leq n$. The corresponding frequent itemset of f_i due to global recoding is denoted to be $f'_j = G(f_i)$. The recoding distance between F and F' is defined as:

$$RD(F, F') = \sum_{i=1}^{n} TD(f_i, G(f_i)).$$

∎

Example 6.2: Following up Example 4.1, we compute the (global) recoding distortion of generalizing (`MSE`, `manager`) to (`Deg.`, `manager`). Figure 6.1 shows the attribute hierarchy of `Edu`. The recoding distortion $RD(\{$(`MSE`, `manager`)$\}, \{$(`Deg.`, `manager`)$\})$, RD, can be computed as follows.

$$\begin{aligned} RD &= TD((\texttt{MSE}, \texttt{manager}), (\texttt{Deg.}, \texttt{manager})) \\ &= VD(\texttt{MSE}, \texttt{Deg.}) + VD(\texttt{manager}, \texttt{manager}) \\ &= \sum_{i=0}^{2} \frac{i \cdot RDist(G_i)}{h} = \frac{1 \times 3}{2} + \frac{2 \times 0}{2} = 1.5 \end{aligned}$$

∎

Distortion metric for local recoding. As discussed in Section 4, single-dimensional global recoding may often lead to over-generalization. Since we have adopted local recoding, we extend the recoding distortion to local recoding. Regarding local recoding, we remark that there are two unique challenges in calculating the recoding distance (see Figure 3 (b)).

(1) An itemset in F having no correspondence in F'. Local recoding allows part of the tuples that share the same attribute values to be generalized. Such recoding may generalize some supporting tuples of a frequent itemset which makes the itemset (in the original or generalized form) not frequent anymore. To address this, we measure the distortion of the disappeared frequent itemset to the most general

form. The reason behind this is that the frequent itemset can be trivially recovered when the entire dataset is generalized to the most general form.

Specifically, given a frequent itemset f in F, if we cannot find a corresponding frequent itemset in F', we may first create an artificial itemset, f_{max}, which generalizes each value in f to it most general form. Then, we can calculate the recoding distance (RD) between f and f_{max}.

Example 6.3: Reconsider the dataset in Table 1. Suppose we recode the `Edu`. attribute of Records 1 and 2 to `Deg`. When σ is 40%, {`BA`} and {`MSE`} were frequent itemsets (not minimal for illustration purpose) before recoding and there is no frequent itemset after recoding. ∎

(2) An itemset in F having more than one corresponding itemsets in F'. As discussed, local recoding may generalize a frequent itemset f in F into more than one correspondences in F', denoted as F_f. In this case, we calculate the tuple distance of each of the corresponding itemsets in F_f and take the minimum tuple distance as the tuple distance of f. This is because the itemset with the minimum tuple distortion has been revealed in F' even there may be some other more distorted itemsets.

With the above considerations, we have the following recoding distance for local recoding:

Definition 6.5: *Recoding Distance for Local Recoding (RD_{local}):* Let $F = \{f_1, f_2 \dots f_n\}$ be a set of *σ-frequent itemsets* in D and $F' = \{f'_1, f'_2 \dots f'_m\}$ be the set of *σ-frequent itemsets* in D'. The corresponding frequent itemset(s) of f_i due to local recoding is denoted as $F_f = G(f_i)$. The recoding distance between F and F' is defined as:

$$RD_{local}(F, F') = \sum_{i=1}^{n} \frac{TD_{local}(f_i, G(f_i))}{TD_{local}(f_i, f_{max})}$$

where $TD_{local}(f_i, G(f_i)) =$

$$\begin{cases} \theta_q \times TD(f_i, G(f_i)), & \text{if } f \text{ has 1 correspondent in } F' \\ (1-\theta_q) \times TD(f_i, f_{max}), & \text{if } f \text{ has no correspondent in } F' \\ \theta_q \times min(TD(f_i, f_j)), & \\ \quad where\ f_j \in G(f_i), & \text{otherwise,} \end{cases}$$

θ_q is a parameter that specifies the importance between the itemsets that are distorted and those disappeared due to G and $TD_{local}(f_i, f_{max})$ at the denominator is used to normalized RD_{local}. ∎

Example 6.4: Following up the local recoding in Example 6.1, when σ is 30%, the frequent itemset {(`BA`)} corresponds to the frequent itemsets {(`BA`), (`Deg`)} in the recoded datasets. ∎

6.2 Metric for the change in growth rate

The second component in our heuristics concerns the growth rate of the emerging patterns. Intuitively, we aim at a recoding that significantly reduces the growth rate of the emerging patterns, in order to hide them. Given an emerging pattern e and the result of a local recoding e', the reduction in growth rate due to the recoding can be easily defined as the growth rate of e minus the growth rate of e'. Then, the growth rate reduction of E due to a local recoding G, denoted as $RG_{local}(G, E)$, can be defined as the total reduction in growth rate of e in E divided by the total growth rate of e in E.

Putting all these together. Based on the derivations from Section 6.1 and Section 6.2, the utility gain due to a local recoding G on a set of emerging patterns E is defined as:

$$\texttt{util\_gain}(G, E) = \theta_p RG_{local}(G, E) - (1-\theta_p) RD_{local}(F, F')$$

This utility gain is used in our heuristic algorithm, presented in Figure 2. There are two parameters θ_p and θ_q specified by users.

It is worth mentioning that *jumping emerging patterns* are a special case in measuring the reduction in growth rate. Recall that jumping emerging patterns have an infinite growth rate. Hence, whenever a recoding that either hides jumping emerging patterns or converts them into non-jumping emerging patterns would yield an infinite reduction in growth rate. Our heuristic algorithm will tend to hide the jumping emerging patterns prior to the non-jumping ones.

7 Implementation Optimization

In this section, we discuss some implementation issues for optimizing the computation of the proposed algorithm.

1. The maintenance of the equivalence classes. Local recoding relies on equivalence classes (Lines 03, 06 and 07 in `local-recoding` in Figure 3). A local recoding would change the equivalence classes in the datasets slightly. We used a hashtable to keep track of the update of the classes caused by a recoding (Line 07). Since an emerging pattern may not be hidden by simply one recoding, we note that we may compute the equivalence class of attributes multiple times (Line 03). With the hashtable, Line 03 does not recompute existing equivalence classes.

2. An index for checking correspondents of F in F'. Given two sets of frequent itemsets F and F', we check the correspondents of an itemset in F to measure distortion between F and F' (`util_gain`). The core of this is to check whether a value v is a generalized version of another value in an attribute hierarchy. While an attribute hierarchy is often a small tree, these checks occur in every iteration of `hide-eps`. We apply an index [39] for computing the ancestor-descendant relationship of nodes in a tree. This significantly reduces the runtime of our algorithm.

3. A data structure for checking correspondents of E in E'. The other task of in computing `util_gain` is to keep

track of the change of emerging patterns during local recoding, which is neccessary to measure the reduction in growth rate. Hence, we associate an emerging pattern of e to its records. By comparing the records of e and e', we obtain the correspondence between e and e'.

8 Experimental Evaluation

To verify the effectiveness of our proposed algorithms, we have conducted an experimental study of our algorithm on two benchmark datasets.

We have implemented both our algorithm in simulated annealing style in Figure 2 and a greedy-search version of this algorithm, denoted as SA and Greedy, respectively. The implementation is written in JAVA SDK 1.6. We have run our experiment on a desktop PC with a Quad CPU at 2.4GHz and 3.25GB RAM. The desktop PC runs a Windows XP operating system. We have used system calls to invoke the implementations from [41] and [26] to determine emerging patterns and frequent itemsets, respectively.

We have applied our implementation on two datasets, namely Adult [36] and Mushroom [37]. Adult is a census dataset which is used to predict whether a person's income exceeds \$50k/year. Each record in Adult contains eight attributes. We removed the records that contain missing values. Adult has two classes of people – people who earn more than \$50k/year (7508 records) and people who do not (22654 records). We used the attribute hierarchy presented in [15] for local recoding. Mushroom describes physical characteristics, classification and poisonous/edible properties of mushrooms. Our discussions will mainly focus on Adult as its results demonstrate the properties of our proposed algorithm better.

The effect of the parameters θ_p and θ_q. We performed a set of experiments to verify the effects on the parameters θ_p and θ_q on the heuristic algorithm. The performance metric used was given in distortion on the frequent itemsets / the number of missing frequent itemsets, unless otherwise specified. We used the Adult dataset and Greedy in this experiment. σ and ρ were set to 40% and 5, respectively. The frequent itemsets are:

(Husband, Married-civ-spouse, Male)
(Married-civ-spouse, White)
(Married-civ-spouse, United-States)
(Male, Private, White)
(Male, Private, United-States)
(Male, White, United-States)
(Private, White, United-States).

When we recode all attributes to All in the frequent itemsets, we obtain the maximum distortion of the frequent itemsets of Adult 623.1.

To illustrate the possible recoding in the frequent itemsets, we list the frequent itemsets after applying Greedy, where θ_p and θ_q were both set to 0.8:

(Relationship, United-States)
(Married, White, United-States)
(Male, Private, White)
(Male, Private, United-States)
(Male, White, United-States)
(Private, White, United-States).

The distortion obtained is 21.5 (out of 623.1).

Table 2. The effect of the parameters in util_gain on Greedy's performance on Adult

$\theta_p \backslash \theta_q$	0.0	0.2	0.4	0.6	0.8	1.0
0	0/0	50/1	50/1	50/1	50/1	NA
0.2	46.7/1	73.3/1	21.5/1	21.5/1	21.5/1	7.5/3
0.4	46.7/1	73.3/1	21.5/1	21.5/1	21.5/1	7.5/3
0.6	46.7/1	73.3/1	42.5/1	42.5/1	21.5/1	7.5/3
0.8	46.7/1	73.3/1	21.5/1	42.5/1	42.5/1	7.5/4
1.0	7.5/4	7.5/4	7.5/4	7.5/4	7.5/4	7.5/4

Next, we varied θ_p and θ_q and measured the distortion of frequent itemsets and runtime of our algorithm. The results are shown in Table 2 and Table 3.

We make a few observations from Table 2 and Table 3. Firstly, when θ_p is set to 0, the algorithm only concerns distortion (regardless of the corresponding reduction in growth rate) during local recodings. In such a case, the distortion in frequent itemsets of various θ_q's is in general large. We note that the corresponding runtime in Table 3 is also relatively high. We used DNF to denote "did not finish in 360 mins". The reason is that when θ_p is 0, the heuristics do not effectively reduce the growth rate and the search takes more recodings that are not relevant to hiding emerging patterns. This results in a relatively large distortion and runtime.

Secondly, when θ_p is 1, util_gain concerns only the reduction in growth rate. Table 3 shows that util_gain finished quickly. However, four frequent itemsets disappeared.

Thirdly, when we set θ_q to 1 and varied θ_p, we do not consider the frequent itemsets that disappear. Hence, such recodings lose relatively more frequent itemsets. Similarly, when we set θ_q to 0, we consider only the distortion of those that do not disappear. Since there is in fact one frequent itemset that disappears during recodings, overlooking this frequent itemset would lead to more distortion.

Fourthly, we obtained no distortion with no missing frequent itemset when θ_p was 1 and θ_q was 0. We speculate that this is an outlier (although a good outlier), as we benchmarked our the algorithm with a real dataset.

In all, we found that on the Adult dataset, Greedy may yield frequent itemsets with a distortion of 21.5 (out of 623.1) and one (out of seven) missing frequent itemset when θ_p is moderate (0.2 - 0.6) and θ_q is large (0.8).

Simulated annealing search. After verifying the effect of the parameters θ_p and θ_q on Greedy, we applied SA to Adult. We set the temperature of SA to be low with a high cooling rate (T = 10 and α = 0.4). Hence, SA initially has some chance to avoid local sub-optimas and then converges to Greedy quickly. SA is allowed to restart five times and

Table 3. The effect of the parameters in `util_gain` on `Greedy`'s runtime (min) on `Adult`

$\theta_p \backslash \theta_q$	0.0	0.2	0.4	0.6	0.8	1.0
0	54	311	305	214	319	DNF
0.2	107	128	120	102	116	123
0.4	135	109	120	111	117	108
0.6	121	137	139	128	122	109
0.8	101	122	103	130	139	131
1.0	66	62	66	59	66	59

Table 4. The effect of the parameters in `util_gain` on `SA`'s performance on `Adult`, where α = 0.4 and T = 10

$\theta_p \backslash \theta_q$	0.0	0.2	0.4	0.6	0.8	1.0
0	23.3/2	61.6/1	61.6/1	35/1	50/1	42.5/1
0.2	61.6/1/1	23.3/0	21.5/1	35/4	61.6/1	0/3
0.4	21.5/1	26.6/1	0/3	23.3/1	28.5/1	61.6/2
0.6	61.6/1	21.5/1	0/0	0/3	77/1	0/3
0.8	61.6/1	33.3/1	23.3/1	50/1	0/1	61.6/3
1.0	0/0	0/0	50/1	50/1	50/2	50/3

we report the best of the five runs. The results are shown in Table 4 and 5.

As expected, Table 4 shows that `SA` introduced a certain randomness in our results. `SA` also often performs well at a moderate θ_p and a large θ_q. Under many combinations of θ_p and θ_q, `SA` produces comparable or better results, for example when (p, q) are (0.6, 0.4) and (0.8, 0.8). `SA` may sometimes lose more frequent itemsets when compared to `Greedy`, for example (0.4, 0.4) and (0.6, 0.6).

Table 5 shows that `SA` did not finished more often. The randomness in simulated annealing may lead the search to a place where there are few effective recodings. We tackle this by restarting `SA` when it did not finish in 360 minutes.

Experiments with `Mushroom`. In addition to `Adult`, we tested `Greedy` on the `Mushroom` dataset. We divided `Mushroom` into two datasets: (i) edible mushrooms (3488 records) and (ii) poisonous mushrooms (2156 records). We considered the nominal attributes only. For nominal attributes, we derived our own attribute hierarchies. The attributes of a mushroom concern mostly color and smell. We show the hierarchies of these attributes in Figure 5. We have tested `Greedy` with various combinations of p and q. We set σ and ρ to be 40% and 5, respectively. We omitted the discussion of the runtime of `Greedy` on `Mushroom` since it is approximately 10 mins. The results are shown in Table 6.

Table 5. The effect of the parameters in `util_gain` on `SA`'s runtime (min) on `Adult`, where α = 0.4 and T = 10

$\theta_p \backslash \theta_q$	0.0	0.2	0.4	0.6	0.8	1.0
0	713	472	366	629	738	417
0.2	953	644	935	DNF	523	1074
0.4	652	557	820	1012	871	893
0.6	611	DNF	881	849	638	954
0.8	408	677	1214	664	894	703
1.0	576	1084	781	940	DNF	DNF

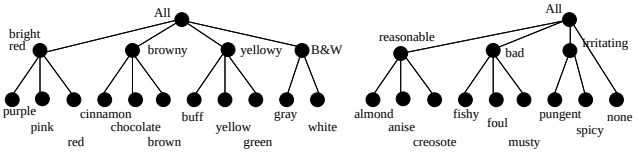

(a) Color (b) Smell

Figure 5. Attribute hierarchies of `Mushroom`

Table 6. `Greedy`'s performance on `Mushroom`

$\theta_p \backslash \theta_q$	0.0	0.2	0.4	0.6	0.8	1.0
0	92.7/0	92.7/0	92.7/0	92.7/0	92.7/0	92.7/0
0.2	92.7/0	74.7/0	74.7/0	74.7/0	74.7/0	74.7/0
0.4	92.7/0	74.7/0	74.7/0	74.7/0	74.7/0	74.7/0
0.6	92.7/0	74.7/0	74.7/0	74.7/0	74.7/0	55.3/1
0.8	92.7/0	74.7/0	92.7/0	53.3/1	0/1	55.3/1
1.0	92.7/0	92.7/0	92.7/0	NA	NA	74/0

Table 6 shows that our algorithm can often hide emerging patterns without losing any frequent itemsets. However, the distortion is often relatively severe. For example, we often obtained a distortion of 74.7 out of a maximum distortion of 116 in various combinations θ_p and θ_q. And the frequent itemsets in `Mushroom` are {(`odor=none`, `veil=white`), (`stalk-color-above-ring=white`, `stalk-color-below-ring=white`, `veil=white`)}. This may be due to the properties of the `Mushroom` dataset. (i) We found that the height of our attribute hierarchy of `color` and `smell` is rather small. When we recode attributes to hide emerging patterns, the recoded values often reach `All`. (ii) The attribute hierarchies carry certain semantics of the class, for example edible mushrooms often have a pale color. In order to hide emerging patterns, `All` is often used. For instance, recoding `purple`, and `red` into `brightred` may not notably reduce the growth rate of `eps`.

Similarly, we applied `SA` to `Mushroom`. The results are shown in Table 7. The results show that it is still possible to use `SA` to avoid some local sub-optimas. The best recoding leads to a distortion of 18 and no missing frequent itemsets.

9 Conclusions and Future Work

In this paper, we studied a particular case of `PPDP` where we hide emerging patterns of a dataset and at the same time preserve its frequent itemsets as far as possible. We have presented a heuristic local-recoding algorithm for this problem, where some metrics carefully derived for measuring the reduction of the growth rate of emerging patterns and the distortion of frequent itemsets are used to guide the re-

Table 7. `SA`'s performance on `Mushroom`, where α = 0.4 and T = 10

$\theta_p \backslash \theta_q$	0.0	0.2	0.4	0.6	0.8	1.0
0	55.3/0	55.3/0	55.3/0	55.3/0	55.3/0	55.3/0
0.2	55.3/0	55.3/0	55.3/0	36.7/0	55.3/0	92.7/0
0.4	55.3/1	55.3/0	55.3/0	55.3/0	92.7/0	92.7/0
0.6	55.3/0	55.3/0	55.3/0	55.3/0	55.3/0	92.7/0
0.8	55.3/0	18/0	18/0	36.7/0	55.3/0	55.3/0
1.0	55.3/0	55.3/0	92.7/0	55.3/0	74/0	55.3/0

coding process. We have implemented the proposed algorithm and tested it with two benchmark datasets. Our experimental results show that the algorithm is effective in hiding emerging patterns while minimizing the distortion on the frequent itemsets. To the best of our knowledge, this is the first work on hiding emerging patterns in a transactional dataset using recoding generalization.

Future work. While the proposed algorithm has shown to be effective in emerging pattern hiding, there remains a number of open research issues worth future research effort. Firstly, the heuristic algorithm hides emerging patterns in a greedy manner and one by one (`next-overlapping-ep`). It will be interesting to investigate if more advanced search strategies could be adopted to explore more effectively the *generalization space* to further minimize the frequent itemset distortion. Possible ideas include hiding a group of emerging patterns instead of hiding them one-at-a-time, and guiding the recoding process to avoid generating new emerging patterns as far as possible. Secondly, our algorithm invokes some existing implementations of frequent itemset and emerging pattern mining. It may be possible to further optimize our algorithm by incorporating our algorithm into the native implementations of those data mining techniques. Thirdly, since recoding approaches require attribute hierarchies, the frequent itemset distortion could be better measured by considering multilevel frequent itemsets. The corresponding change will be replacing Line 03 in `hide-eps`. The computational complexity for multilevel frequent itemset mining is high though.

References

[1] N. R. Adam and J. C. Worthmann. Security-control methods for statistical databases: A comparative study. *ACM Computing Surveys*, 21(4):515–556, 1989.

[2] D. Agrawal and C. Aggarwal. On the design and quantification of privacy preserving data mining algorithms. In *Proc. of PODS*, 2001.

[3] J. Bailey, T. Manoukian, and K. Ramamohanarao. Fast algorithms for mining emerging patterns. In *Proc. of ECML/PKDD*, 2002.

[4] J. R. Bayardo. Efficiently mining long patterns from databases. In *Proc. of SIGMOD*, pages 85–93, 1998.

[5] R. Bayardo and R. Agrawal. Data privacy through optimal k-anonymization. In *Proc. of ICDE*, pages 217–228, 2005.

[6] G. Dong and J. Li. Efficient mining of emerging patterns: Discovering trends and differences. In *Proc. of SIGKDD*, pages 43–52, 1999.

[7] G. Dong, X. Zhang, and L. Wong. CAEP: Classification by aggregating emerging patterns. In *Proc. of DS'99*, pages 30–42, 1999.

[8] W. Du and Z. Zhan. Using randomized response techniques for privacy-preserving data mining. In *Proc. of SIGKDD*, 2003.

[9] Y. Du, T. Xia, Y. Tao, D. Zhang, and F. Zhu. On multidimensional k-anonymity with local recoding generalization. In *Proc. of ICDE*, pages 1422–1424, 2007.

[10] A. Evfimievski, R. Strikant, R. Agrawal, and J. Gehrke. Privacy preserving mining of association rules. In *Proc. of SIGKDD*, 2002.

[11] H. Fan and K. Ramamohanarao. A Bayesian approach to use emerging patterns for classification. In *Proc. of ADC*, pages 39–48, 2003.

[12] B. Fung, K. Wang, R. Chen, and P. Yu. Privacy-preserving data publishing: A survey on recent developments. *ACM Computing Surveys*, in press.

[13] B. Fung, K. Wang, A. Fu, and P. Yu. *Privacy-Preserving Data Publishing: Concepts and Techniques*. Chapman & Hall/CRC, 2010.

[14] B. Fung, K. Wang, L. Wang, and M. Debbabi. A framework for privacy-preserving cluster analysis. In *Proc. of ISI*, page 4651, 2008.

[15] B. Fung, K. Wang, and P. Yu. Top-down specialization for information and privacy preservation. In *Proc. of ICDE*, pages 205–216, 2005.

[16] B. Fung, K. Wang, and P. Yu. Anonymizing classification data for privacy preservation. *TKDE*, 10(5):711–725, 2007.

[17] H. F. K. Ramamohanarao. Pattern based classifiers. In *Proc. of WWW*, pages 71–83, 2007.

[18] H. Kargupta, S. Datta, Q. Wang, and K. Sivakumar. Random-data perturbation techniques and privacy-preserving data mining. *KAIS*, 7(4):387–414, 2005.

[19] K. LeFevre, D. Dewitt, and R. Ramakrishnan. Incognito: Efficient full-domain k-anonymity. In *Proc. of SIGMOD*, pages 49–60, 2005.

[20] K. LeFevre, D. Dewitt, and R. Ramakrishnan. Mondrian multidimensional k-anonymity. In *Proc. of ICDE*, page 25, 2006.

[21] J. Li, H. Liu, J. Downing, A.-J. Yeoh, and L. Wong. Simple rules underlying gene expression profiles of more than six subtypes of acute lymphoblastic leukemia (all) patients. In *Bioinformatics*, volume 19(1), pages 71–78, 2003.

[22] J. Li, H. Liu, S.-k. Ng, and L. Wong. Discovery of significant rules for classifying cancer ddiagnosis data. In *Bioinformatics*, volume 19(Suppl. 2), pages ii93–ii102, 2003.

[23] J. Li, R. Wong, A. Fu, and J. Pei. Anonymization by local recoding in data with attribute hierarchical taxonomies. *TKDE*, 20(9):1181–1194, 2008.

[24] T. Li and N. Li. On the tradeoff between privacy and utility in data publishing. In *Proc. of SIGKDD*, 2009.

[25] A. Machanavajjhala, D. Kifer, J. Gehrke, and M. Vēnkitasubramaniam. L-diversity: Privacy beyond k-anonymity. *TKDD*, 1(1):3, 2007.

[26] MAFIA. *Mining Maximal Frequent Itemsets*. http://himalaya-tools.sourceforge.net/Mafia/.

[27] K. Mandl, P. Szolovits, and I. Kohane. Public standards and patients' control: How to keep electronic medical records accessible but private. *British Medical Journal*, 322(7281):283–287, 2001.

[28] A. Meyerson and R. Williams. On the complexity of optimal k-anonymity. In *Proc. of PODS*, pages 223–228, 2004.

[29] G. Moustakides and V. Verykios. A maxmin approach for hiding frequent itemsets. *DKE*, 65(1):75–79, 2008.

[30] S. Oliveira and O.R.Zaiane. Privacy preserving frequent itemset mining. In *Proc. of ICDM Workshop on Privacy, Security and Data Mining*, volume 14, pages 43–54, 2002.

[31] Y. Saygin, V. Verykios, and C. Clifton. Using unknowns to prevent discovery of association rules. *SIGMOD Record*, 30(4):45–54, 2001.

[32] T. Server. Sharing real-time market research data to increase customer satisfaction. *Information Management Magazine*, July 2008.

[33] X. Sun and P. Yu. A border-based approach for hiding sensitive frequent itemsets. In *Proc. of ICDM*, pages 426–433, 2005.

[34] L. Sweeney. Achieving k-anonymity privacy protection using generalization and suppression. *IJUFKS*, 10(5):571–588, 2002.

[35] L. Sweeney. k-anonymity: A model for protecting privacy. In *IJUFKS*, pages 557–570, 2002.

[36] UCI Machine Learning Repository. *Adult Data Set*. http://archive.ics.uci.edu/ml/datasets/Adult.

[37] UCI Machine Learning Repository. *Mushroom Data Set*. http://archive.ics.uci.edu/ml/datasets/Mushroom.

[38] Z. Wang, H. Fan, and K. Ramamohanarao. Exploiting maximal emerging patterns for classification. In *Proc. of AUS-AI*, pages 1062–1068, 2004.

[39] X. Wu, M. L. Lee, and W. Hsu. A prime number labeling scheme for dynamic ordered xml trees. In *Proc. of ICDE*, pages 66–78, 2004.

[40] J. Xu, W. Wang, J. Pei, X. Wang, B. Shi, and A. Fu. Utility-based anonymization using local recoding. In *Proc. of SIGKDD*, pages 785–790, 2006.

[41] X. Zhang, G. Dong, and K. Ramamohanarao. Exploring constraints to efficiently mine emerging patterns from large high-dimensional datasets. In *Proc. of SIGKDD*, pages 310–314, 2000.

Estimation of the Number of Relevant Images in Infinite Databases

Xiaoling Wang

Abstract

In image retrieval the most commonly used performance measures are precision and recall. However, to determine the number of relevant images in an infinite database presents a significant challenge as the relevant parameters are not directly observable. In our research, we use internet as a vehicle to investigate this problem, and evaluate search results from major image search engines. We also investigate whether the cumulative relevance of images in different results pages follows particular stochastic behaviors, such as the Independent Model or the Markov Chain Distribution. From such models, we shall estimate the total number of relevant images for major image search engines.

1. Introduction and Related Works

Due to the increased importance of the Internet, the use of image search engines such as Google, Yahoo, and Msn is becoming increasingly widespread. However, for many image search engines, it is difficult for users to make a decision as to which image search engine should be selected. It is obvious that the more effective the system is, the more it will offer satisfaction to the user. Therefore, retrieval effectiveness becomes one of the most important parameters to measure the performance of image retrieval systems [18, 19, 20]. As we know, the most commonly used performance measures are the precision P and recall R[1, 2, 3, 13, 14], but to compute recall R is rather difficult as the total number of relevant images is not directly observable in such a potentially infinite database.

Many researchers have conducted studies to evaluate the retrieval effectiveness of image search engines. Ece Çakır et al. [4] described the retrieval effectiveness of image search engines based on various query topics. Fuat Uluç et al. [10] described the impact of the number of query words on image search engines. However, none of these studies describe how to estimate the total number of relevant images for the image search engines. All of them only view the first two page results. In the study by Sprink and Jansen [20], data collected from Dogpile was analyzed and one of the findings was that the percentages of the users that viewed only the first page and those that viewed only the first two pages of document search results were about 71.9% and 15.8%, respectively. Although many works used recall as the measure to evaluate the image search engine, not many papers work on the estimation of the number of relevant images in infinite databases. An algorithm called sample-resample is presented in by Si and Callan [6]; in environments containing resource descriptions already created by query-based sampling, the sample-resample method uses several additional queries to provide an estimate of the database size. Therefore, if the database size has been known, then the distribution of relevant images can be estimated.

In our paper, we model the probabilistic behavior of the distribution of relevant images among the returned results by evaluating the performance of some widespread image search engines.

2. Basic Models and Empirical Evaluation

2.1 Independent Distribution

The cumulative relevance of images in different results pages may follow the independent distribution. We let P_k denote the probability that the cumulative relevance of all the images in Page k. In general, it is normally true that, for search engines, the first pages provide a larger probability, so that

$P_1 \geq P_2 \geq \ldots \geq P_k \geq P_{k+1} \geq \ldots$

And in practice, we may take that after a certain number of retrieved results, the inequalities in the above will become strict ones. Since the relevant outcomes of different ranked images are not mutually exclusive

events and that the search results do not feasibly terminate, we have in general $\sum_{k=1}^{\infty} P_k >> 1$ and that $P_k \to 0$, as $k \to \infty$. We shall model such probability sequence by independent distribution laws which conform to the above characterization and validate these experimentally. We shall also investigate the usefulness of the quadratic formula:

$P_k = \beta_1 k^2 + \beta_2 k + \alpha$,

where $k=1, 2, 3\ldots$

in representing results relevance over the different pages. Therefore, after determining the parameters using the least square method, we can use the non-linear model to estimate the number of relevant images page by page.

Therefore, from this model we can estimate the total number of relevant images for the major image search engines.

2.2 Markov Chain Model

Since in internet image search, results are returned in units of pages, we shall focus on the integer-valued stochastic process $X_1, X_2,\ldots$, where X_J represents the aggregate relevance of all the images in page J, which may be estimated by $X_J = \sum_{i \in J} Y_{Ji}$, where $Y_{Ji}=1$ if the ith image on page J is relevant, and $Y_{Ji}=0$ if the ith image on page J is not relevant. For this stochastic modeling of cumulative page image relevance, we shall investigate in particular the Markov Chain Model.

Here, we model the sequence $X=\{X_1, X_2, \ldots\}$ by a Markov Chain [11, 16, 17]. That is, we assume that the number of relevant images X_J in a page J only depends on X_{J-1} and not on the cumulative number of relevant images returned in $X_1, X_2, \ldots X_{J-2}$. We take the conditional probability of the number of relevant images in X_J given the number of relevant images in X_{J-1} to be the transition probability $p_{(J-1),J}$. From this, we construct the transition probability matrix.

$$P = \begin{pmatrix} p_{00} & p_{01} & \cdots & p_{0n} \\ p_{10} & p_{11} & \cdots & p_{1n} \\ \cdots & \cdots & \cdots & \cdots \\ p_{n0} & p_{n1} & p_{n2} & p_{nn} \end{pmatrix},$$

Where n is the number of images contained in a page. We can effectively estimate the initial probabilities if the sample is reasonably large. The probabilities are placed in a vector of state probabilities:

$\pi(J)$ = vector of state probabilities for page J

$= (\pi_0, \pi_1, \pi_2, \pi_3, \cdots, \pi_n)$

Where π_k is the probability of having k relevant images

Therefore, from this model, we can estimate the number of relevant images by pages by using the formula in page J:

$\pi(J) = \pi(J-1)*P,\ J=1, 2, 3, \ldots, n$

2.3 Queries Selection

We shall evaluate the top image search engines, namely, Google [7], Yahoo [8], and Msn [9], whose market shares are 64%, 16.3%, and 9.9%, respectively [10].By using 72 example queries. The queries consist of one-word, two-word and more than three-word queries, which range from simple words like apple to more specific query like apple computers and finally progressing to rather specific search. In the table below I only list part of queries.

Categories	Sample Queries
One-word query	Apple
	Dolphin
	Octopus
	Facebook
	Roxy
	Wildlife
	Skiing
	Alleyway
	Maldives
	Puppy
Two-word query	Apple Computer
	Plane Crash
	Octopus Card
	Outer Space

	Night Scene
	Daisy Flower
	Street-Art
	Baby Cry
	Afghan Child
	Twin Towers
More than Three-word query	Man Wearing Hat
	Macro Fly Eyes
	Sunrise and Sunset
	Jordan Basketball Nike
	Black and White Portrait
	HongKong Night Scene
	Flowing in the Wind
	Michael Schumacher Ferrari
	Chinese Opera Mask
	Victoria Harbour Hong Kong

Table 1. Part of Sample Query list

Categories	Test Queries
One-word query	Volcano
Two-word query	Tibetan Girl
Three-word query	Desert Camel Shadow

Table 2. Test Query list

2.4 Test Image Search Engines

The Test Image Search Engines we have selected are listed as follows.

Google(www.google.com)

Yahoo(www.yahoo.com)

Msn(www.msn.com)

Each query is run on the selected image search engines separately. Based on Spink and Jansen's study [12], evaluating the images in first two pages is enough. Such a finding seems useful for the users who only want to find less than forty images, but not so useful for users who need a lot of images. Therefore, we will model the independent model or the Markov Chain Model to help us to estimate the number of relevant images per page while we have the initial probability and transition probability matrix in a specific ISE, and it will also guide us as to when we should stop viewing.

3. Experimental Results

The search results for every query in Google, Yahoo and Msn are shown in Appendix 1, Appendix 2 and Appendix 3 respectively. In Appendix 1, the search results show that Google performs quite well except for the query "apple". The ISE Yahoo also shows us that it performs well except for the queries "apple", "roxy", "plane crash", "octopus card", and "outer space" in Appendix 2. Appendix 3 shows that the Msn Search Engine also performs well except for the queries "Apple", "octopus card", "outer space", "black and white portrait" and "HK night scene".

3.1 Independent Distribution

If the cumulative relevance of images in different results pages is independent, we try to create a formula to estimate the number relevant images in pages. In this experiment, we search 69 queries, and we totally review page by page to calculate the number of relevant images. The data are shown in Appendix 1. We can obtain a mean number of relevant images for each pages based on the data we collected. We plot the results for Google, Yahoo and Msn as follows.

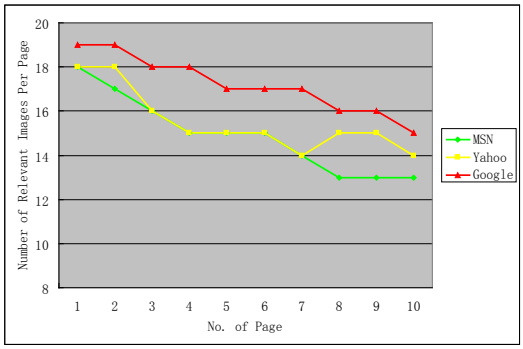

Figure 1. The Mean of the Number of Relevant Images for All the ISEs

The figure below shows the formula that we can use to estimate the number of relevant image page by page.

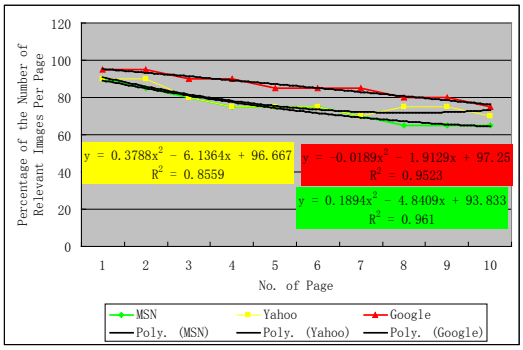

Figure 2. The Formula Created for All the ISEs

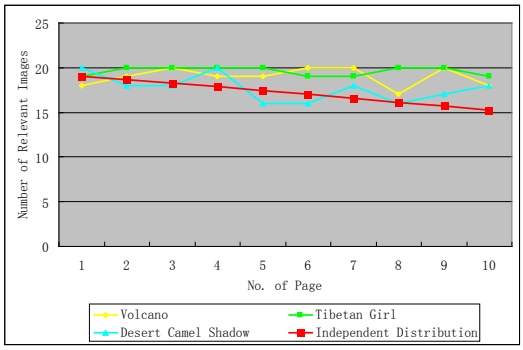

Figure 3. Search Result of Testing Queries and Independent Distribution Model for Google

From the figure above, we can find that the formula for the image search engine Google is

$P_k = -0.0189\,k^2 - 1.9129k + 97.25$ (1)

where k=1, 2, 3,…..

We can also get that the R-square is equal to *0.9523*, which represents the square of the sample correlation coefficient between the outcomes and their predicted values. And as we known, the larger the R^2 the better the model is.

Meanwhile, the formula for Yahoo and Msn are as follows respectively,

$P_k=0.3788\,k^2 - 6.1364k + 96.667$ (2)

$R^2 = 0.8559$

$P_k= 0.1894\,k^2 - 4.8409k + 93.833$ (3)

$R^2 = 0.961$

Therefore, we can use these three formulas to estimate the number of relevant images page by page for the testing ISEs respectively. Meanwhile, according to R-square, the formula given by MSN is the most precise, following by Google and Yahoo provide.

Another fact that we can observe from the figure is the Google returned the best result, and it decline slowly. The second one is Yahoo, which decrease a little quicker than Google dose and the probability of the number of relevant images for each page are smaller than Google provides. Msn shows the worst result, it reduces more sharply and the probability of the number of relevant images per page is the smallest. Therefore, we can conclude that Google perform a best result if we think the cumulative relevance of images in different results pages is independent.

Now, we will testing these formulas by using the test query we have listed before. The charts are shown below and we will discuss the findings.

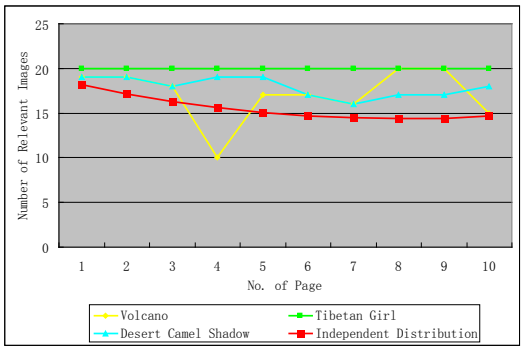

Figure 4. Search Result of Testing Queries and Independent Distribution Model for Yahoo

Figure 4 tells us that the searching result of testing queries and Independent Model we obtain from the example queries for Yahoo. From this figure, we can see that the independent model seems to provide a worse result than the actual data. However, in my opinion, we can still use this model to estimate the number of relevant images for engine, because apparently the distinction is not very large and we know the mean of the number is reasonable.

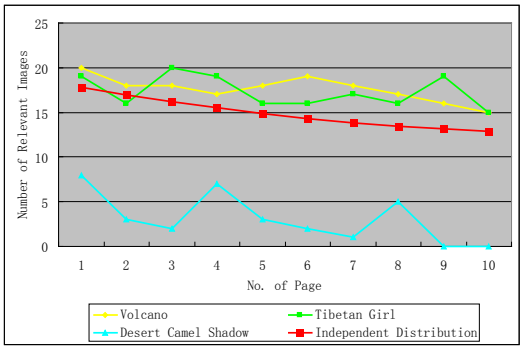

Figure 5. Search Result of Testing Queries and Independent Distribution Model for Msn

Figure 5 illustrates the searching result of testing queries and Independent Model we obtain from the example queries for Msn. The Figure shows us that the Independent Model seems fit the testing queries good too for one word query and two words query, and the trend seems quite the same although there are some fluctuation. But apparently, this model looks worse than we get from Google and Yahoo for rather specific searching term.

3.2 Markov Chain Model

According to these queries, we want to find whether the cumulative relevant images in different pages follows one-step Markov Chain Distribution. And we shall apply Markov Chain Model to estimate the number of relevant images in infinite databases.

The transition probability matrix and the vector of state probabilities for pages for all ISEs are shown in Appendix 1, Appendix 2 and Appendix 3 respectively.

In the following, the Markov Chain Model and test results will be shown. And we will discuss the findings.

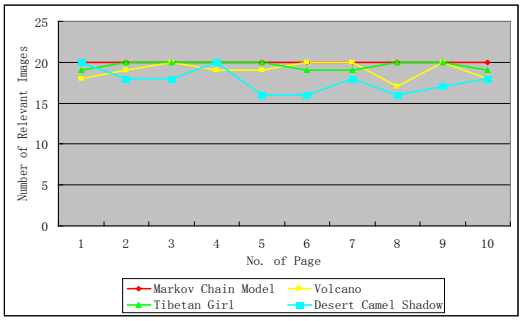

Figure 6. Search Result of Testing Queries and Markov Chain Model for Google

Figure 6 illustrates the searching result of testing queries and Markov Chain Model we obtain from the example queries for Google. According to this figure, we can see that the Markov Chain Model fits the testing queries rather well, no matter for the one-word query, two-word query or three-word query, although there are some distinctions. But apparently, we can't apply this model to query "apple" because this is a special case.

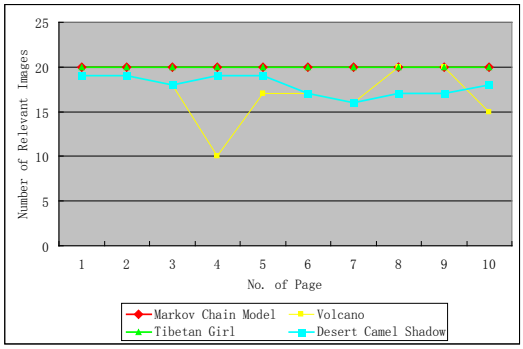

Figure 7. Search Result of Testing Queries and Markov Chain Model for Yahoo

Figure 7 illustrates the searching result of testing queries and Markov Chain Model we obtain from the example queries for Yahoo. The Figure shows us that the Markov Chain Model also fits the testing queries quite good. Especially for the two words query, the model fit the data perfectly, but for the single word query, some point is so bad apparently. But in whole, it is a good predicting model although it fits the data a little worse than Google does.

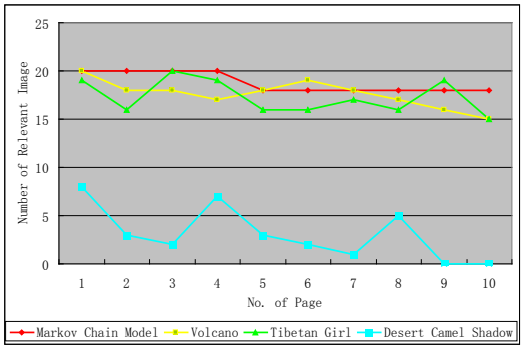

Figure 8. Search Result of Testing Queries and Markov Chain Model for Msn

Figure 8 illustrates the searching result of testing queries and Markov Chain Model we obtain from the example queries for Msn. The Figure tells us that the Markov Chain Model fits the testing queries well for the one-word query and two-word query but so bad for the three-word queries although the trend between them

seems the same. Apparently, this model looks worse than we get from Google and Yahoo. And we can also get a conclusion that the Msn is not good at searching rather specific searching term.

Although all the equation can fit data quite well, but it can not fit all queries very well; the following is a special example. The Figure 9 shows us the searching result for query “apple” in all the ISEs we want to test.

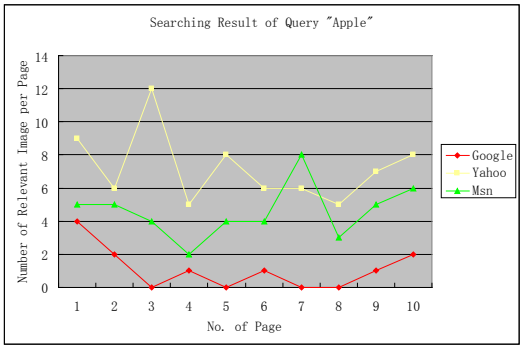

Figure 9. Search Result for Query “apple” in All the ISEs

We can see from the Fig 9 that the searching results are so bad in all ISE, although Yahoo perform better than Msn and Msn perform better than Google. For the query “apple”, it is equivocal for the ISE, because the ISE can’t differentiate what we want to search, the fruit or the brand of computer? Therefore, the searching results are so bad. But in all, for one-word query, we can see from the Appendix that the Google gives the best result and Msn displays the worst result.

For the two-word query, we choose query “apple computer” to compare the ISEs.

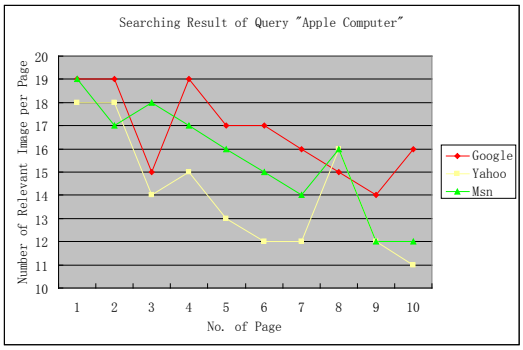

Figure 10. Search Result for Query “apple computer” in All the ISEs

From the Fig 10, we can see all the ISEs display good searching result when we give a more specific search term. And it shows us that Google give us the best result, Yahoo following it and Msn display the worst result.

For the three-word query, we pick query “black and white portrait” to compare.

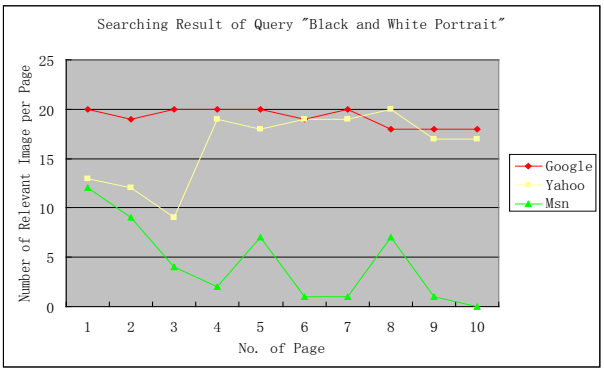

Figure 11. Search Result for Query “black and white portrait” in All the ISEs

When we give a rather specific query, Google perform rather well, the Yahoo displays well also, but Msn give us a quite bad result. Msn returned so many colorful images; it seems it can’t differentiate “black and white” and “colorful”. This illustrates Msn is not good at searching rather specific searching term but good at simple word.

4. Conclusion and Future Work

Currently, estimating the number of relevant images in the infinite image search engines is quite hard, but it is so important for us. Therefore, we develop a set of image queries to investigate models to estimate the number of relevant images in infinite ISEs. And using some queries to test the model we obtain.

If the stochastic process follows independent distribution, we can get equation (1) (2) (3) respectively for Google, Yahoo and Msn. We can observe that the Google returned the best results, and it decline slowly. Meanwhile it fits the data very well. The second one is Yahoo, which decrease a little quicker than Google dose and the probability of the number of relevant images for each page are smaller than Google provides. Msn shows the worst results when three-word query is given, and it reduces more sharply and the probability of the number of relevant images per page is the smallest. Therefore, we can conclude that Google performs the best results if we think the cumulative relevance of images in different

results pages is independent. And the most important thing is that we can use these formulas to estimate the number of relevant images for ISEs.

If the stochastic process follows Markov Chain Distribution, we can find that the Markov Chain Model we obtain for Google is the best, because it fits the data quite well, especially for the quite specific queries. Yahoo comes in 2nd. The model fits the specific query quite well, but for the special specific query, the result is a little worse than Google have done. Msn seems the worst among these three ISEs when a rather specific query is given. But it fits easy word and specific query quite good. In a word, according to our experiment, we can use Independent Model and Markov Chain Model to estimate the total number of relevant images in infinite image search engines. But apparently, the equivocal character of the query “apple” made all the Independent Model and Markov Chain Model incapable of estimating.

For infinite image repositories, it is generally impractical to step through the interminable set of search results presented. Therefore, our future work is to find an optimal stopping rule. According to what we have done above, it seems using Markov Chain could provide us a good stopping rule.

5. Reference

[1] K. Stevenson and C. Leung, “Comparative Evaluation of Web Image Search Engines for Multimedia Applications”, *In Proceedings of IEEE International Conference on Multimedia and Expo*, July 2005

[2] Ishioka, T. 2003, “Evaluation of Criteria for Information Retrieval”, *In Proceedings of the 2003 IEEE/WIC International Conference on Web Intelligence* (October 13 - 17, 2003). Web Intelligence IEEE Computer Society, Washington, DC, 425

[3]Raquel Kolitski Stasiu, Carlos A. Heuser, and Roberto da Silva, “Estimating Recall and Precision for Vague Queries in Databases”, *In Proceedings of Springer-Verlag Berlin Heidelberg, CAiSE 2005, LNCS 3520, pp. 187-200, 2005*

[4] Ece Çakır, Hüseyin Bahçeci, Yıltan Bitirim, "An Evaluation of Major Image Search Engines on Various Query Topics," icimp, pp.161-165, 2008. *In Proceedings of the Third International Conference on Internet Monitoring and Protection*, 2008

[5] F. Uluç, E. Emirzade and Y. Bitirim, “The Impact of Number of Query Words on Image Search Engines”, *In Proceedings of Second International Conference on Internet and Web Applications and Services* (ICIW), pp. 50, 2007

[6] Si, L. and Callan, J. 2003, “Relevant document distribution estimation method for resource selection”, *In Proceedings of the 26th Annual international ACM SIGIR Conference on Research and Development in informaion Retrieval* Toronto, Canada, July 28 - August 01, 2003. SIGIR '03. ACM, New York, NY, 298-305

[7] Google Search Engine www.google.com

[8] Yahoo Search Engine www.yahoo.com

[9] Msn Search Engine www.msn.com

[10] Nielsen//NetRatings, “Goole accounts for more than half of all web searches, while Yahoo and Msn combined account more than one fourth, according to Nielson//Netrating”, April 2009. http://www.polepositionmarketing.com/emp/april-2009-search-engine-2/

[11] Render, R., R. M. Stair Jr., and M. E. Hanna. “Quantitative Analysis for Management-Chapter 16”, 10th Edition, Prentice Hall, 2009

[12] A.Sprink and B.J.Jansen, “Searching Multimedia Federated Content Web Collections”, Online Information Review, Vol.30, No.5, pp. 485-495,2006

[13] Jin, X. and French, J. C. 2003. Improving ima ge retrieval effectiveness via multiple queries. *In Pr oceedings of the 1st ACM international Workshop o n Multimedia Databases* (New Orleans, LA, USA, November 07 - 07, 2003). MMDB '03. ACM, New York, NY, 86-93. DOI= http://doi.acm.org/10.1145/951676.951692

[14] Nottelmann, H. and Fuhr, N. 2003. Evaluating different methods of estimating retrieval quality for resource selection. In *Proceedings of the 26th Annual international ACM SIGIR Conference on Research and Development in informaion Retrieval* (Toronto, Canada, July 28 - August 01, 2003). SIGIR '03. ACM, New York, NY, 290-297. DOI=

http://doi.acm.org/10.1145/860435.860489

[15] Thomas W. Miller, *Data and Text Mining: A Business Applications Approach.* Upper Saddle River, N.J. : Pearson Prentice Hall, c2005

[16]W.S. Kendall, F. Liang, J.-S. Wang, *Markov chain Monte Carlo : innovations and applications*, Singapore ; Hackensack, NJ : World Scientific, c2005

[17]Dani Gamerman, *Markov chain Monte Carlo : stochastic simulation for Bayesian inference***,** London ; New York : Chapman & Hall, 1997

[18] Shirahatti, N. V. and Barnard, K. 2005. Evaluating Image Retrieval. *In Proceedings of the 2005 IEEE Computer Society Conference on Computer Vision and Pattern Recognition (Cvpr'05) - Volume 1 - Volume 01* (June 20 - 26, 2005). CVPR. IEEE Computer Society, Washington, DC, 955-961. DOI= http://dx.doi.org/10.1109/CVPR.2005.147

[19] Black Jr, J. A., Fahmy, G., and Panchanathan, S. 2002. A Method for Evaluating the Performance of Content-Based Image Retrieval Systems. *In Proceedings of the Fifth IEEE Southwest Symposium on Image Analysis and interpretation* (April 07 - 09, 2002). SSIAI. IEEE Computer Society, Washington, DC, 96.

[20] Münevver Tugçe Elagöz , Mehtap Mendeli , Remziye Zeden Manioglulari , Yiltan Bitirim, "An Empirical Evaluation on Meta-Image Search Engines," ICDT, pp.135-139, 2008. *In Proceedings of the Third International Conference on Digital Telecommunications* (ICDT 2008), 2008

Appendix 1: The Searching Result for All Queries in Google

Query / Number of Relevant Images / Page Number	Apple	Dolphin	Octopus	Facebook	Roxy	Wildlife
1	4	20	18	20	20	18
2	2	20	20	20	19	17
3	0	20	19	20	18	18
4	1	20	17	20	18	16
5	0	19	17	20	17	13
6	1	19	18	20	17	15
7	0	19	15	20	16	10
8	0	19	14	19	15	5
9	1	18	14	19	12	11
10	2	18	13	19	12	11
	Apple Computer	Plane Crash	Octopus Card	Outer Space	Night Scene	Daisy Flower
1	19	19	20	20	20	20
2	19	18	18	17	20	18
3	15	18	16	16	20	18
4	19	20	17	18	20	18
5	17	19	15	14	18	16
6	17	18	13	13	17	17
7	16	18	15	15	18	17
8	15	17	10	10	15	17
9	14	18	7	9	14	15
10	16	17	4	3	15	12
	Man Wearing	Macro Fly Eyes	Sunrise and Sunset	Jordan Basketball	Black and White	HK Night Scene

	Hat			Nike	Portrait	
1	20	18	19	20	20	19
2	19	18	20	19	19	19
3	18	16	20	19	20	20
4	18	16	20	20	20	19
5	19	16	19	18	20	20
6	16	16	20	17	19	19
7	17	15	16	19	20	20
8	18	15	17	20	18	18
9	17	10	15	20	18	19
10	20	11	15	19	18	18

Query / Number of Relevant Images / Page Number	Starbucks	Skiing	Alleyway	Maldives	Puppy	Twilight
1	20	19	20	19	20	20
2	20	19	20	19	20	20
3	20	20	20	18	20	20
4	20	19	18	18	20	20
5	19	17	20	18	19	20
6	20	16	19	20	19	20
7	18	17	20	20	19	20
8	18	18	19	17	20	18
9	16	14	19	18	19	17
10	18	13	17	13	18	19
	Macro Abstract	Street-art	Baby Cry	Afghan Child	Twin Towers	Toilet Icon
1	19	19	17	20	19	14
2	18	20	19	20	19	8
3	18	20	16	19	18	14
4	17	20	13	20	19	9
5	16	19	10	20	17	13
6	18	20	10	20	18	5
7	17	19	4	17	19	9
8	18	17	8	19	18	3
9	14	16	4	17	19	4
10	18	17	6	19	18	2
	Eagle Catching Fish	Blowing in the Wind	Michael Schumacher Ferrari	Chinese Opera Mask	Victoria Harbour Hong	Star Wars and Pepsi

					Kong	
1	19	20	19	19	20	19
2	18	20	19	20	19	19
3	17	18	19	19	18	18
4	19	18	18	18	19	18
5	18	18	20	19	18	17
6	20	19	19	20	18	17
7	17	19	19	19	20	17
8	18	20	18	18	19	19
9	18	18	18	17	18	15
10	18	19	18	16	19	17

Query Number of Relevant Images / Page Number	Headphone	Gundam	Yelling	Transformers	Chair	Scrat
1	19	20	20	20	19	20
2	20	20	20	20	20	19
3	19	20	19	20	20	20
4	18	20	19	20	20	20
5	19	20	18	20	19	20
6	20	20	18	20	20	20
7	20	20	16	20	18	19
8	18	19	15	19	20	20
9	17	19	14	16	20	19
10	20	19	14	18	19	20
	Kiehl's Lotion	Colorful Candy	Jennifer Aniston	Doraemon Figure	Yoga Poses	Amazon Rainforest
1	19	19	20	19	20	20
2	19	18	20	20	20	20
3	19	16	20	19	20	20
4	18	16	20	19	19	19
5	19	15	19	19	17	19
6	19	17	20	18	16	20
7	18	16	20	19	18	19
8	19	14	20	14	16	19
9	19	12	20	18	16	18
10	15	13	20	15	14	18
	Great White Shark	Rock n Roll	Heart Shaped Cookies	Drink Vending Machine	Butterfly on Yellow Flower	Lily of the Valley

1	20	20	19	20	20	16
2	20	20	18	20	19	18
3	20	20	16	19	19	17
4	20	20	16	19	15	18
5	20	20	16	16	14	16
6	19	20	18	16	13	16
7	20	20	16	15	13	15
8	18	20	17	18	11	16
9	20	20	16	16	9	15
10	20	18	16	15	16	15

Query Number of Relevant Images / Page Number	Tornado	Tired	Fisheye	Windmill	Steak	Piano
1	19	18	20	20	18	14
2	18	18	20	20	20	12
3	20	14	20	18	18	9
4	17	16	20	18	18	11
5	17	15	20	18	18	3
6	19	15	20	17	19	4
7	11	12	20	17	18	6
8	15	14	20	17	20	3
9	15	11	20	15	18	4
10	8	9	20	15	18	2
	Outdoor Wedding	Dior Catwalk	BMW Z4	African Art	Solar Eclipse	Icy Tree
1	20	20	20	20	18	20
2	20	20	20	20	17	19
3	19	20	20	20	19	20
4	20	20	20	20	19	20
5	20	20	20	19	20	19
6	20	19	20	19	18	17
7	20	19	20	19	20	20
8	19	17	20	20	20	20
9	19	16	20	19	20	20
10	20	16	20	20	20	20
	Bee on Sunflower	Sailing on San Francisco	Front View of Garden Cottage	Couple in Beach Chairs	Pink Room Design	Messy Working Desk

		Bay				
1	20	19	17	16	20	16
2	20	19	16	15	19	13
3	20	17	14	15	19	14
4	17	19	15	17	14	12
5	16	17	14	17	15	15
6	18	16	17	15	15	15
7	16	15	13	12	15	14
8	16	17	12	10	14	13
9	18	19	14	11	11	13
10	18	20	15	7	10	14

Appendix 1: Google Transition Probability Matrix

Number of Relevant Images	0	1	2	3	4	5	6	7	8	9	10	11	12	13	14	15	16	17	18	19	20
0	0.5	0.5	0	0	0	0	0	0	0	0	0	0	0	0	0	0	0	0	0	0	0
1	0.6667	0	0.3333	0	0	0	0	0	0	0	0	0	0	0	0	0	0	0	0	0	0
2	1	0	0	0	0	0	0	0	0	0	0	0	0	0	0	0	0	0	0	0	0
3	0	0	0	0	1	0	0	0	0	0	0	0	0	0	0	0	0	0	0	0	0
4	0	0	0.5	0	0	0	0.3333	0	0.1667	0	0	0	0	0	0	0	0	0	0	0	0
5	0	0	0	0	0	0	0	0	0	0	0	1	0	0	0	0	0	0	0	0	0
6	0	0	0	0.5	0	0	0	0	0	0.5	0	0	0	0	0	0	0	0	0	0	0
7	0	0	0	0	1	0	0	0	0	0	0	0	0	0	0	0	0	0	0	0	0
8	0	0	0	0	0.3333	0	0	0	0	0.3333	0	0	0	0	0.3333	0	0	0	0	0	0
9	0	0	0	0.4	0	0	0	0	0	0	0	0.2	0	0.2	0	0	0.2	0	0	0	0
10	0	0	0	0	0.1429	0.1429	0	0.1429	0	0.1429	0.1429	0.2857	0	0	0	0	0	0	0	0	0
11	0	0	0	0.1429	0	0	0	0.1429	0	0.1429	0.1429	0.2857	0	0	0	0.1429	0	0	0	0	0
12	0	0	0	0	0	0	0	0	0	0.1429	0.1429	0	0.1429	0.1429	0.2857	0.1429	0	0	0	0	0
13	0	0	0	0	0	0	0.0909	0	0	0	0.0909	0.0909	0.0909	0.1818	0.1818	0.2727	0	0	0	0	0
14	0	0	0	0	0	0	0	0	0.04	0.04	0	0.04	0.12	0.2	0.08	0.24	0.08	0.08	0.08	0	0
15	0	0	0	0	0	0	0	0	0.0294	0	0.1176	0	0.1176	0.0294	0.2353	0.2941	0.0294	0.0882	0.0294	0.0294	0
16	0	0	0	0	0	0	0	0	0	0	0	0	0	0.0682	0.0682	0.2273	0.2727	0.1591	0.2045	0	0
17	0	0	0	0	0	0	0	0	0	0	0	0	0	0.0175	0	0.0877	0.2456	0.193	0.2105	0.193	0.0526
18	0	0	0	0	0	0	0	0	0	0	0	0	0	0.0105	0.0421	0.0316	0.1368	0.1789	0.3053	0.1579	0.1368
19	0	0	0	0	0	0	0	0	0	0	0	0.0074	0	0	0.0148	0.0296	0.0296	0.0889	0.2593	0.2963	0.2741
20	0	0	0	0	0	0	0	0	0	0	0	0	0	0	0	0	0.0051	0.0303	0.0909	0.2626	0.6111

Appendix 1: The table below shows us that the number of relevant images for Sixteen Pages. The result shows us the probability and index, which get from the program we have done with Matlab.

Page Number	Probability	Index	Number of Relevant Images
1	0.5139	21.0000	20
2	0.4068	21.0000	20
3	0.3406	21.0000	20
4	0.2965	21.0000	20
5	0.2649	21.0000	20
6	0.2410	21.0000	20
7	0.2222	21.0000	20
8	0.2067	21.0000	20
9	0.1938	21.0000	20
10	0.1828	21.0000	20
11	0.1732	21.0000	20
12	0.1648	21.0000	20
13	0.1573	21.0000	20
14	0.1506	21.0000	20
15	0.1445	21.0000	20
16	0.1389	21.0000	20

The original vector is as follows:

$\pi(0)$=[0, 0, 0, 0, 1/72, 0, 0, 0, 0, 0, 0, 0, 0, 0, 2/72, 0, 3/72, 2/72, 6/72, 21/72, 37/72]

The testing result for Google:

Model and Testing / Query / Page Number	Markov Chain Model	Volcano	Tibetan Girl	Desert Camel Shadow
1	20	18	19	20
2	20	19	20	18
3	20	20	20	18
4	20	19	20	20
5	20	19	20	16
6	20	20	19	16
7	20	20	19	18
8	20	17	20	16
9	20	20	20	17
10	20	18	19	18

Appendix 2: The Searching Result for All Queries in Yahoo

Query / Number of Relevant Images / Page Number	Apple	Dolphin	Octopus	Facebook	Roxy	Wildlife
1	9	19	19	19	20	15
2	6	19	19	17	20	16
3	12	20	18	9	15	17
4	5	15	13	5	5	13
5	8	15	16	6	10	13
6	6	13	11	7	12	14
7	6	16	14	5	14	15
8	5	16	9	5	6	12
9	7	11	8	6	9	13
10	8	16	14	4	4	10
	Apple Computer	Plane Crash	Octopus Card	Outer Space	Night Scene	Daisy Flower
1	18	18	13	19	20	19
2	18	18	3	17	19	20
3	14	16	8	4	19	18
4	15	4	2	1	20	19
5	13	11	5	1	18	19
6	12	9	8	3	19	16
7	12	8	7	0	20	18
8	16	7	6	1	19	18
9	12	7	4	0	19	17
10	11	7	8	0	18	15
	Man Wearing Hat	Macro Fly Eyes	Sunrise and Sunset	Jordan Basketball Nike	Black and White Portrait	HK Night Scene
1	19	20	18	19	13	20
2	17	19	16	20	12	20
3	15	19	17	20	9	20
4	17	19	15	20	19	20
5	18	20	19	20	18	19
6	18	20	19	20	19	18
7	19	18	18	18	19	20
8	17	19	19	20	20	20
9	18	19	19	19	17	19
10	18	19	19	19	17	19

Query / Number of Relevant Images / Page Number	Starbucks	Skiing	Alleyway	Maldives	Puppy	Twilight
1	19	19	19	19	20	20
2	17	12	18	19	20	20
3	19	11	17	19	20	19
4	13	9	17	19	19	6
5	17	5	19	19	18	3
6	18	10	17	20	17	5
7	16	9	20	20	18	5
8	18	9	18	19	15	2
9	19	12	17	17	20	5
10	16	10	17	19	19	5
	Macro Abstract	Street-art	Baby Cry	Afghan Child	Twin Towers	Toilet Icon
1	20	19	5	17	19	20
2	20	20	5	11	20	20
3	20	19	8	17	19	20
4	18	20	8	19	19	20
5	19	19	8	12	14	20
6	19	20	10	18	17	20
7	18	19	8	17	13	20
8	19	20	11	16	12	20
9	19	20	6	16	12	20
10	17	20	10	17	13	20
	Eagle Catching Fish	Blowing in the Wind	Michael Schumacher Ferrari	Chinese Opera Mask	Victoria Harbour Hong Kong	Star Wars and Pepsi
1	19	19	20	20	20	20
2	18	19	19	19	20	17
3	19	20	20	20	20	17
4	18	20	20	20	20	16
5	16	20	20	20	20	16
6	15	19	20	19	20	15
7	15	20	20	20	20	9
8	14	20	20	18	20	0
9	13	20	20	20	20	0
10	14	19	19	19	19	0

Query / Number of Relevant Images / Page Number	Headphone	Gundam	Yelling	Transformers	Chair	Scrat
1	19	9	18	20	20	20
2	12	17	18	20	20	20
3	7	8	17	18	20	14
4	6	0	17	18	20	12
5	7	1	16	18	19	7
6	7	4	14	18	18	6
7	9	8	13	17	19	8
8	9	15	13	18	19	8
9	12	20	6	20	19	10
10	11	17	7	18	20	5
	Kiehl's Lotion	Colorful Candy	Jennifer Aniston	Doraemon Figure	Yoga Poses	Amazon Rainforest
1	6	17	20	19	20	20
2	19	20	20	20	16	17
3	19	19	20	18	14	20
4	18	16	20	13	20	20
5	19	19	18	11	19	17
6	12	19	20	8	17	15
7	14	20	20	7	18	15
8	13	18	20	0	17	17
9	13	17	20	0	18	17
10	14	17	20	0	17	20
	Great White Shark	Rock n Roll	Heart Shaped Cookies	Drink Vending Machine	Butterfly on Yellow Flower	Lily of the Valley
1	20	20	20	19	20	16
2	20	19	20	20	17	16
3	20	14	20	19	15	17
4	19	18	20	19	11	20
5	19	20	19	19	13	17
6	20	20	19	18	14	15
7	18	7	18	19	12	11
8	18	10	16	18	15	16
9	19	18	16	20	13	20
10	19	20	17	19	11	18

Query / Number of Relevant Images / Page Number	Tornado	Tired	Fisheye	Windmill	Steak	Piano
1	18	18	20	20	20	17
2	19	17	20	18	16	18
3	11	17	20	18	17	16
4	8	17	20	16	18	13
5	8	16	20	19	18	15
6	11	17	20	18	17	11
7	6	16	20	16	17	9
8	5	18	20	16	17	13
9	7	16	20	18	17	11
10	6	18	20	16	16	12
	Outdoor Wedding	Dior Catwalk	BMW Z4	African Art	Solar Eclipse	Icy Tree
1	19	20	20	20	17	20
2	19	19	20	20	20	20
3	19	20	20	18	17	20
4	20	20	20	18	11	20
5	19	19	20	20	17	19
6	18	12	20	20	20	20
7	18	17	20	19	16	20
8	17	19	20	20	17	20
9	19	19	19	20	17	20
10	19	19	19	20	14	20
	Bee on Sunflower	Sailing on San Francisco Bay	Front View of Garden Cottage	Couple in Beach Chairs	Pink Room Design	Messy Working Desk
1	20	19	11	11	16	18
2	18	19	15	9	17	16
3	18	19	12	3	12	16
4	18	18	12	5	11	15
5	20	19	11	4	10	16
6	20	20	12	5	4	16
7	20	19	13	0	6	15
8	18	19	12	2	14	15
9	19	18	8	2	6	14
10	20	17	9	0	11	13

Appendix 2: Yahoo Transition Probability Matrix

Number of Relevant Images	0	1	2	3	4	5	6	7	8	9	10	11	12	13	14	15	16	17	18	19	20
0	0.625	0.25	0.125	0	0	0	0	0	0	0	0	0	0	0	0	0	0	0	0	0	0
1	0.25	0.25	0	0.25	0.25	0	0	0	0	0	0	0	0	0	0	0	0	0	0	0	0
2	0.25	0	0.25	0	0	0.5	0	0	0	0	0	0	0	0	0	0	0	0	0	0	0
3	0.25	0	0	0	0	0.5	0	0	0.25	0	0	0	0	0	0	0	0	0	0	0	0
4	0	0.1667	0	0	0	0.1667	0.1667	0	0.3333	0	0	0.1667	0	0	0	0	0	0	0	0	0
5	0.0625	0	0.0625	0	0.0625	0.25	0.125	0.125	0.1875	0	0.125	0	0	0	0	0	0	0	0	0	0
6	0	0	0.0625	0.0625	0.125	0.125	0.0625	0.1875	0.0625	0.0625	0.0625	0.0625	0	0	0.0625	0	0	0	0	0.0625	0
7	0.0833	0	0	0	0	0.0833	0.3333	0.25	0.0833	0.0833	0.0833	0	0	0	0	0	0	0	0	0	0
8	0.0625	0	0.0625	0	0	0	0.0625	0.1875	0.25	0	0.125	0.125	0	0	0.0625	0.0625	0	0	0	0	0
9	0.0667	0	0	0.0667	0.0667	0.1333	0.0667	0	0.1333	0.1333	0	0	0.1333	0.0667	0	0	0	0.0667	0	0.0667	0
10	0	0	0	0	0.1667	0.1667	0	0	0.1667	0.1667	0	0	0.1667	0	0	0	0	0	0.1667	0	0
11	0	0	0	0	0	0	0.1111	0	0.1111	0.2222	0.0556	0	0.1111	0.0556	0.0556	0.0556	0.1111	0.1111	0	0	0
12	0	0	0	0	0	0.04	0.04	0.08	0.04	0.08	0.04	0.2	0.12	0.12	0.08	0.04	0.04	0.04	0.04	0	0
13	0	0	0	0.05	0	0	0	0	0	0	0.05	0.15	0.2	0.15	0.2	0.05	0.1	0.05	0	0	0
14	0	0	0	0	0	0	0.1538	0	0	0.0769	0	0	0.1538	0.2308	0	0.1538	0	0.0769	0.0769	0	0.0769
15	0	0	0	0	0	0.0435	0	0	0	0.0435	0	0.1304	0.087	0.1304	0.087	0.1739	0.087	0.087	0	0.0435	0.087
16	0	0	0	0	0.0294	0	0	0	0	0	0	0.0588	0.0294	0.0294	0.0588	0.1176	0.2647	0.2059	0.1176	0.0588	0.0294
17	0	0	0	0	0.0175	0	0	0	0.0175	0.0175	0	0.0351	0.0175	0.0351	0.0175	0.1053	0.1053	0.2456	0.1404	0.1053	0.1404
18	0	0	0	0	0	0	0	0	0	0	0	0	0	0.0274	0.0137	0.0137	0.1507	0.1918	0.2466	0.2329	0.1233
19	0	0	0	0	0	0	0.0088	0	0	0	0	0.0088	0.0439	0.0088	0.0175	0	0.0263	0.0877	0.1754	0.3596	0.2632
20	0	0	0	0	0	0	0	0.006	0	0	0	0	0	0	0.006	0.0119	0.0179	0.0536	0.1131	0.25	0.5417

Appendix 2: The table below shows us that the number of relevant images for Sixteen Pages. The result shows us the probability and index, which get from the program we have done with Matlab.

Page Number	Probability	Index	Number of Relevant Images
1	0.4028	21.0000	20
2	0.3282	21.0000	20
3	0.2809	21.0000	20
4	0.2498	21.0000	20
5	0.2278	21.0000	20
6	0.2112	21.0000	20
7	0.1980	21.0000	20
8	0.1872	21.0000	20
9	0.1781	21.0000	20
10	0.1703	21.0000	20
11	0.1636	21.0000	20
12	0.1577	21.0000	20
13	0.1525	21.0000	20
14	0.1479	21.0000	20
15	0.1438	21.0000	20
16	0.1402	21.0000	20

The original vector:

π (0)= [0,0,0,0,0,1/72,1/72,0,0,2/72,0,2/72,0,2/72,0,1/72,2/72,4/72,7/72,21/72,29/72]

The Testing Result for Yahoo:

Model and Testing / Page Number / Query	Markov Chain Model	Volcano	Tibetan Girl	Desert Camel Shadow
1	20	19	20	19
2	20	19	20	19
3	20	18	20	18
4	20	10	20	19
5	20	17	20	19
6	20	17	20	17
7	20	16	20	16
8	20	20	20	17
9	20	20	20	17
10	20	15	20	18

Appendix 3: The Searching Result for All Queries in Msn

Query / Number of Relevant Images / Page Number	Apple	Dolphin	Octopus	Facebook	Roxy	Wildlife
1	5	20	19	18	20	20
2	5	17	19	17	18	19
3	4	18	18	18	18	19
4	2	16	17	17	17	18
5	4	14	18	17	18	16
6	4	11	16	15	17	15
7	8	10	16	18	16	13
8	3	8	15	18	14	15
9	5	7	15	18	14	15
10	6	11	13	17	14	14
	Apple Computer	Plane Crash	Octopus Card	Outer Space	Night Scene	Daisy Flower
1	19	17	18	16	19	17
2	17	17	14	13	16	16
3	18	17	6	11	17	15
4	17	16	11	8	16	16
5	16	16	9	11	15	13
6	15	15	6	5	16	13
7	14	17	8	4	16	12
8	16	12	8	1	12	10
9	12	18	6	7	14	9
10	12	16	5	7	15	9
	Man Wearing Hat	Macro Fly Eyes	Sunrise and Sunset	Jordan Basketball Nike	Black and White Portrait	HK Night Scene
1	18	15	19	12	18	18
2	17	12	19	9	14	17
3	16	14	16	4	13	16
4	14	13	19	2	10	14
5	15	16	16	7	4	15
6	15	15	16	1	7	15
7	13	11	17	1	7	13
8	11	14	17	7	0	11
9	6	11	19	1	0	6
10	10	12	20	0	0	10

Query / Number of Relevant Images / Page Number	Starbucks	Skiing	Alleyway	Maldives	Puppy	Twilight
1	20	19	19	20	18	19
2	17	20	17	20	16	18
3	17	20	16	19	14	18
4	16	19	16	20	15	15
5	17	19	13	15	13	17
6	16	19	14	17	17	19
7	14	19	14	18	13	14
8	17	15	12	17	14	13
9	16	18	14	17	12	12
10	16	19	11	16	15	14
	Macro Abstract	Street-art	Baby Cry	Afghan Child	Twin Towers	Toilet Icon
1	18	20	7	19	20	0
2	18	20	5	17	17	1
3	16	19	3	15	18	1
4	16	17	3	15	17	0
5	15	16	3	11	15	2
6	14	16	2	10	14	1
7	16	15	1	10	16	0
8	18	15	2	10	14	3
9	15	12	1	10	10	1
10	16	16	2	6	16	1
	Eagle Catching Fish	Blowing in the Wind	Michael Schumacher Ferrari	Chinese Opera Mask	Victoria Harbour Hong Kong	Star Wars and Pepsi
1	20	18	20	20	13	20
2	18	17	20	17	12	18
3	16	16	18	18	11	18
4	15	12	20	14	9	19
5	12	8	20	13	12	18
6	11	13	20	7	17	18
7	10	10	20	10	15	16
8	8	9	20	11	13	14
9	7	8	18	7	9	12
10	9	7	20	10	17	12

Query / Number of Relevant Image / Page Number	Headphone	Gundam	Yelling	Transformers	Chair	Scrat
1	20	20	19	17	20	20
2	18	20	19	19	20	19
3	20	20	18	20	18	19
4	20	19	15	19	20	19
5	18	20	17	19	20	18
6	20	20	17	20	20	19
7	20	20	16	20	20	19
8	17	20	16	20	19	17
9	16	20	17	20	20	17
10	17	20	17	20	19	15
	Kiehl's Lotion	Colorful Candy	Jennifer Aniston	Doraemon Figure	Yoga Poses	Amazon Rainforest
1	19	15	19	19	20	20
2	19	15	20	17	20	20
3	18	12	19	16	19	20
4	17	8	20	14	17	19
5	18	8	20	11	18	18
6	16	9	20	13	19	20
7	15	6	20	5	15	20
8	13	6	20	5	15	18
9	13	7	20	2	18	18
10	12	8	20	2	15	19
	Great White Shark	Rock n Roll	Heart Shaped Cookies	Drink Vending Machine	Butterfly on Yellow Flower	Lily of the Valley
1	20	20	17	19	15	13
2	19	20	17	19	8	10
3	19	20	17	15	6	13
4	18	20	15	20	6	14
5	16	20	14	19	6	9
6	18	20	16	16	6	11
7	17	20	15	17	6	8
8	18	18	16	18	4	12
9	17	20	15	17	2	10
10	18	19	9	16	4	6

Query / Number of Relevant Images / Page Number	Tornado	Tired	Fisheye	Windmill	Steak	Piano
1	18	19	20	18	19	17
2	18	17	20	18	20	17
3	14	17	19	18	20	17
4	12	16	19	18	16	17
5	13	17	19	18	19	14
6	13	17	20	18	18	17
7	10	17	19	16	18	17
8	13	15	17	16	17	15
9	13	16	18	16	18	17
10	10	15	18	20	16	15
	Outdoor Wedding	Dior Catwalk	BMW Z4	African Art	Solar Eclipse	Icy Tree
1	19	17	20	20	16	19
2	18	19	20	20	12	18
3	19	16	20	19	15	16
4	20	18	20	19	14	14
5	18	19	20	20	13	17
6	18	19	20	19	10	16
7	18	18	20	20	11	18
8	15	15	19	17	8	17
9	17	17	20	19	12	17
10	13	14	20	20	11	12
	Bee on Sunflower	Sailing on San Francisco Bay	Front View of Garden Cottage	Couple in Beach Chairs	Pink Room Design	Messy Working Desk
1	20	17	16	9	11	20
2	19	15	16	6	10	18
3	20	16	15	5	8	17
4	17	17	14	3	9	10
5	16	19	16	4	3	13
6	17	17	15	4	4	12
7	16	17	12	2	2	9
8	18	18	14	1	4	8
9	16	15	14	1	6	8
10	13	17	12	2	3	5

Appendix 3: Msn Transition Probability Matrix

Number of Relevant Images	0	1	2	3	4	5	6	7	8	9	10	11	12	13	14	15	16	17	18	19	20
0	0.4	0.2	0.2	0.2	0	0	0	0	0	0	0	0	0	0	0	0	0	0	0	0	0
1	0.25	0.3333	0.25	0	0	0	0	0.1667	0	0	0	0	0	0	0	0	0	0	0	0	0
2	0	0.4444	0.1111	0	0.3333	0	0	0.1111	0	0	0	0	0	0	0	0	0	0	0	0	0
3	0	0.1429	0.1429	0.2857	0.2857	0.1429	0	0	0	0	0	0	0	0	0	0	0	0	0	0	0
4	0	0.0833	0.4167	0	0.1667	0	0.1667	0.0833	0.0833	0	0	0	0	0	0	0	0	0	0	0	0
5	0	0	0.1429	0.2857	0.2857	0.2857	0	0	0	0	0	0	0	0	0	0	0	0	0	0	0
6	7	8	9	10	11	12	13	14	15	16	17	18	19	20	21	22	23	24	25	26	27
7	0.0909	0.1818	0	0	0	0.0909	0	0.1818	0.0909	0.0909	0.1818	0.0909	0	0	0	0	0	0	0	0	0
8	0	0	0	0.0625	0	0.0625	0.125	0.1875	0.1875	0.125	0	0.0625	0.125	0.0625	0	0	0	0	0	0	0
9	0	0	0	0.0909	0.0909	0	0.2727	0	0.1818	0.0909	0	0.0909	0.0909	0	0	0	0	0.0909	0	0	0
10	0	0	0	0	0.0588	0	0.1176	0	0.1765	0.1176	0.1765	0.1176	0	0.1765	0	0	0.0588	0	0	0	0
11	0	0	0	0	0	0.0667	0.0667	0.0667	0.2	0.1333	0.2667	0	0.0667	0.0667	0.0667	0	0	0	0	0	0
12	0	0	0	0	0	0	0	0	0.0952	0.0952	0.0952	0.1429	0.0476	0.0476	0.2381	0.0952	0.0476	0.0476	0.0476	0	0
13	0	0	0	0	0	0.037	0	0.037	0	0.037	0.2222	0.0741	0.2222	0.1481	0.1111	0.037	0.037	0.037	0	0	0
14	0	0	0	0	0	0	0.0313	0	0	0.0313	0.0313	0.125	0.1563	0.1563	0.125	0.0938	0.1563	0.0938	0	0	0
15	0	0	0	0	0	0	0	0	0.0208	0.0208	0	0.0417	0.1042	0.125	0.1458	0.1458	0.1458	0.1667	0.0625	0	0.0208
16	0	0	0	0	0	0	0	0	0	0	0	0	0.0625	0.0625	0.1406	0.2656	0.1875	0.1563	0.0781	0.0313	0.0156
17	0	0	0	0	0	0	0	0	0	0	0.0123	0	0.0247	0.0247	0.0247	0.1235	0.2593	0.2469	0.2099	0.0741	0
18	0	0	0	0	0	0	0	0	0	0	0	0	0	0	0.0533	0.0933	0.2133	0.24	0.2	0.1067	0.0933
19	0	0	0	0	0	0	0	0	0	0	0	0	0	0	0.0145	0.0435	0.087	0.1304	0.2174	0.2609	0.2464
20	0	0	0	0	0	0	0	0	0	0	0	0	0	0	0	0.0108	0.0108	0.0753	0.129	0.2258	0.5484

Appendix 3: The table below shows us that the number of relevant images for Sixteen Pages. The result shows us the probability and index, which get from the program we have done with Matlab.

Page Number	Probability	Index	Number of Relevant Images
1	0.3194	21.0000	20
2	0.2500	21.0000	20
3	0.1927	21.0000	20
4	0.1527	21.0000	20
5	0.1304	18.0000	18
6	0.1245	18.0000	18
7	0.1179	18.0000	18
8	0.1114	18.0000	18
9	0.1051	18.0000	18
10	0.0992	18.0000	18
11	0.0937	18.0000	18
12	0.0886	18.0000	18
13	0.0839	18.0000	18
14	0.0796	18.0000	18
15	0.0757	18.0000	18
16	0.0720	18.0000	18

The Original Vector:

π (0)= [1/72,0,0,0,0,1/72,0,1/72,0,1/72,0,1/72,1/72,2/72,0,3/72,3/72,7/72,9/72,18/72,23/72]

The Testing Result for Msn:

Model and Testing / Page Number / Query	Markov Chain Model	Volcano	Tibetan Girl	Desert Camel Shadow
1	20	20	19	8
2	20	18	16	3
3	20	18	20	2
4	20	17	19	7
5	18	18	16	3
6	18	19	16	2
7	18	18	17	1
8	18	17	16	5
9	18	16	19	0
10	18	15	15	0

Patient Journey Optimization Using A Multi-Agent Approach

Chung Ho CHOI

Abstract

With the increasing expectation from patients and the regulations enacted by the government, exploring ways to shorten patient journey has caught increasing attention. Patient journey optimization typically involves treatment operation scheduling at multiple medical units. The decentralized nature of the problem makes conventional centralized operation research methods inapplicable in general and motivates the use of the multi-agent approach. In this paper, we focus on cancer patient treatment. We model patients and medical units as autonomous agents which interact locally via a bidding process and a coordination process for patient journey optimization. With reference to a dataset containing more than five thousand different cancer patient journeys, the effectiveness of the proposed algorithm under different settings of implementation has been experimentally evaluated via experimental simulations.

1 Introduction

Shortening the length of patient journey is always an expectation of patients. Also, it is one of the vital key performance indicators for evaluating the effectiveness of healthcare service providers. In order to best utilize the existing resources to raise healthcare service level, careful application of scheduling algorithms is crucial [7]. While conventional operations research methods have been found effective for scheduling related problems found in different medical units [8, 9, 4], most of them take the centralized approach and are not designed to be applied to decentralized situations where multiple resources at multiple hospitals are to be coordinated [5, 7, 2].

The multi-agent approach is characterized by emphasizing on local interaction and self-organization of different entities being modeled. These properties make it especially suitable for tackling complex tasks with a lot of stakeholders [11, 1]. Multi-agent methods have found applications in a variety of problem domains, such as airport resource scheduling [3], load allocation in transportation logistics [6], supply chain management [10], etc. Recently, it has also been applied to patient scheduling in [5, 7] with some initial success demonstrated. And yet, there are limitations. Paulussen *et al.*, in [5], assume that a quantified health state can be accurately derived as a utility measure for guiding the scheduling process. In [7], Vermeulen *et al.* did not consider the temporal constraints between the treatment operations during the scheduling process.

In this paper, we focus on the problem of improving the healthcare experience of cancer patients by optimizing their patient journeys. It is common that many developed cities have established a number of cancer centers to pool up resources for best utilization and yet to ensure that the centers are properly located to cater for the needs in different regions of the cities. However, the geographical distribution of the patient demand is dynamic in general and hard to be accurately predicted at different time points. The objective of this study is to explore the extent to which patient journey can be improved by better coordinating and mobilizing resources distributed at different cancer centers. In particular, we formulate the problem based on the healthcare system for cancer treatment in Hong Kong. We propose the use of a multi-agent approach where each patient and each unit of resources are modeled as autonomous agents which can interact with others to arrive an effective overall schedule with reduced amount of patient waiting times. To evaluate the effectiveness of the proposed approach, we made use of a patient identity anonymized data set collected by Hospital Authority in Hong Kong which contains 5819 cancer patients with an admission period spanning over 6 months, and have carried out simulations with the proposed approach given different settings of the environment.

The rest of the paper is organized as follows. The patient scheduling problem formulation is described in Section 2. Section 3 and Section 4 present the details of the proposed agent-based scheduling algorithm. Section 5 presents some preliminary experimental results and Section 6 concludes the paper.

2 PROBLEM FORMULATION

In this section, we first briefly describe the establishment of the cancer centers in Hong Kong. Then, we formulate the patient scheduling problem for cancer treatment as an optimization problem and explain how a particular multi-

agent approach can be adopted to address the distributed nature of the problem.

2.1 Cancer Patient Treatment - A Hong Kong Scenario

In Hong Kong, there are seven cancer centers. Figure 1 shows the geographical distribution of the seven cancer centers in Hong Kong. With the objective not to reveal the performance of individual centers, we denote the set of the seven centers as $\mathcal{C} = \{\mathcal{C}_1, \mathcal{C}_2, ..., \mathcal{C}_7\}$. Currently, these cancer centers are essentially managed by themselves at the operational level. That is, on-demand information exchange among the centers for scheduling patients is not yet extensively used. That is why it is common for cancer patients to be scheduled for receiving a series of treatments all at only one cancer center, even though the same or some of them could be provided significantly earlier by other centers.

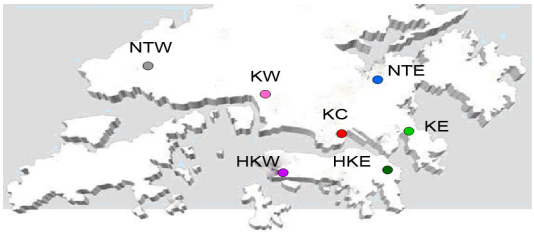

Figure 1. Seven geographically distributed cancer centers in Hong Kong.

Generally speaking, for any patient admitted to a hospital (cancer center), he or she first consults a medical doctor for diagnosis. Once the case is suspected to be cancer, the doctor will specify the patient a treatment plan which contains a sequence of treatment operations. For the application domain being chosen, we denote the set of treatment operations as $\Gamma = \{$radiotherapy planning, radiotherapy, surgery, chemotherapy$\}$.

To carry out the treatment operations, medical resources are needed. As resources are usually limited, related scheduling and allocation are by no means trivial. We denote the set of medical resources (or units) for our domain as $A = \{$radiotherapy planning unit, radiotherapy unit, operation unit, chemotherapy unit$\}$. We assume that one treatment operation can only be performed at one medical unit of the corresponding type. A patient journey is defined as the duration from the date of admission to the date of the last treatment operation completed. The goal of this work is to shorten the patient journey as far as possible.

2.2 Formulation

Let $K := A \times \mathcal{C}$ be the cartesian product of A and $\mathcal{C}$ giving the complete set of medical units, $M := K \rightarrow \Gamma$ be an one-to-one mapping between K and Γ specifying the treatment type of the medical units, and P be the set of cancer patients being scheduled.

Also, given a patient i, let N_Γ^i denote the number of treatment operations needed, D_0^i denote the admission date, D_j^i denote the date of the j^{th} treatment operation where $1 \leq j \leq N_\Gamma^i$, $V_j^i \in K$ be the unit at which the j^{th} treatment operation is performed, $Tr_j^i \in \Gamma$ be the type of treatment for the j^{th} operation, C_k be the daily capacity (i.e., the maximum number of patients that could be treated) of medical unit $k \in K$, T_t be the duration (in days) of treatment type $t \in \Gamma$, and Z be the set of dates on which patient scheduling is being considered.

With the assumption that all the patients are being treated equally in terms of urgency, the scheduling problem can be formulated as:

$$\min_D \sum_{i=1}^{|P|} \sum_{j=1}^{N_\Gamma^i - 1} (|D_j^i - D_{j+1}^i|) \tag{1}$$

with the following constraints to be satisfied:

$$D_{j+1}^i > D_j^i + T_{Tr_j^i} \tag{2}$$

$$\forall d \in Z \quad \left|\{i : D_j^i = d \wedge V_j^i = k\}\right| \leq C_k \tag{3}$$

$$Tr_j^i = M(k) \tag{4}$$

$$D_j^i > D_0^i > 0. \tag{5}$$

The objective function in (1) is to minimize the time lags between treatment operations for cancer patients. Constraint (2) ensures the temporal constraints between treatment operations are not violated, constraint (3) is used to ensure all medical units are operating within their capacities. Constraint (4) ensures that only the right kind of treatments are assigned to each medical unit. Constraint (5) ensures that patients would only be scheduled to receive treatment operations after their admissions.

3 SCHEDULING FRAMEWORK

Theoretically, patient journeys "travelling" possibly different centers could be scheduled by directly optimizing the criterion function (1). However, it is impractical to do so as it is hard to assume that a cancer center is willing to share its real-time resource allocation related data (e.g., C_k) with other centers due to both technical and managerial reasons. So, on one hand, the information sharing infrastructure across different information systems of different centers' medical units has to be ready. Also, each medical unit

is used to be managed by its own staff using its own information system for resource allocation. Having the patient scheduling at different medical units to be effectively coordinated to optimize the patient journey experience poses challenges on how the resource should be managed accordingly even within a hospital, let alone crossing all the hospitals.

In this section, we argue that the use of the multi-agent approach which tries to model each stakeholder as an autonomous agent and allows only local interactions among the agents is particularly suitable for our application. It aims to minimize the information sharing requirement among the hospitals and yet to obtain a good enough suboptimal result for the (global) patient journey optimization. In our proposed framework, there are *patient agents* and *resource agents*. They interact via some designed protocol for achieving the aforementioned optimization.

3.1 Patient Agent

A patient agent is used to represent one cancer patient and is denoted as P_i with $i = 1, 2, ..., |P|$. It stores the patient's treatment plan. As it is common that some treatment operations have to be performed in prior to the others, the set of treatment operations to be received by a patient has to be ordered to satisfy certain temporal constraints. Hence, each patient agent P_i maintains an ordered set $Tr^i = \{Tr^i_1, Tr^i_2, ...Tr^i_{N^i_\Gamma}\}$ as its treatment plan.

3.2 Resource Agent

A resource agent is used to manage a specific medical unit. Here, we denote R_{ab} as a resource agent representing medical unit $a \in A$ at cancer center $b \in \mathcal{C}$. Each resource agent has full access to the schedule of the medical unit it represents, but not those of the others.

3.3 Scheduling Algorithm

We adopt a two-phases scheduling algorithm similar to what being proposed in [5, 7]. For each newly admitted patient, a treatment plan is first designed and then the corresponding treatment operations are initially scheduled with the temporal constraints of the operations and the unit capacity taken into account (initial assignment phase). Then, a time-slot swapping process is enforced for further enhancement in patient journey quality (rescheduling phase). Here we assume that two patient agents with their treatment plans containing operations of the same type but scheduled at different time are willing to be matched by resource agents and to exchange the corresponding timeslots as far as none of their schedules is worsen (as suggested in [7]) and none of the temporal constraints as specified in (2) are violated.[1] Algorithm 1 gives a high-level description of this two-phases scheduling algorithm.

Algorithm 1 Scheduling Algorithm

```
for every patient agent P_i do
    Initial assignment based on P_i's treatment plan
    for each P_i's treatment operation do
        Rescheduled to be performed earlier by exchanging timeslot with another patient agent with the help of the resource agent (rescheduling phase)
        if No involving parties are worsened in terms of their resulting overall schedules then
            The exchanging process is proceeded
        end if
    end for
end for
```

4 AGENT COORDINATION

In this section, more details about the scheduling algorithm are given, including (1) how the patient agents interact with the resource agents to establish candidate patient agent pairs for timeslot swapping consideration, and (2) how some "unnecessary" swappings can be rejected so as to further improve the scheduling optimality.

4.1 A bidding process for agent matchmaking

Figure 2 shows our proposed framework. As what have been introduced in Sections 3.1 and 3.2, there are two types of agents, namely patient agents and resource agents. In order to show clearly the coordination between agents, we further categorize patient agents during a matchmaking process into *initiating patient agents* and *target patient agents*. Initiating patient agents P_I are those patient agents who initiate a request for timeslot exchange. Target patient agents P_G are the others who are willing to participate in the exchanging process.

With the objective to shorten its patient journey, an initiating patient agent P_I first sends out a request of rescheduling one of the treatment operations to the corresponding resource agents R_{ab}. The request includes the earliest possible start date (*EPS*) and the latest possible start date (*LPS*) of its associated treatment operation. In order not to violate the temporal constraints between treatment operations, the *EPS* can be defined as:

$$EPS^I_j = D^I_{j-1} + T_{Tr^I_{j-1}} + \delta_1. \quad (6)$$

[1] This assumption may imply that some policy-wise incentive to be in place so that different medical units are willing to share their resources in this manner, which however is not the main focus of our study.

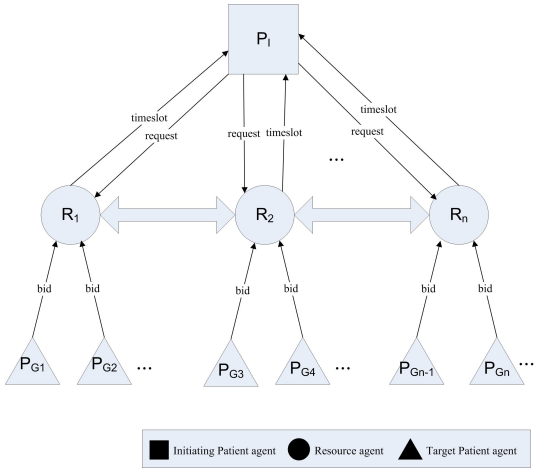

Figure 2. The proposed agent coordination framework for patient scheduling.

Note that δ_1 denotes how many days a patient should be admitted (if needed) before a treatment operation to be carried out. In our experiment, we set to be one. In practice, this value could be designated by healthcare providers in order to better suit their needs. With a similar argument, LPS is defined as:

$$LPS_j^I = D_j^I - 1. \quad (7)$$

Once a resource agent receives a request with EPS and LPS, it will first check whether there are available timeslots released by ceased patients which can fulfill the request. If yes, the released timeslot will be assigned to the initiating patient agent. If not, the resource agent will then pass the request to those patient agents (target patient agents, P_G) which reserved resources of the same type in the period from EPS to LPS. Those target patient agents who have received the request will submit a bid to the resource agent in response.

There are several factors needed to be considered in computing the bid value.

- First, the target patient agent should not have its last operation in its treatment plan to be exchanged, or its last operation has then to be performed later and thus it would end up with a lengthened journey.

- Second, as it is impractical to reschedule a patient's treatment operation without prior notification, we assume that the exchange of timeslots would not be considered if the initiating patient will have less than a week's time of notification.[2]

[2]In general, the time of notification can be adjusted according to the real situation.

- Third, the target patient agent also has to ensure that the temporal constraints between its treatment operations would not be violated after the exchanging process.

Taking into account the above considerations, the bid value submitted by a target patient agent P_G with its j_tth operation that matches with the j_ith operation of the initiating agent P_I as specified in the request (that is $Tr_{j_t}^G = Tr_{j_i}^I$) is formulated as:

$$Bid^G = (D_{j_t}^G - EPS_{j_i}^I) + Last + Noti + Temp, \quad (8)$$

where $Last$, $Noti$ and $Temp$ are three binary variables. $Last = 0$ if the j_tth operation is not the last one for P_G, or ∞ otherwise. $Noti = 0$ if a week's time of notification for the target patient agent to be notified, or ∞ otherwise. $Temp = 0$ if there are no temporal constraints violated, or ∞ otherwise.

Among all the target patient agents, the one with the lowest bid value will be accepted and the timeslot swapping between the initiating agent and target one will be confirmed. If two bids are found to be numerically identical, the resource agent will select one at random.

4.2 A coordination process for rejecting unnecessary swappings

A timeslot swapping confirmed as described in the previous section sometimes does not necessarily lead to ultimate improvement in patient journey. To illustrate that, suppose there is a patient agent with 3 treatment operations to be rescheduled. In case the last treatment operation could not be rescheduled to be performed earlier, any rescheduling of the first 2 treatment operations are essentially useless as the duration of the whole journey remains unchanged (see Figure 3(a)). As another example, even a shortened patient journey can be achieved, rescheduling of the first 2 treatment operations could also be useless if the rescheduling of the last treatment operation cannot be benefited from the rescheduling of the first two (see Figure 3(b)).

In order that these useless swappings can be rejected so as to be reserved for other potentially more useful swappings, the scheduling algorithm could be modified in such a way that a resource agent after identifying the most optimal bid among the target patient agents will not notify the initiating patient agent immediately. Instead, it will pass the bid to the resource agent which is responsible for the succeeding treatment operation of the initiating patient agent. Having received such a bid, the resource agent could derive a new EPS, denoted as ${}^{(new)}EPS_{j_i+1}^I$. Clearly, unnecessary swappings occur if that resource agent could not find a bid among those received from the target patient agent P_G such that ${}^{(new)}EPS_{j_i+1}^I \leq D_{j_t'}^G \leq EPS_{j_i+1}^I$, where

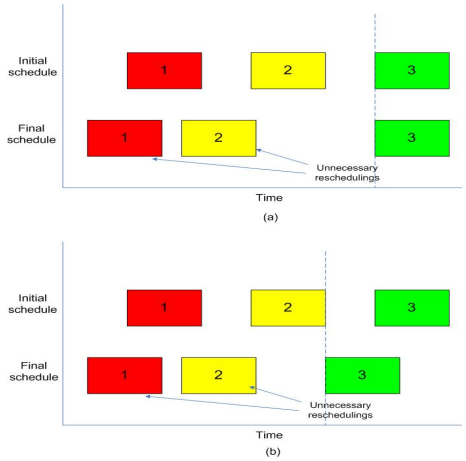

Figure 3. Unnecessary reschedulings.

$Tr^I_{j_i+1} = Tr^G_{j'_t}$. In that case, the resource agent will notify its antecedent to discard the bid such that the corresponding timeslots would not be exchanged. In general, such a succeeding resource agent consultation process can be carried out in a recursive manner.

5 EXPERIMENTAL VALIDATION

To evaluate the effectiveness of the proposed multi-agent approach, we first obtained a dataset containing the scheduled treatment plans of 5819 cancer patients being treated at the seven cancer centers in Hong Kong within an admission period of 6 months (from 1/7/2007 to 31/12/2007). The average length of the patient journey among all cancer centers is 90.7 days. Based on the dataset, we have carried two groups of experimental simulations.

For the first group of simulations, we made use of the scheduled treatment plans in the dataset for the initial assignment and studied to what extent the multi-agent approach can improve the patient journey as a whole. As only swappings and taking timeslots of ceased patients were allowed in our simulations, the capacity requirement is essentially equivalent to that of the original data.

For the second group of simulations, we aim to make the simulation setting more flexible by making use of only the statistics of the scheduled treatment plans and the capacity of the medical units allocated as revealed in the dataset. The initial assignment strategy and the rescheduling strategy can both be specified by the user for evaluation. Also, we tried to increase the capacity value as revealed in the dataset by percentage so as to see to what extent the patient journey can be improved with more resources injected.

5.1 Simulations with initial assignment and unit capacity fixed

Four different settings have been tested so as to demonstrate various aspects of the proposed algorithm. They include

Setting 1: Any patient agent is willing to explore the possibility to swap some or all of its treatment operation schedule with others'.

Setting 2: It is assumed that only 20% of the patients of each center are allowed to undergo timeslot swapping.

Setting 3: It is assumed that patients are reluctant to travel for a long distance even though some of their operations can be scheduled earlier, and thus only swappings between two nearby cancer centers are allowed. In particular, the neighborhood relationships are assumed to be

- $C_1 \rightarrow C_2$ or C_3
- $C_2 \rightarrow C_1$ or C_3
- $C_3 \rightarrow C_1$ or C_2 or C_4 or C_5 or C_6
- $C_4 \rightarrow C_3$ or C_6
- $C_5 \rightarrow C_3$ or C_7
- $C_6 \rightarrow C_3$ or C_4
- $C_7 \rightarrow C_5$

where $\alpha \rightarrow \beta$ implies that patients admitted in cancer center α would only be swapped to its neighboring cancer center β.

Setting 4: Timeslots released by ceased patients are allocated to the patient agents who have the longest patient journeys at a time point.

Figure 4a shows the average length of the patient journeys associated with the seven cancer centers in Hong Kong obtained given the four aforementioned settings.

The experimental results obtained shows that, on average, the average length of journey could be reduced by 9.8 days for those 5819 cancer patients if no restriction is imposed on the exchange of timeslots whenever there is a Pareto improvement (Setting 1). Given only 20% of patients per center are allowed for timeslot exchange (Setting 2), it is found that the average length of journey could still be reduced by an average of 6.1 days. This observation is interesting as even a small percentage of resources being released by each center could already achieve a significant improvement. With the geographical restriction on allowing only swappings between nearby centers as described in Setting 3, the average length of journey can also be reduced by 9.3 days.

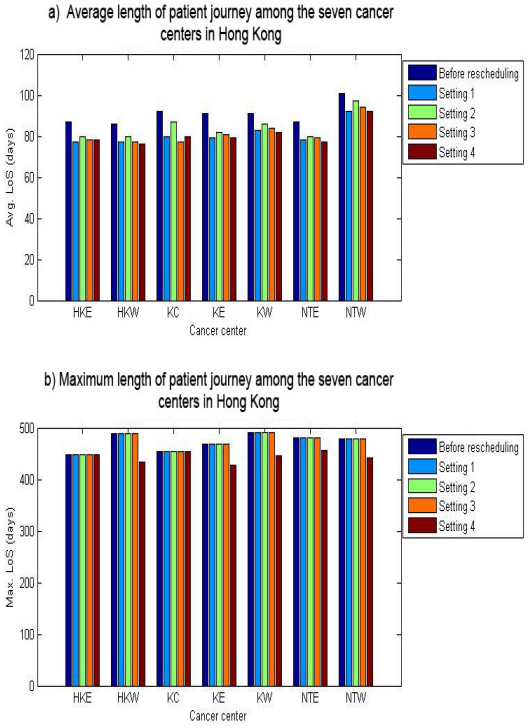

Figure 4. a) Average length of patient journey; b) Maximum length of patient journey among the seven cancer centers in Hong Kong under 4 different experiment settings.

However, it should also be noted that according to Figure 4b, the maximum length of journey remains unchanged. The reason is obvious as no one is willing to swap with those with the longest length of journey and the last day of the treatment to be the end of the period being considered. Improvement on reduction on maximum length of journey can only be observed for Setting 4 where the released timeslots due to ceased patients are allocated to those with long length of journey.

5.2 Simulations revealing the effects of varying initial assignment and unit capacity

Contrary to the group of simulations previously presented, we tried to simulate also the initial assignment process using again the treatment plan of the 5819 cancer patients. However, all the treatment operations were not scheduled according to the data but simulated based on the statistics of the inter-operation duration obtained from the dataset. In particular, during the initial assignment phase, patient agents would be assigned an initial schedule one by one based on their admission orders. For each treatment operation, each patient agent would be assigned with the next earliest available timeslot. However, it is obvious that there should be a minimum time lag between two subsequent treatment operations due to different medical reasons. We first used the average inter-operation duration computed based on the dataset to set the related parameters as shown in Table 1 and then performed the simulation. The average length of journey computed right after the initial assignment is found to be 83.3 days. Figure 5 shows that the improvements obtained due to the different settings are not very much different from those obtained in the previous section.

Table 1. Average time lags between treatment operations (RTP - Radiotherapy planning; RT - Radiotherapy; OT - Operation; CHEM - Chemotherapy).

Antecedent treatment operation (A)	Subsequent treatment operation(S)	Average time lag (days) between the start date of (A) and (S)
RTP	RT	21
RTP	OT	44
RTP	CHEM	23
RT	OT	94
RT	CHEM	39
RT	RTP	27
OT	RTP	55
OT	RT	67
OT	CHEM	54
CHEM	RTP	104
CHEM	RT	56
CHEM	OT	97

According to the dataset, the minimum days between any two treatment operations was found to be one only. This implies that treatment operation sometimes could be started one day after another if the resource is available. We have also tried to set the minimum days to be one in our initial assignment phase and compared the results obtained based on those presented in Table 1. By Figure 6, while we observed some improvements in performance, the enhancement however is not very significant. Hence, setting some reasonable time lags between treatment operations does not have too big an impact on lengthening too much the length of journey. Of course, there should always be medical reasons for setting a bigger minimum threshold.

For all the results presented so far, it is assumed that the capacity of each medical unit is fixed. To study the cost-effectiveness of increasing the units' capacities for patient journey optimization, we increased the capacity by the same percentage for all the medical units. According to Figure 7,

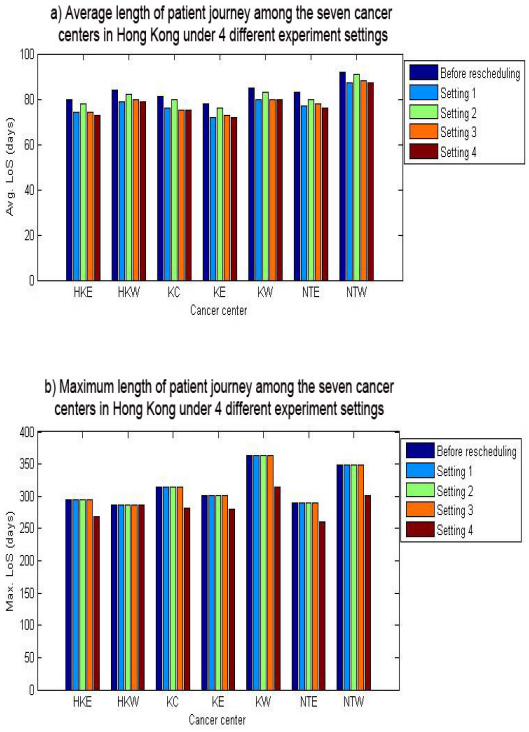

Figure 5. a) Average length of patient journey and; b) Maximum length of patient journey among the seven cancer centers in Hong Kong under 4 different experiment settings in Experiment B.

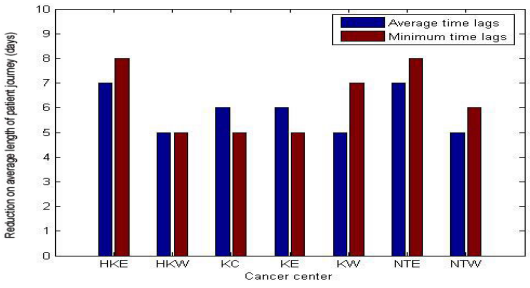

Figure 6. Reduction on average length of patient journey (Setting 4) by varying the time lags between treatment operations.

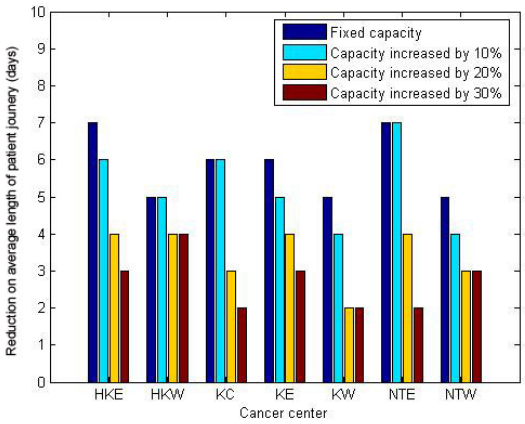

Figure 7. Reduction on average length of patient journey (Setting 4) by varying capacities.

it is found that when all the resource capacities are increased incrementally (10%, 20%, 30%), the reduction on average length of patient journey will then drop accordingly. In particular, it is found that a higher increase in capacities will cause a greater drop as a result. In fact, such drop could be attributed to the fact that when the resource capacities are increased, patients would then be scheduled with less idle times between treatment operations; and hence with less chance to exchange timeslots with others.

6 CONCLUSIONS

In this paper, a multi-agent approach was proposed for patient journey optimization. Particularly, by applying the approach, the shortening of the overall patient journey will not result in any single patient with its length of journey lengthened as a result. Also, all the temporal constraints among the treatment operations for each patient would not be violated during the scheduling process.

The effectiveness of the proposed approach has been demonstrated by applying it to a dataset containing 5819 scheduled treatment plans of cancer patients admitted to hospitals in Hong Kong. The effects of varying the initial assignment and the unit capacity on the overall reduction in length of patient journey are also studied.

Currently, since we are using a Pareto improvement approach, it is assumed that no single patient (agent) would get a lengthened schedule after swapping timeslots with another. In the future, we are going to see whether there would be a greater improvement in achieving a reduced overall length of patient journey when the above assumption is relaxed. In particular, we are going to see whether the bid as formulated in Section 4.1 could be defined in a more sophisticated way such that a greater reduction on length of patient journey could be achieved by the matchmaking process.

ACKNOWLEDGEMENT

This is to acknowledge Hong Kong Hospital Authority for providing the patient journey dataset to support this research study.

References

[1] H. Czap and M. Becker. Multi-agent systems and microeconomic theory: A negotiation approach to solve scheduling problems in high dynamic environments. In *HICSS '03: Proceedings of the 36th Annual Hawaii International Conference on System Sciences (HICSS'03) - Track 3*, page 83.2, Washington, DC, USA, 2003. IEEE Computer Society.

[2] K. Decker, J. Li, and Y. Demazeau. Coordinating mutually exclusive resources using gpgp. *Autonomous Agents and Multi-Agent Systems*, 3:200–0, 2000.

[3] X. Mao, A. Mors, N. Roos, and C. Witteveen. Coordinating competitive agents in dynamic airport resource scheduling. In *MATES '07: Proceedings of the 5th German conference on Multiagent System Technologies*, pages 133–144, Berlin, Heidelberg, 2007. Springer-Verlag.

[4] J. Patrick and M. Puterman. Reducing wait times through operations research: optimizing the use of surge capacity. *Healthc Q*, 11(3):77–83, 2008.

[5] T. O. Paulussen, I. S. Dept, K. S. Decker, A. Heinzl, and N. R. Jennings. Distributed patient scheduling in hospitals. In *Coordination and Agent Technology in Value Networks. GITO*, pages 1224–1232. Morgan Kaufmann, 2003.

[6] V. Robu, H. Noot, H. La Poutré, and W.-J. van Schijndel. An interactive platform for auction-based allocation of loads in transportation logistics. In *AAMAS '08: Proceedings of the 7th international joint conference on Autonomous agents and multiagent systems*, pages 3–10, Richland, SC, 2008. International Foundation for Autonomous Agents and Multiagent Systems.

[7] I. Vermeulen, S. Bohte, K. Somefun, and H. La Poutre. Improving patient activity schedules by multi-agent pareto appointment exchanging. In *CEC-EEE '06: Proceedings of the The 8th IEEE International Conference on E-Commerce Technology and The 3rd IEEE International Conference on Enterprise Computing, E-Commerce, and E-Services*, page 9, Washington, DC, USA, 2006. IEEE Computer Society.

[8] J. Vissers and R. Beech. *Health operations management : patient flow logistics in health care*. Routledge, 2 Park Square, Milton Park, Abingdon, Oxon OX14 4RN, 2005.

[9] J. Vissers, J. Bekkers, and I. Adan. Patient mix optimization in tactical cardiothoracic surgery planning: a case study. *IMA Journal of Management Mathematics*, 16, 2005.

[10] M. Wang, J. Liu, H. Wang, W. K. Cheung, and X. Xie. On-demand e-supply chain integration: A multi-agent constraint-based approach. *Expert Systems with Applications*, 34(4):2683 – 2692, 2008.

[11] G. Weiss. *Multiagent systems : a modern approach to distributed artificial intelligence*. Cambridge, Mass. : MIT Press, 1999.

Commentary-based Video Categorization and Concept Discovery

Janice Kwan-Wai Leung

Abstract

Social network contents are not limited to text but also multimedia. Dailymotion, YouTube, and MySpace are examples of successful sites which allow users to share videos among themselves. Due to the huge amount of videos, grouping videos with similar contents together can help users to search videos more efficiently. Unlike the traditional approach to group videos into some predefined categories, we propose a novel comment-based matrix factorization technique to categorize videos and generate concept words to facilitate searching and indexing. Since the categorization is learnt from users feedback, it can accurately represent the user sentiment on the videos. Experiments conducted by using empirical data collected from YouTube shows the effectiveness of our proposed methodologies.

1 Introduction

Starting from last decade, World Wide Web is developed into the second generation Web 2.0. Thanks to this newest development, people can control over the data in the Internet instead of just retrieve data. Furthermore, it led to the evolution of web-based communities. Social networks such as forums, blogs, video sharing sites are examples of applications.

Recent years online video sharing systems are burgeoning. In video sharing sites, users are allowed to upload and share videos with other users. YouTube is one of the most successful and fast-growing systems. In YouTube, users can share their videos in various categories. Among these video categories, music is the most popular one and the number of music videos overly excess that of other categories [1, 7]. Users are not only allowed to upload videos but tag videos and leave comments on them as well. With more than 65,000 new videos being uploaded every day and 100 million video views daily, YouTube becomes a representative community among video sharing sites.

Due to the incredible growth of video sharing sites, video searching is no longer a easy task and more effort should be paid by users to search their desire videos from the entire video collection. To address this problem, grouping videos with similar contents together is necessary. Currently, videos on YouTube are only coarsely grouped into some predefined high level categories (e.g. music, entertainment, sports, etc). Videos in a single category still span through a wide range of varieties. For example, in the music category, we may find music from various countries or with different musical styles. Though some other video sharing sites, such as DailyMotion and MySpace, have a lower level of category for music videos, the categorizes just follow the basic music genre. However, people interests on music are not limited to these simple genre. Furthermore, the predefined categories maybe too subjective to capture the real interest of the majority of users since they are only defined by a small group of people. Finally, the current categories on YouTube are fixed and it is hard to add/remove categories too often. As time goes by, some categories may become obsolete and some new topics may be missing from the categories.

These observations motivate us to explore a new way of video categorization. In this work, we propose a novel comment-based clustering technique by utilizing user comments for achieving this goal. Unlike the traditional approaches of predefining some categories by human, our categorization is learnt from the user comment. The advantage of our proposed approach is three-fold. First, our approach can capture user interests more accurately and fairly than that of the predefined categories approach. The reason is that we have taken the user opinions into consideration. In other words, the resulting categories are contributed by public users rather than a small group of people; Second, since user interest can be changed from time to time, the categories of our method can be changed dynamically according to the recent comments by users; Finally, as users comments are in the form of natural language, users can describe their opinions in detailed. Therefore, by comment-based clustering, we can obtain clusters which represent fine-grained level ideas.

In the literature, various clustering techniques have been proposed for video categorization [5, 12]. However, this type of techniques did not take user opinion into consideration and thus the clustering results do not capture user interests. On the other hand, researchers have proposed to use the user tags on videos for clustering [6, 4]. Though

user tags can somehow reflect user feelings on videos, tags are, in many cases, too brief to represent the complex ideas of users and thus the resulting clusters may only carry high-level concepts. Another stream of works which use commonly fetched objects of users for clustering [2] also suffer similar shortcomings as tag-based clustering. In [11], they proposed to adopt a multi-modal approach for video categorization. However, their work required lots of human efforts to first identified different categories from a large amount of videos.

We want to remark that although comment-based clustering can theoretically obtain more fine-grained level clusters, it is much more technically challenging than that of tag-based clustering. The reason is that user comments are usually in the form of natural language and thus pre-processing is necessary for us to clean up the noisy data before using them for clustering.

The rest of the paper is organized as follows. Section 2 discusses previous works in the context of social network mining. Section 3 explains our proposed approach for video categorization in video sharing sites. Section 4 briefly introduces our web crawler. Section 5 presents the details of pre-processing of the raw data grabbed by our crawler. Section 6 describes our video clustering algorithm. Section 7 presents and discusses our experimental results. Section 8 concludes the paper.

2 Related Works

Since the late eighties, data mining has became a hot research field. Due to the advancing development of technologies, there is an increasing number of applications involving large amount of multimedia. For this reason, researches in the field of data mining are not limited to text mining but multimedia mining. Qsmar R. Zaine et al. [12] developed a multimedia data mining system prototype, MulitMediaMiner, for analyzing multimedia data. They proposed modules to classify and cluster images and videos based on the multimedia features, Internet domain of pares referencing the image of video, and HTML tags in the web pages. The multimedia features used include size of image or videos, width and height of frams, date on which the image or video was created, etc. S. Kotsiantis et al. [5] presented a work to discover relationships between multimedia objects based on the features of a multimedia document. In their work, features of videos such as color or grayscale histograms, pixel information, are used for mining the content of videos.

Motivated by the bloom of social networks, plenty of works have been done involving the study or analysis of online social networks. Different approaches are proposed to discover user interests and communities in social networks. Tag-based approach is one of the invented methods. In [6], Xin Li et al. developed a system to found common user interests, and clustered users and their saved URLs by different interest topics. They used the dataset from a URLs bookmarking and sharing site, del.icio.us. User interests discovery, and user and URLs clustering were done by using the tags users used to annotate the content of URLs. Another approach introduced to study user interests is user-centric which detects user interests based on the social connection among users. M. F. Schwartz et al. [8] discover people's interests and expertise by analyzing the social connections between people. A system, Vizster [3], was designed and developed to visualize online social networks. The job of clustering networks into communities was included in the system. For this task, Jeffrey and Danah identified group structures based on linkage. Except the use of sole tag-based or user-centric approaches, there are works done with a hybrid approach by combing the two methods. In [4], user interests in del.icio.us are modeled using the hybrid approach. Users are able to make friends with other users to form social ties in the URLs sharing network. Julia Stoyanovich et al. examined user interests by utilizing both the social ties and tags users used to annotate content of URLs. Some researchers proposed the object-centric approach for social interests detection. In this approach, user interests are determined with the analysis of commonly fetched objects in social communities. Figuring out common interests is also a useful task in peer-to-peer networks since shared interests facilitate the content locating of desire objects. Guo et al. [2] and K. Sripanidkulchai [9] presented in their works the algorithms of examining shared interests based on the common objects users requested and fetched in peer-to-peer systems.

3 Interest-based Video Categorization for Video Searching

With the ceaseless growth of media content, it is increasingly a tense problem for video searching. It is usual that users hardly find their desire videos from the immense amount of videos. There are two main directions to ease the process of video searching, one is enhancing the text-based search engine whilst the other one is designing a better directory. In this paper, we focus on the former approach.

Though many video sharing sites allowed tagging function for users to use tag to annotate videos during the upload process, it is very common for user to tag videos by some high level wordings. As such, tags are usually too brief for other users to locate the videos by using the text-based search engine. In our method, as user comments usually describe the video in details, we can use them for video clustering to obtain fine-grained categories. By identifying the concept words for each categories, we can use them as latent tags for the corresponding categories in order to facil-

itate the video searching process.

In music domain, music videos in sharing systems are always categorized according to their types of musical sounds (e.g. pop, metal, country, etc.) under the music genre. However, except music styles, people may have many different attitudes and preferences (e.g. appearance of singers, event of performance, age of songs, etc) towards music in different regions. Therefore, to categorize music based on people interests, music genre is not a good categorical construct for video searching.

Our aim is to find a categorization where videos in each video group are representing a popular topic of interest. In our algorithm, interests are modeled by clustering videos into groups with the utilization of user-left comments. Previously, computer scientists have tried many ways to find user interests. Tags are very popular to help in this context [6]. However, two disadvantages would be raised in this manner. First, tags on a video are manually given by the one who uploads the video, thus the tags are just expressing a single user's feeling about the video. Therefore, tags on a video would have a strong bias and are not fair enough to exactly describe what the video is actually about. Furthermore, single-user given tags are definitely not representative of public feelings about the video. Second, videos are often tagged with a small number of words. As such, often fails to give enough description on the video. Therefore, tags are insufficient to provide detailed information about videos. Since comments can be given by any users on any videos as feedbacks, they express different users thoughts about a video. Thus, containing more in-depth information about the videos. Also, allowing every user to leave feedbacks, the number of comments on a video are usually much more than that of tags. Hence, utilizing comments to find out interests instead of tags can solve the above difficulties.

Beside tag-based, some researchers proposed the content-based approach to categorize videos. Using video content as categorizing materials can group similar videos together according to their actual content. Nevertheless, video content itself only provide information about the videos but nothing about users' idea. Consequently, this approach fails to group videos according to user interests. In contrast, user-left comments include users' view about the videos. Therefore, comments can, undoubtedly, be used to categorize videos based on popular user interests.

Video features can also be used to achieve the goal of cluster videos [5]. Video features, however, are hard to be extracted automatically. Due to the limitation of human resources, automatic information retrieval from mass amount of data is preferred. Also, using video features to cluster videos suffers the same shortcomings of content-based as well. Because of information retrieval dealing with text is much easier than video features extraction, and comments, in addition to video content, provide users' views on videos, user-left comments are significant for clustering videos.

4 Data set collection

YouTube is a video sharing platform which users can upload their own videos for sharing purpose. Along with each video, a short description can be entered by the uploading user and also comments can be given by other registered users. In this paper, we focused on the user comments of music videos of Hong Kong singers in YouTube.

We first defined a set of 102 Hong Kong singer/group names. Given the set of singer/group names, we developed a crawler to firstly visit the YouTube web site and automatically searches from the site the related videos based on video titles and video descriptions. From the resulting videos, the crawler saves the URL of each videos for further process. For the convenience of gathering user comments, the crawler transforms the fetched URLs to links which link to the pages of "all comments" mode of corresponding videos. With all the transformed video URLs, for each link, the crawler is able to scrape the video web page and grab the video title, all the user comments and user name of who left comments on the video.

In the data set acquired by our crawler, there are 19305 videos, 102 singers and 7271 users in total.

5 Data Pre-processing

To ease the process of video searching by discovering the user interest and categorizing videos, larger amount of data is required from video sharing sites. However, just the large-sized collection of text-formatted raw data is not applicable for further processing. Large-sized dataset always need to undergo data pre-processing in the field of data mining. Here is no exception in our algorithm. After crawling YouTube, the mass data need to be pre-processed before performing video clustering.

Here are two steps of data pre-processing involved in our introduced algorithm,

1) Data Cleaning

2) Text Matrix Generation

5.1 Data Cleaning

As the comments left on YouTube videos are written in natural languages which consist lots of non-informative words, such as "thank" , "you", etc, text processing with such materials must be caution. To avoid resulting a poor clustering,data cleaning is necessary for handling the noisy words.

In natural languages, there are many words that are not informative for clustering. These words would make the

entire dataset very noisy. Applying a stoplist is one of the ways to clean up these words. Since some words are obviously not informative, it is easy to define a stoplist of noise. With a predefined stoplist non-informative or distractive words can be strained from the dataset. After removing all the useless words by the stoplist, the dataset is then passed to the process of matrix generation.

5.2 Text Matrix Generation

Text-formatted data is not easy for further processing, it is more convenient to transform the data from text to matrix representation beforehand.

For example, the dataset can be represented by matrix A of size $n \times m$ where n is number of videos in the dataset and m equals to number of unique case-insensitive words in the dataset. In A, each row is a vector of video words and element $a_{i,j}$ is the frequency count of word j occurs in comments left on video i.

A dictionary is firstly built with the case-insensitive words in all the comments in the dataset. As comments are all in texts, linguistically, there exist many meaningless words in comments. These meaningless words, e.g. "is", "am", "the", "a", always occur in an extremely high frequency. Therefore, words occur in frequency exceeding a threshold should be discarded. On the other hand, words that seldom occur are probably not important, so words with few occurrence should also be neglected. Therefore, we set an upper bound and a lower bound for word occurring frequency. All the words with frequency less than the lower bound or larger than the upper bound are filtered out. After filtering all the meaningless words, dictionary can then be built and matrix can be generated as well.

6 Popular Interests Discovery and Video Categorization via Clustering

In order to facilitate the video searching process, constructing a video category based on the user interests is crucial.

With the reason that users' interests are reflected from the comments they left on videos, grouping similarly commented videos together is a possible way to provide a good video categorization. Since the objective of clustering is to distinguish substantial amount of data and group similar objects together, clustering is an adequate algorithm for constructing a video category that can guide user to his/her desire videos.

Figure 1 shows the procedures of discovering popular interests and categorizing Hong Kong singer videos from YouTube.

6.1 Video Clustering

For our purpose of building a good video category for easier video searching, Non-negative Matrix Factorization (NMF) is the chosen clustering algorithm [10]. We propose to apply NMF for clustering based on three reasons. First of all, NMF is a bi-clustering method. With a bi-clustering algorithm, comment words and videos can be clustered simultaneously. Thus, the main characteristics of video groups can be drawn while grouping videos with similar user views together. Additionally, NMF does not provide an absolute assignment of videos to groups. Absolute assignment clustering algorithms are not suitable for singer video clustering. In practice, a video can belongs to multiple groups. For example, a classic music video can be performed by a singer who is passed away. The video is said to be in both "classic" group and "died singer" group. As NMF calculates possibility coefficients of each video to different groups, a single video can be assigned videos to multiple groups. Finally, NMF is effective for clustering. Since we need to cluster a large amount of data, effectiveness is one of the concerns. An effective low-dimensional linear factor model is desired.

Comments on a video often capture users feelings about the video or describe the video. Videos are clustered into the same group if they bear comments with similar contents. Similar videos, therefore, can be grouped together and with their characteristics be revealed as popular user-interests.

Let A be the $n \times m$ video-word matrix generated in the process of data pre-processing, where n and m are the number videos and number of words in dictionary respectively. As all the elements in A are the occurrence counts of words in documents, they are greater or equal to zero. This makes matrix A a non-negative matrix.

Since the importance of a term to a document can be reflected by it's number of appearance, the well-known keyword measure in Information Retrieval $tf - idf$ is adopted for extracting important words. Within the dataset, all the comments of a video is aggregated and considered as a document. Importance of term i in document j is $w_{i,j}$ which is computed by using $tf_{i,j}$ (term frequency of term i in document j) and idf_i (inverse document frequency of term i). Terms that are important to a document are expected to appear many times in the document. For this reason, the term frequency is used to measure the normalized frequency of a term in a document. Suppose there are t distinct terms in document j, $tf_{i,j}$ can be computed as,

$$tf_{i,j} = \frac{f_{i,j}}{\sqrt{\sum_{k=1}^{t} f_{k,j}^2}} \quad (1)$$

where $f_{i,j}$ is the number of times that term i appears in document j. As words appear in many documents are not useful for distinguishing documents, a measure idf is used

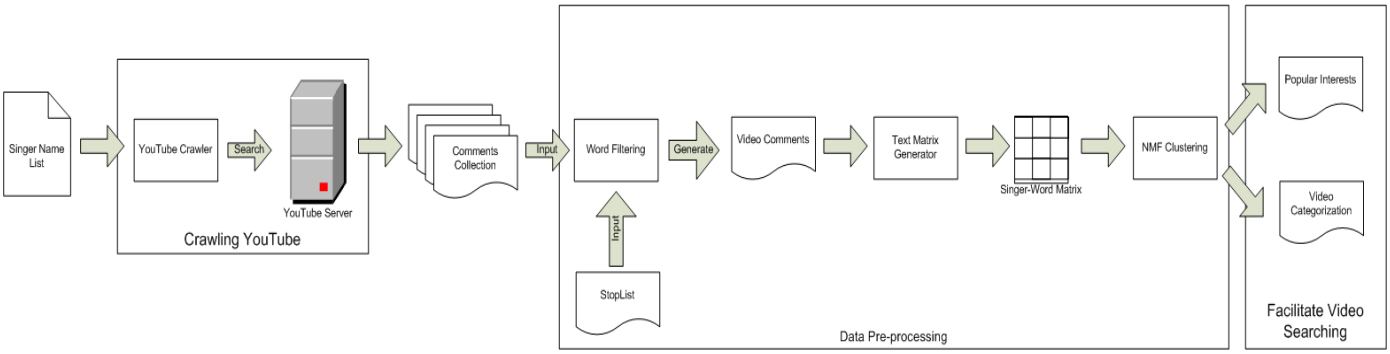

Figure 1. Popular interests discovery and video categorization of Hong Kong singer videos in YouTube

.

to scale down the importance of these widely-used terms. The inverse document frequency of term i is defined as,

$$idf_i = log\frac{N}{n_i} \tag{2}$$

where N is the total number documents in the dataset, and n_i is number of documents that containing term i.

After computing the term frequency and inverse document frequency, the importance weight of a term i in document j is defined as the combination of $tf_{i,j}$ and idf_i,

$$w_{i,j} = tf_{i,j} \times idf_i \tag{3}$$

The greater the weighting, the more the important is the term to the respecting document.

From matrix A, a non-negative matrix X can be produced by calculating the importance weights. Each element in X is defined as,

$$x_{i,j} = w_{i,j} = \frac{a_{i,j}}{\sqrt{\sum_{k=1}^{t} a_{k,j}^2}} \times log\frac{N}{n_i} \tag{4}$$

By fitting a k-factor model to matrix X, where k equals to number of groups to be obtained, X is decomposed to two non-negative matrices W and H, such that $X = WH + U$. After matrix decomposition, W is in size of $n \times k$ and H is in size of $k \times m$.

Our objective is to find W and H such that $X \approx WH$. By iteratively updating W and H, we can obtain W and H by minimizing the following function,

$$F(W, H) = ||X - WH||^2 \tag{5}$$

with respect to W and H and subject to constraints that $W, H \geq 0$.

Figure 2 shows the decomposition of video dataset matrix. From the resulting matrices, relationships between words videos and clusters are revealed. Matrix W shows the relationships between videos and different clusters, whilst H clarifies the relationships between words and clusters. In W, value held in $w_{n,k}$ is the coefficient indicated how likely video n belongs to cluster k. To fit the purpose of our research, we have refined the method of group assigning in NMF. The original NMF algorithm assigns an object to a group in a maximum coefficient approach. However, in our method, a video n is treated to be in group k if $w_{n,k}$ has the a value greater than a threshold β_k within vector n in W, where the value of threshold β_k is data dependent. The threshold should be chosen in a coefficient distribution depend manner. Videos can then be grouped into clusters based on their similarities. We define the set of cluster for video V_n that it belongs to as,

$$C_n = \{k \in K \mid \forall\, W_{n,k} > \beta_k\} \tag{6}$$

where K is set of all clusters.

Matrix H provides the information about the characteristics of the video groups. Concept words of a cluster can be found with H as $h_{k,m}$ is the coefficient of the term m belongs to cluster k. For each cluster, the top 10 words, with respect to the term-cluster coefficient, are considered to be the concept words for the cluster. Hence, stating the properties of a group of videos.

7 Experimental Evaluation

A proof-of-concept experiment was done to study the Hong Kong social culture in regional music domain. An Intel(R) Core(TM)2 Quad 2.40GHz PC with 4GB RAM was used to conduct our experiment. Our web crawler was implemented in VC++ and the core algorithm was implemented in Matlab.

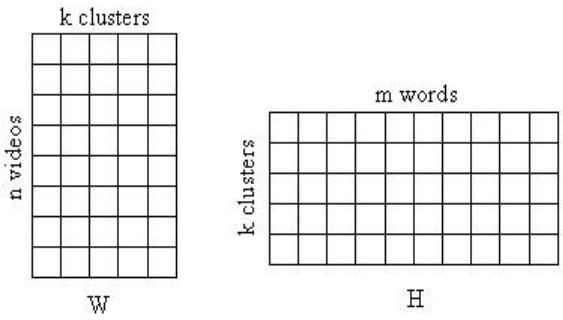

Figure 2. NMF decomposition for video clustering.

7.1 Empirical Setting

As the videos were grabbed by searching from the YouTube site with predefined list of singer names, there are possibilities that some videos are grabbed more than one time. For those videos preformed by more than one singer, as long as there are more than one singer names annotated in the video title, the video will be collected in times equals to the number of hits the predefined singer name hits the video title. To achieve a more accurate clustering result, duplicated videos are removed form the dataset.

In comments, users are used to mention the singer names when they are commenting on him/her. This will make the singer names dominate in every group of concept words. However, it is not conspicuous enough to reveal interests by singers. Therefore, in our experiment, we add singer names to the stoplist as well.

Furthermore, some videos are less popular or just been uploaded for a short time that only have a few comments. These videos which have relatively few words are informativeless for video clustering. Videos which have less than 30 valid words are eliminated.

The videos are clustered into k groups with the clustering algorithm discussed in section 7, where k is experimentally set as 20. The experiment was done twice, once with threshold β_i regarding cluster i to be mean coefficient of all videos,

$$\beta_i = meanCoef_i = \frac{\sum_{j=1}^{n} w_{j,i}}{n} \tag{7}$$

To compensate the poor performance caused by the extremely uneven distribution of coefficient, we chose the threshold to be mean coefficient plus standard deviation of all videos for the second experiment. β_i regarding cluster i is defined as,

Group	Concept Words
1	beautiful lyrics melody
2	female makeup dress
3	cute pretty handsome
4	sex photos scandal
5	funny hilarious laughing
6	rap raps hip
7	movie film story
8	cantonese mandarin language
9	commercial pepsi coke
10	piano piece ear grade
11	japanese japan korean
12	china olympic games
13	old classic memories
14	dance dancer moves
15	guitar band rock
16	award tvb gold
17	english chinese accent
18	sad legend died
19	together couple two
20	voice pretty talent

Table 1. Latent video categories discovered in Hong Kong music video domain from YouTube

$$\beta_i = meanSdCoef_i = \sqrt{\frac{1}{n}\sum_{j=1}^{n}(w_{j,i} - meanCoef_i)^2} \tag{8}$$

where n is total number of videos being clustered.

7.2 Video Categorization

Since video clustering is a complete clustering analysis, music categories and trends in Hong Kong can be found by clustering the videos. We deployed NMF as our clustering method. Applied the clustering algorithm to the video dataset in the way discussed in Section 5.2, with the experimentally chosen number of cluster of 18, videos were clustered into groups based on the words in their comments. The mean coefficient of videos to a cluster is set as the critical point. Videos with coefficient higher than the critical point of a cluster are said to be in that cluster. Under this strategy, videos can belong to several clusters as they may have multiple characteristics. Table 1 shows the discovered categories from our dataset.

Unlike the generic music video categorization of some famous video sharing sites, such as DailyMotion divides music videos into eight classes (Pop, Rock, Rap, R&B,

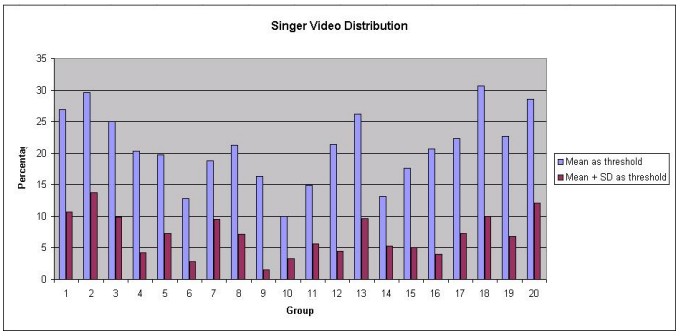

Figure 3. Singer video distribution in YouTube.

		Precision	
Group	Concept Words	Mean as Threshold	Mean + SD as Threshold
A	sex photos scandal	21.64%	81.58%
B	old classic memories	61.04%	78.16%
C	sad legend died	35.86%	60.34%
D	together couple two	64.44%	79.82%
Average		45.75%	74.96%

Table 2. Precision of objective clusters

Jazz, Metal, Covers, and Electros), we categorized videos of local singers into twenty classes which are far more specific.

From our clustering result, we noticed that videos of singers are not only limited to general music videos, but also funny clips, award presentations, commercial advertisements as well as event promotion clips. Looking at the music videos alone, by clustering users' comments, we found that people's attitude towards Hong Kong music are not only target on the music styles. There are also other features of music people are interested at, like languages, age of music, music instruments, type of singers, singer's voice, composition goodness, etc.

Furthermore, categorize singer videos with the proposed clustering algorithm, people can identify dance-oriented videos (Group 14), cross-culture produced music (Group 11) or even movie theme songs (Group 7) easily. Other than simply categorizing singer video clips, some up-to-date news in the local music circle, like scandals (Group 4), can also be found.

Figure 3 illustrates the distribution of Hong Kong singer videos in YouTube according to the proposed algorithm using mean and mean + sd as thresholds. From the figure, we can see that the distribution of videos diverse over different threshold values. With the mean coefficient as the threshold, compared to the video groups resulted from the algorithm with mean + SD coefficient as threshold, larger groups of videos can be obtained. In the other words, algorithm associated with a smaller group assigning threshold would result heavier overlapped video groups.

The video clustering results are evaluated by human experts. To make the evaluation less controvertible, we only show the precisions of objective video groups in Table 2 where groups A, B, C, D are cluster 4, 13, 18, 19 in our clustering. In the table, we noticed that assigning videos to groups with a smaller threshold may sometimes lower the precision. This will be caused in the groups which are very distinct to others. As a video group is too specific, the video-group coefficients to the group hold the extreme values. Also, closely related videos to the distinct group is always much fewer than videos which do not. Hence, videos are condense at the lower extreme side. As a result, lowered the mean coefficient and caused the poor precision. On the other hand, we can see that the algorithm which assigns videos into groups with a larger threshold yields far better precisions. The average precision of the larger-threshold clustering groups in the table is 74.96% whilst that of the lower-threshold clustering is just 45.75%. The difference between the precisions resulted from clustering with the two different thresholds reflects the degree of extraordinary of the video group. The larger the difference, the more the special the group is. For example, in group 4, the two precisions differ from each other by a large percentage at about 60%, and from the concept words we can know that this group is about scandal of singers involving their sex photos. This is obviously an extremely distinct group.

7.3 User Comments vs User Tags

As tags are believed to be an accurate description of an object and have been widely used for finding user interests and grouping objects, it is necessary to examine the virtues of user comments over tags before utilizing comments to capture popular interests and categorize videos to facilitate the video search in video sharing sites. One important observation from our experimental results is that user comments usually contains more in-depth information than that of user tags. Table 3 shows both the top 10 concept words found from user comments and the top 10 user tags of four clustered groups. From the concept words in the user comments, we can make a reasonable prediction that cluster I is about some music videos of some old songs. From the user tags, however, we can only find some singer names or some high-level descriptions (e.g. music, mv, mtv). Same as cluster II, from the concept words, this cluster is probably talking about some superstars who are already died. Nevertheless, the most frequent tags are only names of those dead superstars which do not reveal the low-level description of the group. Cluster III is the similar case as the above

Cluster I	Top 10 concept words in user comments	old classic memories drama childhood love 80s memory loved san
	Top 10 frequent user tags	chinese chan mv cheung wong love music mtv top anita
Cluster II	Top 10 concept words in user comments	sad legend two died missed heaven star superstar crying talented
	Top 10 frequent user tags	cheung chan leslie anita mui chinese mv danny hong wong
Cluster III	Top 10 concept words in user comments	guitar solo band rock cover drummer chords intro crap violin
	Top 10 frequent user tags	chinese beyond wong kong cheung ka kui hong nicholas paul
Cluster IV	Top 10 concept words in user comments	sex photos stupid fake victims private innocent scandal girls stop
	Top 10 frequent user tags	gillian chung sex photo edison chen gill cheung cecilia chan

Table 3. Examples of user comments and user tags in four video clusters

		Concept Words from Group			
		A	B	C	D
Percentage of Videos from Group	A	34.04%	4.02%	0%	2.13%
	B	0%	15.79%	0%	0%
	C	0.84%	0.84%	7.58%	0.84%
	D	0%	10.17%	3.39%	5.26%

Table 4. Percentage of videos with tags covering concept words across groups

two clusters. Concept words from user comments state that this group is about the band sound and rock music but the tags only list out the name of a local popular band, "Beyond", and some of the band members. Tags of the other clusters suffer the similar problem as the above mentioned clusters. From the table, we can see that the user tags actually agree with our discovered concept words though the tags just exhibit the high-level sketch of the groups. In the other words, our algorithm gives an in-depth characterization of the videos with the concept words which the characterization cannot be exposed by the user tags, and in the mean time, the concept words achieve a strong agreement with the tags.

From this observation, we can conclude that if we want to obtain clustering results in a more fine-grained level, using comment-based clustering technique is more suitable. For the purpose of social culture discovery, it is beyond doubt that fine-grained level clustering result is more desirable.

To give a more in-depth analysis of comments and tags, we have compared concept words against tags in different clusters. Table 4 record the portion of videos whose tags cover the concept words of different groups and there are two major observations from the table. First, we can see that there are at least 65% of videos whose tags cannot cover the concept words of the group they belongs to. This implies tag-based clustering cannot completely capture user opinions and video content. Second, we can see that the concept words of each group are mostly covered by tags of its own group. This once again verify the accuracy of our proposed method.

7.4 Relationship Discovery via Clustering

Apart from video categorizing and indexing, we can also discover the relationships between singers with the video comments. Music videos always include singers in it. When users leaving comments on a video, the content of the comment is not limited to the video itself but also the singers. Within the comments, some talk about properties of singers, such as styles, the active ages, appearance, etc. Practically, except characteristics, users also tend to talk and discuss the recent hot news about singers. As such, in addition to the videos, user-left comments also describe the singers. In this context, singer relationships can be found from video comments.

To reveal the relationships between singers, singers should be clustered into groups based on their similarities and relatedness. To this end, the set of comments should be reorganized to a form that suits the purpose of singer clustering. In this context, comments are no longer grouped by videos but by singers according to the singers presentence in the videos. Each singer has his/her collection of comments. The adopted clustering algorithm tends to group singers with similar descriptive words together. As such, with all the descriptions and hot news about singers, singers can be grouped based on their style, characteristics or special relationships. From the clustering result, not only the common properties of singers can be found, but also their relationships like members of a band sound, couple, etc.

Applying the same clustering algorithm introduced before with matrix X in the algorithm set to be the singer-word matrix, singers can be clustered into groups. Here

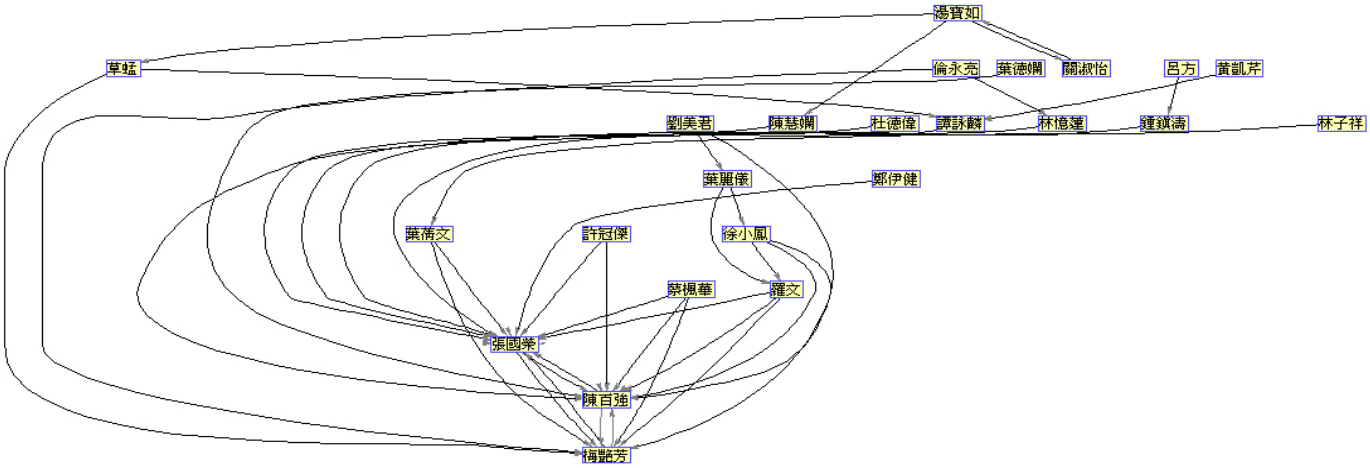

Figure 4. Singer Relationship.

we visualize the relationships between singers in a singer network based on their similarities reflected from the comments. With a visualized singer network, not only the relationships between singers can be shown but also the hidden phenomenon. Due to the paper size, Figure 4 illustrate only partial of the singer network. In this graph, the singers are relatively closely connected to each others than to other singers and thus form a subnetwork. In this subnetwork, all the nodes are active singers in 80s, this is one of their relationships. The network is a directed graph which the singer being pointed to is highly referenced by the singer who points to him/her. Grasshopper, at the top left corner is pointing to Anita Mui at the bottom as the members of Grasshopper are students of Anita Mui. Leslie Cheung, Danny Chan and Anita Mui are famous singers and many other singers have used their songs for performance. This can be reflected in the graph: many other singers points to these three singers.

8 Conclusion and Future Work

In this paper, we have proposed a comment-based video categorization approach by using NMF. Experimental results showed that our comment-based clustering yields better performance than that of tag-based approach which was proposed previously in the literature. On the other hand, we have successfully discovered some non-trivial categories among the videos of Hong Kong singers. Since our categorization is learnt from user feedbacks, it can provide an easy way for users to reach their desire videos via our list of categories. Additionally, our comment-based clustering can reveal relationships among singers within the social network which can help in the context of social culture study.

In our future work, we plan to extend the comment-based technique from video and singer clustering to user clustering. After we have obtained the three types of cluster, we can acquire the relationships among different videos, singers and users by analyzing the inter-cluster similarity. As such, social culture can be studied by combining and analyzing the discovered relationships. With the video-video, singer-singer, user-singer, and user-user relationships found by clustering, we can know the changes in music styles and singer styles over the ages, the trend of music, the ways people appreciate music, and even the special relationships of singers reflected by news, and more. Relationships observed by clustering are not only useful for social scientists to study social culture, but also beneficial for businesses, entertainment companies, fans clubs, social network systems and system users. With the help of examined user-user relationships, businesses can be profited from reducing advertising costs by advertise only to the potential customer groups. User-signer relationships define user-idol groups, entertainment companies can effectively promote to the target groups. Determining the user-singer relationships, in addition to profits for entertainment companies, fans groups can easily be managed. Other than the advantages for some specific parties, general users are also benefited. Well-clustered groups of videos and singers equipped with a batch of indicative words leads to a effort saving video searching for users. Also, social network systems are able to detect and refine incorrect tags with the indicative words resulted from clustering. As a result, introductions to videos are more precise and thus improves the video searching function.

References

[1] X. Cheng, C. Dale, and J. Liu. Understanding the characteristics of internet short video sharing: Youtube as a case study. *In CoRR abs*, Jul 2007.

[2] L. Guo, S. Jiang, L. Xiao, and X. Zhang. Fast and low-cost search schemes by exploiting localities in p2p networks. *J. Parallel Distrib. Comput.*, 65(6):729–742, 2005.

[3] J. Heer and D. Boyd. Vizster: Visualizing online social networks. *IEEE Symposium on Information Visualization, 2005*.

[4] C. M. C. Y. Julia Stoyanovich, Sihem Amer-Yahia. Leveraging tagging to model user interests in del.icio.us. In *AAAI '08: Proceedings of the 2008 AAAI Social Information Spring Symposium*. AAAI, 2008.

[5] P. P. Kotsiantis S., Kanellopoulos D. Multimedia mining. In *WSEAS Transactions on Systems, Issue 10, Volume 3*, pages 3263–3268, December 2004.

[6] X. Li, L. Guo, and Y. E. Zhao. Tag-based social interest discovery. In *WWW '08: Proceeding of the 17th international conference on World Wide Web*, pages 675–684, New York, NY, USA, 2008. ACM.

[7] C. G. R. A. A. F. L. Rodrygo L. T. Santos, Bruno P. S. Rocha. Characterizing the youtube video-sharing community. 2007.

[8] M. F. Schwartz and D. C. M. Wood. Discovering shared interests using graph analysis. *Commun. ACM*, 36(8):78–89, 1993.

[9] K. Sripanidkulchai, B. Maggs, and H. Zhang. Efficient content location using interest-based locality in peer-to-peer systems. In *INFOCOM 2003. Twenty-Second Annual Joint Conference of the IEEE Computer and Communications Societies. IEEE*, volume 3, pages 2166–2176 vol.3, 2003.

[10] W. Xu, X. Liu, and Y. Gong. Document clustering based on non-negative matrix factorization. In *SIGIR '03: Proceedings of the 26th annual international ACM SIGIR conference on Research and development in informaion retrieval*, pages 267–273, New York, NY, USA, 2003. ACM.

[11] L. Yang, J. Liu, X. Yang, and X.-S. Hua. Multi-modality web video categorization. In *MIR '07: Proceedings of the international workshop on Workshop on multimedia information retrieval*, pages 265–274, New York, NY, USA, 2007. ACM.

[12] O. R. Zaïane, J. Han, Z.-N. Li, S. H. Chee, and J. Y. Chiang. Multimediaminer: a system prototype for multimedia data mining. In *SIGMOD '98: Proceedings of the 1998 ACM SIGMOD international conference on Management of data*, pages 581–583, New York, NY, USA, 1998. ACM.

Implementation of Multiple-precision Modular Multiplication on GPU

Kaiyong Zhao

Abstract

Multiple-precision modular multiplications are the key components in security applications, like public-key cryptography for encrypting and signing digital data. But unfortunately they are computationally expensive for contemporary CPUs. By exploiting the computing power of the many-core GPUs, we implemented a multiple-precision integer library with CUDA. In this paper, we will investigate the implementation of two approaches of multiple-precision modular multiplications on GPU. We will analyze the detail of the instructions of multiple-precision modular multiplication on the GPU and find the hit issues, and then we propose to use the inline ASM to improve the implementation of this function. Our experimental results show that the performance of multiple-precision modular multiplication has been improved by 20%.

Keywords

GPU computing, CUDA, Multiple-precision Modular Multiplication, Karatsuba multiplication, Montgomery modular multiplication

1. Introduction

In recent years, peer-to-peer (P2P) content distribution applications such as BitTorrent and ppLive, have become the most popular Internet applications due to their scalability and robustness. Network coding has been proposed as an effective mechanism to improve the performance of such P2P applications [14]. However, P2P applications with network coding suffer from the notorious pollution attacks: a malicious node can send out bogus packets which will be merged into other genuine packets and propagated into the whole network at an exponential speed. To resolve this problem, homomorphic hash functions have to be applied such that the hash of any encoded packet can be effectively derived from the hashes of the original packets, which enables the detection of bogus packets before a peer encodes it with other packets [12]. Unfortunately homomorphic hash functions rely on multiple-precision modular operations and are computationally expensive [10] [12].

Recent advances in Graphics Processing Units (GPUs) open a new era of GPU computing [20]. For example, commodity GPUs like NVIDIA's GTX 280 has 240 processing cores and can achieve 933 GFLOPS of computational horsepower. More importantly, the NVIDIA CUDA programming model makes it easier for developers to develop non-graphic applications using GPU [1] [4]. In CUDA, the GPU becomes a dedicated coprocessor to the host CPU, which works in the principle of Single-Program Multiple Data (SPMD) where multiple threads based on the same code can run simultaneously.

In this paper, we present our study of using GPUs for multiple-precision modular multiplication, which is the key component of not only the homomorphic hashing, but also a number of security applications that make use of public-key cryptography. We implement two methods of multiple-precision modular multiplications on NVIDIA GPUs using CUDA. One is Coarsely Integrated Operand Scanning (CIOS) Montgomery method; the second one is Karatsuba multiplication with Montgomery. In order to achieve the highest performance, we analyze the ptx code (i.e., the assembly code for NVIDIA GPUs) of the implementation. As the CUDA PTX standard is not open to the public, we rely on the decuda tool to disassemble the compiled binary cubin file and search for the bottleneck for an improvement.

The contribution of this work is twofold:

- First, we designed and implemented two approaches of multiple-precision modular multiplication on the CUDA architecture.
- Second, we analyze the implementation of the directive instructions, and use inline ASM to optimize the Montgomery algorithm.

The rest of the paper is organized as follows. Section 2 provides background information on Karatsuba Mulitiplication, Montgomery algorithm, GPU architecture, and CUDA programming model. Section 3 presents the design of multiple-precision modular arithmetic on GPU. Section 4 presents the decuda analysis, and then presents our inline ASM implementation of the 32-bit integer multiplication. Experimental results are presented in Section 5, and we conclude the paper in Section 6.

2. Background and Related Work

In this section, we provide the required background knowledge of Karatsuba multiplication, Montgomery multiplication algorithm, GPU architecture, and CUDA programming model.

2.1 Karatsuba multiplication

The Karatsuba multiplication algorithm has been described by Knuth, which is possible to perform multiplication of large numbers in (many) fewer operations than the usual brute-force technique of "long multiplication". As discovered by Karatsuba [25]， multiplication of two *n*-digit numbers can be done with a bit complexity of less than n^2 steps using identities of the form

$$(a+b\cdot 10^n)(c+d\cdot 10^n) = a\cdot c + [(a+b)(c+d) - a\cdot c - b\cdot d]$$

The inputs x and y are treated as each split into two parts of equal length (or the most significant part one limb shorter if N is odd).

Let *b* be the power of 2 where the split occurs, ie. if x_0 is k limbs (y_0 the same) then $b=2^{(k \cdot mp\_bits\_per\_limb)}$. With that $x=x_1 \cdot b+x_0$ and $y=y_1 \cdot b+y_0$, and the following holds,

$$x\cdot y = (b^2+b)x_1y_1 - b\cdot(x_1-x_0)\cdot(y_1-y_0) + (b+1)\cdot x_0\cdot y_0$$

This formula means doing only three multiplies of $N^2/4$ limbs, whereas a base case multiply of N^2 limbs is equivalent to four multiplies of $N^2/4$. The factors (b^2+b) etc represent the positions where the three products must be added. [3]

The term $(x_1-x_0)\cdot(y_1-y_0)$ is best calculated as an absolute value, and the sign used to choose to add or subtract. Notice the sum $high(x_0 \cdot y_0) + low(x_1 \cdot y_1)$ occurs twice, so it is possible to do $5\cdot k$ limb additions, rather than $6\cdot k$.

Squaring is similar to multiplying, but with $x = y$ the formula reduces to an equivalent with three squares,

$$x^2 = (b^2+b)x_1^2 - b(x_1-x_0)^2 + (b+1)x_0^2$$

The final result is accumulated from those three squares the same way as for the three multiplies above. The middle term $(x_1-x_0)^2$ is now always positive.

A similar formula for both multiplying and squaring can be constructed with a middle term $(x_1+x_0)\cdot(y_1+y_0)$. But those sums can exceed k limbs, leading to more carry handling and additions than the form above.

Karatsuba multiplication is asymptotically an $O(N^{1.585})$ algorithm, the exponent being log(3)/log(2), representing 3 multiplies each 1/2 the size of the inputs. This is a big improvement over the base case multiply at $O(N^2)$ and the advantage soon overcomes the extra additions Karatsuba performs.

2.2 Montgomery Multiplication

The classical modular multiplication is suitable for normal operations. However, when performing modular exponentiations, Montgomery multiplication shows much better performance advantage [5]. The following gives the Montgomery reduction and Montgomery multiplication algorithms.

Montgomery reduction is an algorithm introduced in 1985 by Peter Montgomery that allows modular arithmetic to be performed efficiently when the modulus is large (typically several hundred bits).

Let m be a positive integer, and let R and A be integers such that $R > m$, $gcd(m, R) = 1$, and $0 \le A < m\cdot R$. The Montgomery reduction of A modulo m with respect to *R* is defined as $A\cdot R^{-1} \bmod m$. In our applications, *R* is chosen as b^n to simply the calculation.

Algorithm 1 Multiple-precision Montgomery Reduction

INPUT: integer *m* with *n* radix *b* digits and gcd(*m*, *b*) = 1, $R = b^n$, $m' = -m^{-1} \bmod b$, and integer *A* with 2*n* radix *b* digits and $A < m\cdot R$.

OUTPUT: $T = A\cdot R^{-1} \bmod m$.

1: $T \leftarrow A$;
2: **for** (*i* **from** 0 **to** $n-1$)
3: $u_i \leftarrow T_i \cdot m' \bmod b$;
4: $T \leftarrow T + u_i \cdot m \cdot b^i$;
5: **end for**
6: $T \leftarrow T / b^n$;
7: **if** ($T \ge m$) **then** $T \leftarrow T - m$;
8: **return** *T*;

Algorithm 2 Multiple-precision Montgomery Multiplication

INPUT: non-negative integer *m*, *x*, *y* with *n* radix *b* digits, $x < m$, $y < m$, and gcd(*m*, *b*) = 1, $R = b^n$, $m' = -m^{-1} \bmod b$.

OUTPUT: $T = x\cdot y\cdot R^{-1} \bmod m$.

1: $T \leftarrow 0$;
2: **for** (*i* **from** 0 **to** $n-1$)
3: $u_i \leftarrow (T_0 + x_i \cdot y_0)\cdot m' \bmod b$;
4: $T \leftarrow (T + x_i \cdot y + u_i \cdot m) / b$;
5: **end for**
6: **if** ($T \ge m$) **then** $T \leftarrow T - m$;
7: **return** *T*;

2.3 GPU Computing and CUDA

GPUs are dedicated hardware for manipulating computer graphics. Due to the huge computing demand for real-time and high-definition 3D graphics, the GPU has evolved into a highly parallel, multithreaded, manycore processor. The advances of computing power in GPUs have driven the development of general-purpose computing on GPUs (GPGPU). The first generation of GPGPU requires that any non-graphics application must be mapped through graphics application programming interfaces (APIs).

Recently one of the major GPU vendors, NVIDIA, announced their new general-purpose parallel programming model, namely Compute Unified Device Architecture (CUDA) [1] [4], which extends the C programming language for general-purpose application development. Meanwhile,

another GPU vendor AMD also introduced Close To Metal (CTM) programming model which provides an assembly language for application development [2]. Intel also exposed Larrabee, a new many-core GPU architecture specifically designed for the market of GPU computing this year [23].

Since the release of CUDA, it has been used for speeding up a large number of applications [17] [18] [20] [21] [22].

The NVIDIA GeForce 8800 has 16 Streaming Multiprocessors (SMs), and each SM has 8 Scalar Processors (SPs), resulting a total of 128 processor cores. The SMs have a Single-Instruction Multiple-Data (SIMD) architecture: At any given clock cycle, each SP of the SM executes the same instruction, but operates on different data. Each SP can support 32-bit single-precision floating-point arithmetic as well as 32-bit integer arithmetic.

Each SM has four different types of on-chip memory, namely registers, shared memory, constant cache, and texture cache. For GeForce 8800, each SM has 8192 32-bit registers, and 16 Kbytes of shared memory which are almost as fast as registers. Constant cache and texture cache are both read-only memories shared by all SPs. Off-chip memories such as local memory and global memory have relatively long access latency, usually 400 to 600 clock cycles [4]. The properties of the different types of memories have been summarized in [4] [17]. In general, the scarce shared memory should be carefully utilized to amortize the global memory latency cost. Shared memory is divided into equally-sized banks, which can be simultaneously accessed. If two memory requests fall into the same bank, it is referred to as bank conflict, and the access has to be serialized.

In CUDA model, the GPU is regarded as a coprocessor capable of executing a great number of threads in parallel. A single source program includes host codes running on CPU and also kernel codes running on GPU. Compute-intensive and data-parallel kernel codes run on GPU in the manner of Single-Process Multiple-Data (SPMD). The threads are organized into blocks, and each block of threads are executed concurrently on one SM. Threads in a thread block can share data through the shared memory and can perform barrier synchronization. Each SM can run at most eight thread blocks concurrently, due to the hard limit of eight processing cores per SM. As a thread block terminate, new blocks will be launched on the vacated SM. Another important concept in CUDA is warp, which is formed by 32 parallel threads and is the scheduling unit of each SM. When a warp stalls, the SM can schedule another warp to execute. A warp executes one instruction at a time, so full efficiency can only be achieved when all 32 threads in the warp have the same execution path. Hence, if the number of threads in a block is not a multiple of warp size, the remaining instruction cycles will be wasted.

3. Multiple-Precision Modular Arithmetic for CUDA

In this section, we present a set of library functions of multiple-precision modular arithmetic implemented on GPUs. These library functions are the cornerstones of the network coding system and homomorphic hash functions. It is of critical importance to implement these library functions efficiently. In modular arithmetic, all operations are performed in a group Z_m, i.e., the set of integers $\{0,1,2,\cdots,m-1\}$. In the following, the modulus m is represented in radix b as $(m_n m_{n-1}\cdots m_1 m_0)_b$ where $m_n \neq 0$. Each symbol m_i, $0 \le i \le n$, is referred to as a radix b digit. Non-negative integers x and y, $x < m$, $y < m$, are represented in radix b as $(x_n x_{n-1}\cdots x_1 x_0)_b$ and $(y_n y_{n-1}\cdots y_1 y_0)_b$ respectively.

We have implemented the following multiple-precision library functions for CUDA:

- Multiple-precision comparison
- Multiple-precision subtraction
- Multiple-precision modular addition
- Multiple-precision modular subtraction
- Multiple-precision multiplication
- Multiple-precision division
- Multiple-precision multiplicative inversion

In this paper, we only present the implementation details in the Montgomery multiplication and the optimization in this paper.

3.1 CIOS Montgomery Reduction

The Coarsely Integrated Operand Scanning method improves on the first one by integrating the multiplication and reduction steps. Specifically, instead of computing the entire product *ab*, then reducing, we alternate between iterations of the outer loops for multiplication and reduction. We can do this since the value of *m* in the *i*th iteration of the outer loop for reduction depends only on the value *t*[*i*], which is completely computed by the *i*th iteration of the outer loop for the multiplication. This leads to the following algorithm:

Algorithm 3 Multiple-precision Montgomery multiplication

INPUT: integer *m* with *n* radix *b* digits and gcd(*m*, *b*) = 1, $R = b^n$, positive integer *x and y* with *n* radix *b* digits and $x < m$.

OUTPUT: $x*y*R^{-1} \bmod m$.

```
1.  for (i from 0 up to s-1)
2.      C: = 0
3.      for ( j from 0 up to s-1)
4.          (C,S) := t[j] + a[j]*b[i] + C
5.          t[j] := S
```

```
6.      end for
7.      (C,S) := t[s] + C
8.      t[s] := S
9.      t[s+1] := C
10.     C := 0
11.     m := t[0]*n'[0] mod W
12.     for (j from 0 up to s-1)
13.        (C,S) := t[j] + m*n[j] + C
14.        t[j] := S
15.     end for
16.     (C,S) := t[s] + C
17.     t[s] := S
18.     t[s+1] := t[s+1] + C
19.     for (j from 0 up to s)
20.        t[j] := t[j+1]
21.     end for
22. end for
```

Note that the array t is assumed to be set to 0 initially. The last j-loop is used to shift the result one word to the right (i.e., division by 2^w), hence the references to *t[j]* and *t[0]* instead of *t[i+j]* and *t[i]*. A slight improvement is to integrate the shifting into the reduction as follows:

```
m := t[0]*n'[0] mod W
(C,S) := t[0] + m*n[0]
for (j from 1 up to s-1)
   (C,S) := t[j] + m*n[j] + C
   t[j-1] := S
end for
(C,S) := t[s] + C
t[s-1] := S
t[s] := t[s+1] + C
```

The auxiliary array *t* uses only *s* + 2 words. This is due to the fact that the shifting is performed one word at a time, rather than *s* words at once, saving *s* - 1 words. The final result is in the first *s*+1 words of array *t*. A related method, without the shifting of the array (and hence with a larger memory requirement), is described in [2].

The CIOS method (with the slight improvement above) requires $2s^2+s$ multiplications, $4s^2+4s+2$ additions, $6s^2+7s+2$ reads, and $2s^2+5s+1$ writes, including the final multi-precision subtraction, and uses $s+3$ words of memory space. The memory reduction is a significant improvement over the SOS method.

We say that the integration in this method is "coarse" because it alternates between iterations of the outer loop. In the next method, we will alternate between iterations of the inner loop [24].

3.2 Karatsuba Montgomery Reduction

Modular multiplication can be spared into two parts, one is multiplication and one is modular reduction. In this method, we choose the Karatsuba multiplication to implement the multiplication, and then perform Montgomery reduction.

Algorithm 4 Multiple-precision Karatsuba and Montgomery Multiplication

INPUT: integer *m* with *n* radix *b* digits and gcd(*m*, *b*) = 1, $R = b^n$, positive integer *x and y* with *n* radix *b* digits and $x < m$.

OUTPUT: $x*y*R^{-1} \bmod m$.

```
1.  Karatsuba(x,y)
2.  for (i from 0 up to s-1)
3.     C := 0
4.     m := t[i]*n'[0] mod W
5.     for (j from 0 up to s-1)
6.        (C,S) := t[i+j] + m*n[j] + C
7.        t[i+j] := S
8.     end for
9.     ADD (t[i+s],C)
10. end for
11. for (j from 0 up to s)
12.    u[j] := t[j+s]
13. end for
14. B := 0
15. for (i from 0 up to s-1)
16.    (B,D) := u[i] - n[i] - B
17.    t[i] := D
18. end for
19. (B,D) := u[s] - B
20. t[s] := D
21. if B=0 then return t[0], t[1], ... , t[s-1]
22. else return u[0], u[1], ... , u[s-1]
```

4. Improving the Montgomery Multiplication

To achieve a high performance, we analyze the implementation of the instructions of the Montgomery Multiplication. We use the decuda tool to disassemble the cubin file of the CUDA binary codes. We will tell the details as below.

4.1 ASM of Integer Multiplication

When we use the decuda tool disassemble the cubin. We get that the 32bit multiplication 32bit integer is not only using one instruction but using ten to twenty instructions.

We can see the MULT64X64LO need more than 20 instructions, but the MULT32X32WIDE only need 10 instructions. So, we use inline ASM to limit the compiler

compile the 32bit multiplication 32bit work with the 10 instructions. eg.:

Algorithm 5 32bit integer multiplication

INPUT: 32bit integer *A* multiplicative with 32bit integer *B*.

OUTPUT: *A*B*.

```
1.  static inline __device__ unsigned __int64
    mul_32x32(unsigned A, unsigned B) {
2.    unsigned __int64 out;
3.    asm("mul.wide.u32  %0, %1, %2;" : "=l"(out) : "r"(A),
    "r"(B));
4.    return out;
5.  }
```

5. Implementation and Experimental Results

We tested these implementations on T61 NVIDIA Quadro NVS140M graphic card which contains an NVIDIA Quadro G86M GPU. The G86M GPU uses the G80 architecture with 16 processing cores working at 0.8 GHz. The implementation of modular multiplication is in 1024-bit integer. All the implementation is 1024-bit multiplied by 1024-bit modular 1024-bit.

5.1 Comparing Karatsuba Method and CIOS Method

In Fig. 1, the X-coordinate represents the number of threads. As Fig. 1 shows, the karatsuba Montgomery multiplication is slow than the CIOS method of Montgomery multiplication. The karatsuba Montgomery multiplication method needs 60 registers and 5132 local memories. But the CIOS method only needs 14 register and no local memory at all. The blue block shows the CIOS method of the Montgomery Multiplication. The red block shows the method with K-MM (Karatsuba Montgomery Multiplication). The K-MM method needs more variables in the implementation, because that can't use callback function in the CUDA model recently, so the 1024bit integer multiplication will be translate into 2 256bit integer function, and 256bit to 128bit, and so on. So the K-MM method is slow than the CIOS method on the recently GPU model.

The CIOS method only needs 14 registers and using unrolling method unroll the loop.

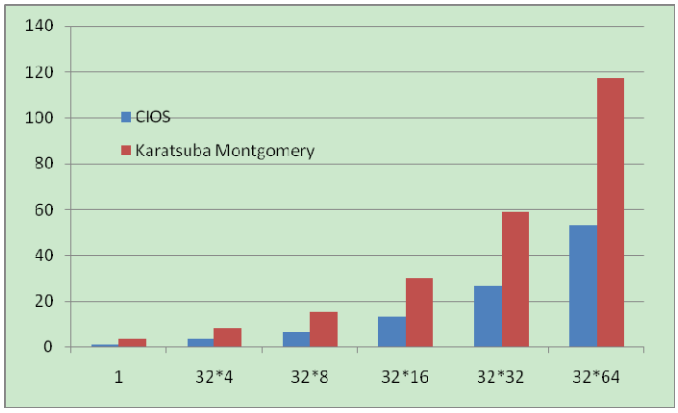

Figure 1. Throughput of Montgomery multiplication and karatsuba Montgomery multiplication on GPU using Algorithm 3&4, with different number of threads.

5.2 Montgomery Multiplication with inline ASM

We use the inline ASM to limit the instruction work with the Short instruction. The experimental results are shown in Fig. 2. The performance has been improved by 20% as compared with the one without using our inline ASM code.

The blue and red block all use the CIOS method. But the red one, as the Fig. 2 shows is 20% faster than blue one. Because the inside ASM function used to solve the 32bit multiplicative 32bit integer. In the decuda code we can see that each loop the CIOS-ASM method is 11 instructions little than the CIOS method.

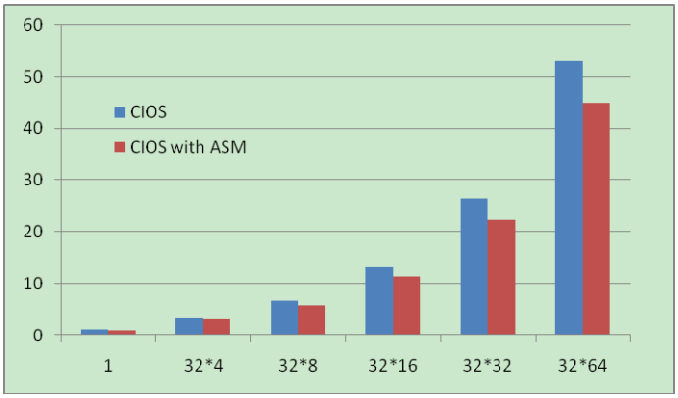

Figure 2. Throughput of inline ASM in CIOS on GPU, with different number of threads

6. Conclusions

Multiple-precision modular multiplication is an important component in public-key cryptography for encrypting and signing digital data. In this paper, we describe the design, implementation and optimization of multiple-precision modular multiplication using GPU and CUDA. Although Karasuba multiplication is theoretically advantageous, we

found that it is not practical for the current GPU platform due to the high cost of comparing large integers. Nevertheless, we improved the performance of the CIOS method by developing an inline ASM implementation of 32-bit integer multiplication.

7. References

[1] NVIDIA CUDA. http://developer.nvidia.com/object/cuda.html

[2] AMD CTM Guide: Technical Reference Manual. 2006. http://ati.amd.com/companyinfo/researcher/documents/ATI_CTM_Guide.pdf

[3] GNU MP Arithmetic Library. http://gmplib.org/

[4] NVIDIA CUDA Compute Unified Device Architecture: Programming Guide, Version 2.0beta2, Jun. 2008.

[5] Montgomery, P., 1985. Multiplication without trial division, Math. Computation, vol. 44, 1985, 519-521.

[6] Menezes, A., van Oorshot, P., and Vanstone S., 1996. Handbook of applied cryptography. CRC Press, 1996.

[7] Ahlswede, R., Cai, N., Li S. R., and Yeung, R. W. 2000. Network information flow. IEEE Transactions on Information Theory, 46(4), July 2000, 1204-1216.

[8] Ho, T., Koetter. R., Médard, M., Karger, D.R. and Effros, M. 2003. The benefits of coding over routing in a randomized setting. In Proceedings of IEEE ISIT, 2003.

[9] Li, S.-Y.R., Yueng, R.W., and Cai, N. 2003. Linear network coding. IEEE Transactions on Information Theory, vol. 49, 2003. 371-381.

[10] Krohn, M., FreedMan, M., and Mazieres, D. 2004. On-the-fly verification of rateless erasure codes for efficient content distribution. In Proceedings of IEEE Symposium on Security and Privacy, Berkeley, CA, 2004.

[11] Gkantsidis, C. and Rodriguez, P. 2005. Network coding for large scale content distribution. In Proceedings of IEEE INFOCOM 2005.

[12] Gkantsidis, C. and Rodriguez, P. 2006. Cooperative security for network coding file distribution. In Proceedings of IEEE INFOCOM'06, 2006.

[13] Li, Q., Chiu, D.-M., and Lui, J. C.S. 2006. On the practical and security issues of batch content distribution via network coding. In Proceedings of IEEE ICNP'06, 2006, 158-167.

[14] Chou, P. A. and Wu, Y. 2007. Network coding for the Internet and wireless networks. Technical Report. MSR-TR-2007-70, Microsoft Research.

[15] Wang, M. and Li, B. 2007. Lava: a reality check of network coding in peer-to-peer live streaming. In Proceedings of IEEE INFOCOM'07, 2007.

[16] Wang, M. and Li, B. 2007. R^2: random push with random network coding in live peer-to-peer streaming. In IEEE Journal on Selected Areas in Communications, Dec. 2007, 1655-1666.

[17] Ryoo, S., Rodrigues, C. I., Baghsorkhi, S. S., Stone, S. S., Kirk, D. B., and Hwu, W. 2008. Optimization principles and application performance evaluation of a multithreaded GPU using CUDA. In Proceedings of ACM PPoPP'08, Feb. 2008.

[18] Falcao, G., Sousa, L., and Silva, V. 2008. Massiv parallel LDPC decoding in GPU. In Proceedings of ACM PPoPP'08, Feb. 2008.

[19] Yu, Z., Wei, Y., Ramkumar, B., and Guan, Y. 2008. An efficient signature-based scheme for securing network coding against pollution attacks. In Proceedings of IEEE INFOCOM'08, Apr. 2008.

[20] Owens, J. D., Houston, M., Luebke, D., Green, S., Stone, J. E., and Phillips, J. C. 2008. GPU computing. IEEE Proceedings, May 2008, 879-899.

[21] Al-Kiswany, S., Gharaibeh, A., Santos-Neto, E., Yuan, G., and Ripeanu, M. 2008. StoreGPU: exploiting graphics processing units to accelerate distributed storage systems. In Proceedings of IEEE Symposium on High Performance Distributed Computing (HPDC), Jun. 2008.

[22] Silberstein, M., Geiger, D., Schuster, A., Patney, A., Owens, J. D. 2008. Efficient computation of sum-products on GPUs through software-managed cache. In Proceedings of the 22nd ACM International Conference on Supercomputing, Jun. 2008.

[23] Seiler, L., et. al., 2008. Larrabee: a many-core x86 architecture for visual computing. ACM Transactions on Graphics, 27(3), Aug. 2008.

[24] Cetin Kaya Koc and Tolga Acar， Burton S. Kaliski Jr，Analyzing and Comparing Montgomery Multiplication Algorithms, IEEE Micro, 16(3):26-33, June 1996

[25] A. Karatsuba and Yu. Ofman (1962). "Multiplication of Many-Digital Numbers by Automatic Computers". In Proceedings of the USSR Academy of Sciences 145: 293–294.

L-BFGS and Delayed Dynamical Systems Approach for Unconstrained Optimization

Xiaohui XIE

Abstract

The dynamical (or ode) systems approach for optimization problems has existed for two decades. The main feature of this approach is that a continuous path starting from the initial point can be generated and eventually the path will converge to the solution. This approach is quite different from conventional optimization methods where a sequence of points, or a discrete path, is generated. An advantage of the dynamical systems approach is that it is more suitable for large scale problems. Common examples of this approach are ode's based on the steepest descent direction or the Newton's direction. In this research we apply the L-BFGS scheme to the ode model, hopefully to improve on the rate of convergence over the steepest descent direction, but not to suffer from the large amount of computational work in the Newton's direction.

1 Problem background and introduction

This paper studies computational methods for a local or the global minimizer of an unconstrained optimization problem. Optimization problems are classified into:
(a) Unconstrained Problem:

$$\min_{x\in R^n} f(x) \qquad f: R^n \to R^1 \qquad (UP)$$

(b) Equality Constrained Problem:

$$\begin{aligned} \min_{x\in R^n} & f(x) \\ h(x) &= 0 \qquad h: R^n \to R^p \end{aligned}$$

(c) Inequality Constrained Problem:

$$\begin{aligned} \min_{x\in R^n} & f(x) \\ g(x) &\le 0 \qquad h: R^n \to R^p \end{aligned}$$

(d) General Constrained Problem:

$$\begin{aligned} \min_{x\in R^n} & f(x) \\ g(x) &\le 0 \\ h(x) &= 0 \end{aligned}$$

The motivation of unconstrained methods is to generate a sequence of points $\{x_k\}$ (x_0 given) such that (1) $f(x_k) > f(x_{k+1})$;(2) $\{x_k\}$ is convergent, and (3) the limit point of the sequence is a stationary point of (UP). Different methods advance from x_k to x_{k+1} differently. Well-known methods include the steepest descent method, Newton's method and quasi-Newton method. A common theme behind all these methods is to find a direction $p \in R^n$ so that there exists an $\bar{\epsilon} > 0$ such that

$$f(x + \epsilon p) < f(x) \qquad \forall \epsilon \in (0, \bar{\epsilon})$$

This direction is called a descent direction of $f(x)$ at x. Once we have found a descent direction, we may go along this direction to approach one more step toward the optimum solution.

The following paragraphs summarize the advantages and disadvantages of these methods.

1.1 Steepest descent method

Using directional derivative in multivariable calculus, it is clear that for (UP), p is a descent direction

at $x \Leftrightarrow \nabla f(x)^T p < 0$. Hence $p = -\nabla f(x)$, or equivalently, $p = -\nabla f(x)/\|\nabla f(x)\|_2$ is obviously a descent direction for $f(x)$. This direction is called the steepest descent direction.

Method of Steepest Descent: At each iteration k: find the lowest point of f in the direction $-\nabla f(x_k)$ from x_k, i.e., find λ_k that solves

$$\min_{\lambda>0} f(x_k - \lambda \nabla f(x_k))$$

Then $x_{k+1} = x_k - \lambda \nabla f(x_k)$.

Unfortunately, the steepest descent method converges only linearly, and sometimes very slowly linearly. In fact, if $\{x_k\}$, which is generated by the steepest descent method, converges to a local minimizer x^* where $\nabla^2 f(x^*)$ is positive definite (p.d.), and λ_{max} and λ_{min} are the largest and smallest eigenvalues of $\nabla^2 f(x^*)$, then one can show that $\{x_k\}$ satisfies

$$\lim_{k\to\infty} sup \frac{\|x_{k+1} - x^*\|}{\|x_k - x^*\|} \leq c, \quad c = \frac{\lambda_{max} - \lambda_{min}}{\lambda_{max} + \lambda_{min}},$$

in a particular weighted l_2 norm, and the bound on c is tight for some starting x_0. This property indicates that the steepest descent method is q-linearly convergent. When λ_{max} and λ_{min} are far apart, then c is close to 1, and the convergence will be slow.

1.2 Newton's method

At point x_k, if $\nabla^2 f(x_k)$ is p.d., the function $f(x)$ can be approximated by a quadratic function based on the Taylor expansion:

$$\begin{aligned} f(x) \cong\ & f(x_k) + \nabla f(x_k)^T (x - x_k) \\ & + \frac{1}{2}(x - x_k)^T \nabla^2 f(x_k)(x - x_k) \end{aligned} \tag{1}$$

Then the minimizer of (1) is given by

$$\begin{aligned} \nabla f(x) &= 0 \\ &\Rightarrow \quad \nabla f(x_k) + \nabla^2 f(x_k)(x - x_k) = 0 \\ &\Rightarrow \quad x = x_k - [\nabla^2 f(x_k)]^{-1} \nabla f(x_k), \end{aligned}$$

where $-[\nabla^2 f(x_k)]^{-1} \nabla f(x_k)$, is called the Newton's direction. Then we define

$$x_{k+1} = x_k - [\nabla^2 f(x_k)]^{-1} \nabla f(x_k),$$

and the resulting method of computing x_k is called the Newton's method.

Newton's method

Given x_0, compute

$$x_{k+1} = x_k - [\nabla^2 f(x_k)]^{-1} \nabla f(x_k), \qquad k \leftarrow k + 1.$$

A key requirement for Newton's method is the p.d. of $\nabla^2 f(x_k)$. Descent directions guarantee that $f(x)$ can be further reduced and therefore they form the basis of some global methods. However, in some real applications, if the starting point is far away from the optimal solution, or the Hessian is not positive definite, Newton's direction is not adopted. Although Newton's method converges very fast ($\{x_k\}$ converges to x^* q-quadratically), the Hessian matrix is difficult to compute. So we would like to find more feasible methods with (A) no second-order information, i.e., no Hessian; and (B) fast convergence. A rule of thumb is that first-order information normally gives slow (linear) convergence, while second-order information normally gives fast (quadratic) convergence. Let us discuss several practical considerations. In general, the convergence is quadratic: the error is essentially squared at each step (that is, the number of accurate digits doubles in each step). There are some caveats, however. Firstly, Newton's method requires that the derivative be calculated directly. (If the derivative is approximated by the slope of a line through two points on the function, the secant method results; this can be more efficient depending on how one measures computational effort.) Secondly, if the initial value is too far from the true zero, Newton's method can fail to converge. Because of this, most practical implementations of Newton's method put an upper limit on the number of iterations and perhaps on the size of the iterates. Thirdly, if the root being sought has multiplicity greater than one, the convergence rate is merely linear (errors reduced by a constant factor at each step) unless special procedures are taken. Finding the inverse of the Hessian is an expensive operation. Therefore the descent direction $-[\nabla^2 f(x)]^{-1} \nabla f(x)$ is often solved approximately (but to great accuracy) using methods such as the conjugate gradient method. There also exist various quasi-Newton methods, where an approximation for

the Hessian is used instead.

Table 1 compares the advantages and disadvantages between the steepest descent method and the Newton's method.

Table 1: **Comparison of the methods**

	Advantage	Disadvantage
Steepest descent method	Simple and inexpensive, guarantees descent	Slow convergence
Newton's method	Very fast convergence if applicable	Expensive, second-order information matrix inversion

1.3 Quasi-Newton method—BFGS

Instead of using the Hessian matrix, the quasi-Newton methods approximate it.

Quasi-Newton methods are based on Newton's method to find the stationary point of $f(x)$, where the gradient $\nabla f(x)$ is 0. In Quasi-Newton methods the Hessian matrices of second derivatives of $f(x)$ do not need to be computed. The Hessian is updated by analyzing successive gradient vectors instead. Quasi-Newton methods are a generalization of the secant method to find the root of the first derivative for multidimensional problems. In multi-dimensions the secant equation is under-determined, and quasi-Newton methods differ in how they constrain the solution, typically by adding a simple low-rank update to the current estimate of the Hessian.

In quasi-Newton methods, the inverse of the Hessian matrix is approximated in each iteration by a p.d. matrix, say H_k, where k is the iteration index. Thus, the k th iteration has the following basic structure:
(a) set $p_k = -H_k g_k, \quad (g_k = \nabla f(x_k))$,
(b) line search along p_k giving $x_{k+1} = x_k + \lambda_k p_k$,
(c) update H_k giving H_{k+1}.

The initial matrix H_0 can be any positive definite symmetric matrix, although in the absence of any better estimate, the choice $H_0 = I$ often suffices. Potential advantages of the method are:
(1) only first-order information is required;
(2) H_k being symmetric and p.d. implies the descent property; and
(3) $O(n^2)$ multiplications per iteration.

The most important quasi-Newton formula was suggested by Broyden, Fletcher, Goldfarb, and Shanno independently in 1970, and is subsequently known as the BFGS formula. It is used to solve an unconstrained nonlinear optimization problem.

$$H_{k+1}^{BFGS} = H_k + \left(1 + \frac{y_k^T H_k y_k}{s_k^T y_k}\right) \frac{s_k s_k^T}{s_k^T y_k} - \left(\frac{s_k y_k^T H_k + H_k y_k s_k^T}{s_k^T y_k}\right) \tag{2}$$

where $s_k = x_{k+1} - x_k$,
$y_k = \nabla f(x_{k+1}) - \nabla f(x_k) = g_{k+1} - g_k$.

We have the following theorem.

Theorem 1.1 *If H_k^{BFGS} is a p.d. matrix, and $s_k^T y_k > 0$, then H_{k+1}^{BFGS} in (2) is also positive definite.*

Proof: For any $z \neq 0$, it is sufficient to prove that

$$z^T \left[H_k + \left(1 + \frac{y_k^T H_k y_k}{s_k^T y_k}\right) \frac{s_k s_k^T}{s_k^T y_k} - \left(\frac{s_k y_k^T H_k + H_k y_k s_k^T}{s_k^T y_k}\right) \right] z > 0,$$

In the rest of the proof, the subscript k will be omitted. Since H is p.d., we can write $H = LL^T$, and let
$a = L^T z$ and $b = L^T y$, then

$$
\begin{aligned}
z^T H_{k+1} z &= z^T \left[H_k + \left(1 + \frac{y_k^T H_k y_k}{s_k^T y_k}\right) \frac{s_k s_k^T}{s_k^T y_k} \right. \\
&\quad \left. - \left(\frac{s_k y_k^T H_k + H_k y_k s_k^T}{s_k^T y_k} \right) \right] z \\
&= z^T \left[H + \left(1 + \frac{y^T H y}{s^T y}\right) \frac{s s^T}{s^T y} - \left(\frac{s y^T H + H y s^T}{s^T y} \right) \right] z \\
&= a^T a + \frac{z^T b^T b s s^T z}{(s^T y)^2} + \frac{(z^T s)^2}{s^T y} - \frac{z^T s b^T a}{s^T y} - \frac{a^T b s^T z}{s^T y} \\
&= \left(a - \frac{z^T s b}{s^T y}\right)^T \left(a - \frac{z^T s b}{s^T y}\right) + \frac{(z^T s)^2}{s^T y} \\
&= \left\| a - \frac{z^T s b}{s^T y} \right\|^2 + \frac{(z^T s)^2}{s^T y} \\
&\geq 0
\end{aligned}
$$

If the norm above equals zero, i.e.,

$$
\left\| a - \frac{z^T s b}{s^T y} \right\| = 0,
$$

then we have

$$
a = \frac{z^T s b}{s^T y}, \text{ or } L^T z = \frac{z^T s L^T y}{s^T y},
$$

which means that $y \propto z$.

However, since $s^T y > 0$,

$$
\frac{(z^T s)^2}{s^T y} > 0,
$$

as $y \propto z$. Thus the theorem is proved. □

1.4 Limited-Memory Quasi-Newton Methods—L-BFGS

Limited-memory quasi-Newton methods are useful for solving large problems whose Hessian matrices cannot be computed at a reasonable cost or are not sparse. These methods maintain simple and compact approximations of Hessian matrices: instead of storing fully dense $n \times n$ approximations, they save only a few vectors of length n that represent the approximations implicitly. Despite these modest storage requirements, they often yield an acceptable rate of convergence. Various limited-memory methods have been proposed; we focus mainly on an algorithm known as L-BFGS, which, as its name suggests, is based on the BFGS updating formula. The main idea of this method is to use curvature information from only the most recent iterations to construct the Hessian approximation. Curvature information from earlier iterations, which is less likely to be relevant to the actual behavior of the Hessian at the current iteration, is discarded in the interest of saving storage.

As we have discussed in section 1.3, each step of the BFGS method has the form

$$
x_{k+1} = x_k - \alpha_k H_k \nabla f_k,
$$

where α_k is the step length and H_k is updated at every iteration by means of the formula

$$
H_{k+1} = V_k^T H_k V_k + \rho_k s_k s_k^T, \tag{3}
$$

where

$$
\rho_k = \frac{1}{y_k^T s_k}, \qquad V_k = I - \rho_k y_k s_k^T, \tag{4}
$$

and

$$
s_k = x_{k+1} - x_k, \qquad y_k = \nabla f_{k+1} - \nabla f_k. \tag{5}
$$

Since the inverse Hessian approximation H_k will generally be dense, the cost of storing and manipulating it is prohibitive when the number of variables is large. To circumvent this problem, we store a modified version of H_k implicitly, by storing a certain number (say, m) of the vector pairs $\{s_i, y_i\}$ used in the formulas (3)-(5). The product $H_k \nabla f_k$ can be obtained by performing a sequence of inner products and vector summations involving ∇f_k and the pairs $\{s_i, y_i\}$. After the new iterate is computed, the oldest vector pair in the set of pairs $\{s_i, y_i\}$ is replaced by the new pair $\{s_k, y_k\}$ obtained from the current step (5).

We now describe the updating process in a little more detail. At iteration k, the current iterate is x_k and the set of vector pairs is given by $\{s_i, y_i\}$ for $i = k - m, \ldots, k - 1$. We first choose some initial

Hessian approximation H_0 (in contrast to the standard BFGS iteration, this initial approximation is allowed to vary from iteration to iteration) and find by repeated application of the formula (3) that the L-BFGS approximation H_{k+1} satisfies the following formula [12]:

In general, we have for $k+1 \leq m$ the usual BFGS updated

$$\begin{aligned} H_{k+1} &= V_k^T V_{k-1}^T \cdots V_0^T H_0 V_0 \cdots V_{k-1} V_k \\ &\quad + V_k^T \cdots V_1^T \rho_0 s_0 s_0^T V_1 \cdots V_k \\ &\quad \vdots \\ &\quad + V_k^T V_{k-1}^T \rho_{k-2} s_{k-2} s_{k-2}^T V_{k-1} v_k \\ &\quad + V_k \rho_{k-1} s_{k-1} s_{k-1}^T V_k \\ &\quad + \rho_k s_k s_k^T. \end{aligned} \tag{6}$$

For $k+1 > m$ we have the update

$$\begin{aligned} H_{k+1} &= V_k^T V_{k-1}^T \cdots V_{k-m+1}^T H_0 V_{k-m+1} \cdots V_{k-1} V_k \\ &\quad + V_k^T \cdots V_{k-m+2}^T \rho_{k-m+1} s_{k-m+1} s_{k-m+1}^T \\ &\quad \cdot V_{k-m+2} \cdots V_k \\ &\quad \vdots \\ &\quad + V_k^T V_{k-1}^T \rho_{k-2} s_{k-2} s_{k-2}^T V_{k-1} V_k \\ &\quad + V_k \rho_{k-1} s_{k-1} s_{k-1}^T V_k \\ &\quad + \rho_k s_k s_k^T. \end{aligned} \tag{7}$$

A method for choosing H_0 that has proved effective in practice is to set $H_0 = \gamma_k I$, where

$$\gamma_k = \frac{s_{k-1}^T y_{k-1}}{y_{k-1}^T y_{k-1}}.$$

The strategy of keeping the m most recent correction pairs $\{s_i, y_i\}$ works well in practice; indeed no other strategy has yet proved to be consistently better. However, the main weakness of the L-BFGS method is that it converges slowly on ill-conditioned problems — specifically, on problems where the Hessian matrix contains a wide distribution of eigenvalues. On certain applications, the nonlinear conjugate methods are competitive with limited-memory quasi-Newton methods.

Algorithm (L-BFGS)

Choose starting point x_0, integer $m > 0$;
$k \leftarrow 0$;
repeat
  Choose H_0
  Compute $p_k \leftarrow -H_k \nabla f_k$
  Compute $x_{k+1} \leftarrow x_k + \alpha_k p_k$ where α_k is chosen to satisfy the Wolfe conditions;
  if $k > m$
    Discard the vector pair $\{s_{k-m}, y_{k-m}\}$ from storage;
  Compute and save
    $s_k \leftarrow x_{k+1} - x_k, y_k = \nabla f_{k+1} - \nabla f_k$;
  $k \leftarrow k+1$;
until convergence.

2 Analysis for dynamical systems with time delay

2.1 Introduction of dynamical systems

For the easiness of reading, the (UP) problem is reproduced here:

$$\min_{x \in R^n} f(x) \qquad f : R^n \to R^1 \tag{8}$$

It is very important that the optimization problem (8) itself is posted in the continuous form, i.e., x can be changed continuously. In the literature, the necessary and sufficient conditions of a local optimum are also presented in the continuous form. Furthermore, almost all the theoretical study for problem (8) is in the continuous form. However, it is very interesting to say that when it comes down to the numerical solution of (8), most of the conventional methods, such as the gradient/ steepest descent method, Newton's method and quasi-Newton's method, are all addressed in the discrete form. This interesting situation is mainly due to the fact that the computer's computation can be only done discretely. However, is it possible to study both the optimization problem and the solution methods in its original form, i.e., continuous form? In this sense, we may use the dynamical system approach or neural network approach to

solve the original optimization problem.

• Dynamical system approach. The essence of this approach is to convert problem (8) into a dynamical system or an ordinary differential equation (ode) so that the solution of problem (8) corresponds to a stable equilibrium point of this dynamical system.

• Neural network approach. The mathematical representation of neural network is an ordinary differential equation which is asymptotically stable at any isolated solution point. A companion of this neural network is an energy function which is a Lyapunov function. And as time evolves, the solution of the ode will converge to the optimum, and in this whole process, the energy function will decrease monotonically in time.

The following discussion reviews the research results in the dynamical system approach, and identifies the merits of this approach.

Consider the following simple dynamical system or ordinary differential equation

$$\frac{dx(t)}{dt} = p(x). \tag{9}$$

We first state some classical result on the existence and uniqueness of the solution, and some stability definitions for the dynamical system (9) [21,24].

Theorem 2.1 [24] *Assume that $p(x)$ is a continuous function from R^n to R^n. Then for arbitrary $t_0 \geq 0$ and $x_0 \in R^n$ there exists a local solution $x(t)$ satisfying $x(t_0) = x_0$, $t \in [t_0, \tau)$ to (9) for some $\tau > t_0$. If furthermore $p(x)$ is locally Lipschitz continuous at x_0, then the solution is unique, and if $p(x)$ is Lipschitz continuous in R^n then τ can be extended to ∞.*

Definition 2.2 *(Equilibrium point) A point $x^* \in R^n$ is called an equilibrium point of (9) if $p(x^*) = 0$.*

Definition 2.3 *(Stablility in the sense of Lyapunov) Let $x(t)$ be the solution of (9). An isolated equilibrium point x^* is Lyapunov stable if for any $x_0 = x(t_0)$ and any scalar $\epsilon > 0$, there exists a $\delta > 0$ such that if $\|x(t_0) - x^*\| < \delta$, then $\|x(t) - x^*\| < \epsilon$ for $t \geq t_0$.*

Definition 2.4 *(Convergence) Let $x(t)$ be the solution of (9). An isolated equilibrium point x^* is convergent if there exists a $\delta > 0$ such that if $\|x(t_0) - x^*\| < \delta$, $x(t) \to x^*$ as $t \to \infty$.*

A dynamical system or ode (9) arising from an optimization problem needs to have $p(x)$ being a descent direction for the objective function $f(x)$. Some well-known versions are:

Dynamical system based on the steepest descent direction:

$$\frac{dx(t)}{dt} = -\nabla f(x(t))$$

Dynamical system based on the Newton direction:

$$\frac{dx(t)}{dt} = -[\nabla^2 f(x(t))]^{-1} \nabla f(x(t)) \tag{10}$$

As in the discrete optimization methods in the previous chapter, the steepest descent direction has a slow convergence rate - meaning that it takes a very "large" value of t to approach the equilibrium point. The Newton direction has a much faster convergence rate, but the amount of work in evaluating the Jacobian is much greater.

Some other dynamical systems in the literature are:

$$\frac{dx(t)}{dt} = s(t) \cdot p(x(t)), \tag{11}$$

$$a(t) \cdot \frac{d^2x(t)}{dt^2} + b(t) \cdot B(x(t)) \cdot \frac{dx(t)}{dt} = p\left(x(t)\right), \tag{12}$$

where $p(x)$is a descent direction for $f(x)$, $B(x) \in R^{n \times n}$ is a positive definite matrix, $a(t)$ and $b(t)$ are scalar functions in t, and $s(t)$ is a positive scalar function in t and bounded above.

A major advantage of the dynamical systems approach is that very large problems can be solved [13]. No matter whether we use any of (9)-(12), existing ode methods are quite mature to tackle these problems. Solving systems with tens or hundreds of thousands of unknowns poses no problem to ode solvers. The problem size handled can be much larger than traditional methods described in Chapter 1, which are of order of magnitude in the thousands. The research in the ode approach is to find a "good" $p(x)$ in (9) that balances the convergence rate and the amount of work.

The dynamical systems approach normally consists of the following three steps:

(a) to establish an ode system;

(b) to study the convergence of the solution $x(t)$ of the ode as $t \to \infty$; and

(c) to solve the ode system numerically.

The convergence study of $x(t)$ as $t \to \infty$ and the stability of the corresponding dynamical system have mostly been addressed on a case by case base. No standard theory and/or methodology are given. This phenomenon certainly limits the systematic study of the dynamical system approach and its application potential as well. Two papers are worth mentioning, one by Tanabe [18] which used the stability theory of the dynamical system to study the ode system, and the other one by Yamashita [24] which employed Lyapunov's direct method to study the ode system.

Even though the solutions of ode systems are continuous, yet the actual computation has to be done discretely. In all the dynamical systems (10)-(12), the numerical solutions were mainly solved by either discrete optimization methods or finite difference methods.

In summary, the main attractiveness of this approach is its simplicity and its originality in pursuing the continuous form. Furthermore, there is not any restriction on the form of the objective function $f(x)$ in (8).

2.2 Delayed dynamical systems approach

As stated above, the steepest descent direction and the Newton direction of the dynamical systems approach both have their weakness. The main idea in this paper is to apply the theme of the L-BFGS algorithm in Chapter 1 to the dynamical systems approach, making it a bridge between the steepest descent direction and the Newton direction. The resulting dynamical system is a delayed ode, thus we call it the delayed dynamical systems approach.

The delayed dynamical systems approach solves the delayed ode:

$$\frac{dx(t)}{dt} = -H(x(t), x(t-\tau_1(t), \ldots, x(t-\tau_m(t)))) \cdot \nabla f(x(t)), \quad (13)$$

where H and $t-\tau_1(t), \ldots, t-\tau_m(t)$ are to be defined below.

As the delayed ode (13) is numerically solved, we compute approximations $x_0, x_1, \ldots, x_k, x_{k+1}, \ldots$ to $x(t)$ at time points $t_0, t_1, \ldots, t_k, t_{k+1}, \ldots$. We define $H = H_k$ to be a different function in the interval $(t_{k-1}, t_k]$ iteratively by:

Given $t_0, x(t_0) = x_0$, and an initial H_0, for $t_0 \le t$, we define

$$\begin{aligned} H(x(t), x(t_0)) &:= H_1(x(t), x(t_0)) \\ &:= V_0(t)^T H_0 V_0(t) + \rho_0(t) s_0(t) s_0(t)^T, \end{aligned}$$

where

$$s_0(t) = x(t) - x_0,$$

$$y_0(t) = \nabla f(x(t)) - \nabla f(x_0),$$

$$\rho_0(t) = 1/y_0(t)^T s_0(t),$$

$$V_0(t) = I - \rho_0(t) y_0(t) s_0(t)^T,$$

in the R.H.S. of (13) and determine a stepsize $h_1 = (t_1 - t_0)$ to compute, using some numerical ode method, an approximation x_1 to $x(t_1)$ at t_1. Then for $t_1 \le t$, we define

$$\begin{aligned} &H(x(t), x(t_1), x(t_0)) \\ &\quad := H_2(x(t), x(t_1), x(t_0)) \\ &\quad := V_1(t)^T V_0(t_1)^T H_0 V_0(t_1) V_1(t) \\ &\qquad + V_1(t)^T \rho_0(t_1) s_0(t_1) s_0(t_1)^T V_1(t) \\ &\qquad + \rho_1(t) s_1(t) s_1(t)^T \end{aligned}$$

where

$$s_1(t) = x(t) - x(t_1),$$

$$y_1(t) = \nabla f(x(t)) - \nabla f(x(t_1)),$$

$$\rho_1(t) = 1/y_1(t)^T s_1(t),$$

$$V_1(t) = I - \rho_1(t) y_1(t) s_1(t)^T,$$

in the R.H.S. of (13) and determine a stepsize $h_2 = (t_2 - t_1)$ to compute, using some numerical ode method, an approximation x_2 to $x(t_2)$ at t_2. Of course, computationally x_1 is used instead of $x(t_1)$.

This process is repeated until we have accepted x_{m-1} at t_{m-1}. Then for $t_{m-1} \le t$, we use

$$\begin{aligned}
&H(x(t), x(t_{m-1}), \ldots, x(t_1), x(t_0)) \\
&\quad := H_m(x(t), x(t_{m-1}), \ldots, x(t_1), x(t_0)) \\
&\quad := V_{m-1}(t)^T V_{m-2}(t_{m-1})^T \ldots V_1(t_2)^T V_0(t_1)^T \\
&\qquad \cdot H_0 V_0(t_1) V_1(t_2) \ldots V_{m-2}(t_{m-1}) V_{m-1}(t) \\
&\qquad + V_{m-1}(t)^T V_{m-2}(t_{m-1})^T \ldots V_1(t_2)^T \\
&\qquad \cdot \rho_0(t_1) s_0(t_1) s_0(t_1)^T V_1(t_2) \ldots V_{m-2}(t_{m-1}) \\
&\qquad \cdot V_{m-1}(t) \\
&\qquad + \ldots \\
&\qquad + V_{m-1}(t)^T \rho_{m-2}(t_{m-1}) s_{m-2}(t_{m-1}) \\
&\qquad \cdot s_{m-2}(t_{m-1})^T V_{m-1}(t) \\
&\qquad + \rho_{m-1}(t) s_{m-1}(t) s_{m-1}(t)^T \qquad (13A)
\end{aligned}$$

where

$$\begin{aligned}
s_{m-1}(t) &= x(t) - x(t_{m-1}), \\
y_{m-1}(t) &= \nabla f(x(t)) - \nabla f(x(t_{m-1})), \\
\rho_{m-1}(t) &= 1/y_{m-1}(t)^T s_{m-1}(t), \\
V_{m-1}(t) &= I - \rho_{m-1}(t) y_{m-1}(t) s_{m-1}(t)^T.
\end{aligned}$$

to compute x_m at t_m. Beyond this point we save only m previous values of x. The definition of H is now, for $m \le k$,
for $t_k \le t$,

$$\begin{aligned}
&H(x(t), x(t_k), \ldots, x(t_{k-m+2}), x(t_{k-m+1})) \\
&\quad := H_{k+1}(x(t), x(t_k), \ldots, x(t_{k-m+2}), x(t_{k-m+1})) \\
&\quad := V_k(t)^T V_{k-1}(t_k)^T \ldots V_{k-m+2}(t_{k-m+3})^T \\
&\qquad \cdot V_{k-m+1}(t_{k-m+2})^T H_0 V_{k-m+1}(t_{k-m+2}) \\
&\qquad \cdot V_{k-m+2}(t_{k-m+3}) \ldots V_{k-1}(t_k) V_k(t) \\
&\qquad + V_k(t)^T V_{k-1}(t_k)^T \ldots V_{k-m+2}(t_{k-m+3})^T \\
&\qquad \cdot \rho_{k-m+1}(t_{k-m+2}) s_{k-m+1}(t_{k-m+2}) \\
&\qquad \cdot s_{k-m+1}(t_{k-m+2})^T V_{k-m+2}(t_{k-m+3}) \ldots \\
&\qquad \cdot V_{k-1}(t_k) V_k(t) \\
&\qquad + \ldots \\
&\qquad + V_k(t)^T \rho_{k-1}(t_k) s_{k-1}(t_k) \\
&\qquad \cdot s_{k-1}(t_k)^T V_k(t) \\
&\qquad + \rho_k(t) s_k(t) s_k(t)^T \qquad (13B)
\end{aligned}$$

where

$$\begin{aligned}
s_k(t) &= x(t) - x(t_k), \\
y_k(t) &= \nabla f(x(t)) - \nabla f(x(t_k)), \\
\rho_k(t) &= 1/y_k(t)^T s_k(t), \\
V_k(t) &= I - \rho_k(t) y_k(t) s_k(t)^T.
\end{aligned}$$

It is obvious that the delayed ode (13) is a continuous version of the L-BFGS scheme. The $H = H_k$ in (13) attempts to approximate the inverse of the Jacobian in the Newton method. It is worth mentioning that the matrix H_k is never computed explicitly. We only need to compute the R.H.S. of (13), i.e., the product of H_k and a vector.

2.3 Uniqueness property of dynamical systems

The positive definite property of the dynamical system (13) is proved in Appendix I, hence we conclude that the solution exists. The next step is to show the Lipschitz continuity of this system, which implies that the solution is also unique.

2.3.1 Definition of Lipschitz continuity

Let $F : R^n \to R^m$ be a function, we say that F is **Lipschitz continuous** with **Lipschitz constant** L if there is a nonnegative constant L such that

$$\|F(x_1) - F(x_2)\| \le L\|x_1 - x_2\|$$

for all x_1 and x_2 in R^m.

2.3.2 Lipschitz continuity of method (13)

By Theorem 2.1, the solution of our new unconstrained optimization method (13) is unique if the right-handed-side of (13) is Lipschitz continuous. We firstly rewrite (13) as

$$\frac{dx(t)}{dt} = -H(x(t), x(t-\tau))\nabla f(x(t)) \ .$$

Let $u = x(t)$ and $w = x(t-\tau)$, then our aim is to prove that $-H(u, w)\nabla f(u)$ is Lipschitz continuous

with respect to u and w. In other words, we want to prove that

$$\|H(u,w)\nabla f(u)-H(\bar{u},w)\nabla f(\bar{u})\| \le L_1\|u-\bar{u}\|, \quad (14)$$

$$\|H(u,w)\nabla f(u) - H(u,\bar{w})\nabla f(u)\| \le L_2\|w-\bar{w}\|. \quad (15)$$

This problem is a difficult one and the following theorem may give some hint to our goal:

Theorem 2.5 *(Kurdyka, subanalytic, semi-algebraic) Let F: $X \subset R^n \to R$ be a definable C^1-function such that*

$$\left|\partial F/\partial x_i\right| < M$$

for some M and each i.
Then there exist a finite partition of X and $C > 0$ such that on each piece, the restriction of F to this piece is C-Lipschitz.
Moreover, this finite partition only depends on X and not on F. (And C only depends on M and n.)

It is obvious that $H(u,w)\nabla f(u)$ is a column vector. In order to transform a vector into a scalar we can use $e_i^T H(u,w)\nabla f(u)$ and problem (14) and (15) can be converted to

$$\left|\frac{\partial}{\partial u}[e_i^T H(u,w)\nabla f(u)]\right| < M_1,$$

$$\left|\frac{\partial}{\partial w}[e_i^T H(u,w)\nabla f(u)]\right| < M_2$$

Equation (13B) shows that $H(u,w)$ depends in a complicated way on

$$y(u,w) = \nabla f(u) - \nabla f(w)\ ,$$

$$s(u,w) = u - w\ .$$

The resulting partial derivatives $\frac{\partial}{\partial w}[e_i^T H\nabla f(u)]$ contain so many fractions whose denominators all have terms $y^T s$ that the bound must be controlled properly because the denominators tend to 0. The main problem is therefore to make the numerators and denominators have the same order so that they canceled out each other.

The following lemma seems to play a critical role in this cancellation:

Lemma 2.6 *Let $F : R^n \to R^m$ be continuously differentiable in the open convex set $D \subset R^n$, $x \in D$, and let $J = \frac{\partial F}{\partial x}$ be Lipschitz continuous at x in the neighborhood D, using a vector norm and the induced matrix operator norm and the Liptschitz constant γ. Then, for any $x + p \in D$,*

$$\|F(x+p) - F(x) - J(x)p\| \le \frac{\gamma}{2}\|p\|^2.$$

If we define $x = w, p = u - w = s, F(x) = \nabla f(x)$, then the lemma converts to

$$\|\nabla f(u) - \nabla f(w) - \nabla^2 f(w)(u-w)\| \le \frac{\gamma}{2}\|u-w\|$$

Substituting y and s into the above inequality yields

$$\|y - \nabla^2 f(w)s\| \le \frac{\gamma}{2}\|s\|.$$

3 Numerical testing

Based on the analysis in the previous sections, we hope to conclude that the continuous-time Limited Memory BFGS method has a better performance than other traditional methods. In this section we will show the computational results of several examples.

3.1 The test problems

We have tested method (13) on the following unconstrained optimization problems:
Problem 1: Extended Rosenbrock function

$$f(x) = \sum_{i=1}^{n}[100(x_{2i} - x_{2i-1}^2)^2 + (1 - x_{2i-1})^2],$$
$$[x_0]_{2i-1} = -1.2, [x_0]_{2i} = 1, [x^*]_i = 1, f(x^*) = 0.$$

Problem 2: Penalty function I

$$f(x) = \sum_{i=1}^{n} 10^{-5}(x_i - 1)^2 + [(\sum_{i=1}^{n} x_i^2) - \frac{1}{4}]^2,$$
$$[x_0]_i = i.$$

Problem 3: Variable dimensioned function

$$f(x) = \sum_{i=1}^{n}(x_i - 1)^2 + [\sum_{i=1}^{n} i(x_i - 1)]^2,$$
$$+[\sum_{i=1}^{n} i(x_i - 1)]^4,$$
$$[x_0]_i = 1 - i/n, [x^*]_i = 1, f(x^*) = 0.$$

Problem 4: Linear function-rank 1

$$f(x) = \sum_{i=1}^{m}[i(\sum_{j=1}^{n} jx_j) - 1]^2, (m \geq n)$$
$$[x_0]_i = \frac{1}{i}, f(x^*) = \frac{m(m-1)}{2(2m+1)} \text{ at any point}$$
$$\text{where } \sum_{j=1}^{n} jx_j = \frac{3}{2m+1}.$$

3.2 Comparison between continuous-time L-BFGS and continuous-time steepest descent

Our main platform of numerical computation is Matlab. The Matlab library contains nonstiff ode solvers ode113, ode23, and ode45, and stiff ode solvers ode15s, ode23s, and ode23tb. There is also a nonstiff delayed differential solver ddesd. Nonstiff solvers are efficient for ode problems without a wide-spread spectrum of eigenvalues, whereas stiff solvers are good for problems with both large and small eigenvalues.

The difficulty with solving (13) is the time delay. In order to get familiar with the ode solvers, and eventually to take into account the delayed equation, we first test ode (and not dde) solvers on the above test problems.

In the first phase we start with solving a modified form of Problem 1:

Modified Extended Rosenbrock function:

$$f(x) = \sum_{i=1}^{n}[100(x_{2i} - x_{2i-1})^2 + (1 - x_{2i-1})^2],$$
$$[x_0]_{2i-1} = -1.2, [x_0]_{2i} = 1, [x^*]_i = 1, f(x^*) = 0.$$

The difference between the original Rosenbrock and the modified one is the square of x_{2i-1} in the first part of the right-handed-side.

We use the nonstiff ode solver ode113 on this problem with dimension $n = 100$ and tolerance $= 10^{-4}$. The result is given in the following table, where t denotes the iteration time, *value* denotes the computed optimal solution value, and *step* denotes the number of iterations.

Table 2: **Modified Rosenbrock Problem using ode113**

	t	value	step
L-BFGS	2	0	497
Steepest descent	23.2813	0.0006	53557

We can see that the continuous-time L-BFGS is obviously faster than the continuous-time steepest descent method in the value of t and number of integration steps.

Based on the performance in phase 1, we then move on to the second phase, where the delayed equation solver ddesd is used. This time we focus on all the test problems mentioned above and also use the original Extended Rosenbrock. However, the numerical results are not so good as we have expected – the continuous-time steepest descent method shows better performance than the continuous-time L-BFGS. After an analysis on the problems, it is found that many of them have a wide spectrum of eigenvalues. In other words, the problems are stiff.

In the third phase, the Matlab stiff ode solver ode15s is being used on the above four problems. Matlab does not have a stiff solver, and hence we are unable to take into account the effect of time delay. In the following tables, P denotes the problem number, N the dimension of variables. Table 4 to Table 6 give the performance on function value when the solution reach to the optimum value.

Table 3: **Comparison of the two methods for $m = 2$ on function value**

P	*N*	*Steepest descent*	*Limited-Memory BFGS*
1	10^3	0	5.8852×10^3
2	10^3	1.2030×10^5	9.7257×10^{-3}
3	10^3	5.2945×10^{-4}	42.307
4	10^3	6.0317	1.3153×10^{23}

Table 4: **Comparison of the two methods for $m = 4$ on function value**

P	N	*Steepest descent*	*Limited-Memory BFGS*
1	10^3	0	4.2692×10^3
2	10^3	1.5114×10^5	9.7304×10^3
3	10^3	0	2.9868×10^{-1}
4	10^3	6.0317	32.595

Table 5: **Comparison of the two methods for $m = 6$ on function value**

P	N	*Steepest descent*	*Limited-Memory BFGS*
1	10^3	0	1.1273×10^3
2	10^3	1.5068×10^5	9.7296×10^{-3}
3	10^3	7.1928×10^{-8}	1.0795×10^{-5}
4	10^3	6.0317	6.0317

Table 7 to Table 9 focus on the comparison for the norm of gradient as solution tends to the optimum value.

Table 6: **Comparison of the norm of gradient of the two methods for $m = 2$**

P	N	*Steepest descent*	*Limited-Memory BFGS*
1	1000	0	57.060
2	1000	1.4146×10^3	6.9366×10^{-5}
3	1000	4.6056×10	3.1173
4	1000	8.5570×10^{-7}	2.8544×10^{15}

Table 7: **Comparison of the norm of gradient of the two methods for $m = 4$**

P	N	*Steepest descent*	*Limited-Memory BFGS*
1	1000	0	6.5250
2	1000	1.6787×10^3	1.8992×10^{-4}
3	1000	0	8.1280×10
4	1000	2.1221×10^{-7}	1.9531×10^2

Table 8: **Comparison of the norm of gradient of the two methods for $m = 6$**

P	N	*Steepest descent*	*Limited-Memory BFGS*
1	1000	0	3.1648
2	1000	1.6749×10^3	1.7542×10^{-4}
3	1000	5.3639×10^{-1}	1.5238
4	1000	3.7336×10^{-7}	3.7253×10^{-5}

By comparing these tables one may find that the continuous-time L-BFGS performs better in Problem 2, while the continuous-time steepest descent method performs better in Problem 4. In Problems 1 and 3, there is not much difference.

In order to show the full potential of the continuous-time L-BFGS, it is our next goal to use a stiff dde solver, which will be performed in the next phase of this research.

3.3 A new code using Radar5

For stiff problems, including differential-algebraic and neutral delay equations with constant or state-dependent (eventually vanishing) delays, the code RADAR5 written by Ernest Hairer is more appropriate. This code uses collocation methods based on Radau nodes and solves dde's of the type

$$My'(t) = f\left(t, y(t), y(t - \alpha_1(t, y(t))), \ldots, y(t - \alpha_m(t, y(t)))\right)$$

$$y(t_0) = y_0,\ y(t) = g(t) \quad \text{for} \quad t < t_0,$$

where M is a constant $d \times d$ matrix and $\alpha_i(t, y(t)) < t$ for all $t \geq t_0$ and for all i. The value $g(t_0)$ may be different from y_0, allowing for a discontinuity at t_0. (Collocation methods have been proved to have excellent stability properties for delay equations.)

The code RADAR5 is written in ANSI Fortran-90 and is made up of several routines. Because our main test programs are written in MATLAB, we need to call FORTRAN from MATLAB. This is not an easy task and will be tackled in the next phase of our research.

4 Main stages of this research

(A) Prove that the function H in (13) is positive definite. (Done and shown in Appendix I).

(B) Prove that H is Lipschitz continuous. (Still ongoing)

(C) Show that the solution to (13) is asymptotically stable. (A simple consequence of (B).)

(D) Show that (13) has a better rate of convergence than the dynamical system based on the steepest descent direction.

(E) Perform numerical testing.

(F) Apply this new optimization method to practical problems.

APPENDIX I: To show that H in (13) is positive definite.

Without loss of ambiguity, in the subsequent proof, we drop the $t, t_0, t_1, \ldots, t_k, t_{k+1}$, ect. in $s_k(t), y_k(t), V_k(t)$, and so on below.

Property 1 If H_0 is positive definite, the matrix H defined by (13) is positive definite (provided that $y_i^T s_i > 0$ for all i).

Proof: We prove the result by induction. From the above discussion we know that (13), the continuous analog of the L-BFGS formula, has two cases. Hence our proof needs to cater for each of them.

For the first case $k+1 > m$, note that when $m = 1$

$$\begin{aligned} H_{k+1} &= V_k^T H_0 V_k + \rho_k s_k s_k^T \\ &= H_0 - \frac{H_0 y_k s_k^T}{y_k^T s_k} - \frac{s_k y_k^T H_0}{y_k^T s_k} \\ &\quad + \frac{s_k y_k^T H_0 y_k s_k^T}{(y_k^T s_k)^2} + \frac{s_k s_k^T}{y_k^T s_k} \end{aligned}$$

It is obvious that the proof of p.d. of this matrix is the same as that of Theorem 1 in section 1.3. Therefore, H_{k+1} is p.d. when $m = 1$.

Now suppose they are true for $m = l$, we show that they are true for $m = l + 1$.

When $m = l$, we have (denoting H_{k+1} by H_{k+1}^l to emphasize $m = l$)

$$\begin{aligned} H_{k+1}^l &= V_k^T V_{k-1}^T \cdots V_{k-l+1}^T H_0 V_{k-l+1} \cdots V_{k-1} V_k \\ &\quad + \{V_k^T \cdots V_{k-l+2}^T \rho_{k-l+1} s_{k-l+1} s_{k-l+1}^T \\ &\qquad \cdot V_{k-l+2} \cdots V_k \\ &\quad + V_k^T \cdots V_{k-l+3}^T \rho_{k-l+2} s_{k-l+2} s_{k-l+2}^T \\ &\qquad \cdot V_{k-l+3} \cdots V_k \\ &\quad \vdots \\ &\quad + V_k^T V_{k-1}^T \rho_{k-2} s_{k-2} s_{k-2}^T V_{k-1} V_k \\ &\quad + V_k \rho_{k-1} s_{k-1} s_{k-1}^T V_k \\ &\quad + \rho_k s_k s_k^T \}. \end{aligned}$$

being positive definite. (There are $l + 1$ terms in H_{k+1}^l)

If $m = l + 1$, from (13B)

$$\begin{aligned} H_{k+1}^{l+1} &= V_k^T V_{k-1}^T \cdots V_{k-l}^T H_0 V_{k-l} \cdots V_{k-1} V_k \\ &\quad + V_k^T \cdots V_{k-l+1}^T \rho_{k-l} s_{k-l} s_{k-l}^T \\ &\qquad \cdot V_{k-l+1} \cdots V_k \\ &\quad + \{V_k^T \cdots V_{k-l+2}^T \rho_{k-l+1} s_{k-l+1} s_{k-l+1}^T \\ &\qquad \cdot V_{k-l+2} \cdots V_k \\ &\quad + V_k^T \cdots V_{k-l+3}^T \rho_{k-l+2} s_{k-l+2} s_{k-l+2}^T \\ &\qquad \cdot V_{k-l+3} \cdots V_k \\ &\quad \vdots \\ &\quad + V_k^T V_{k-1}^T \rho_{k-2} s_{k-2} s_{k-2}^T V_{k-1} V_k \\ &\quad + V_k \rho_{k-1} s_{k-1} s_{k-1}^T V_k \\ &\quad + \rho_k s_k s_k^T \}. \end{aligned}$$

(There are $l + 2$ terms in H_{k+1}^{l+1}.)

Comparing these two equations we find that the terms in curly braces are the same, and let

$$\begin{aligned} (*) &= V_k^T \cdots V_{k-l+2}^T \rho_{k-l+1} s_{k-l+1} s_{k-l+1}^T \\ &\qquad \cdot V_{k-l+2} \cdots V_k \\ &\quad + V_k^T \cdots V_{k-l+3}^T \rho_{k-l+2} s_{k-l+2} s_{k-l+2}^T \\ &\qquad \cdot V_{k-l+3} \cdots V_k \\ &\quad \vdots \\ &\quad + V_k^T V_{k-1}^T \rho_{k-2} s_{k-2} s_{k-2}^T V_{k-1} V_k \\ &\quad + V_k \rho_{k-1} s_{k-1} s_{k-1}^T V_k \\ &\quad + \rho_k s_k s_k^T \end{aligned}$$

Thus,

$$\begin{aligned} H_{k+1}^l &= V_k^T V_{k-1}^T \cdots V_{k-l+1}^T H_0 V_{k-l+1} \cdots V_{k-1} V_k \\ &\quad + (*) \end{aligned}$$

$$\begin{aligned} H_{k+1}^{l+1} &= V_k^T V_{k-1}^T \cdots V_{k-l}^T H_0 V_{k-l} \cdots V_{k-1} V_k \\ &\quad + V_k^T \cdots V_{k-l+1}^T \rho_{k-l} s_{k-l} s_{k-l}^T \\ &\qquad \cdot V_{k-l+1} \cdots V_k + (*) \\ &= V_k^T V_{k-1}^T \cdots V_{k-l+1}^T (V_{k-l}^T H_0 V_{k-l} + \rho_{k-l} \\ &\qquad \cdot s_{k-l} s_{k-l}^T) V_{k-l+1} \cdots V_{k-1} V_k + (*) \end{aligned}$$

Since we have assumed that H_{k+1}^l is p.d., if we try to prove that H_{k+1}^{l+1} is also p.d., we should prove that

$V_{k-l}^T H_0 V_{k-l} + \rho_{k-l} s_{k-l} s_{k-l}^T$ and H_0 have the same property, i.e., $V_{k-l}^T H_0 V_{k-l} + \rho_{k-l} s_{k-l} s_{k-l}^T$ is also p.d..

Now we move forward to prove that $V_{k-l}^T H_0 V_{k-l} + \rho_{k-l} s_{k-l} s_{k-l}^T$ is p.d..

From the proof before, we have the following conclusion:

Consider the formula

$$B = V_k^T A V_k + \rho_k s_k s_k^T \qquad k = 0, 1, \cdots$$

(The definition of V_k, ρ_k, s_k are the same as in the L-BFGS formula.) If we know A is a p.d. matrix, then B is also p.d..

In this sense, it is easy to know that $V_{k-l}^T H_0 V_{k-l} + \rho_{k-l} s_{k-l} s_{k-l}^T$ is p.d.. As we have assumed that H_{k+1}^l is p.d. when H_0 is p.d., we conclude that H_{k+1}^{l+1} is p.d..

For the second case $k + 1 \leq m$,

$$\begin{aligned} H_{k+1} &= V_k^T V_{k-1}^T \cdots V_0^T H_0 V_0 \cdots V_{k-1} V_k \\ &\quad + V_k^T \cdots V_1^T \rho_0 s_0 s_0^T V_1 \cdots V_k \\ &\quad \vdots \\ &\quad + V_k^T V_{k-1}^T \rho_{k-2} s_{k-2} s_{k-2}^T V_{k-1} v_k \\ &\quad + V_k \rho_{k-1} s_{k-1} s_{k-1}^T V_k \\ &\quad + \rho_k s_k s_k^T. \end{aligned}$$

We also use induction to prove H_{k+1} is p.d..

Firstly, $H_1 = V_0^T H_0 V_0 + \rho_0 s_0 s_0^T$ from above, so it is clearly that H_1 is p.d..

Secondly, assumed that H_k is p.d.. We are going to prove that H_{k+1} is also p.d.. We have assumed

$$\begin{aligned} H_k &= V_{k-1}^T V_{k-2}^T \cdots V_0^T H_0 V_0 \cdots V_{k-2} V_{k-1} \\ &\quad + V_{k-1}^T \cdots V_1^T \rho_0 s_0 s_0^T V_1 \cdots V_{k-1} \\ &\quad + V_{k-1}^T \cdots V_2^T \rho_1 s_1 s_1^T V_2 \cdots V_{k-1} \\ &\quad \vdots \\ &\quad + V_{k-1} \rho_{k-2} s_{k-2} s_{k-2}^T V_{k-1} \\ &\quad + \rho_{k-1} s_{k-1} s_{k-1}^T. \end{aligned}$$

is p.d.. Hence,

$$\begin{aligned} H_{k+1} &= V_k^T V_{k-1}^T \cdots V_0^T H_0 V_0 \cdots V_{k-1} V_k \\ &\quad + V_k^T \cdots V_1^T \rho_0 s_0 s_0^T V_1 \cdots V_k \\ &\quad \vdots \\ &\quad + V_k^T V_{k-1}^T \rho_{k-2} s_{k-2} s_{k-2}^T V_{k-1} v_k \\ &\quad + V_k \rho_{k-1} s_{k-1} s_{k-1}^T V_k \\ &\quad + \rho_k s_k s_k^T \\ &= V_k^T (V_{k-1}^T V_{k-2}^T \cdots V_0^T H_0 V_0 \cdots V_{k-2} V_{k-1} \\ &\quad + V_{k-1}^T \cdots V_1^T \rho_0 s_0 s_0^T V_1 \cdots V_{k-1} \\ &\quad + V_{k-1}^T \cdots V_2^T \rho_1 s_1 s_1^T V_2 \cdots V_{k-1} \\ &\quad + \cdots + V_{k-1} \rho_{k-2} s_{k-2} s_{k-2}^T V_{k-1} \\ &\quad + \rho_{k-1} s_{k-1} s_{k-1}^T) V_k + \rho_k s_k s_k^T \\ &= V_k^T H_k V_k + \rho_k s_k s_k^T. \end{aligned}$$

Therefore, we have proved that H_{k+1} is p.d. when $k + 1 \leq m$.

So we have proved the property for both cases $k + 1 \leq m$ and $k + 1 > m$. □

The proof of the property above is part of our work on the delayed dynamical systems approach for unconstrained optimization. The requirement that $y_i^T s_i > 0$ for all i in Property 1 is not a major issue, because we work with a continuous ode and the numerical method can always be restarted.

References

[1] Aluffi-Pentini, F., Parisi, V. and Zirilli, F. Algorithm 617 DAFNE: A differential equations algorithm for nonlinear equations, ACM Trans. on Math. Software, 10 (3), 1984, 317-324.

[2] Boggs, P. T., The solution of nonlinear systems of equations by A-stable integration techniques, SIAM J. Numer. Anal. 8 (4), 1971, 767-785.

[3] Botsaris, C. A. and Jacobson, D. H., A Newton-type curvilinear search method for optimization, JMAA, 54, 1976, 217-229.

[4] Brown, A. A. and Bartholomew-Biggs, M. C., ODE versus SQP methods for constrained optimization, JOTA 62 (3), 1989, 371-386.

[5] Chen, Y. H. and Fang, S. C., Solving convex programming problem with equality constraints by neural networks, Computers Math. Appl. 36, 1998, 41-68.

[6] Chu, M. T., On the continuous realization of iterative processes, SIAM Review 30 (3), 1988, 375-387.

[7] Han, Q., Liao, L.-Z., Qi, H. and Qi, L., Stability analysis of gradient-based neural networks for optimization problems, J. Global Optim. 19 (4), 1962, 363-381.

[8] Hassan, N. and Rzymowski, W., An ordinary differential equation in nonlinear programming. Nonlinear Analysis, Theory, Method & Applications 15 (7), 1990, 597-599.

[9] aykin, S. S., Neural Networks: A Comprehensive Foundation, Prentice-Hall, Englewood Cliffs, NJ, 1994.

[10] He, B. S., Inexact implicit methods for monotone general variational inequalities, Mathematical Programming, 86 (1), 1999, 199-217.

[11] Incerti, S., Parisi, V. and Zirilli, F., A new method for solving nonlinear simultaneous equations, SIAM J. Numer. Anal. 16, 1979, 779-789.

[12] Jorge Nocedal, Updating Quasi-Newton Matrices With Limited Storage, Mathematics of Computation, Vol 35, No 151, July 1980, pp. 773-782.

[13] Liao, L.-Z. and Qi, H., A neural network for the linear complementarity problem, Math. Comput. Modelling 29 (3), 1999, 9-18.

[14] L.Z. Liao, L.Q. Qi, and H.W. Tam, A gradient-based continuous method for large-scale optimization problems, Journal of Global Optimization, Vol 31 , Apr 2005, pp. 271-286.

[15] Liao, L.-Z., Qi, H. and Qi, L., Solving nonlinear complementarity problems with neural networks: a reformulation method approach, JCAM 131 (12), 2001, 343-359.

[16] LI-ZHI LIAO, HOUDUO QI and LIQUN QI, (2004), Neurodynamical Optimization, Journal of Global Optimization 28: 175-195.

[17] Novakovi?c, Z. R., Solving systems of non-linear equations using the Lyapunov direct method, Computers Math. Applic. 20 (12), 1990, 19-23.

[18] Tanabe, K., A geometric method in nonlinear programming, JOTA 30 (2), 1980, 181-210.

[19] Tank, D. W. and Hopfield, J. J., Simple neural optimization networks: An A/D convert, signal decision circuit, and a linear programming circuit, IEEE Trans. Circuits Syst. 33, 1986, 533-541.

[20] Wilde, N. G., A note on a differential equation approach to nonlinear programming, Management Science 15 (11), 1969, 739-739.

[21] Williems, J. L., Stability Theory of Dynamical Systems, Nelson, 1970.

[22] Wu, X., Xia, Y., Li, J. and Chen, W. K., A high performance neural network for solving linear and quadratic programming problems, IEEE Trans. Neural Networks, 7, 1996, 643-651.

[23] Xia, Y., A new neural network for solving linear programming problems and its applications, IEEE Trans. Neural Networks 7, 1996, 525-529.

[24] Yamashita, H., A differential equation approach to nonlinear programming, Math. Prog. 18,1980, 155-168.

[25] Zabcayk, J ., Mathematical Control Theory: An Introduction, Birkhauser, Boston, 1992.